

**Vaccine potential of Perfringolysin O (PFO) of
Clostridium perfringens and its mutants**

Thesis submitted to the Jawaharlal Nehru University in partial
fulfillment of the requirement for the award of the degree of

DOCTOR OF PHILOSOPHY
IN
BIOTECHNOLOGY
BY

Ankita Singh



2021

**School of Biotechnology
Jawaharlal Nehru University
New Delhi- 110 067**



**School of Biotechnology
Jawaharlal Nehru University
New Delhi-110067**

Dated: 18/05/2021

CERTIFICATE

This is to certify that the work entitled '**Vaccine potential of Perfringolysin O (PFO) of *Clostridium perfringens* and its mutants**' submitted to the School of Biotechnology, Jawaharlal Nehru University, New Delhi in partial fulfillment of the requirement for the award of the degree of Doctorate of Philosophy, embodies faithful record of the original research work carried out by **Ms. Ankita Singh**. She has worked under my guidance and supervision. This work is original and has not been submitted so far in part or full for any other degree or diploma of any other University.

Ankita Singh

Ankita Singh

Candidate

Aparna Dixit

Prof. Aparna Dixit

Supervisor

School of Biotechnology

JNU, New Delhi-110067

Devapriya Choudhury

Dr. Devapriya Choudhury

Supervisor

School of Biotechnology

JNU, New Delhi-110067

Pawan K. Dhar

Prof. Pawan K. Dhar

Dean

School of Biotechnology

Jawaharlal Nehru University

New Delhi-110067

Acknowledgment

योगेश्वराय महादेवाय
त्त्रयंबकाय त्रिपुरान्तकाय
त्रिकाग्नि कलया कालाग्निरुद्रया
नीलकण्ठाय मृतुन्जय
त्रिगुणी कलया कालाग्निरुद्रया
सर्वेसराय सदा शिवाय
महादेवाय: नमः

First and foremost, I would like to express deep love, devotion, and gratitude to almighty for showering immense love, care, will, courage, and infinite power, to complete this journey of Ph.D. very patiently. The unconditional support, love, and faith of my parents and brothers always keep me motivated in every situation. The unconditional love and support of my husband has been instrumental in accomplishing my Ph.D. work. I want to thank my father-in-law and all family members for the endless support.

The Accomplishment of the thesis was not possible without the immense support of my supervisor **Prof. Aparna Dixit** Professor, School of Biotechnology, Jawahar Lal Nehru University-Delhi I would like to thank her for her caring and concerning nature that constantly push me to complete the thesis work. I also express deep appreciation to **Dr. Devapriya Chaudhary, Dr. Swati Tiwari** for their keen interest & valuable inputs in my study.

I want to thank the Dean, **Prof. Pawan K. Dhar**, for the moral support and providing for instrument facilities in the department. My sincere thanks and acknowledgment My sincere thanks to **Prof. Rajiv Bhat** and other faculty members for their constant support and encouragement. I would like to thank Dr. Lalit C. Garg for his support, encouragement, Special thanks go to Naresh bhaiya for helping me in animal handling and Rinku bhaiya for maintaining an efficient working environment in the lab. **Sheenu** and **Geeta** are acknowledged and sincerely thanked for all the paperwork. I genuinely acknowledge the **Manish bhaiya** and other CIF staff. **Tiwari sir, Ajay ji, Sajjan ji, and Yadav ji** are sincerely appreciated for their administrative services and cooperation. **Pandeyji's** help from the animal house facility is strongly appreciated which helped me finish my animal experiments in time.

I genuinely thank my seniors **Gaurav sir, Rachna mam, Zaheer sir, Sapna mam, Ankita mam, Shailesh sir, Sunita mam, Mahima mam, Alka mam, Radha,** and **Jasvir kaur** for their everlasting support and valuable suggestions. I will never forget **Mahima mam, Alka mam, Radha,** and **Jasvir** for their support every time. I especially thank Jasvir for supporting me like my sister, and I always feel very blessed to have such a genuine friend. I especially thank Sweta for her outstanding support in accomplishing my experimental work. I genuinely thank my juniors Jeetesh, Roshan, and Rohit for their willing and ready help whenever needed. I would like to thank my batchmates **Monika, Kritika, Urvider Kaur, Akanksha, Priyanka, Usuf, Rajkamal, Ashwathi** for some very essential lessons that I learned from them. Help was always provided to me whenever asked for at NII by **Amit sir,** and **Himani mam.** Financial assistance from **JNU** and **UGC** is sincerely acknowledged. I extend my gratitude AIRF, JNU, New Delhi for providing me with different technical facilities that helped me perform my experiments.

I dedicate this thesis to my family members!

Ankita

Table of Contents

| Contents | Page No. |
|---|--------------|
| Abbreviations | |
| Chapter 1 Introduction | 1-11 |
| Chapter 2 Review of Literature | 12-67 |
| Chapter 3 Materials and methods | 68-95 |
| 3.1 Materials | |
| 3.2 Methods | |
| 3.2.1 Bacterial cell cultures | |
| 3.2.2 Cryopreservation of the bacterial cells | |
| 3.2.3 Medium preparation for animal cell culture | |
| 3.2.4 Animal cell culture | |
| 3.2.5 Cell counting | |
| 3.2.6 Cryopreservation of the animal cells | |
| 3.2.7 Plasmid isolation at mini scale (Miniprep) | |
| 3.2.8 Plasmid isolation in large scale (Midiprep) | |
| 3.2.9 Restriction enzyme Digestion analysis | |
| 3.2.10. Agarose gel electrophoresis | |
| 3.2.11. DNA quantification | |
| 3.2.12. Competent cell preparation | |
| 3.2.13. Transformation | |
| 3.2.14. Confirmation of sequence of synthesized gene constructs by gene sequencing | |
| 3.2.15. Expression analysis of WTrPFO and its mutants | |
| 3.2.16. Analysis of localization of expression of the recombinant protein | |
| 3.2.17. Optimization of expression of the recombinant protein | |
| 3.2.18. Purification of the recombinant proteins (WTrPFO and rPFOC-ter) from the soluble fraction | |
| 3.2.19. Purification of recombinant proteins (rPFOV208C, rPFOA212C, and rPFOR467A) from inclusion bodies | |
| 3.2.20. Protein concentration estimation | |

| | |
|--|----------------|
| 3.2.21. Sodium dodecyl sulfate-polyacrylamide gel electrophoresis (SDS-PAGE) | |
| 3.2.22. Western blotting /Immunoblotting analysis | |
| 3.2.23. Oligomerization behavior of WTrPFO and its mutants | |
| 3.2.24. Hemolytic assay | |
| 3.2.25. Cytotoxicity activity assay | |
| 3.2.26. Pore formation analysis | |
| 3.2.27. Mice immunization | |
| 3.2.28. Enzyme-linked immunosorbent assay(ELISA) | |
| 3.2.29. Antibody Isotyping | |
| 3.2.30. Lymphocyte proliferation assay | |
| 3.2.31. Cytokine ELISA | |
| 3.2.32. <i>In vitro</i> inhibition of the hemolytic activity of WTrPFO by the antisera | |
| 3.2.33. <i>In vitro</i> neutralization capacity of the antisera towards cytotoxicity of the WTrPFO in phagocytic cells | |
| Chapter 4 Results | 96-137 |
| 4.1 Sequence confirmation of the synthetic gene constructs (pET22.PFO_{wt}, and its mutants) | |
| 4.2 Recombinant expression analysis and purification of WTrPFO its mutants | |
| 4.3 Biological activity of the WTrPFO toxin and its mutants | |
| 4.4 Evaluation of immune response generated against recombinant PFO and its mutants | |
| 4.5 Assessment of neutralization potential of immunization with the WTrPFO and its mutant against the wild type rPFO toxicity | |
| Chapter 5 Discussion | 138-149 |
| Chapter 6 Summary | 150-152 |
| Publications and conference presentation | |
| Appendices | |

Abbreviations

| Abbreviations | Full form |
|-----------------------|------------------------------------|
| % | Percentage |
| × | Times |
| ± | Plus-minus |
| ≤ | Less than or equal to |
| ≥ | Greater than or equal |
| °C | Degree Celsius |
| μg | Microgram/s |
| μl | Microliter/s |
| μM | Micromolar |
| A | Absorbance |
| Å | Armstrong |
| ACH | Amplitudes characteristics |
| AP | Alkaline phosphatase |
| APS | Ammonium persulphate |
| ATP | Adenosine triphosphate |
| BCA | Bicinchoninic acid |
| bp | Base pairs |
| BSA | Bovine serum albumin |
| CaCl ₂ | Calcium chloride |
| CFA | Complete Freund's Adjuvant |
| Cfu | Colony forming unit |
| CH ₃ COOK | Potassium acetate |
| CH ₃ COONa | Sodium acetate |
| cm | Centimeter |
| Con A | Concanavalin A |
| CTLs | Cytotoxic T-lymphocytes |
| Da | Dalton |
| DMEM | Dulbecco's Modified Eagle's Medium |
| DMSO | Dimethyl sulfoxide |
| DNA | Deoxyribonucleic acid |
| DNase | Deoxyribonuclease |
| dNTPs | Deoxynucleotide triphosphates mix |
| dpi | Days post immunization |
| DTT | Dithiothreitol |
| EDTA | Ethylenediaminetetraacetic acid |
| ELISA | Enzyme Linked immunosorbent assay |
| FBS | Fetal bovine serum |
| h | Hour |
| HCl | Hydrochloride acid |
| HRP | Horse radish peroxide |
| IFA | Incomplete Freund's adjuvant |
| IFN-γ | Interferon gamma |

Abbreviations

| | |
|----------------------------------|--|
| IgG | Immunoglobulin G |
| IgG1 | Immunoglobulin G isotype IgG1 |
| IgG2a | Immunoglobulin G isotype IgG2a |
| IgG2b | Immunoglobulin G isotype IgG2b |
| IgM | Immunoglobulin M |
| IgA | Immunoglobulin A |
| IL-4 | Interleukin 4 |
| IPTG | Isopropyl β -D-1-thiogalctopyranoside |
| K ₂ HPO ₄ | Dipotassium phosphate |
| Kb | Kilo basepair |
| kDa | Kilodalton |
| KH ₂ PO ₄ | Monopotassium phosphate |
| L | Liter(s) |
| LB | Luria bertani broth |
| LTB | Subunit B heat labile enterotoxin of E. Coli |
| M | Molar |
| Mg | Milligrams |
| MgCl ₂ | Magnesium chloride |
| Min | Minutes(s) |
| ml | Milliliter(s) |
| mM | Millimoles |
| MQ | milliQ water |
| MTT | 3-(4,5-dimethylthiazol-2-yl)-2,5-diphenyltetrazolium bromide |
| LDH | Lactate dehydrogenase |
| N | Normal |
| NaHPO ₄ | Disodium phosphate |
| NaCl | Sodium chloride |
| NaH ₂ PO ₄ | Monosodium phosphate |
| NaOH | Sodium hydroxide |
| NC | Nitrocellulose membrane |
| NEB | New England biolabs |
| ng | Nanogram |
| Ni ²⁺ -NTA | Nickel nitrilotriacetic acid |
| nm | Nanometer |
| O/N | Overnight |
| OD | Optical density |
| PI | Pre immune sera |
| PAGE | Polyacrylamide gel electrophoresis |
| PBS | Phosphate buffered saline |
| PBST | Phosphate buffered saline with tween-20 |
| PCR | Polymerase chain reaction |
| PEG | Polyethelene glycol |
| pH | $-\log[H^+]$ |

Abbreviations

| | |
|---------------|--|
| PI | Proliferation index |
| pm | Picomoles |
| PNPP | Para-Nitrophenylphosphate |
| PVDF | Polyvinylidene acid |
| RNA | Ribonucleic acid |
| RNase | Ribonuclease |
| rpm | Revolutions per minutes |
| RPMI-1640 | Roswell Park Memorial institute medium |
| RT | Room Temperature |
| S.D. | Standard deviation |
| SDS | Sodium dodecyl sulphate |
| sec | Seconds(s) |
| TAE | Tris-acetate-EDTA buffer |
| TE | Tris-EDTA buffer |
| TEMED | Tetramethylethylenedaimine |
| Th1 | T helper cell subset 1 |
| Th2 | T helper cell subset 2 |
| TNF- α | Tumor necrosis factor alpha |
| U | Unit(s) |
| UV | Ultraviolet |
| V | Volts |
| v/v | Volume/Volume |
| w/v | Weight/volume |
| w/w | Weight/weight |
| XTT | 2,3-Bis-(2-Methoxy-4-Nitro-5-Sulfophenyl)-2H-Tetrazolium-5-Carboxanilide |
| α | Alpha |
| β | Beta |
| γ | Gamma |
| λ | Lambda |

Chapter 1

Introduction

All organisms encounter an unfathomable number of microorganisms present in the environment. Majority of the infectious diseases that the humans and animals suffer from are caused by pathogenic bacteria. The number of bacterial infections is far more than the viral, parasitic and fungal infections altogether. Some of these bacteria are highly infectious and the infected organism die in the absence of curative treatment. *Clostridium* genus comprise many such highly infectious bacteria including *C. perfringens* responsible for gangrene, food poisoning, and enterotoxemia, *C. difficile* responsible for pseudomembranous colitis, *C. tetani*, the causative agent of neurodamaging disease tetanus, *C. botulinum* responsible for botulism, and *Clostridium noyvi* responsible for gas gangrene and infectious necrotic hepatitis infectious, that cause heavy mortality, if not treated timely^{1, 2}.

Clostridium perfringens is one of the Gram-positive, rod-shaped pathogenic anaerobe of the genus *Clostridium* belonging to the Bacillaceae family³. The bacterium is also characterized by rapid proliferation and heat resistant spore formation⁴. *C. perfringens* is widely distributed in the environment including soils, food, sewage, aquatic ecosystem (marine, estuarine, and freshwater), and also colonizes in the gastrointestinal tract of various animals and humans^{5, 6, 7}. Its ubiquitous presence in the environment is responsible for causing a number

¹Brüggemann, H. Genomics of clostridial pathogens: implication of extrachromosomal elements in pathogenicity. *Current opinion in microbiology*. **8(5)**, 601-605 (2005).

²Cohen, J.E., Wang, R., Shen, R.F., Wu, W.W., and Keller, J.E. Comparative pathogenomics of *Clostridium tetani*. *PloS one*. **12(8)**, e0182909 (2017).

³Lebrun, M., Mainil, J. G. and Linden, A. Cattle enterotoxaemia and *Clostridium perfringens*: Description, diagnosis and prophylaxis. *Veterinary Record*. **167**, 13–22 (2010).

⁴Labbe, R. G. and Juneja, V. K. *Clostridium perfringens*. *Foodborne Diseases: Third Edition*. **32**, 235-24 (2017).

⁵Hughes, K.A. and Thompson, A. Distribution of sewage pollution around a maritime Antarctic research station indicated by faecal coliforms, *Clostridium perfringens* and faecal sterol markers. *Environmental Pollution*. **127(3)**, 315-321 (2004)

⁶Miller, W.A., Miller, M.A., Gardner, I.A., Atwill, E.R., Byrne, B.A., Jang, S., Harris, M., Ames, J., Jessup, D., Paradies, D. and Worcester, K. *Salmonella spp.*, *Vibrio spp.*, *Clostridium perfringens*, and *Plesiomonas shigelloides* in marine and freshwater invertebrates from coastal California ecosystems. *Microbial ecology*. **52(2)**, 198-206 (2006).

⁷Athira, C.K., Milton, A.A.P., Reddy, A., Rajendrakumar, A.M., Verma, M.R., Kumar, A., Nagaleekar, V.K. and Agarwal, R.K. Diversity of toxin-genotypes among *Clostridium perfringens* isolated from healthy and diarrheic neonatal cattle and buffalo calves. *Anaerobe*. **49**, 99-102 (2018).

of histotoxic and enteric diseases⁸. Different strains of this bacterium secrete a broad range of toxins including extracellular toxins, enzymes (hydrolases, phosphatases, etc.), and an enterotoxin, which are the causative agents for several pathogenic conditions in humans and animals^{8,9}. Further, *C. perfringens* infections also cause fatal disease in livestock including goat, sheep, chicken, etc. after infection, resulting in heavy economic losses to animal husbandry industry^{10,11,12}. It is established that the toxins secreted by *C. perfringens* are responsible for causing different diseases. Based on the secretion of a particular combination of typing toxins (α , β , ϵ , ι , CPE and NetB), the bacterium has recently been classified into seven toxinotypes A-G. Each toxinotype (Type A-G) is responsible for a variety of diseases in humans and animals^{13,14}. Besides these typing toxins, all these seven strains of *C. perfringens* also secrete β 2-toxin, and PFO (Perfringolysin O; earlier referred to as θ toxin) that are potentially virulent toxins and play a very important role in the pathogenicity of *C. perfringens*. Of the various toxins produced by different strains of *C. perfringens*, the α -toxin, PFO and β 2 toxins are produced by all the seven toxinotypes and have been associated with various human and animal diseases¹⁵. The α -toxin, θ -toxin, collagenase, μ -hyaluronidase, and neuraminidases are encoded by the virulent genes located in chromosome, β 1-toxin, β 2-toxin, ϵ -

⁸Uzal, F. A., Freedman, J. C., Shrestha, A., Theoret, J. R., Garcia, J., Awad, M. M. and McClane, B. A. Towards an understanding of the role of *Clostridium perfringens* toxins in human and animal disease. *Future Microbiology*. **9**(3), 361–377 (2014).

⁹Revitt-Mills, S.A., Rood, J.I. and Adams, V. *Clostridium perfringens* extracellular toxins and enzymes: 20 and counting. *Microbiology Australia*. **36**(3), 114-117 (2015).

¹⁰Uzal, F. A. and Songrer, J. G. Diagnosis of *Clostridium perfringens* intestinal infections in sheep and goats. *Journal of Veterinary Diagnostic Investigation*. **20**, 253–265 (2008).

¹¹Van Immerseel, F., Rood, J.I., Moore, R.J. and Titball, R.W. Rethinking our understanding of the pathogenesis of necrotic enteritis in chickens. *Trends in microbiology*. **17**(1), 32-36 (2009).

¹² Skinner, J.T., Bauer, S., Young, V., Pauling, G. and Wilson, J. An economic analysis of the impact of subclinical (mild) necrotic enteritis in broiler chickens. *Avian diseases*. **54**(4), 1237-1240 (2010).

¹³Rood, J.I., Adams, V., Lacey, J., Lyras, D., McClane, B.A., Melville, S.B., Moore, R.J., Popoff, M.R., Sarker, M.R., Songer, J.G. and Uzal, F.A. Expansion of the *Clostridium perfringens* toxin-based typing scheme. *Anaerobe*. **53**, 5-10 (2018).

¹⁴Uzal, F.A., Navarro, M.A., Li, J., Freedman, J.C., Shrestha, A. and McClane, B.A. Comparative pathogenesis of enteric clostridial infections in humans and animals. *Anaerobe*. **53**, 11-20 (2018).

¹⁵Kiu, R. and Hall, L.J. An update on the human and animal enteric pathogen *Clostridium perfringens*. *Emerging microbes & infections*. **7**(1), 1-15 (2018)

toxin, ι -toxin, and l-protease are encoded by plasmid or extrachromosomal genes^{16, 17}. The presence of virulent genes in the mobile plasmid is believed to be the source of biodiversity in *C. perfringens* strains¹⁸.

Besides the main toxins namely alpha, beta, epsilon, iota and enterotoxin, the pore forming toxin perfringolysin O (PFO), secreted by all the *C. perfringens* types, has also been implicated in the onset and progression of some *Clostridial* diseases¹⁵.

Though the α -toxin and PFO are secreted by all the seven *C. perfringens* strains, they are secreted in large amounts by Type A¹⁵. After the *C. perfringens* encounters an open soft tissue, the α -toxin, a primary toxin, and the PFO a secondary toxin are secreted which destroy the tissues and help in the persistence of infection, resulting in gas gangrene (myonecrosis)^{19, 20}. In small ruminants, *C. perfringens* type A causes bovine enterotoxaemia, also known as necrohemorrhagic enteritis, characterized by sudden death without any clinical symptoms^{21, 22, 23}. The infected animals suffer from 100 % mortality, which makes enterotoxaemia caused by *C. perfringens* A an economically important disease.

¹⁶Katayama, S., Dupuy, B., Cole, S.T., Daube, G. and China, B. Genome mapping of *Clostridium perfringens* strains with I-CeuI shows many virulence genes to be plasmid-borne. *Molecular and General Genetics*. **251(6)**, 720-726 (1996)

¹⁷Popoff, M.R. and Bouvet, P. Genetic characteristics of toxigenic Clostridia and toxin gene evolution. *Toxicon*. **75**, 63-89 (2013).

¹⁸Petit, L., Gibert, M. and Popoff, M. R. *Clostridium perfringens*: Toxinotype and genotype. *Trends in Microbiology*. **7**, 104–110 (1999).

¹⁹Titball, R.W. Gas gangrene: an open and closed case. *Microbiology*. **151(9)**, 2821-2828 (2005).

²⁰Awad, M.M., Ellemor, D.M., Boyd, R.L., Emmins, J.J. and Rood, J.I. Synergistic effects of alpha-toxin and perfringolysin O in *Clostridium perfringens*-mediated gas gangrene. *Infection and Immunity*. **69(12)**, 7904-7910 (2001).

²¹Verherstraeten, S., Goossens, E., Valgaeren, B., Pardon, B., Timbermont, L., Vermeulen, K., Schauvliege, S., Haesebrouck, F., Ducatelle, R., Deprez, P. and Van Immerseel, F. The synergistic necrohemorrhagic action of *Clostridium perfringens* perfringolysin and alpha toxin in the bovine intestine and against bovine endothelial cells. *Veterinary research*. **44(1)**, 1-8 (2013).

²²Lebrun, M., Mainil, J. and Linden, A. Cattle enterotoxaemia and *Clostridium perfringens*: description, diagnosis and prophylaxis. *Veterinary Record: Journal of the British Veterinary Association*. **167**, 13-22. (2010).

²³Valgaeren, B.R., Pardon, B., Verherstraeten, S., Goossens, E., Timbermont, L., Haesebrouck, F., Ducatelle, R., Deprez, P.R. and Van Immerseel, F. Intestinal clostridial counts have no diagnostic value in the diagnosis of enterotoxaemia in veal calves. *Veterinary Record*, **172(9)**, 237-237 (2013).

To control the infection, several approaches, such as removal of the infected limb or all infected dead tissues and administration of antibiotics especially penicillin and clindamycin at the same time along with providing hypobaric oxygen at the infected area are adopted to prevent the growth of the anaerobe, and improve the healing potential of the adjacent healthy tissues in gas gangrene²⁴. However, extensive and rapid destruction of infected tissue, shock leads to death of organism suffering from gas gangrene. In calves, the animals die very quickly after exposure to *C. perfringens* without any apparent premonitory clinical signs of necrohemorrhagic enteritis. This demands a safe and efficient preventive measures such as vaccination as the curative treatment for *Clostridial* infections^{18, 25}. Since the onset of *C. perfringens*-associated disease is linked to the production of one or more causative toxins, producing antibodies directed against these toxins could be more promising for disease control. However, since the native toxins are often highly toxic, denatured toxoids have been evaluated against different *C. perfringens* toxins. Several recent studies demonstrated that active immunization with crude toxoid preparations was protective in experimental infections^{26, 27, 28}. Denatured toxoid based vaccine has also been reported to be effective in confirming protection in important livestock against the ϵ -toxin produced by *C. perfringens* type D^{29, 30}.

²⁴Stephens, L.M.B., Gas gangrene: potential for hyperbaric oxygen therapy. *Postgraduate medicine*. **99**, 217-224(1996).

²⁵Muylaert, A., Lebrun, M., Duprez, J.N., Labrozzi, S., Theys, H., Taminiau, B. and Mainil, J. Enterotoxaemia-like syndrome and *Clostridium perfringens* in veal calves. *Veterinary Record*. **167**, 64–65 (2010).

²⁶Stevens, D.L., Titball, R.W., Jepson, M., Bayer, C.R., Hayes-Schroer, S.M. and Bryant, A.E. Immunization with the C-Domain of α -Toxin Prevents Lethal Infection, Localizes Tissue Injury, and Promotes Host Response to Challenge with *Clostridium perfringens*. *Journal of Infectious Diseases*. **190**, 767–773 (2004).

²⁷Nagahama, M., Ochi, S., Oda, M., Miyamoto, K., Takehara, M. and Kobayashi, K. Recent Insights into *Clostridium perfringens* Beta-Toxin. *Toxins (Basel)*. **7**, 396–406 (2015).

²⁸US8980283B2 - *C. perfringens* alpha toxoid vaccine Google Patents <https://patents.google.com/patent/US8980283B2/en>.

²⁹Chandran, D., Naidu, S.S., Sugumar, P., Rani, G.S., Vijayan, S.P., Mathur, D., Garg, L.C. Development of a recombinant epsilon toxoid vaccine against enterotoxemia and its use as a combination vaccine with live attenuated sheep pox virus against enterotoxemia and sheep pox. *Clinical and Vaccine Immunology*. **17**, 1013–1016 (2010).

³⁰Lobato, F.C., Lima, C.G., Assis, R.A., Pires, P.S., Silva, R.O., Salvarani, F.M., Carmo, A.O., Contigli, C. and Kalapothakis, E. Potency against enterotoxemia of a recombinant *Clostridium perfringens* type D epsilon toxoid in ruminants. *Vaccine*. **28**, 6125–6127 (2010).

Likewise, immunization with the alpha toxoid has been found to confer protection in mice model of gas gangrene^{31,32}. However, variability in efficacy of toxoids and possible contamination of other toxoids made interpretations of the results difficult. Also, immune response and protective efficacy of the formaldehyde denatured toxoid was significantly less in comparison to the native toxins in the intestinal loop model for bovine necrohemorrhagic enteritis³³. There are few reports on strain-specific recombinant polyvalent, multi-toxin fusion and subunit vaccines against the *C. perfringens* infections^{34, 35}.

In relation to *C. perfringens* type A infection, it has been found that the serum of calves infected with the bacterium had abundant antibodies against both α -toxin and PFO in the serum of calves³³. These studies suggest potential of these two proteins as vaccine candidates. Although the use of native toxins is an efficient strategy for vaccine development, the active toxins cannot be regarded as safe and efficient vaccines owing to their very high toxicity. Therefore, genetically modified inactivated toxins (generated by site-directed mutagenesis of residues critical for toxicity) or non-toxic fragments of the essential toxins offer safe and better choice as vaccine candidates. Towards the development of such recombinant vaccines against *C. perfringens* type A, the studies have been

³¹Boyd, N.A., Thomson, R.O. and Walker, P.D. The prevention of experimental *Clostridium novyi* and *C. perfringens* gas gangrene in high-velocity missile wounds by active immunisation. *Journal of medical microbiology*. **5**, 467-472(1972).

³²Evans, D.G. The In-Vitro Production of α Toxin, θ Haemolysin and Hyaluronidase by Strains of *C. welchii* Type A, and the relationship of In-Vitro Properties to Virulence for Guinea-Pigs. *Journal of Pathology and Bacteriology*. **57**, 75-85 (1945).

³³Goossens, E., Verherstraeten, S., Valgaeren, B.R., Pardon, B., Timbermont, L., Schauvliege, S., Rodrigo-Mocholí, D., Haesebrouck, F., Ducatelle, R., Deprez, P.R. and Van Immerseel, F. Toxin-neutralizing antibodies protect against *Clostridium perfringens*-induced necrosis in an intestinal loop model for bovine necrohemorrhagic enteritis. *BMC veterinary research*. **12**, 1-8 (2016).

³⁴Song, X., Sun, Y., Liu, Y., Zhang, C., Yang, L. and Wang, C. Expression and Purification of Multi-toxin Fusion Protein of *Clostridium perfringens* and the Preparation of Genetically Engineered Multivalent Subunit Vaccine. *Applied Biochemistry and Microbiology*. **55**, 231-236 (2019).

³⁵Katalani, C., Nematzadeh, G., Ahmadian, G., Amani, J., Kiani, G. and Ehsani, P. In silico design and in vitro analysis of a recombinant trivalent fusion protein candidate vaccine targeting virulence factor of *Clostridium perfringens*. *International journal of biological macromolecules*. **146**, 1015-1023 (2020).

conducted only with α -toxin and its C-terminal fragment^{26, 36, 37, 38}. The PFO has remained as “the Underrated *C. perfringens* toxin” with not many studies on its various aspects and its potential as vaccine, though it contributes significantly to disease progression and has an established role in pathogenicity of the bacterium.

PFO, a pore-forming cytolysin of *C. perfringens* belongs to the largest family of bacterial β Pore-forming toxins (β -PFTs), chiefly secreted by Gram-positive bacteria³⁹. It is also known as cholesterol-dependent cytolysin (CDC)⁴⁰. Few Gram-negative bacteria such as *Desulfobulbus propionicus*, and *Enterobacter lignolyticus* have also been reported to secrete CDC⁴¹. The cholesterol, a common component of mammalian cells is mandatory in a significant amount for binding and assembly of CDCs or PFO in the membrane for pore formation and cytolysis⁴². The PFO is encoded by a virulent *pfo* or *pfoA* gene located on the chromosome of more than 90% of *C. perfringens* strains. Its expression is regulated by the VirS/VirR two-component regulatory system and agr system

³⁶Titball, R.W., Williamson, E.D., Havard, H.L., Oyston, P.C. and Payne, D.W. UK Secretary of State for Defence. *Clostridium perfringens*. vaccines. U.S. Patent 6,403,094 (2002).

³⁷Stevens, D.L., Titball, R.W., Jepson, M., Bayer, C.R., Hayes-Schroer, S.M. and Bryant, A.E., Immunization with the C-domain of α -toxin prevents lethal infection, localizes tissue injury, and promotes host response to challenge with *Clostridium perfringens*. *Journal of Infectious Diseases*. **190**, 767-773 (2004)

³⁸Forti, K., Cagiola, M., Pellegrini, M., Anzalone, L., Di Paolo, A., Corneli, S., Severi, G. and De Giuseppe, A. Generation of recombinant baculovirus expressing atoxic C-terminal CPA toxin of *Clostridium perfringens* and production of specific antibodies. *BMC biotechnology*. **20**, 1-8 (2020)

³⁹Heuck, A.P., Moe, P.C. and Johnson, B.B. The cholesterol-dependent cytolysin family of gram-positive bacterial toxins. In Cholesterol Binding and Cholesterol Transport Proteins. *Springer, Dordrecht*. **51**, 551-577 (2010).

⁴⁰Tweten, Rodney K. Cholesterol-dependent cytolysins, a family of versatile pore-forming toxins. *Infection and immunity*. **73**, 6199-6209(2005).

⁴¹Hotze, E.M., Le, H.M., Sieber, J.R., Bruxvoort, C., McInerney, M.J. and Tweten, R.K. Identification and characterization of the first cholesterol-dependent cytolysins from Gram-negative bacteria. *Infection and immunity*. **81**, 216-225 (2013).

⁴²Morton, C. J., Sani, M. A., Parker, M. W. & Separovic, F. Cholesterol-Dependent Cytolysins: Membrane and Protein Structural Requirements for Pore Formation. *Chemical Reviews*. **119**, 7721–7736 (2019).

(accessory gene regulator system)^{43, 44, 45}. Although PFO is encoded by all the strains *C. perfringens*, its role in virulence in synergy with the α -toxin in gas gangrene and necrohemorrhagic enteritis is clearly established^{20, 21, 46}. In addition, it has also been reported to augment the virulence of ϵ -toxin in mouse model of type D enteroxaemia⁴⁷. The PFO has been reported as the second-most immunogenic toxin of *C. perfringens* after the alpha-toxin which highlights the importance of PFO as a strong candidate for vaccine development against *C. perfringens*³³. Thus, PFO could be a progressive and emerging candidate for generating immune responses and can be a supportive candidate along with the other toxins in vaccine development against all types of *C. perfringens*, as it is secreted by all the 7 types. Recently a Non-toxic PFO derivative, PFO^{L491D}, has been reported to significantly neutralize the cytotoxic effect of *C. perfringens* type A in bovine endothelial. The neutralization was found to be augmented with combination of the anti-PFO^{L491D} antisera and anti- α -toxin derivative GST-cpa247-370 antisera⁴⁸.

The present study therefore was undertaken to assess the vaccine potential of the recombinant PFO of *C. perfringens* type A and generate its not-toxic variants. In order to develop non-toxic variants, it is necessary to have an insight into structural-functional relationship of any toxin and to identify the target residues critical for the biological activity of the toxin. Structure and function of PFO

⁴³Rood, J.I. and Lyrstis, M., Regulation of extracellular toxin production in *Clostridium perfringens*. *Trends in microbiology*. **3**,192-196 (1995).

⁴⁴Ohtani, K., Yuan, Y., Hassan, S., Wang, R., Wang, Y. and Shimizu, T., Virulence gene regulation by the agr system in *Clostridium perfringens*. *Journal of bacteriology*. **191**, 3919-3927 (2009).

⁴⁵Vidal, J.E., Chen, J., Li, J. and McClane, B.A. Use of an EZ-Tn5-based random mutagenesis system to identify a novel toxin regulatory locus in *Clostridium perfringens* strain 13. *PLoS One*. **4**, 1-13 (2009).

⁴⁶O'Brien, D.K. and Melville, S.B. Effects of *Clostridium perfringens* alpha-toxin (PLC) and perfringolysin O (PFO) on cytotoxicity to macrophages, on escape from the phagosomes of macrophages, and on persistence of *C. perfringens* in host tissues. *Infection and immunity*. **72**, 5204-5215 (2004).

⁴⁷Fernandez-Miyakawa, M.E., Jost, B.H., Billington, S.J. and Uzal, F.A. Lethal effects of *Clostridium perfringens* epsilon toxin are potentiated by alpha and perfringolysin-O toxins in a mouse model. *Veterinary microbiology*. **127**, 379-385 (2008).

⁴⁸Verherstraeten, S., Goossens, E., Valgaeren, B., Pardon, B., Timbermont, L., Haesebrouck, F., Ducatelle, R., Deprez, P. and Van Immerseel, F. Non-toxic perfringolysin O and α -toxin derivatives as potential vaccine candidates against bovine necrohaemorrhagic enteritis. *The Veterinary Journal*. **217**, 89-94 (2016).

has been worked on and understood to a great extent. The PFO is secreted as a water-soluble, elongated monomer (115 Å×30 Å×55 Å) of a polypeptide of 500 amino acid residues (molecular mass 52,469 Da), of which 27 amino acid residues serve as the signal sequence for the general secretory pathway⁴⁹. Primary structure of the PFO is very conserved and shows 40 %-70 % similarity with the primary structure of other CDCs produced by other bacterial genera such as Alveolysin of *Bacillus alvei*, (71.4%), Hemolysin of *Bacillus cereus* (66.9%) Streptolysin O of *Streptococcus pyogenes* (63.5%), Pneumolysin of *Streptococcus pneumonia* (46.1%); and Listeriolysin of *Listeria monocytogenes* (42.5%)¹⁸. These data suggest that the PFO shares similarity in structure and pore-formation mechanism with other CDCs. PFO was the CDCs whose crystal structure was first determined⁵⁰. Therefore, it has been considered as a model system to study the conformational changes during binding and oligomerization of the CDCs in cholesterol-containing membranes⁵¹. Crystal structure of the PFO monomer revealed that it could be divided into four domains; N-terminal domain or domain 1, domain 2, domain 3, and the C-terminal domain or domain 4, and all the domains are dominated by β -strands⁵⁰. The amino acid residues present in three domains are not in a continuous way including domain 1 (residues 37-53, 90-178, 229-274, 350-373), domain 2 (residues 54-89, 374-390), domain 3 residues 179-228, 275-349). However, in the C-terminal domain or domain 4, the residues are continuous (residues 391-500). The C-terminal domain of PFO and other CDCs is the most conserved region which is very crucial for the recognition and binding of the cholesterol-containing membrane by the

⁴⁹Verherstraeten, S., Goossens, E., Valgaeren, B., Pardon, B., Timbermont, L., Haesebrouck, F., Ducatelle, R., Deprez, P., Wade, K.R., Tweten, R. and Van Immerseel. Perfringolysin O: The Underrated *Clostridium perfringens* Toxin? *Toxins (Basel)*.7, 1702–1721 (2015).

⁵⁰Rosjohn, J., Feil, S. C., McKinstry, W. J., Tweten, R. K. & Parker, M. W. Structure of a cholesterol-binding, thiol-activated cytolysin and a model of its membrane form. *Cell* .89, 685–692 (1997).

⁵¹Dunstone, M.A. and Tweten, R.K. Packing a punch: the mechanism of pore formation by cholesterol dependent cytolysins and membrane attack complex/perforin-like proteins. *Current opinion in structural biology*. 22, 342-349 (2012).

cholesterol recognition motif^{52, 53}. All the domains of PFO participate in the pore formation mechanism in a very coordinated manner, which starts with the recognition and binding of the C-terminal domain (D4 domain) to cholesterol in the membrane⁵¹. Upon binding, the molecule undergoes conformation changes leading to association of D3 domain of each monomer (40-50 monomers) and oligomerization to form the pre-pore complex. Subsequently, two stranded amphipathic β -sheet or trans-membrane complex (TMH1 and TMH2; residues Q191-A213) get inserted and span the membrane to form a β -barrel pore complex of between 300 and 450 Å, depending upon the number of monomers involved in pore formation⁵⁴. Thus, pore formation is a multi-step process and any change or variation in the sequence of any domain could disrupt the binding, oligomerization and subsequently pore formation. Such residues that are critical for any of these steps can therefore be targeted to generate a non-toxic PFO as vaccine alone or in combination with the immunogenic non-toxic mutants of α -toxin or others toxins for combating *C. perfringens* infection.

Several PFO mutants, V208C, A212C, R467A (with reference to GenBank accession no.M36704), and N-terminal deletion variant of PFO, harboring only C-terminal domain of PFO have been shown to have declined pore formation

⁵²Farrand, A.J., LaChapelle, S., Hotze, E.M., Johnson, A.E. and Tweten, R.K. Only two amino acids are essential for cytolytic toxin recognition of cholesterol at the membrane surface. *Proceedings of the National Academy of Sciences*. **107**,4341-4346 (2010).

⁵³Dowd, K.J. and Tweten, R.K. The cholesterol-dependent cytolysin signature motif: a critical element in the allosteric pathway that couples membrane binding to pore assembly. *PLoS pathogens*. **8**, 1002787 (2012).

⁵⁴Tweten, R.K. Cholesterol-dependent cytolysins, a family of versatile pore-forming toxins. *Infection and immunity*. **73**, 6199-6209 (2005).

ability, haemolytic activity, and destabilization of the structure^{55, 56, 57}. The amino acid residue V208 and A212 are present at the trans-membrane helix (TMH) in domain 3 of the PFO molecule that mediates the insertion of the molecule through the membrane in pore formation. The residue R467 is present in the most conserved tryptophan-rich region termed undecapeptide (457-ECTGLAWEWWR-467) in the D4 domain involved in allosteric coupling and insertion of β -barrel in the membrane⁵¹. The mutation, R467A destabilized the structure of the PFO leading to functional disability and pore formation.

Therefore, to begin with we targeted these residues to assess their immunogenic and vaccine potential, together with wild type PFO and C-terminal domain of PFO. Since these mutants are defective in critical steps involved in pore formation, it is hypothesized that these PFO mutants will be safe and effective candidates for vaccine development, as only one residue is mutated and rest of immunodominant epitopes would be retained in the recombinant mutant proteins.

With this background, the present study envisages to evaluate the immunogenic and neutralizing potential of the recombinant C-terminal domain of PFO and considered PFO mutants (rV208C, rA212C, rR467A) in murine model. Defined objectives of the study are:

⁵⁵Shimada, Y., Maruya, M., Iwashita, S. and Ohno-Iwashita, Y. The C-terminal domain of perfringolysin O is an essential cholesterol-binding unit targeting to cholesterol-rich micro domains. *European journal of biochemistry*. **269**, 6195-6203 (2002).

⁵⁶Shepard, Laura A., Alejandro P. Heuck, Brian D. Hamman, Jamie Rossjohn, Michael W. Parker, Kathleen R. Ryan, Arthur E. Johnson, and Rodney K. Tweten. Identification of a membrane-spanning domain of the thiol-activated pore-forming toxin *Clostridium perfringens* perfringolysin O: an α -helical to β -sheet transition identified by fluorescence spectroscopy. *Biochemistry*. **37**, 14563-14574(1998).

⁵⁷Kulma, M., Kacprzyk-Stokowiec, A., Kwiatkowska, K., Traczyk, G., Sobota, A. and Dadlez, M. R468A mutation in perfringolysin O destabilizes toxin structure and induces membrane fusion. *Biochimica et Biophysica Acta (BBA)-Biomembranes*. **1859**, 1075-1088 (2017).

- Identification of mutations that affect the activity of the toxin.
- Recombinant expression analysis and purification of WTrPFO toxin and its mutants.
- Determination of the biological activity of the WTrPFO toxin and its mutants:
- Evaluation of immune response generated against recombinant PFO and its mutants.
- Assessment of neutralization potential of immunization with the PFO and its mutant against the wild type rPFO cytotoxicity

Chapter 2

Review of Literature

It has always been a big challenge to protect humans and animals from the infectious diseases caused by various pathogenic bacteria present in the environment. The ubiquitous presence of bacteria in the background, including soil, water, and other organisms, including animals and plants, presents more difficulties for animals and humans. *Clostridium perfringens* is one of the widely spread pathogenic bacteria present ubiquitously in the environment, including sewage, food, feces, and gut of the animals and humans^{1, 2, 3}. This bacterium's pathogenic behavior is proved by its ability to secrete a wide range of toxins (about 30 toxins), including extracellular toxins, enzymes (hydrolases, phosphatases, etc.), and an enterotoxin^{4,5}. *C. perfringens*, are classified into seven strains; type A (α -toxin), type B (α -, β - and ϵ -toxins), type C (α - and β -toxins), type D (α - and ϵ -toxins), type E (α - and ι -toxins), type F (α -toxin and CPE) and type G (α - and NetB toxins) by typing method based on the production of certain toxins (typing toxins) by each strain linked to the specific syndrome⁶. Some other virulent toxins including enterotoxin, PFO, B, Lux S, elongation factor Tu (EF-Tu), pyruvate: ferredoxin oxidoreductase (PFOR) and A/B toxin are also reported produced by the bacterium^{7, 8}.

¹Hughes, K.A. and Thompson, A. Distribution of sewage pollution around a maritime Antarctic research station indicated by faecal coliforms, *Clostridium perfringens* and faecal sterol markers. *Environmental Pollution*. **127**(3), 315-321 (2004).

²Athira, C.K., Milton, A.A.P., Reddy, A., Rajendrakumar, A.M., Verma, M.R., Kumar, A., Nagaleekar, V.K. and Agarwal, R.K. Diversity of toxin-genotypes among *Clostridium perfringens* isolated from healthy and diarrheic neonatal cattle and buffalo calves. *Anaerobe*. **49**, 99-102 (2018).

³Uzal, F. A., Freedman, J. C., Shrestha, A., Theoret, J. R., Garcia, J., Awad, M. M., McClane, B. A. Towards an understanding of the role of *Clostridium perfringens* toxins in human and animal disease. *Future Microbiology*. **9**(3), 361–377 (2014).

⁴Pawaiya, R.S., Gururaj, K., Gangwar, N.K., Singh, D.D., Kumar, R. and Kumar, A. The Challenges of Diagnosis and Control of Enterotoxaemia Caused by *Clostridium perfringens* in Small Ruminants. *Advances in Microbiology*. **10**(5), 238-273 (2020).

⁵Li, M., Huang, L., Zhu, Y. and Wei, Q. Growth of *Clostridium perfringens* in roasted chicken and braised beef during cooling—One-step dynamic analysis and modeling. *Food Control*. **106**, 106739 (2019).

⁶Rood, J.I., Adams, V., Lacey, J., Lyras, D., McClane, B.A., Melville, S.B., Moore, R.J., Popoff, M.R., Sarker, M.R., Songer, J.G. and Uzal, F.A. Expansion of the *Clostridium perfringens* toxin-based typing scheme. *Anaerobe*. **53**, 5-10 (2018).

⁷Lee, K., Lillehoj, H.S., Li, G., Park, M.S., Jang, S.I., Jeong, W., Jeoung, H.Y., An, D.J. and Lillehoj, E.P. Identification and cloning of two immunogenic *Clostridium perfringens* proteins, elongation factor Tu (EF-Tu) and pyruvate: ferredoxin oxidoreductase (PFO) of *C. perfringens*. *Research in Veterinary Science*. **91**(3), e80-e86 (2011).

⁸Silva, R.O.S., Santos, R.L.R., Pires, P.S., Pereira, L.C., Pereira, S.T., Duarte, M.C., Assis, R.A.D. and Lobato, F.C.F. Detection of A/B toxin and isolation of *Clostridium difficile* and *Clostridium perfringens* from foals. *Equine Veterinary FJournal*. **45**:671-675 (2013)

Although a single strain does not produce all the toxins, only certain toxins are produced by a single strain that might act synergistically for the pathogenesis.⁹ All the strains (type A-G) are pathogenic for the animals, whereas type A, C, and F are also reported pathogenic for humans¹⁰. This bacterium is associated with different types of histotoxic, enteric, and systemic pathogenic conditions in humans and animals, as mentioned in the **figure 1**^{11,12,13,14}. Different types of pathogenic conditions are based on the production or encountering of toxins in different body locations. *C. perfringens* associated enterotoxaemia is found mild in humans but it is very lethal and harmful for farm animals, including goats, sheep, chickens, cattle, etc. Therefore, this bacterium is also associated with heavy economic losses, especially for farming industries.^{11,15, 16} Further, this bacterium was found to be associated with a large number of bovine deaths, about 500,000 annually only in Brazil that causes a considerable loss of approximately US\$350 million¹⁷. Also, It was reported as the second most common bacteria responsible for food-associated infections in the USA, nearly 1,000,000 cases yearly that reflects the high economic burden

⁹Kiu, R.; Hall, L.J. An update on the human and animal enteric pathogen *Clostridium perfringens*. *Emerging microbes & infections*. **7**, 1–15 (2018).

¹⁰Li, J.; Uzal, F.A.; McClane, B.A. *Clostridium perfringens* sialidases: Potential contributors to intestinal pathogenesis and therapeutic targets. *Toxins*. **8**, 341 (2018).

¹¹Uzal, F.A. and Songer, J.G. Diagnosis of *Clostridium perfringens* Intestinal Infections in Sheep and Goats. *Journal of Veterinary Diagnostic Investigation*. **20**, 253-265 (2008).

¹²Heida, F.H., van Zoonen, A.G., Hulscher, J.B., teKieft, B.J., Wessels, R., Kooi, E.M., Bos, A.F., Harmsen, H.J. and de Goffau, M.C. A necrotizing enterocolitis-associated gut microbiota is present in the meconium: results of a prospective study. *Clinical Infectious Diseases*. **62(7)**, 863-870 (2016).

¹³Carney, T., Perry, J. D., Ford, M., Majumdar, S., and Gould, F. K. Evidence for antibiotic induced *Clostridium perfringens* diarrhoea. *Journal of clinical pathology*. **55(3)**, 240 (2002).

¹⁴Dittmar, E., Beyer, P., Fischer, D., Schäfer, V., Schoepe, H., Bauer, K. and Schlösser, R. Necrotizing enterocolitis of the neonate with *Clostridium perfringens*: diagnosis, clinical course, and role of alpha toxin. *European journal of paediatrics*. **167(8)**, 891-895 (2008).

¹⁵Van Immerseel, F., Rood, J.I., Moore, R.J. and Titball, R.W. Rethinking our understanding of the pathogenesis of necrotic enteritis in chickens. *Trends in microbiology*. **17(1)**, 32-36 (2009).

¹⁶Skinner, J.T., Bauer, S., Young, V., Pauling, G. and Wilson, J. An economic analysis of the impact of subclinical (mild) necrotic enteritis in broiler chickens. *Avian diseases*. **54(4)**, 1237-1240 (2010).

¹⁷ Manteca, C.; Daube, G.; Jauniaux, T.; Linden, A.; Pirson, V.; Dettleux, J.; Ginter, A.; Coppe, P. Kaeckenbeeck, A.; Mainil, J. A role for the *Clostridium perfringens* β 2 toxin in bovine enterotoxaemia? *Veterinary microbiology*. **86**, 191–202 (2002).

listed as US\$ 382 million¹⁸. The outbreak of *clostridia* gastroenteritis and food poisoning was also reported in some other countries, including Japan, England, and Wales from 1992 to 2012, the eastern region of Ghana, and very recently in Northern Greece^{19, 20}. Some enterotoxigenic *C. perfringens* strains were also reported in several regions of India^{21, 22}. The incidence rates of enterotoxaemia in different countries worldwide were found to range from 24.13% to 100%.

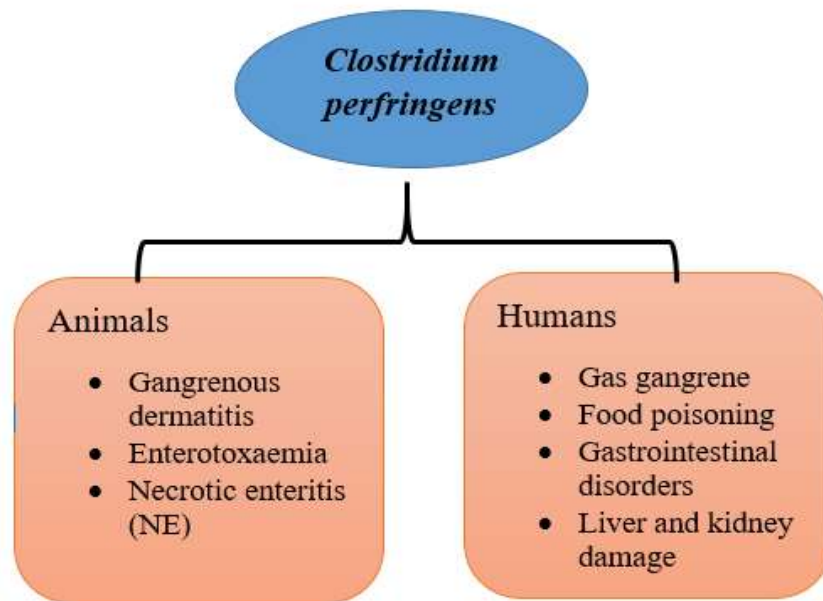


Figure 1. Different types of pathogenic conditions in humans and animals caused by *C. perfringens*.

¹⁸Grass, J. E., Gould, L. H., and Mahon, B. E. Epidemiology of foodborne disease outbreaks caused by *Clostridium perfringens*, United States, 1998-2010. *Foodborne pathogens and disease*. **10(2)**, 131–136 (2013).

¹⁹Hailegebreal, G. A review on *clostridium perfringens* food poisoning. *Global Research Journal of Public Health and Epidemiology*. **4 (3)**, 104-109 (2017).

²⁰Mellou, K., Kyritsi, M., Chrysostomou, A., Sideroglou, T., Georgakopoulou, T., and Hadjichristodoulou, C. *Clostridium perfringens* Foodborne Outbreak during an Athletic Event in Northern Greece, June. *International journal of environmental research and public health*. **16(20)**, 3967 (2019).

²¹Gurmu, E.B., Hazarika, R.A., Borah, P. and Barua, A.G. Presence of enterotoxigenic *Clostridium perfringens* in foods of animal origin, Guwahati, India. *Journal of Environmental and Occupational Health*. **2(1)**, 45-50 (2013).

²²Kumar, N.V., Sreenivasulu, D. and Reddy, Y.N. Prevalence of *Clostridium perfringens* toxin genotypes in enterotoxemia suspected sheep flocks of Andhra Pradesh. *Veterinary World*. **7(12)**, 1132-1136 (2014).

Additionally, about 5-15% of total antibiotic-associated diarrhea cases (AAD) were reported as caused by *C. perfringens*²³. Also, AAD has been reported about 2.6% caused by *C. perfringens* in an Indian hospital²⁴. Type A is the most common type of *C. perfringens* that produces mainly two virulent toxins, CPA (α -toxin) and PFO (θ -toxin). Although almost all the strains express PFO toxin, its pathogenic effect was observed in acting synergistically with α -toxin secreted by type A strains for causing gas gangrene in animals only²⁵. The synergistic effect of PFO and α -toxins were also reported for developing a type of enterotoxaemia called enteric necrohemorrhagic enteritis in calves²⁶. PFO was also reported for enhancing virulence of ϵ -toxin in causing type D enterotoxaemia in a mouse model²⁷. Type A strains are very pathogenic and are proven by their high mortality rates in human adults, around 67% to 100% within 24h after the infection²⁸. Also, Type A is mainly associated with ovine enterotoxaemia (sheep)⁴. Ovine enterotoxaemia was mainly reported in some countries, including India, Italy, United Kingdom, and Turkey^{29,30,31,32}.

²³Carman, R.J. *Clostridium perfringens* in spontaneous and antibiotic-associated diarrhoea of man and other animals. *Reviews in Medical Microbiology*, **8**, S46 (1997).

²⁴Joshy L, Chaudhry R, Dhawan B, Kumar L, Das BK. Incidence and characterization of *Clostridium perfringens* isolated from antibiotic-associated diarrhoeal patients: a prospective study in an Indian hospital. *Journal of Hospital Infection*. **63(3)**, 323-9 (2006).

²⁵Junior, C.A.O., Silva, R.O., Lobato, F.C., Navarro, M.A. and Uzal, F.A. Gas gangrene in mammals: a review. *Journal of Veterinary Diagnostic Investigation*. **32(2)**, 175-183 (2020).

²⁶Verherstraeten, S., Goossens, E., Valgaeren, B., Pardon, B., Timbermont, L., Vermeulen, K., Schauvliege, S., Haesebrouck, F., Ducatelle, R., Deprez, P. and Van Immerseel, F. The synergistic necrohemorrhagic action of *Clostridium perfringens* perfringolysin and alpha toxin in the bovine intestine and against bovine endothelial cells. *Veterinary research*. **44(1)**, 1-8 (2013).

²⁷Fernandez MME, Jost BH, Billington SJ, Uzal FA. Lethal effects of *Clostridium perfringens* epsilon toxin are potentiated by alpha and perfringolysin-O toxins in a mouse model. *Veterinary Microbiology*. **127**, 379-385 (2008).

²⁸Lee, H.L., Cho, S.Y., Lee, D.G., Ko, Y., Hyun, J.I., Kim, B.K., Seo, J.H., Lee, J.W. and Lee, S. A. fatal spontaneous gas gangrene due to *Clostridium perfringens* during neutropenia of allogeneic stem cell transplantation: Case report and literature review. *Infeccion&Chemotherapy*. **46**, 199-203 (2014).

²⁹Miserez, R., Frey, J., Buogo, C., Capaul, S., Tontis, A., Burnens, A. and Nicolet, J. Detection of Alpha- and Epsilon-Toxigenic *Clostridium perfringens* Type D in Sheep and Goats Using a DNA Amplification Technique (PCR). *Letters in Applied Microbiology*. **26**, 382-386 (1998).

³⁰Greco, G., Madio, A., Buonavoglia, D., Totaro, M., Corrente, M., Martella, V. and Buonavoglia, C. *Clostridium perfringens* Toxin-Types in Lambs and Kids Affected with Gastroenteric Pathologies in Italy. *The Veterinary Journal*. **170**, 346-350 (2005).

³¹Radostitis, O.M., Gay, C.C., Hinchcliff, K.H. and Constable, P.D. *Veterinary Medicine*. 10th Edition, Saunders Elsevier, London (2007).

³²Tutuncu, M., Kilicoglu, Y., Guzel, M., Pekmezci, D. and Gulhan, T. Prevalence and Typing of *Clostridium perfringens* Enterotoxins in Small Ruminants of Samsun Province, Northern Turkey. *Journal of Animal & Plant Sciences*. **28**, 1204-1207 (2018).

Furthermore, the incidence of enterotoxaemia in sheep was extensively studied in Iran that represented the incidence rate, 0.14%, and the case fatality rate ranged between 0% to 80%³³. In another study, the incidence of enterotoxaemia in sheep and goats was also reported as 31% and 22%, respectively³⁴.

2.1 *Clostridium perfringens*

C. perfringens is a bacterium of the genus *Clostridium* and *Firmicutes* phylum characterized by a group of spore-forming, rod-shaped, non-motile, oxygen-tolerant anaerobic, and Gram-positive bacteria³⁵. Although *C. perfringens* previously described as *Bacillus aerogenes capsulatus*, *Bacterium welchii*, and *Clostridium welchii*, the species name *welchii* was replaced by *perfringens* in the fifth edition of Bergey's Manual of Determinative Bacteriology^{36,37,38}. William H. Welch first identified it in the infected blood vessels of a 38-year-old man during an autopsy in 1891³⁸. Notably, the gas bubbles formation was reported in *C. perfringens* infected tissues in British and French soldiers during World War I, which was linked with gas gangrene symptoms^{39,40}.

C. perfringens is a fast-growing ubiquitous bacterium present in environments including soil, food, aquatic ecosystem (marine, estuarine, and freshwater). It

³³Tooloei, M. and Masodei, M.H. The Distribution and Prevalence Rate of Enterotoxaemia in Sheep in East Azerbaijan Province, Northwestern Iran in Spring 2008. *Journal of Animal and Veterinary Advances*. **7**, 1434-1439 (2008)

³⁴Maqbool, B., Iqbal, M.K., Ijaz, M., Aslam, M.B., Ahmad, H.I. and Hussain, K. Prevalence and Chemotherapy of Enterotoxemia (*Clostridium perfringens*) in Diarrheic Sheep and Goats. *JIB-Research*, **1**, 30-35 (2017).

³⁵Galperin, M.Y. Genome diversity of spore-forming Firmicutes. *Microbiology spectrum*. **1(2)**, TBS-0015 (2013).

³⁶Lucey, B. P. and Hutthins, G. M. William H. Welch, MD, and the discovery of *Bacillus welchii*. *Archives of Pathology & Laboratory Medicine*. **128**, 1193-1195 (2004).

³⁷Veillon, A. and Zuber, A. Recherches sur quelques microbes strictement anaérobies et leur rôle en pathologie. *Archives de Médecine Expérimentale et d'Anatomie Pathologique*. **10**, 517-545 (1898).

³⁸Welch, W. H. and Nuttall, G. H. F. A gas producing bacillus (*Bacillus aerogenes capsulatus*, Nov Spec) capable of rapid development in the blood vessels after death. *Bulletin of the Johns Hopkins Hospital*. **3**, 81-91 (1892).

³⁹Roberts, E.J., Martucci, J.A. and Wu, D. The Unusual Presence of Gas From a Puncture Wound: A Case Report. *J Foot Ankle Surgery*. **57(4)**, 785-789 (2018).

⁴⁰Brown, P.W. and Kinman, P.B. Gas gangrene in a metropolitan community. *JBJS*. **56(7)**, 1445-1451 (1974).

also resides in the gut of warm-blooded animals and even in healthy humans⁴¹. Generally, the value of *C. perfringens* in healthy adults usually ranges from 103–105 per gram, but an increase in the population of bacteria from 106–108 per gram can outbreak the infection⁴². Since *C. perfringens* was present in the fecal matter, which is one of the components of sewage-polluted water, it is also considered the sewage-pollution marker and a specific parameter for the water quality localities⁴³. Indeed, the presence of *C. perfringens* in seawater and great depth of marine sediments around Rothera Research Station, and the Antarctic Peninsula, is described as a sewage pollution marker⁴⁴.

2.2 Isolation and identification of the *C. perfringens*

Several methods of isolation and identification of *C. perfringens* are described in **tables 1** and **2**, respectively.

| Isolation | |
|----------------------------------|---|
| Methods | Description |
| Direct plating on TSC medium | Culturing of samples on tryptose-sulfite-cycloserine (TSC) medium resulted in black precipitates due to reduction of sulfite to sulfide ¹ . |
| Direct plating in TSC-EYA medium | Directly culturing of samples on tryptose-sulfite-cycloserine with egg yolk agar (TSC-EYA) medium at 37 °C for 24 in anaerobic conditions resulted in black, lecithinase-positive colonies for the confirmation of <i>C. perfringens</i> ¹ . |
| Most Probable Number (MPN) | Streaking of diluted samples on boiled (to expel the oxygen) and cooled before the use of DRCM (Differential Reinforced Clostridial Medium) resulted in blacking of medium after incubation for 24h or 48h at 37°C in air ¹ . |
| Ethanol pre-treatment | Plating of sample pre-treated (50% ethanol) for 30 min on fastidious anaerobe agar resulted in appearing of colonies of <i>C. perfringens</i> exhibited beta-haemolysis ¹ |

Table 1. Methods used for isolation of the *C. perfringens*

⁴¹Songer, J.G. Clostridial Enteric Diseases of Domestic Animals. *Clinical Microbiology Reviews*. **9**, 216-234 (1996).

⁴²McClane, B.A., Robertson, S.L. and Li, J. *Clostridium perfringens*. *Food microbiology: fundamentals and frontiers*. 465-489 (2012).

⁴³Miller-Pierce, M.R. and Rhoads, N.A. *Clostridium perfringens* testing improves the reliability of detecting non-point source sewage contamination in Hawaiian coastal waters compared to using Enterococci alone. *Marine pollution bulletin*. **144**, 36-47 (2019).

⁴⁴Hughes, K.A. and Thompson, A. Distribution of sewage pollution around a maritime Antarctic research station indicated by faecal coliforms, *Clostridium perfringens* and faecal sterol markers. *Environmental Pollution*. **127(3)**, 315-321 (2004).

Table 2. Methods used for identification of the *C. perfringens*

| Identification | |
|-----------------------------|--|
| Method | Description |
| MALDI-TOF Mass Spectrometry | A very quick identification method of bacterial species based upon the protein profiling of whole bacterial cells to analyze the most conserved ribosomal proteins by directly putting on bacterial colonies onto the MALDI-TOF metal target followed by appropriate analysis ⁴⁵ . |
| Nagler's reaction | Based on the identification of α -toxin by incubating sample spread in egg-yolk agar medium containing anti-toxin in one half of the medium at 35-37°C for 24-48 hrs in anaerobic condition. The positive result is defined as a zone of opacity in half of the anti-toxin-free medium and absence of turbidity in anti-toxin containing medium due to neutralization ⁴⁶ . |
| PCR with specific primers | Based on the identification of <i>C. perfringens</i> potentially producing enterotoxin by PCR using primers for the <i>cpe</i> gene. ⁴⁷ |
| Reverse CAMP test | Based on the synergistic hemolysis by α -toxin of <i>C. perfringens</i> and CAMP factor produced by <i>S. agalactiae</i> , both bacteria were streaked perpendicular to each other in sheep blood agar medium. Subsequent anaerobic incubation for 24-48 h at 37°C resulted in appearing of the “bow-tie” zone of increased hemolysis ⁴⁸ . |

⁴⁵Sauer, S., Freiwald, A., Maier, T., Kube, M., Reinhardt, R., Kostrzewa, M. and Geider, K. Classification and identification of bacteria by mass spectrometry and computational analysis. *PLoS one*. **3(7)**, e2843 (2008).

⁴⁶Ezzeldeen, N.A., Ammar, A.M., Shalaby, B., Haririr, M.E. and Omar, W.S. Rapid detection of *Clostridium perfringens* in seafood. *Advances in Environmental Biology*. **10(4)**,174-182 (2016).

⁴⁷Labbe, R. G. and Juneja, V. K. *Clostridium perfringens*. *Foodborne Diseases: Third Edition*. **32**, 235-24 (2017).

⁴⁸Scheven, M. Detection of *Clostridium perfringens* in mixed infection patient samples using a modified reverse CAMP test. *Zeitschrift für die gesamte Hygiene und ihre Grenzgebiete*. **37(2)**, 90 (1991).

2.3 Characteristics of the *C. perfringens*

2.3.1 Oxygen-tolerant

Although *C. perfringens* is a strict anaerobic bacterium, it can survive in the aerobic environment (soil, arterial blood, and surface in hospital wards)⁴⁹. It can also cause pathogenic conditions in the aerobic environment, such as infants' and adults' gut and other conditions like gas-gangrene. Due to aero-tolerant behavior, it can also escape phagocytosis by macrophages in both aerobic and anaerobic conditions⁵⁰. *C. perfringens* seemed to contain a specialized gene system to respond to peroxides for encoding superoxide dismutase (SOD), superoxide reductase, and alkyl hydro-peroxide reductase, but the mechanism is still unknown⁵¹.

2.3.2 Stress-resistant spore-formation

The formation of resistant spores is an essential characteristic of the *C. perfringens* that makes it more vulnerable to the transmission of food-borne (food-poisoning and enteritis necroticans), non-food borne (antibiotic-associated diarrhea and enterotoxaemia), and histotoxic illnesses (*Clostridial* myonecrosis/gas gangrene)⁵². Unfavorable environmental and physiological conditions, including nutrients starvation for the growth and proliferation, are responsible for triggering the spore formation by *C. perfringens*. Inorganic phosphate (Pi) is an essential component for initiating the sporulation process present in the bacterium and humans' gut. The lethal enterotoxin CPE, secreted during sporulation, causes diarrhea and thus mediates dormant spores' spread in the environment.

⁴⁹Machida, Y., Yano, Y., Yano, T., Seshimo, T., Ohtani, H. and Ujiiye, A. An outbreak of enterocolitis due to *Clostridium perfringens* in a hospital for the severely disabled. *KansenshogakuZassh.* **63**, 410–416 (1989).

⁵⁰O'Brien, D.K. and Melville, S.B. The anaerobic pathogen *Clostridium perfringens* can escape the phagosome of macrophages under aerobic conditions. *Cellular microbiology.* **2(6)**, 505-519 (2000).

⁵¹Jean, D., Briolat, V. and Reysset, G. Oxidative stress response in *Clostridium perfringens*. *Microbiology*, **150(6)**, 1649-1659 (2004).

⁵²Stevens, DL.; Rood, JI. Histotoxic Clostridia. In: Fischetti, VA.; Novick, RP.; Ferretti, JJ.; Portnoy, DA.; Rood, JI., editors. Gram-positive pathogens. 2nd. ASM press; Washington, DC, (2006).

Resistant spores help the bacterium to survive in unfavorable conditions and cause disease after exposure to favorable conditions. Food environment stress (extreme temperature, osmotic pressure, chemical preservatives, and pH) related resistant property of the spore is very critical to *C. perfringens* to cause food-borne illness. The spores responsible for food-poisoning are believed to be heat resistant as spores can survive even in boiling temperature for one hour or longer^{53,54}. Spo0A initiates the bacterium's spore formation, a transcriptional factor encoded by *spo0A* and regulated by Sigma factors, including SigF, SigE, SigG, and SigK⁵⁵. The role of some other proteins, transcriptional regulator CcpA (encoded, by *ccpA*) and an Agr-like quorum-sensing system, potentially promoted by the *codY* gene in food poisoning strain type A, were also reported in regulating the spore-formation process^{56,57}.

2.3.3 Spore germination

C. perfringens spores can survive for an extended period in extreme environmental conditions (temperature, osmotic pressure, chemical preservatives, and pH). In the exposure of favorable conditions, spores turned back into live condition and able to grow within 20 min. Spore germination plays a significant role in the *C. perfringens* associated food-borne disease, CPE-associated non-food-borne human GI diseases, and other *C. perfringens* diseases, including clostridial myonecrosis transmission. Spore requires some small molecules to initiate germination called germinates, *i.e.*, sugars,

⁵³ Ma M, Li J., Mc Clane, BA. Genotypic and phenotypic characterization of *Clostridium perfringens* isolates from Darmbrand cases in post-World War II Germany. *Infection and Immunity*. **80**:4354–4363 (2012).

⁵⁴Sarker, MR., Shivers, RP., Sparks, SG., Juneja, VK., McClane, BA. Comparative experiments to examine the effects of heating on vegetative cells and spores of *Clostridium perfringens* isolates carrying plasmid genes versus chromosomal enterotoxin genes. *Applied and Environmental Microbiology*. **66**, 3234–3240 (2000).

⁵⁵Li, J., Paredes-Sabja, D., Sarker, M.R. and McClane, B.A. *Clostridium perfringens* Sporulation and Sporulation-Associated Toxin Production. *The Bacterial Spore: from Molecules to Systems*. 331-347 (2016).

⁵⁶Li, J., Chen, J., Vidal, J. E. and McClane, B. A. The Agr-like quorum-sensing system regulates sporulation and production of enterotoxin and beta2 toxin by *Clostridium perfringens* type A non-food-borne human gastrointestinal disease strain F5603. *Infection and Immunity*. **79**, 2451–2459 (2011).

⁵⁷Li, J., Freedman, J. C., Evans, D. R. and McClane, B. A. CodY promotes sporulation and enterotoxin production by *Clostridium perfringens* type A strain SM101. *Infection and Immunity*. **85**, (2017).

nucleosides, amino acids, salts, purines, primary bile acids (including glycocholate, cholate, and taurocholate). Different germinates were found very specific for different bacterial species and strains that seemed to be adapted for different environmental niches. Indeed, *C. perfringens* food poisoning isolates are adapted to nutrients including KCl, NaPi, L-asparagine, or exogenous 1:1 chelate of Ca²⁺ Ca-DPA-rich food niches that are required for the spore germination. In contrast, non-food-borne GI disease isolates are better adapted to germinate in the host's intestinal epithelium in the presence of L-alanine, L-valine, and with the mixture of KCl and L-asparagine. Further, numerous host-derived components like lysozyme released by Peyer patches in the small intestine are also essential for spore germination. The germinant is recognized by germinant receptor (GRs), including GerKC present in the spore's inner membrane to initiate the germination.

2.3.4 Rapid proliferation

C. perfringens is one of the fastest-growing bacteria. It can generate a two-fold quicker than other intestinal commensals like wild-type *Escherichia coli* (typically 20–30 min in Luria-Bertani broth)⁹. The generation time has been reported 8–12 min at 37 °C while culturing *C. perfringens* at 43 °C in optimal media showed generation time of 12–17 min at 37°C. This bacterium's fast-growing nature makes it more pathogenic and predisposes to infection in avian NE cases, bovine necrohemorrhagic enteritis (could be <5 h), and gas gangrene^{58, 59}.

2.3.5 Host specificity

Different *C. perfringens* toxinotypes are present in the different hosts. Type A is generally present in the environment and the intestine of the animals. Further, gas gangrene causing type A exclusively present in humans. While other toxinotypes, including type C, type D, type E, and type G are found in

⁵⁸Shojadoost, B., Vince, A.R. and Prescott, J.F. The successful experimental induction of necrotic enteritis in chickens by *Clostridium perfringens*: a critical review. *Veterinary research*. **43(1)**, 1-12 (2012).

⁵⁹Uzal, F.A., McClane, B.A., Cheung, J.K., Theoret, J., Garcia, J.P., Moore, R.J. and Rood, J.I. Animal models to study the pathogenesis of human and animal *Clostridium perfringens* infections. *Veterinary microbiology*. **179(1-2)**, .23-33 (2015).

pigs, ruminants (sheep), calves, and poultry⁶⁰. Moreover, the host for type F is not well determined. The bacterium's host specificity is based on the toxin type and its specific colonizing property of the strain in the host. For example, type C can colonize in the intestine villi through capsule polysaccharides⁶¹.

2.3.6 Genetic diversity

The variations in chromosomal and plasmid profile analyzed by the multiple-locus variable-number tandem repeat analysis, multiple-locus (MLVA), and Pulse field gel electrophoresis (PFGE) were reported among the *C. perfringens* strains isolated from the different sources including food and soils, humans, domestic animals from the various geographical areas⁶². In the previous study, genomic analysis of *C. perfringens* revealed its large pangenome that contained only 12.6% core genes and remaining variable gene content that indicated the plasticity or openness nature of *C. perfringens* genome⁶³. Further, the highest open index value of *C. perfringens* estimated in a study also suggested that a large proportion of this bacterial genome is occupied by the accessory genes responsible for the diverse functions⁶⁴. The genome's high openness supports the bacterium's ability to obtain the genes from the surrounding, making it more adaptive to survive in antagonistic survival conditions. Contrary, the genome of other human pathogens, including *Bordetella pertussis* and *Mycobacterium tuberculosis*, was found relatively more conserved and having small genetic changes with the lowest OI (Openness Index) that supported the relation in genetic diversity and genome

⁶⁰Lepp, D., Zhou, Y., Ojha, S., Gohari, I.M., Carere, J., Yang, C., Prescott, J.F. and Gong, J. *Clostridium perfringens* produces an adhesive pilus required for the pathogenesis of necrotic enteritis in poultry. *Journal of Bacteriology*. 00578-20 (2021).

⁶¹Walker, P.D., Murrell, T.G.C. and Nagy, L.K. Scanning electronmicroscopy of the jejunum in enteritis necroticans. *Journal of medical microbiology*. **13(3)**, 445-450 (1980).

⁶²Park, M., Deck, J., Foley, S.L., Nayak, R., Songer, J.G., Seibel, J.R., Khan, S.A., Rooney, A.P., Hecht, D.W. and Rafii, F. Diversity of *Clostridium perfringens* isolates from various sources and prevalence of conjugative plasmids. *Anaerobe*. **38**, 25-35 (2016).

⁶³Kiu, R., Caim, S., Alexander, S., Pachori, P. and Hall, L.J. Probing genomic aspects of the multi-host pathogen *Clostridium perfringens* reveals significant pangenome diversity, and a diverse array of virulence factors. *Frontiers in Microbiology*. **8**, 2485 (2017).

⁶⁴Feng, Y., Fan, X., Zhu, L., Yang, X., Liu, Y., Gao, S., Jin, X., Liu, D., Ding, J., Guo, Y. and Hu, Y. Phylogenetic and genomic analysis reveals high genomic openness and genetic diversity of *Clostridium perfringens*. *Microbial genomics*. **6(10)**, (2020).

openness^{65,66}. The low GC content (~28.0 %) and high proliferation rate (as short as ~7 min) were believed to be the major contributor to the *C. perfringens* genome's openness.

Additionally, the relatively lacking *C. perfringens* in the clustered regularly interspaced short palindromic repeats (CRISPER) system compared to other bacteria in the study also indicated the genetic diversity caused by horizontal gene transfer⁶⁷. The antibiotic resistance gene (ARG) was found to increase with time in the bacterium compared to virulent genes that reflect its ability to acquire the ARG genes from the other bacterium present in the environment, especially from the genera *staphylococcus* and *streptococcus* that have ARGs sufficiently^{68, 69}. The increasing antibiotic resistance steadily relatively compared to virulence nature might also be due to selective antibiotics in both animals and humans. The phages and *C. perfringens* interaction were also reported for causing genetic variation in the bacterium as about 14.1% of gene functions accounted for the total gene functions in the accessory genome of the *C. perfringens*.

2.4 Classification of *C. perfringens*

Firstly, *C. perfringens* isolates were classified based on their ability to produce acid and gas by fermentation of carbohydrate (glycerine and inulin) present in the culturing medium and spore formation^{70, 71}. Afterward, the classification of *C. perfringens* was established into four types (toxintypes A to D) by Wilsdon based on the production of three toxins named W toxin (now known as α -

⁶⁵Wan, X., Koster, K., Qian, L., Desmond, E., Brostrom, R., Hou, S. and Douglas, J.T. Genomic analyses of the ancestral Manila family of *Mycobacterium tuberculosis*. *PLoS One*. **12(4)**, e0175330 (2017).

⁶⁶Mooi, F.R. *Bordetella pertussis* and vaccination: the persistence of a genetically monomorphic pathogen. *Infection, Genetics and Evolution*. **10(1)**, 36-49 (2010).

⁶⁷McAllister, K.N. and Sorg, J.A. CRISPR genome editing systems in the genus *Clostridium*: a timely advancement. *Journal of bacteriology*. **201(16)**, e00219-19 (2019).

⁶⁸Lerminiaux, N.A. and Cameron, A.D. Horizontal transfer of antibiotic resistance genes in clinical environments. *Canadian journal of microbiology*. **65(1)**, 34-44 (2019).

⁶⁹Frieden, T. Antibiotic resistance threats in the United States. *Centers Dis Control Prev*. **114** (2013).

⁷⁰ Simonds, J.P. Classification of the *Bacillus welchii* group of bacteria. *The Journal of Infectious Diseases*. **16**, 31-4, (1915).

⁷¹Bergey, D.H. *Bergey's manual of determinative bacteriology*. Second ed. London: Bailliere, Tindall & Cox; (1926).

toxin), X toxin (ϵ -toxin), and Z toxin (β -toxin), and Bull and Pritchard demonstrated that⁷². This toxin-based classification of *C. perfringens* by Wilsdon was performed by toxin-antitoxin neutralization tests using antisera produced against culture supernatants. A different strain termed type E was successfully isolated from a calf in 1943, characterized by producing α -toxin and another toxin named ι -toxin⁷³. Recently, the toxin typing scheme was expanded by classifying the strains into seven toxinotypes A to G based on the secretion of a particular combination of typing toxins (α , β , ϵ , ι , CPE and NetB) by each strain (**Table 3**)^{6, 74}. Further, several other toxins secreted from the strains categorized as non-typing toxins (PFO, β 2-toxins, and λ -toxin) are potentially virulent and play a vital role in the pathogenesis along with other typing toxins⁹. Notably, the α -toxin, PFO, and β 2 toxins are believed to produce all the seven toxinotypes associated with various human and animal diseases⁹. The toxins encoding genes produced by each toxinotypes A to F were identified by Multiplex PCR method using PCR primer specific for the α -toxin (*plc* or *cpa*), β -toxin (*cpb*), ϵ -toxin (*etx*), ι -toxin (*iap*), CPE (*cpe*), and NetB (*netB*) genes.

2.5 Genomic and plasmid insight of *C. perfringens*.

2.5.1 Genome

Gas gangrene-associated *C. perfringens* (strain 13) was the first-ever sequenced Gram-positive anaerobic pathogen (published in early 2002). That highlighted the virulent genes encoding different toxins and enzymes, anaerobic fermentation pathways, and the absence of amino acid synthesis

⁷²Glenny, A.T., Barr, M., Llewellyn-Jones, M., Dalling, T. and Ross, H.E. Multiple toxins produced by some organisms of the *Cl. welchii* group. *Journal of Pathology and Bacteriology*. **37**, 53-74 (1933).

⁷³ Bosworth, T.J. On a new type of toxin produced by *Clostridium welchii*. *Journal of Comparative Pathology and Therapeutics*. **53**, 245-552 (1943).

⁷⁴Uzal, F.A., Navarro, M.A., Li, J., Freedman, J.C., Shrestha, A. and McClane, B.A. Comparative pathogenesis of enteric clostridial infections in humans and animals. *Anaerobe*. **53**, 11-20 (2018).

Table 3. Classification of the *Clostridium perfringens*

| Toxinotype | Typing toxins | | | | | | Non-typing toxins | | |
|------------|------------------------|-----------------------|--------------------------|-------------------------------------|-------------------|---------------------|--------------------------|-------------------------|------------------------|
| | α <i>cpa</i> | β <i>cpb</i> | ϵ <i>ctx</i> | ι <i>iap</i> <i>ibp</i> | CPE <i>cpe</i> | NetB <i>netB</i> | $\beta 2$ <i>cpb2</i> | λ <i>lam</i> | Θ <i>pfo</i> |
| A | + | | | | | | + | | + |
| B | + | + | + | | | | + | + | + |
| C | + | + | | | + | | + | | + |
| D | + | | + | | + | | + | + | + |
| E | + | | | + | + | | + | + | + |
| F | + | | | | + | | + | | + |
| G | + | | | | | + | + | | + |

+ Production of toxin; **+** Potential production of toxin

pathways⁷⁵. The genome size of *C. perfringens* ranges from 3.0–4.1 Mb with low GC content of about 27–28%, and the genes estimated in each *C. perfringens* are 2500–3600⁷⁶. Genes encoding virulent toxins including CPA [α -toxin (phospholipase C)] hyaluronidase (μ -toxin), collagenase (κ -toxin), PFO (θ -toxin) are located in the variable arm of the chromosome, whereas, *nan H* and *nan I* genes encoding neuraminidases are located in the conserved region of the chromosome⁷⁷.

⁷⁵Shimizu, T., Ohtani, K., Hirakawa, H., Ohshima, K., Yamashita, A., Shiba, T., Ogasawara, N., Hattori, M., Kuhara, S. and Hayashi, H. Complete genome sequence of *Clostridium perfringens*, an anaerobic flesh-eater. *Proceedings of the National Academy of Sciences*. **99(2)**, 996-1001 (2002).

⁷⁶Fourie, J.C.J., Bezuidenhout, C.C., Sanko, T.J., Mienie, C. and Adeleke, R. Inside environmental *Clostridium perfringens* genomes: antibiotic resistance genes, virulence factors and genomic features. *Journal of Water and Health*. **18(4)**, 477-493 (2020).

⁷⁷Lacey, J.A., Allnutt, T.R., Vezina, B., Van, T.T.H., Stent, T., Han, X., Rood, J.I., Wade, B., Keyburn, A.L., Seemann, T. and Chen, H. Whole genome analysis reveals the diversity and evolutionary relationships between necrotic enteritis-causing strains of *Clostridium perfringens*. *Bmc Genomics*. **19(1)**, 1-22 (2018).

2.5.2 Plasmid

The virulence nature of *C. perfringens* is highly associated with the presence of plasmids. Approximately 16 virulent toxins, including CPE, ϵ -toxin, ι -toxin, NetB, β 2-toxin, and binary enterotoxin encoding and antimicrobials genes present in the large plasmids⁷⁸. Moreover, about three different toxin plasmids (size ranges from ~45kb to ~140kb), encoding different toxins, can be present in each *C. perfringens* strains⁷⁸. Sequences containing locus named *tcp*(transfer of clostridial plasmids) are responsible for horizontal gene transfer⁷⁹. The universal presence of *tcp* locus indicates conjugative plasmid transfer could be a key HGT event for increased virulence of *C. perfringens* strains.

2.6 Characterization of toxins produced by *C. perfringens*

C. perfringens secretes more than 20 toxins and different types of enzymes that act in the host in different ways to proceed with the pathogenesis⁸⁰. Further, these toxins and enzymes could be encoded by either chromosomal or plasmid genes. Some of the major toxins are described as follows:

2.6.1 Chromosomally encoded toxins

Essential toxins of the *C. perfringens* type A, PLC, and PFO are reported to be encoded by chromosome⁸¹. Some other toxins and enzymes include kappa-toxin, collagenase, mu-toxin, hyaluronidase, clostripain, cysteine protease, and sialidases, were also reported to be encoded by chromosome^{82,83}. Alpha-toxin

⁷⁸Li, J., Adams, V., Bannam, T.L., Miyamoto, K., Garcia, J.P., Uzal, F.A., Rood, J.I. and McClane, B.A. Toxin plasmids of *Clostridium perfringens*. *Microbiology and Molecular Biology Reviews*. **77(2)**, 208-233 (2013).

⁷⁹Freedman, J.C., Theoret, J.R., Wisniewski, J.A., Uzal, F.A., Rood, J.I. and McClane, B.A. *Clostridium perfringens* type A–E toxin plasmids. *Research in microbiology*. **166(4)**, 264-279 (2015).

⁸⁰Revitt-Mills, S.A., Rood, J.I. and Adams, V. *Clostridium perfringens* extracellular toxins and enzymes: 20 and counting. *Microbiology Australia*. **36(3)**, 114-117 (2015)

⁸¹Canard, B., Saint-Joanis, B. and Cole, S.T. Genomic diversity and organization of virulence genes in the pathogenic anaerobe *Clostridium perfringens*. *Molecular microbiology*. **6(11)**, 1421-1429 (1992).

⁸²Katayama, S.I., Dupuy, B., Garnier, T. and Cole, S.T. Rapid expansion of the physical and genetic map of the chromosome of *Clostridium perfringens* CPN50. *Journal of bacteriology*. **177(19)**, 5680-5685 (1995).

(PLC), a zinc metallophospholipase C, is secreted by all the *C. perfringens* strains⁹. This toxin is characterized by phospholipase C (PLC) and sphingomyelinase activity, thereby hydrolyzing the cell membrane phospholipids leading to cell lysis and tissue necrosis⁸⁴. This toxin is a main virulent toxin for causing the gas gangrene and other enterotoxemia by type A strains^{25,6}. In myonecrosis or gas gangrene, it plays three important roles 1) facilitates infection by reducing blood supply, 2) transfer of immune cells (neutrophils) to the infected tissues, and also 3) activates the inflammation cascade in the host cell metabolism.^{85,86,87}. Another chromosomally encoded toxin is perfringolysin O (PFO) which was reported to be encoded by almost all the strains of *C. perfringens* (more than 90%). PFO is a type of cholesterol-dependent cytolysin (CDCs) that facilitates pore formation and disruption⁸⁸. Although PFO is not a primary toxin for causing disease, it works synergistically with α -toxin and causes gas gangrene and bovine necrohemorrhagic enteritis by type A strains^{84,89}. The virulent function of both toxins was found organ-dependent as it acts differently in myonecrosis and enterotoxemia that are characterized by different symptoms. Indeed, myonecrosis is characterized by tissue necrosis, thrombosis, and lack of leukocyte infiltration at the infection site, while different symptoms, including

⁸³Li J, Sayeed S, Robertson S, Chen J, McClane BA. Sialidases affect the host cell adherence and epsilon toxin-induced cytotoxicity of *Clostridium perfringens* typed strain CN3718. *PLoS Pathog.* 7, e1002429 (2011).

⁸⁴Sakurai, J., Nagahama, M. and Oda, M. *Clostridium perfringens* alpha-toxin: characterization and mode of action. *Journal of biochemistry.* **136(5)**, 569-574 (2004).

⁸⁵Flores-Díaz, M. and Alape-Girón, A. Role of *Clostridium perfringens* phospholipase C in the pathogenesis of gas gangrene. *Toxicon.* **42(8)**, 979-986 (2003).

⁸⁶Navarro, M.A., McClane, B.A. and Uzal, F.A. Mechanisms of action and cell death associated with *Clostridium perfringens* toxins. *Toxins.* **10(5)**, 212 (2018).

⁸⁷Goossens, E., Valgaeren, B.R., Pardon, B., Haesebrouck, F., Ducatelle, R., Deprez, P.R. and Van Immerseel, F. Rethinking the role of alpha toxin in *Clostridium perfringens*-associated enteric diseases: a review on bovine necro-haemorrhagic enteritis. *Veterinary research.* **48(1)**, 1-17 (2017).

⁸⁸Christie, M.P., Johnstone, B.A., Tweten, R.K., Parker, M.W. and Morton, C.J. Cholesterol-dependent cytolysins: from water-soluble state to membrane pore. *Biophysical reviews.* **10(5)**, 1337-1348 (2018).

⁸⁹Awad, M.M., Ellemor, D.M., Boyd, R.L., Emmins, J.J. and Rood, J.I. Synergistic effects of alpha-toxin and perfringolysin O in *Clostridium perfringens*-mediated gas gangrene. *Infection and Immunity.* **69(12)**, 7904-7910 (2001).

congestion of the capillaries, hemorrhages, and inflammation, appeared in bovine necrohemorrhagic enteritis^{84,90}.

2.6.2 Plasmid encoded toxins

Plasmid encoded toxins include beta-toxin (CPB), beta2-toxin (CPB2), epsilon toxin (ETX), Iota toxin (ITX), NetB toxin, delta toxin, lambda toxin, and NetF toxin. Beta-toxin is a type of pore-forming, trypsin sensitive toxin which resembles 20-28% with several pore-forming toxins of *Staphylococcus aureus*⁹¹. Although Beta2-toxin resembles its name with beta-toxin, the sequence identity is only < 15%⁹². This toxin is found to be very unstable as susceptible to proteases digestion. This toxin is found to be very unstable as susceptible to proteases digestion. Although several variants of Beta2-toxin are reported to be produced by all types of *C. perfringens* and reported to induce hemorrhagic necrosis in the guinea pig intestine, their contribution CPB2 in any disease is still not concluded⁹³. Epsilon-toxin (ETX). Epsilon-toxin (ETX) is one of the most potent pore-forming toxins of the aerolysin family with LD₅₀ of 70 ng/kg body weight⁹⁴. It is secreted as prototoxin or inactive form that becomes active after removing 29 amino acids from C-terminus and 13 aminoacids from N- terminus by chymotrypsin and trypsin proteolytic action *in vitro* by *C. perfringens* lambda-toxin⁹⁵. It is fatal for different organs, including the brain, kidneys, and lungs, and is reported to cause an animal

⁹⁰Silva, R.O., Uzal, F.A., Oliveira, C.A. and Lobato, F.C. Gas gangrene (malignant edema). *Clostridial diseases of animals*. 243-254 (2016).

⁹¹Hunter, S.E., Brown, J.E., Oyston, P.C., Sakurai, J. and Titball, R.W. Molecular genetic analysis of beta-toxin of *Clostridium perfringens* reveals sequence homology with alpha-toxin, gamma-toxin, and leukocidin of *Staphylococcus aureus*. *Infection and Immunity*. **61**, 3958–3965 (1993).

⁹²Gibert, M., Jolivet-Reynaud, C. and Popoff, MR. Beta2 toxin, a novel toxin produced by *Clostridium perfringens*. *Gene* 203:65–73 (1997).

⁹³Fohler, S., Klein, G., Hoedemaker, M., Scheu, T., Seyboldt, C., Campe, A., Jensen, K.C. and Abdulmawjood, A. Diversity of *Clostridium perfringens* toxin-genotypes from dairy farms. *BMC microbiology*. **16**(1), 1-7 (2016).

⁹⁴Bijak, M. Biological Toxins. In *CBRN. Security Manager Handbook* (213-238). Wydawnictwo Uniwersytetu Łódzkiego (2018).

⁹⁵Freedman, J.C., McClane, B.A. and Uzal, F.A. New insights into *Clostridium perfringens* epsilon toxin activation and action on the brain during enterotoxemia. *Anaerobe*. **41**, 27-31 (2016).

(goat and sheep) enterotoxaemia⁹⁶. Iota-toxin is a type of binary toxin that consists of two distinct proteins, IA and IB⁹⁷. Both are secreted as pro-proteins that become active after removing some N-terminus amino acids by host proteases such as chymotrypsin. Both proteins as a holoprotein work together in disassembling the host cell cytoskeleton as IB mediated receptor binding and internalization into host cells followed by ADP-ribosylation of actin by the enzymatic action of IA. NetB toxin, a type of pore-forming toxin secreted from *C. perfringens* strains of type G, is responsible for enteritis in chickens⁹⁸. It resembles other pore-forming toxins, including beta-toxin, α -toxin from *S. aureus*, and δ -toxin from *C. perfringens*. Some other plasmid-encoded toxins and enzymes were also reported, such as lambda-toxin, which is involved in activation of ETX, although its disease-causing feature is still not clear, and delta-toxin⁹⁹.

2.6.3 Toxins encoded by either Chromosome or Plasmid

C. perfringens enterotoxin (CPE)

CPE is one of the most virulent toxins produced by some *C. perfringens* strains of type C, D, E, and F, but any type B strain was not found to secrete this toxin⁹. Although formally CPE secreting strains were grouped into the category of food poisoning type A strains, after revision of typing system for *C. perfringens*, CPE secreting food poisoning strains are classified as type F⁶. The *cpe* gene is present either in the chromosome or in the large plasmid of Type F

⁹⁶Uzal, F.A., Giannitti, F., Finnie, J.W. and García, J.P. Diseases produced by *Clostridium perfringens* type D. *Clostridial Diseases of Animals*; Wiley Blackwell: Ames, IA, USA, 157-172 (2016).

⁹⁷Takehara, M., Takagishi, T., Seike, S., Oda, M., Sakaguchi, Y., Hisatsune, J., Ochi, S., Kobayashi, K. and Nagahama, M. Cellular entry of *Clostridium perfringens* iota-toxin and *Clostridium botulinum* C2 toxin. *Toxins*. **9(8)**. 247 (2017).

⁹⁸Keyburn AL, Boyce JD, Vaz P, Bannam TL, Ford ME, Parker D, Di Rubbo A, Rood JI, Moore RJ. NetB, a new toxin that is associated with avian necrotic enteritis caused by *Clostridium perfringens*. *PLoS Pathog.* **4**, e26 (2008).

⁹⁹Manich M, Knapp O, Gibert M, Maier E, Jolivet-Reynaud C, Geny B, Benz R, Popoff MR. *Clostridium perfringens* delta toxin is sequence related to beta toxin, NetB, and *Staphylococcus* pore-forming toxins, but shows functional differences. *PLoS One*. **3**, e3764 (2008).

strains, but in other strains, it is always present only in the large plasmids (> 70 kb)^{100,101}. CPE encoding *cpe* gene presents only less than 5% *C. perfringens* strains present globally¹⁰². It is a very conserved pore-forming toxin of 319 amino acids produced by *C. perfringens* except produced by type E strains. CPE produced by type E strains is slightly different due presence of mutations in open reading frames or in the functional *cpe* gene that encodes the variant toxin of about ~ten amino acid sequences different from the classical CPE^{103,104}. This toxin is associated with food poisoning and non-food-borne diarrhoea and also responsible for the sporulation^{103,105}.

2.7 Mode of action and other characteristics of the toxins

All the toxin/enzymes secreted from the *C. perfringens* except ITX toxin attack the cell membrane and cause membrane disruption or pore formation through different modes of actions, while ITX toxin acts intracellularly⁸⁷. The toxins of *C. perfringens* with their mode of action and other characteristics (LD₅₀, Molecular weight, and biological functions) are listed in **table 4**¹⁰⁵.

2.8 *C. perfringens* toxinotypes and associated diseases (Pathogenesis)

C. perfringens is a very pathogenic bacterium and responsible for causing many different histotoxic and enterotoxic diseases in humans and animals

¹⁰⁰Gohari, I.M., Kropinski, A.M., Weese, S.J., Whitehead, A.E., Parreira, V.R., Boerlin, P. and Prescott, J.F., 2017. NetF-producing *Clostridium perfringens*: clonality and plasmid pathogenicity loci analysis. *Infection, Genetics and Evolution*. **49**, 32-38 (2017).

¹⁰¹Park, M. and Rafii, F. The prevalence of plasmid-coded *cpe* enterotoxin, β 2 toxin, tpeL toxin, and tetracycline resistance in *Clostridium perfringens* strains isolated from different sources. *Anaerobe*. **56**, 124-129 (2019).

¹⁰²Shrestha, A., Uzal, F.A. and McClane, B.A. Enterotoxic clostridia: *Clostridium perfringens* enteric diseases. *Gram-Positive Pathogens*. 977-990 (2019).

¹⁰³ Miyamoto K, Yumine N, Mimura K, Nagahama M, Li J, McClane BA, Akimoto S. Identification of novel *Clostridium perfringens* type E strains that carry an iota toxin plasmid with a functional enterotoxin gene. *PLoS One*. **6**, e20376 (2011).

¹⁰⁴Billington SJ, Wieckowski EU, Sarker MR, Bueschel D, Songer JG, McClane BA. *Clostridium perfringens* type E animal enteritis isolates with highly conserved, silent enterotoxin gene sequences. *Infection and Immunity*. **66**, 4531-4536 (1998).

¹⁰⁵Pawaiya, R.S., Gururaj, K., Gangwar, N.K., Singh, D.D., Kumar, R. and Kumar, A. The Challenges of Diagnosis and Control of Enterotoxaemia Caused by *Clostridium perfringens* in Small Ruminants. *Advances in Microbiology*, **10(5)**, 238-273 (2020).

Table 4. Characteristics of *C. perfringens* toxins (adapted from Pawatya, R.S. et al., 2020¹⁰⁵)

| Toxins | Gene | MW (kDa) | LD50 (Mice; µg) | Toxin type | Target | Biological functions |
|--------|--------------------------|--------------------------------|-----------------|-------------|--|--|
| α | <i>pic</i> or <i>cpa</i> | 43 | 3 | A-G | Phosphatidylcholine, Sphingomyelin | Hemolysis through phospholipase and sphingomyelinase, Vasoconstriction, Necrosis of intestinal mucosa epithelium and vascular endothelium. |
| β | <i>Cpb</i> | 35 | <0.4 | B and C | Intestinal epithelial, endothelial cells, sensory neurons | Acts primarily on vascular endothelial cells in the mucosa; can also inhibit platelet function. |
| ε | <i>etx</i> | ~33 (inactive) ~32 (active) | 0.070-0.1 | B and D | Endothelial cells, mucosal tight junctions, lymphocytes and all vital organs | Toxic towards neuronal cells via the glutamatergic system or extravasation in the brain. Increases blood pressure, contraction of smooth muscles, and vascular permeability. Causes cerebral edema and necrosis. |
| θ | <i>Pfo</i> | 54 | - | A-G | Enterocytes, endothelial cells | Disrupts cell integrity; acts synergistically with CPA and ETX. |
| λ | <i>lamm</i> | 36 | - | B, D, and E | Endothelial cells | Increases vascular permeability |
| β2 | <i>Cpb2</i> | 28 | - | A | Enterocytes, endothelial cells, leucocytes | Demonecrosis, edema & enterotoxic |
| ι | <i>iota</i> , <i>ib</i> | 47.5, 71.5 | 40 | E | Cytoskeleton (actin) | Disassembles cytoskeleton via ADP-ribosylation of actin, eventually leading to apoptosis and cell death. Increases necrosis of intestinal epithelial cells. |
| δ | | 42 | - | C | Blood cells, GM2 ganglioside on cell membranes | Cytotoxic for many eukaryotic cells including macrophages. |
| CPE | <i>cpe</i> | 35 | 81 | A and F | Claudins of tight junctions | Generates cation-selective pores in epithelial and endothelial cells and activates apoptotic and oncotic cell death. |
| NetB | <i>netB</i> | - | - | G | Enterocytes | Damages extracellular matrix, lamina propria, and intercellular junctions. |

(Figure 1). The bacterium's pathogenicity is associated with a repertoire of toxins they produce. The diseases caused by toxinotypes A to G of *C. perfringens* are host specific and are described as follows:

Type A

The *C. perfringens* type A is a widespread bacterium that is very important for causing histotoxic and enteric diseases in humans and animals. The primary toxins secreted by type A, CPA and PFO are responsible for causing gas gangrene in human beings and other enteric diseases in an animal such as enterotoxaemia in yellow limbs, goat and calves^{106,107}. However, enterotoxaemia in animals is still controversial because type A is ubiquitous even in healthy humans and animals that reduces the pathogenic values of the bacterium. Earlier *C. perfringens* strains secreting CPE and NetB associated with food poisoning in humans and necrosis in chickens were represented as type A. According to the revised classification of *C. perfringens* by toxinotyping method, type A strains are categorized as only alpha-toxin secreting strains and no other typing toxins, i.e., CPB ETX, ITX, and CPE or Net⁶.

Type B

C. perfringens type B, a very pathogenic bacteria, secretes mainly two virulent toxins, including CPB and ETX causing cell lysis, necrosis, necroptosis, and lethal effect mice animals^{108,109,110}. These strains are mainly known for causing

¹⁰⁶Awad, M.M.; Bryant, A.E.; Stevens, D.L.; Rood, J.I. Virulence studies on chromosomal alpha-toxin and theta-toxin mutants constructed by allelic exchange provide genetic evidence for the essential role of alpha-toxin in *Clostridium perfringens*-mediated gas gangrene. *Molecular Microbiology*. **15**(2), 191-202 (1995).

¹⁰⁷Uzal, FA. Diseases produced by *Clostridium perfringens* type A in mammalian species. *Clostridial diseases of animals*. Uzal, FA, Songer, JG, Prescott, J, Popoff, M, eds. Wiley and 809 Blackwell, Ames, IA, 109-116 (2016).

¹⁰⁸Uzal, FA, Songer, JG. Infections by *Clostridium perfringens* type B. *Clostridial diseases of animals*, 139-142 (2016).

¹⁰⁹ Fernandez-Miyakawa, ME, Fisher, DJ, Poon, R, Sayeed, S, Adams, V, Rood, JI, McClane, BA, Uzal, FA. Both epsilon-toxin and beta-toxin are important for the lethal properties of *Clostridium perfringens* type B isolates in the mouse intravenous injection model. *Infection and Immunity*. **75**, 1443-452 (2007).

¹¹⁰Autheman, D, Wyder, M, Popoff, M, D'Herde, K, Christen, S, Posthaus, H. *Clostridium perfringens* beta-toxin induces necrostatin-inhibitable, calpain-dependent necrosis in primary porcine endothelial cells. *PLoS One*. **85**, e64644 (2013).

hemorrhagic, enterotoxaemia in sheep and also found to causing Dysentery in newborn lambs and older lambs (pine), hemorrhagic enteritis in neonatal calves and foals. Therefore, these strains are also associated with a great economic loss. *C. perfringens*, isolates of type B, were mainly found in the border countries such as England and Scotland, Wales, South Africa, and the Middle East as well but rarely in North America¹¹¹. Although type B was not observed for causing disease in humans, recently, it appeared in a young woman's stool suffering from multiple sclerosis (MS)¹¹².

Type C

C. perfringens isolates belonging to type C are responsible for necrohaemorrhagic enteritis and enterocolitis condition in animals, including sheep, cattle, horses and pigs, and human beings¹¹³. The necrotizing condition caused by these strains in humans is referred to as necroticans (EN), pigbel, or armband¹¹⁴. Type C-associated infections are very progressive, resulting in death within 48h after the appearance of symptoms. The main virulent toxins associated with these diseases were demonstrated as alpha-toxin and beta toxin. Some strains belonging to type C were also found secreting CPE and β -toxins¹¹⁵. The β -toxin, a very sensitive to trypsin, is considered a main toxin secreted by type C strains. Therefore, in 1960, malnourished children in Papua New Guinea were affected by these strains.

¹¹¹ENTEROTOXEMIA, T.A. 19 CHAPTER ClostridialEnterotoxemia. *Current Veterinary Therapy-E-Book: Food Animal Practice*. **62** (2008).

¹¹²Rumah, KR, Linden, J, Fischetti, VA, Vartanian, T. Isolation of *Clostridium perfringens* type B in an individual at first clinical presentation of multiple sclerosis provides clues for environmental triggers of the disease. *PLoS One*. **8**, e76359 (2013).

¹¹³Diab, SS, Kinde, H, Moore, J, Shahriar, MF, Odani, J, Anthenill, L, Songer, JG, Uzal, FA. Pathology of *Clostridium perfringens* type C enterotoxemia in horses. *Veterinary Pathology*. **49**, 255-263 (2012).

¹¹⁴ Sayeed, S, Uzal, FA, Fisher, DJ, Saputo, J, Vidal, JE, Chen, Y, Gupta, P, Rood, JI, McClane, BA. Beta toxin is essential for the intestinal virulence of *Clostridium perfringens* type C disease isolate CN3685 in a rabbit ileal loop model. *Molecular Microbiology*. **67**, 15-30 (2008).

¹¹⁵ Fisher, DJ, Fernandez-Miyakawa, ME, Sayeed, S, Poon, R, Adams, V, Rood, JI, Uzal, FA, McClane, BA. Dissecting the contributions of *Clostridium perfringens* type C toxins to lethality in the mouse intravenous injection model. *Infection and Immunity*. **74**, 5200-5210 (2006).

Type D

C. perfringens type D is responsible for causing enterotoxaemia in sheep, goats, and cattle^{11,116}. The main disease-causing toxins secreted by these bacteria are α -toxin (CPA) and ϵ -toxin (ETX). Furthermore, some other strains belonging to this group are also found to secreting CPE or PFO. The outbreak of type D enterotoxaemia in most sheep has been seen during the presence of highly fermentable carbohydrates. The presence of heavy parasites in the intestine is also believed to enhance type D enterotoxaemia. The ϵ -toxin secreted as a proto-toxin in the intestine after infection and activated at the exposure of trypsin and other proteases, including chymotrypsin, by removing amino acids from the C-terminus¹¹⁷. Active ϵ -toxin can get absorbed in the bloodstream and affect the target organs, including the brain, lungs, heart, and kidneys, causing fluid accumulation and edema by increase vascular permeability¹¹⁸.

Type E

C. perfringens type E mainly encodes α -toxin and ι -toxin (ITX). Several individual strains belonging to type E are also found to secrete some additional toxins, CPE or β 2-toxin⁹. *C. perfringens* type E associated diseases are reported in some animal species, including sheep, cattle, and rabbits^{119,120,121}. Although, the involvement of these bacteria in the development of

¹¹⁶Uzal, FA, Hostetter, J, Plattner, B. The alimentary system. In: Maxie MG, ed. Jubb, Kennedy, and Palmer's Pathology of domestic animals. 6th ed. St. Louis, MO: Elsevier. 2, 1-260 (2016).

¹¹⁷Freedman, JC, Li, J, Uzal, FA, McClane, BA. Proteolytic processing and activation of *Clostridium perfringens* epsilon toxin by caprine small intestinal contents. *MBio*. **21**, e01994 (2014).

¹¹⁸Goldstein, J, Morris, WE, Loidl, CF, Tironi-Farinati, C, McClane, BA, Uzal, FA, Fernandez Miyakawa, ME. *Clostridium perfringens* epsilon toxin increases the small intestinal permeability in mice and rats. *PLoS One*. **18**, e7065 (1993).

¹¹⁹Songer, JG, Miskimmins, DW. *Clostridium perfringens* type E enteritis in calves: two cases and a brief review of the literature. *Anaerobe*. **10**, 239-42 (2004).

¹²⁰Redondo, LM, Carrasco, JM, Redondo, EA, Delgado, F, Miyakawa, ME. *Clostridium perfringens* type E virulence traits involved in gut colonization. *PLoS One*. **10**, e 0121305 (2015).

¹²¹Kim, HY, Byun, JW, Roh, IS, Bae, YC, Lee, MH, Kim, B, Songer, JG, Jung, BY. First isolation of *Clostridium perfringens* type E from a goat with diarrhea. *Anaerobe*. **22**, 141-3 (2013).

enterotoxaemia is still uncertain as the reports obtained are based on the presence of type E strains in the intestinal content of enteric animals that are not considered as the diagnostic criteria for the infections¹²². However, a variant *cpe* locus and a variant ITX gene in a plasmid are identified in the individual strains of type E present in the environment or healthy humans' fecal matter¹²³.

Type F

The *C. perfringens* isolates, possessing the structural genes only for the expression of α -toxin and CPE enterotoxin, belong to the toxinotype F. These strains do not carry genes for expression of other significant toxins including β , ι , and ϵ toxins⁶. Earlier, these *C. perfringens* strains secreting α -toxin, and CPE enterotoxin were belonged to the toxinotype A and termed as CPE-positive strains of *C. perfringens* type A. Type F associated diseases are also described as enterotoxigenic infections. These enterotoxigenic infections, including food poisoning and some other non-food-borne intestinal infections, including diarrhea and some other antibiotic-resistant diarrhea, are well documented in humans¹²⁴. Type F-associated infections in animals are not well determined and remain controversial¹²⁵. Type F-associated food poisoning is as second most common bacterial food-borne illness in the world¹²⁶.

Type G

The strains of *C. perfringens* encoding only α -toxin and NetB but no other toxins, i.e., β , ι , and ϵ , belong to the toxinotype G⁶. NetB toxin is a type of β

¹²²Songer, JG. Infections by *Clostridium perfringens* type E. In: *Clostridial diseases of animals*. Uzal, FA, Songer, JG, Prescott, J, Popoff, M, eds. Wiley and Blackwell, Ames, IA. 174-176 (2016).

¹²³Miyamoto, K., Yumine, N., Mimura, K., Nagahama, M., Li, J., McClane, B.A. and Akimoto, S. Identification of novel *Clostridium perfringens* type E strains that carry an iota toxin plasmid with a functional enterotoxin gene. *PLoS One*. **6(5)**, e20376 (2011).

¹²⁴Bueschel, D., Walker, R., Woods, L., Kokai-Kun, J, McClane, B, Songer, JG. Enterotoxigenic *Clostridium perfringens* type A necrotic enteritis in a foal. *J. Am. Vet. Med. Assoc.* 213:1305-1307 (1998).

¹²⁵ Busch, K, Suchodolski, JS, Kühner, KA, Minamoto, Y, Steiner, JM, Mueller, RS, Hartmann, K, Unterer, S. *Clostridium perfringens* enterotoxin and *Clostridium difficile* toxin A/B do not play a role in acute haemorrhagic diarrhoea syndrome in dogs. *Veterinary Record*. **176**, 253 (1998).

¹²⁶Centers for Disease Control and Prevention. *Clostridium perfringens* <https://www.cdc.gov/foodsafety/diseases/clostridium-perfringens.html> (2017).

pore-forming and main virulent toxin of type G strains¹²⁷. These *C. perfringens* are primarily responsible for necrotic enteritis in poultry (chickens). Therefore, it becomes economically crucial and affects the poultry industry worldwide. Formerly, these strains are termed avian necrotic enteritis strains of *C. perfringens* type A. The role of these strains in causing lethality in the poultry was confirmed by epidemiological evidence. Type G strains have not been reported in non-poultry animals and humans^{128,129}.

2.9 Therapeutics in use for *C. perfringens* infections

Therapeutics, including antibiotics, have always been beneficial in curing bacterial infections by targeting them at the molecular and cellular levels. Other preventative measures and antibiotics must be necessary to stop the *C. perfringens* infections as they are a very fast-growing bacterium. This bacterium can lead to animals' death by excessive tissue destruction within hours if not treated timely. It is essential to focus on the inhibition of bacterial proliferation to prevent *C. perfringens* infections. Several antibiotics including, ciprofloxacin, penicillin, and ceftriaxone, are reported as the most effective antibiotics in diarrhoeic sheep and goats¹³⁰. The infection can also be control by preventing the intestinal absorption of toxins produced in the digestive tract using cathartic that increase the defecation and flush out the toxins with fecal matter, but dehydration condition must be kept in mind. Using antitoxin (serotherapy) can be considered the most effective therapy to stop the infection as the rapid proliferating nature of *C. perfringens*¹³¹. The preventive effect of

¹²⁷Keyburn, AL, Boyce, JD, Vaz, P, Bannam, TL, Ford, ME, Parker, D, Di Rubbo, A, Rood, JI, Moore, RJ. NetB, a new toxin that is associated with avian necrotic enteritis caused by *Clostridium perfringens*. *PLoSPathog*4, e26 (2008).

¹²⁸J. F. Prescott, V. R. Parreira, I. MehdizadehGohari, D. Lepp, J. Gong. The pathogenesis of necrotic enteritis in chickens: what we know and what we need to know: a review. *Avian Pathology*.45, 288-94 (2016).

¹²⁹J. I. Rood, A. L. Keyburn, R. J. Moore. NetB and necrotic enteritis: the hole movable story. *Avian Pathology*.43, 295-301 (2016).

¹³⁰Hussain, K., Ijaz, M., Farooqi, S.H., Rizvi, B., Nayab, S., Ali, A., et al. Molecular Characterization of *Clostridium perfringens* Toxino-Types and Type "D" Multidrug Resistance Profile in Diarrheic Sheep. *Pakistan Veterinary Journal*. 38. 271-275 (2018).

¹³¹Aiello, S.E. Merck Veterinary Manual. 8th Edition, Merck and Co., Inc., Whitehouse Station, NJ (2003).

ETX antitoxin for experimental *C. perfringens* type D infection in sheep and goats has been reported¹³².

Nevertheless, antitoxin is not very common in the field due to less availability of toxins and the risk of anaphylaxis (allergic reactions). The use of antibiotics and antisera in combination was reported more effective than antibiotics and antisera alone to treat experimental goats^{133,134}. In case of myonecrosis, the surgical debridement of infected area and removal of all damaged tissue and starting the administration of antibiotics (penicillin G) simultaneously, hyperbaric oxygen and monoclonal antibodies administration can be considered as essential measures to control clostridial infections^{135,136,137}. Therefore, other alternatives, including antitoxin (serotherapy) administration or vaccination against the toxins, could be more promising to control *C. perfringens* infections¹³⁸. However, these treatment methods are not feasible for animals due to quick death after infection without any premonitory symptoms¹³⁹. Therefore, the vaccination could be an excellent preventive measure for *C. perfringens* associated diseases.

¹³²Kotsanas, D., Carson, J.A., Awad, M.M., Lyras, D., Rood, J.I., Jenkin, G.A., Stuart, R.L. and Korman, T.M. Novel Use of TryptoseSulfiteCycloserine Egg Yolk Agar for Isolation of *Clostridium perfringens* during an Outbreak of Necrotizing Enterocolitis in a Neonatal Unit. *Journal of Clinical Microbiology*. **48**, 4263-4265 (2010).

¹³³Phukan, A., Kalita, D. and Das, B. Experimental Production of Enterotoxaemia in Goats and Its Treatment. *Indian Veterinary Journal*. **77**, 1051-1053 (2000).

¹³⁴Islam, K., Rahman, M.S., Ershaduzzaman, M., Taimur, M. and Song, H. J. Experimental Development of Caprine Enterotoxaemia with *Clostridium perfringens* Type D Whole Culture in Natural Host and Its Treatments. *Korean Journal of Veterinary Service*. **30**, 219-231 (1998).

¹³⁵Garcia, J.P., Beingesser, J., Bohorov, O., Bohorova, N., Goodman, C., Kim, D., Pauly, M., Velasco, J., Whaley, K., Zeitlin, L. and Roy, C.J. Prevention and treatment of *Clostridium perfringens* epsilon toxin intoxication in mice with a neutralizing monoclonal antibody (c4D7) produced in *Nicotianabenthiana*. *Toxicon*. **88**, 93–98 (2014).

¹³⁶Carroll, K.C., Butel, J. and Morse, S. *Jawetz, Melnick, & Adelberg's Medical Microbiology*. 27e. McGraw-Hill (2015).

¹³⁷ Massey, P.R., Sakran, J.V., Mills, A.M., Sarani, B., Aufhauser, D.D., Jr.; Sims, C.A., Pascual, J.L., Kelz, R.R. and Holena, D.N. Association for Academic Surgery Hyperbaric oxygen therapy in necrotizing soft tissue infections. *Journal of Surgical Research*. **177**, 146–151 (2012).

¹³⁸Aiello, S.E. Merck Veterinary Manual. 8th Edition, Merck and Co., Inc., Whitehouse Station, NJ (2003).

¹³⁹ Lebrun, M.; Mainil, J.G.; Linden, A. Cattle enterotoxaemia and *Clostridium perfringens*: Description, diagnosis and prophylaxis. *Veterinary Record*. **167**, 13–22 (2010).

2.10 Perfringolysin O (PFO)

PFO is a cholesterol-dependent, β pore-forming toxin that is also termed θ -toxin. It is one of the most virulent toxins of the *C. perfringens* type A that is mainly responsible for the pathogenesis of gas gangrene (humans and animals) and (necrohemorrhagic enteritis) in animals (calves). PFO belongs to the Thiol-activated CDCs, a family of bacterial pore-forming toxins requiring cholesterol in a high amount in the lipid membrane for binding and assembly in the membrane for pore formation cytolysis. However, CDCs are predominantly expressed and secreted by Gram-positive bacteria, including *Clostridium*, *Streptococcus*, *Bacillus*, and *Listeria species*. Some Gram-negative bacteria are also reported for secreting CDCs, such as *Desulfobulbus propionicus* and *Enterobacter lignolyticus*. The essential characteristic of the toxins belonging to CDCs is to share the homology in amino acid sequence or primary structure as PFO exhibited the percentage of identity with other CDCs.

2.10.1 Genetics

The nucleotide sequence of *pfoA gene*, 1.8-kilobase, has been determined on the chromosome's variable arm near to the origin of replication¹⁴⁰. This region (*pfo gene*) on the chromosome is believed to be conserved in almost all the *C. perfringens* strain except enterotoxin-producing food poisoning strains. Expressed product of *pfo gene*, the primary structure of PFO consisting of 500 amino acid residues, with a 27-residues signal peptide, was found to be well conserved despite having a variation on location nucleotide sequence. A region of *pfo gene* encoding a tryptophan-rich loop, termed as undecapeptide region, is the most conserved region of the PFO¹⁴¹.

¹⁴⁰Tweten, R.K. Cloning and expression in *Escherichia coli* of the perfringolysin O (θ -toxin) gene from *Clostridium perfringens* and characterization of the gene product. *Infection and Immunity*. **56**, 3228–3234 (1988).

¹⁴¹Morton, C.J., Sani, M.A., Parker, M.W. and Separovic, F. Cholesterol-dependent cytolysins: membrane and protein structural requirements for pore formation: Focus review. *Chemical reviews*. **119(13)**, 7721-7736 (2019).

2.10.2 Regulation of *pfo* gene expression

The regulation of PFO production in different *C. perfringens* isolates have been reported at transcriptional and expression level by specific gene regulatory systems including, VirS/VirR System, autoinducer 2 (AI-2) system, agr system, and by RNA regulators¹⁴². The VirS/VirR System is a type of Two-Component Regulatory System (TCRs) present in the bacteria's chromosome. It comprises genes *virR* and *virS* for encoding response regulator (VirS) and sensor histidine kinase (VirR). This system was found originally in 1994 in *C. perfringens* type A for regulating the expression of genes *plc* of alpha-toxin, *pfoof* PFO, and *colA* of κ -toxin^{143,144}. The VirS/VirR System regulates the *pfoA* and *pfoR* genes at the transcriptional level. VirR is required to transcribe the *pfoA* gene by putative 2 promoter (p2; major promoter) to express the active PFO toxin and the transcription of *pfoR*, present in the upstream of the *pfoA*, is also regulated by VirR system¹⁴⁴. Additionally, the homolog of the Autoinducer 2 (AI-2) /luxS system and the agr system are also demonstrated to regulate *pfo* gene through cell-cell signaling. The *luxS* gene was found to be involved in the production of AI-2 protein involved in regulating early to late log phase transcription of *pfoA* as *pfoA* transcription was found to be declined in the early to late-log phase in the *luxS* mutant¹⁴⁵. Some RNA regulators, including *virU* and *virT* also involved in *pfo*, *virU* and *virT* regulation. In an experiment, an over-expression showed that *VirU* regulates *pfoA*, *virR*, *ccp*, and *virT* positively, and *VirT* negatively affects the expressions of *pfoA*¹⁴⁶.

¹⁴²Ohtani, K. and Shimizu, T. Regulation of toxin production in *Clostridium perfringens*. *Toxins*, **8**(7), 207 (2016).

¹⁴³ Shimizu, T.; Ba-Thein, W.; Tamaki, M.; Hayashi, H. The *virR* gene, a member of a class of two-component response regulators, regulates the production of the perfringolysin O, collagenase, and hemagglutinin in *Clostridium perfringens*. *Journal of Bacteriology*. **176**, 1616–1623 (1994).

¹⁴⁴Ba-Thein, W.; Lyrstis, M.; Ohtani, K.; Nisbet, I.T.; Hayashi, H.; Rood, J.I.; Shimizu, T. The *virR/virS* locus regulates the transcription of genes encoding extracellular toxin production in *Clostridium perfringens*. *Journal of Bacteriology*. **178**, 2514–2520 (1996).

¹⁴⁵Ohtani, K.; Hayashi, H.; Shimizu, T. The *luxS* gene is involved in cell-cell signaling for toxin production in *Clostridium perfringens*. *Molecular Microbiology*. **44**, 171–179 (2002).

¹⁴⁶Okumura, K.; Ohtani, K.; Hayashi, H.; Shimizu, T. Characterization of genes regulated directly by the *virR/virS* system in *Clostridium perfringens*. *Journal of Bacteriology*. **190**, 7719–7727 (2008).

2.10.3 Structure of PFO

PFO, a soluble monomer of 53 kDa polypeptide containing 500 amino acid residues, is secreted by the general secretory pathway, and signal sequences for extracellular secretion regulate the secretion¹⁴⁷. The similarity in the primary structure of PFO with other CDCs (40-70%) reflects its structural and functional similarity with the CDCs. Therefore, the structure of PFO is seemed to be a model for the study of other CDCs^{148,149}. The structure of PFO was revealed by X-ray crystallography as an elongated monomer, rod-shaped (115Å× 30Å× 55Å), rich in 40% β -sheet secondary structure containing 25 β strands forming five β sheets and eleven α helices and two 3_{10} helices¹⁴¹. The structure is divided into four domains, D1, D2, D3, and D4, that conserved in all the CDCs. Three domains D1, D2, & D3 (**Figure 2a**) of PFO, consist of the discontinuous polypeptide sequence, whereas the C-terminal or D4 domain is a continuous domain. The domains are briefly described in the following sections:

Domain 1: It consists of a discontinuous polypeptide sequence (D1: residues 37-53, 90-178, 229-274, 350-373) made up of α/β secondary structure where α -helices border seven stranded antiparallel β -sheet.

Domain 2: (D2: residues 54–89, 374–390), a linker between the body of the protein and C-terminal domain 4 (D4), consists of four mixed β strands and are associated with the D4 domain by glycine linker at residue 392.

Domain D3: Domain 3 (D3: residues 179–228, 275–349) is an $\alpha/\beta/\alpha$ three-layered structure consisting of one core β -sheet (D3 β 1–5) and two sets of three α -helices present between domains D1 and D4.

¹⁴⁷Hotze, E.M. and Tweten, R.K. Membrane assembly of the cholesterol-dependent cytolysin pore complex. *Biochimica Et BiophysicaActa (BBA)-Biomembranes*. **1818(4)**, 1028-1038 (2012).

¹⁴⁸Wade, K.R., Hotze, E.M. and Tweten, R.K. Perfringolysin O and related cholesterol-dependent cytolysins: mechanism of pore formation. *The Comprehensive Sourcebook of Bacterial Protein Toxins*. **719** (2015).

¹⁴⁹Rezelj, S., Kozorog, M., Švigelj, T., Ulrih, N.P., Žnidaršič, N., Podobnik, M. and Anderluh, G. Cholesterol Enriched Archaeosomes as a Molecular System for Studying Interactions of Cholesterol-Dependent Cytolysins with Membranes. *The Journal of membrane biology*. **251(3)**, 491-505 (2018).

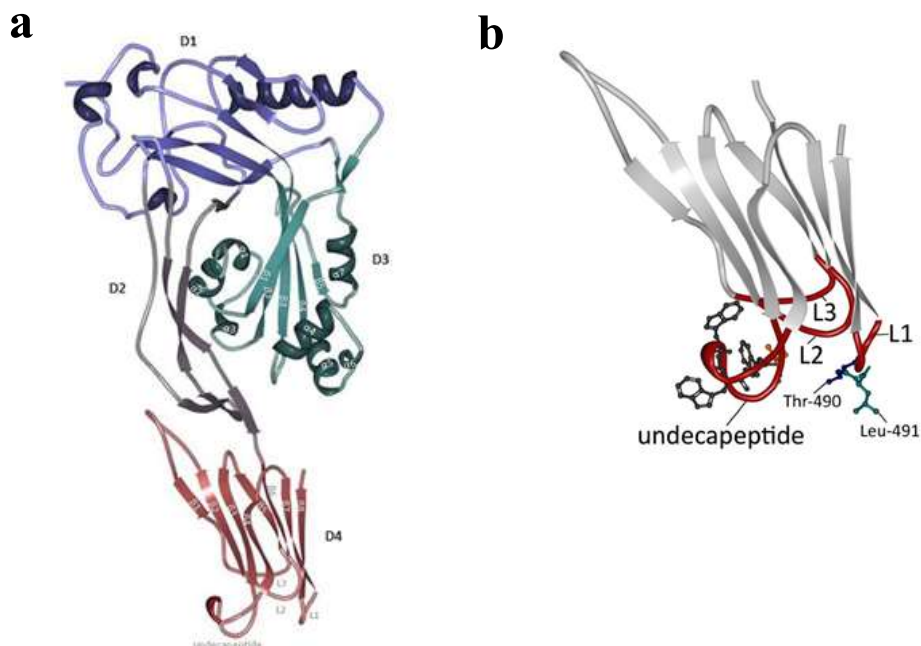


Figure 2. (a) Structure of PFO divided into four domains; D1, D2, D3, and D4 dominated by β -sheets. (b) Structure of C-terminal domain or D4 representing the most conserved region ‘undecapeptide’ of the molecule. The open-access article under the creative commons Attribution on License published in toxins; Perfringolysin O: The Underrated *Clostridium perfringens* Toxin?¹⁵⁰(**appendix no 2.1**).

Domain (D4 or C-terminal domain): Domain 4 (D4: residues 391–500) is a small, packed, β -sandwich structure present at the C-terminus PFO, also termed as C-terminal domain¹⁵¹. This β -sandwich structure is made up of two β -sheets, and each β -sheet is having four β -strands (**Figure 2b**). These β -strands are connected by four loops, L1, L2, L3, and conserved undecapeptide for packing^{152,153}. Furthermore, Loop L1, L2, and undecapeptide loop are more

¹⁵⁰Verherstraeten, S., Goossens, E., Valgaeren, B., Pardon, B., Timbermont, L., Haesebrouck, F., Ducatelle, R., Deprez, P., Wade, K.R., Tweten, R. and Van Immerseel, F. Perfringolysin O: The underrated *Clostridium perfringens* toxin? *Toxins*, **7(5)**, 1702-1721 (2015).

¹⁵¹Johnson, B.B. and Heuck, A.P. Perfringolysin O structure and mechanism of pore formation as a paradigm for cholesterol-dependent cytolysins. *MACPF/CDC Proteins-Agents of Defence, Attack and Invasion*. 63-81 (2014).

¹⁵²Ramachandran, R., Heuck, A. P., Tweten, R. K., & Johnson, A. E. Structural insights into the membrane-anchoring mechanism of a cholesterol-dependent cytolysin. *Nature structural biology*. **9(11)**, 823–827 (2002).

conserved parts of the D4 and form a packet in the protein's distal end. While L3 is least conserved and is located away from the pocket. The pocket is engaged primarily in membrane recognition and binding¹⁵⁴. The undecapeptide loop is a tryptophan-rich, 11 residues (E C T G L A W E W W R) containing the most conserved region of CDCs.

2.10.4 Mechanism of PFO action in cell lysis / β -barrel pore formation by PFO

The pore formation characteristic is a conserved feature of all the CDCs that require cholesterol to recognize and initiate the membrane's pore formation. Although a CDCs, intermedilysin (ILY) produced by *Streptococcus intermedius* was not found to utilize the cholesterol for recognition and binding to the membrane that indicated its presence is not essential for all the CDCs, cholesterol is still a necessary component for the CDCs for their cell lysis activity¹⁵⁵. Interestingly, the binding of soluble PFO monomer to the membrane seems to be supported by the formation of non-specific collisional complex, electrostatic interactions along with non-polar and aromatic amino acids interactions with molecule and lipid bilayer¹⁵⁰. Since the non-polar and aromatic amino acids are rarely present on the surface of water-soluble molecules, conformational changes must localize the hydrophobic residue on the molecule's surface to initiate the insertion of molecules through the membrane. Although the CDCs' pore formation mechanism is still poorly understood, several CDCs are well characterized, including PFO. The successive events, including membrane recognition, binding, oligomerization, pre-pore assembly, and pore-formation (**Figure 3**) that occurred during PFO action in the cholesterol-containing membrane are described in the following section:

¹⁵³Soltani, C.E., Hotze, E.M., Johnson, A.E. and Tweten, R.K. Structural elements of the cholesterol-dependent cytolysins that are responsible for their cholesterol-sensitive membrane interactions. *Proceedings of the National Academy of Sciences*. **104(51)**, 20226-20231 (2007).

¹⁵⁴Savinov, S.N. and Heuck, A.P. Interaction of cholesterol with perfringolysin O: what have we learned from functional analysis? *Toxins*. **9(12)**, 381 (2017).

¹⁵⁵ Giddings, K.S.; Zhao, J.; Sims, P.J.; Tweten, R.K. Human CD59 is a receptor for the cholesterol-dependent cytolysin intermedilysin. *Nature Structural Molecular Biology*. **11**, 1173–1178 (2004).

Membrane recognition and binding is the first event of the PFO action in cell lysis. The two more important factors, cholesterol and D4 domain of the molecules are required to accomplish PFO monomer's binding with the membrane. Some other factors, including cholesterol accessibility in the membrane and the membrane's thickness, also affect molecule binding^{141,156}. Cholesterol, present in the higher eukaryotes, is a critical component of the mammalian cell membrane to carry out physiological functions^{157, 158}. A high amount of cholesterol acts as the receptor for the CDCs binding with the membrane^{159,160}. Initially, the 'lipid raft (cholesterol-rich domain) present in the membrane was believed to be for CDCs recognition, but the presence of cholesterol in the membrane for the CDCs recognition has been confirmed, and the presence of 'Lipid raft' may not be required for the CDCs.

Furthermore, the water-exposed hydrophobic head and deeply embedded aliphatic chains affect the CDCs' binding affinity to the membranes¹⁴¹. The most conserved structure of the CDCs, domain 4 (D4), is critical to initiate the pore formation by CDCs in mammalian membrane^{151,161}. The single residue variation can also affect the binding ability of D4 to the model or cell membranes¹⁶². D4 domain interacts with the membrane only through loops (L1, L2, L3, and undecapeptide) located on the domain's tip rather than by the whole domain⁸⁷. Indeed, the molecule's recognition and binding are chiefly mediated by only two amino acids, threonine-490 and leucine-491 in L1.

¹⁵⁶Das, A., Brown, M.S., Anderson, D.D., Goldstein, J.L. and Radhakrishnan, A. Three pools of plasma membrane cholesterol and their relation to cholesterol homeostasis. *Elife*. **3**, e 02882 (2014).

¹⁵⁷ Simons, K.; Sampaio, J. L. Membrane Organization and Lipid Rafts. *Cold Spring Harbor Perspect. Biol.* **3**, a004697 (2-11).

¹⁵⁸Mouritsen, O. G.; Zuckermann, M. J. What's So Special About Cholesterol? *Lipids*. **39**, 1101–1113 (2004).

¹⁵⁹Nollmann, M.; Gilbert, R.; Mitchell, T.; Sferrazza, M.; Byron, O. The role of cholesterol in the activity of pneumolysin, a bacterial protein toxin. *Biophysical Journal*. **86**, 3141–3151 (2004).

¹⁶⁰ Flanagan, J.J.; Tweten, R.K.; Johnson, A.E.; Heuck, A.P. Cholesterol exposure at the membrane surface is necessary and sufficient to trigger perfringolysin O binding. *Biochemistry*, **48**, 3977–3987 (2009).

¹⁶¹Heuck, A.P.; Savva, C.G.; Holzenburg, A.; Johnson, A.E. Conformational changes that effect oligomerization and initiate pore formation are triggered throughout perfringolysin O upon binding to cholesterol. *Journal of Biological Chemistry*. **282**, 22629–22637 (2007).

¹⁶²Park, S.A., Park, Y.S., Bong, S.M. and Lee, K.S. Structure-based functional studies for the cellular recognition and cytolytic mechanism of pneumolysin from *Streptococcus pneumoniae*. *Journal of structural biology*. **193(2)**, 132-140 (2016).

These amino acids are collectively termed as a cholesterol-recognition motif (CRM) of the PFO¹⁶³. Loop L2 and L3 are essential for anchoring the PFO to the membrane by inserting and stabilizing the molecule's binding¹⁶⁴. While the undecapeptide (UDP) loop of the D4, a conserved tryptophan-rich region of the molecule is involved in PFO anchoring and allosteric coupling required for molecule binding to the membrane followed by oligomer β -barrel pore complex formation¹⁶⁵. The previous studies revealed the importance of the UDP by determining the effect of mutations at the residues R468 and cysteine present in the undecapeptide loop affects the molecule's binding and pore-formation capacity^{166,167}.

The PFO interaction with the membrane by the D4 domain triggers PFO monomers' oligomerization on the membrane surface. Upon binding the D4 domain to the membrane, conformational changes in D3 lead to the rearrangements of β -strands (β 4– β 5) in the core β -sheet present in the D3 domain. D3 is connected to D4 through an interface prepared with both domains D1 and D2. These domains D1 and D2 support the molecule in recognition and connecting to the target membrane⁸⁸. The rearrangements in β -sheet in domain 3 after recognition and binding to membrane results in exposure of β 4 strand to bind the β 1-strand in the core β -sheet of an adjacent monomer to facilitate the oligomer formation on the membrane surface. About 35-50 individual PFO monomers on the membrane surface regularly and form a sizeable ring-shaped complex of ~250-300 Å inner diameter termed as a pre-

¹⁶³Farrand, A.J., LaChapelle, S., Hotze, E.M., Johnson, A.E. and Tweten, R.K. Only two amino acids are essential for cytolytic toxin recognition of cholesterol at the membrane surface. *Proceedings of the National Academy of Sciences*. **107**, 4341-4346 (2010).

¹⁶⁴Farrand, A.J., Hotze, E.M., Sato, T.K., Wade, K.R., Wimley, W.C., Johnson, A.E. and Tweten, R.K. The cholesterol-dependent cytolysin membrane-binding interface discriminates lipid environments of cholesterol to support β -barrel pore insertion. *Journal of Biological Chemistry*, **290(29)**, 17733-17744 (2015).

¹⁶⁵Heuck, A.P., Hotze, E., Tweten, R.K. Johnson AE Mechanism of membrane insertion of a multimeric β -barrel protein: Perfringolysin O creates a pore using ordered and coupled conformational changes. *Molecular Cell*, **6**, 1233–1242 (2000).

¹⁶⁶Polekhina, G., Giddings, K.S., Tweten, R.K. and Parker, M.W. Insights into the action of the superfamily of cholesterol-dependent cytolysins from studies of intermedilysin *Proceedings of the National Academy of Sciences*. **102**, 600–605 (2005).

¹⁶⁷Dowd, K.J. and Tweten, R.K. Correction: The Cholesterol-Dependent Cytolysin Signature Motif: A Critical Element in the Allosteric Pathway that Couples Membrane Binding to Pore Assembly. *PLoS Pathogens*. **8(8)** (2012).

pore complex that regulates the proper alignment of β -strands from the adjacent monomers.

The subsequent process, pre-pore to pore formation, is the last event of PFO action in cell lysis that is believed to be preceded by thermal energy, as low-temperature blocks pre-pore to pore formation. The pre-pore complex's transition to pore formation favored by the unfurling of six α -helices into two amphipathic transmembrane β -hairpins (TMH1 and TMH2) present in the D3 and collapsing of D2 to bring D3 closer to the membrane that was present 40 Å above the membrane surface in the pre-pore complex. The collapsing of D2 favored by the disengagement between D2 and D3. This disengagement is facilitated by stable D1 binding to the membrane¹⁶⁸. Further, the importance of D1 in the disengagement of D2 is also revealed in the previous study by the substitution of tryptophan residue (Trp-165) in D1 that destabilizes the D1 and affects the disengagement of interface between D2 and D3¹⁶⁹.

Additionally, the transition from pre-pore to pore is also supported by the free energy generated during the formation of intermolecular electrostatic interactions after the rotation of β 5 away from the core β -sheet in D3¹⁷⁰. Since the closest of D3 in membrane aid in penetrating transmembrane β -hairpins (TMHs) through the hydrophobic core of the membrane. TMHs span the membrane entirely by forming β -barrel by insertion into the membrane bilayer in a concerted, synchronized manner. The membrane-spanning is facilitated by hydrophobic residues facing the lipid core of the membrane and hydrophilic surfaces exposed to the aqueous pore.

¹⁶⁸Hotze, E.M.; Wilson-Kubalek, E.; Farrand, A.J.; Bentsen, L.; Parker, M.W.; Johnson, A. E. Tweten, R.K. Monomer-monomer interactions propagate structural transitions necessary for pore formation by the cholesterol-dependent cytolysins. *Journal of Biological Chemistry*. **287**, 24534–24543 (2012).

¹⁶⁹Kacprzyk-Stokowiec, A.; Kulma, M.; Traczyk, G.; Kwiatkowska, K.; Sobota, A.; Dadlez, M. Crucial role of perfringolysin O D1 domain in orchestrating structural transitions leading to membrane-perforating pores: A hydrogen-deuterium exchange study. *Journal of Biological Chemistry*. **289**, 28738–28752 (2015).

¹⁷⁰Wade, K.R.; Hotze, E.M.; Kuiper, M.J.; Morton, C.J.; Parker, M.W.; Tweten, R.K. An intermolecular electrostatic interaction controls the prepore-to-pore transition in a cholesterol-dependent cytolysin. *Proceedings of the National Academy of Sciences*. **112**, 2204–2209 (2015).

2.11 Consequences of membrane pore formation in cells by CDCs/PFO

Finally, the consequence of pore formation on cell membrane could be cell death by lysis or programmed cell death. Since the erythrocytes are very sensitive compared to other mammalian cells (HeLa, HEK, and 3T3 cells), readily available and accessible measurement of releasing hemoglobin, therefore the CDCs' activity/PFO has been determined using RBCs for many years¹⁷¹. Interestingly, the macrophages were found more resistant (~10-20) to CDCs than other nucleated cells^{172,173}. Also, differentiated macrophages appeared more resistant to CDCs, streptolysin O (SLO), and anthrolysin O

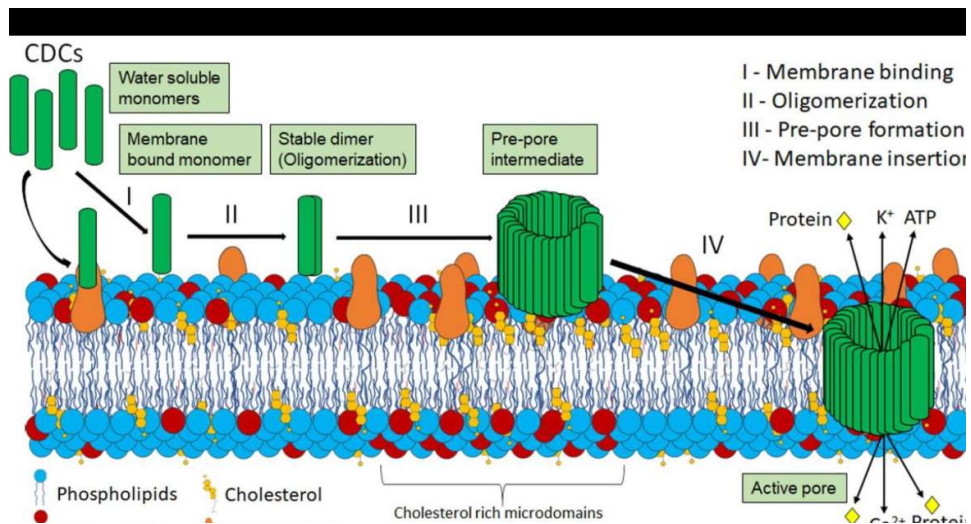


Figure 3. Different stages (I, II, III, and IV) in Pore formation by PFO/CDCs.The open-access article under the creative commons attribution on License published in toxins; Interaction of Macrophages and Cholesterol-Dependent Cytolysins: The Impact on Immune Response and Cellular Survival¹⁴⁵ (appendix no 2.1).

¹⁷¹ Flexner, S.; Noguchi, H. The Influence of Colloids upon the Diffusion of Haemolysins. *Journal of Experimental Medicines*. **8**, 547–563 (1906).
¹⁷² Romero, M.; Keyel, M.; Shi, G.; Bhattacharjee, P.; Roth, R.; Heuser, J.E.; Keyel, P.A. Intrinsic repair protects cells from pore-forming toxins by microvesicle shedding. *Cell Death*. **24**, 798–808 (2017).
¹⁷³ Keyel, P.A.; Roth, R.; Yokoyama, W.M.; Heuser, J.E.; Salter, R.D. Reduction of streptolysin O (SLO) pore-forming activity enhances inflammasome activation. *Toxins*. **5**(6)1105-18 (2013).

(ALO) than THP1 monocytes cell lines and neutrophils^{174,175}. The resistant nature of the macrophages is not still evident. It could be due to a solid and enhanced membrane repair process or declined pore formation compared to other cells. The three membrane repair mechanisms, patch repair, clogging, and intrinsic repair, are believed to trigger the CDCs to resist their lytic action^{172,176,177}. An intrinsic repair mechanism is considered for the PFO as the toxin is shed on microvesicles triggered by oligomerization¹⁷⁸.

Membrane pore-formation also triggers one or more Mitogen-activated Protein Kinase (MAPK) signaling pathways other than programmed cell death pathway, including activation of p38, mitogen-activated protein kinase /ERK kinase (MEK), and c-Jun N-terminus kinases (JNK) pathways) in which p38 is very common and a conserved cellular response to CDCs (**Figure 4**).

2.12 Effect of PFO on macrophages and immune cells

Although many cellular responses of most nucleated cells are common to CDCs, macrophages represent the sign of an infection, including cytokine production and promoting inflammasome activation after directly encountering CDCs/PFO or other virulent closed. CDCs/PFO is also responsible for immune evasion and reducing inflammatory responses by interfering in phagocytosis. The cellular responses generated by macrophages after encountering the CDCs are described below:

2.12.1 Cytokines production

In response to CDCs, macrophages produce some major pro-inflammatory cytokines, including tumor necrosis factor (TNF- α), interleukin (IL)-1 β , IL-6, IL-8, and some other cytokines and chemokines, as shown in **figure 4**.

¹⁷⁴Tanigawa, T.; Suzuki, J.; Ueta, T.; Katsumoto, T.; Tanaka, Y. Different sensitivity to streptolysin-O of cells in macrophage lineage. *Microbiology and Immunology*. **40**, 81–84 (1996).

¹⁷⁵Mosser, E.M.; Rest, R.F. The Bacillus anthracis cholesterol-dependent cytolysin, Anthrolysin O, kills human neutrophils, monocytes and macrophages. *BMC Microbiology*. **6**, 56 (2006).

¹⁷⁶ Cooper, S.T.; McNeil, P.L. Membrane Repair: Mechanisms and Pathophysiology. *Physiological Reviews*. **95**, 1205–1240 (2015).

¹⁷⁷Wolfmeier, H.; Schoenauer, R.; Atanasso, A.P.; Neill, D.R.; Kadioglu, A.; Draeger, A.; Babiychuk, E.B. Ca²⁺-dependent repair of pneumolysin pores: A new paradigm for host cellular defense against bacterial pore-forming toxins. *Biochimica et Biophysica Acta (BBA)-Molecular Cell Research*. **1853**, 2045–2054 (2015).

¹⁷⁸ Ray, S.; Thapa, R.; Keyel, P.A. Multiple Parameters Beyond Lipid Binding Affinity Drive Cytotoxicity of Cholesterol-Dependent Cytolysins. *Toxins*. **11**, 1 (2018).

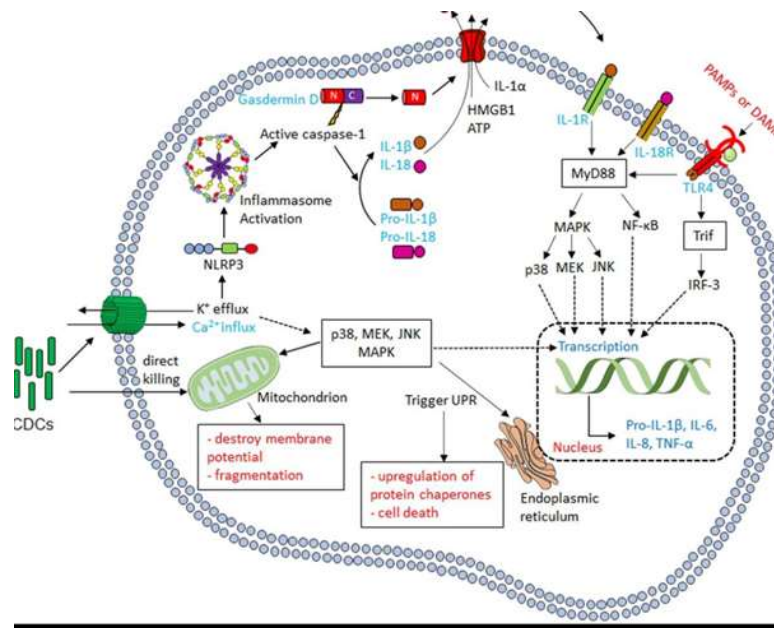


Figure 4. Multiple cellular mechanisms including, Inflammasome activation, and various pathways i.e. mitogen-activated protein kinases (MAPK), p38, mitogen-activated protein kinases /ERK kinase (MEK), and c-Jun N-terminus kinases (JNK) pathways and secretion of the cytokines including TNF- α , IL-6, IL-8, Pro-IL- β triggered by CDCs/ PFO after cell membrane pore formation in *C. perfringens* infections. The open-access article under the creative commons Attribution on License published in toxins; Interaction of Macrophages and Cholesterol-Dependent Cytolysins: The Impact on Immune Response and Cellular Survival¹⁴⁵ (**appendix no 2.1**).

2.12.2 Inflammasome activation

The inflammasome is a complex of the multiple proteins containing cytoplasmic sensory pattern-recognition receptor, the scaffolding protein apoptosis-associated speck-like protein containing a CARD (ASC), and an inflammatory caspase-1 or caspase-11 in mouse and caspase -1,4 or 5 in human)¹⁷⁹. Inflammasome activation is triggered after sensing the various pathogen-associated molecular patterns of CDCs /PFO and membrane pore-formation by nod-like –receptors (NLRs) and nucleotide-binding oligomerization domain-like receptor family, pyrin domain-containing 3

¹⁷⁹Broz, P.; Dixit, V.M. Inflammasomes: mechanism of assembly, regulation and signalling. *Nature Reviews Immunology*. **16**(7), 407-420 (2016).

(NLRP3)^{179,180}. After activation, NLRP3 generates a cascade of the reactions that promote the pro-inflammatory mediators (HMGB1, IL-1 β , IL-18)¹⁸⁰. Although the pro-inflammatory cytokine secretion could be harmful to the extracellular pathogens, in *C. perfringens* associated myonecrosis caused by PFO, inflammasome activation is required¹⁸⁰.

2.12.3 Phagolysosomal Escape

In phagocytosis, the large particles, including extracellular pathogens (>0.5 μ m), are engulfed by innate immune cells (phagocytic cells) including, macrophages, dendritic cells, and neutrophils, to kill them¹⁸¹. Most of the CDCs producing extracellular pathogens cause phagocytosis interference to prevent phagosome and lysosome fusion and escape into the cytoplasm. Further, The listeriolysin O (LLO) and transgenic PFO were observed to promote the phagolysosomal escape of the *L. monocytogenes* or *Bacillus subtilis*^{182,183}. Escaping from the macrophages' phagosome also supports the other extracellular bacteria, including *C. perfringens* and *S. pyogenes*, causing infections^{54,184}.

2.12.4 Innate immune evasion

CDCs are also able to evade innate immune responses such as cytokine reduction. SLO and pneumolysin O (PLY) were reported for reducing cytokine production by interference in phagocytosis. Also, SLO is found for

¹⁸⁰ Yamamura, K.; Ashida, H.; Okano, T.; Kinoshita-Daitoku, R.; Suzuki, S.; Ohtani, K.; Hamagaki, M.; Ikeda, T.; Suzuki, T. Inflammasome Activation Induced by Perfringolysin O of *Clostridium perfringens* and Its Involvement in the Progression of Gas Gangrene. *Frontiers in Microbiology*. **10**, 2406 (2019).

¹⁸¹ Flannagan, R.S.; Jaumouillé, V.; Grinstein, S. The cell biology of phagocytosis. *Annual Review of Pathology: Mechanisms of Disease*. **7**, 61-98 (2012).

¹⁸² Jones, S., Portnoy, D.A. Characterization of *Listeria monocytogenes* pathogenesis in a strain expressing perfringolysin O in place of listeriolysin O. *Infection and Immunity*. **62**, 5608–5613 (1994).

¹⁸³ Portnoy, D.A., Tweten, R.K.; Kehoe, M., Bielecki, J. Capacity of listeriolysin O, streptolysin O, and perfringolysin O to mediate growth of *Bacillus subtilis* within mammalian cells. *Infection and Immunity*. **60**, 2710–2717 (1992).

¹⁸⁴ Hickey, M.J., Kwan, R.Y., Awad, M.M.; Kennedy, C.L., Young, L.F., Hall, P.; Corder, L.M., Lyras, D., Emmins, J.J. and Rood, J.I. Molecular and cellular basis of microvascular perfusion deficits induced by *Clostridium perfringens* and *Clostridium septicum*. *PLoS Pathog.* **4**, e1000045 (2008).

the degradation of IL-1 β by stimulating ubiquitination¹⁸⁵. Similarly, other CDCs, including PLY, also reported reducing pro-IL-1 β , IL-8, IL-12p70, TNF- α , and PFO for reducing TNF- α ¹⁸⁶. Some CDCs, including LLO and PFO, promote immune evasion by blocking NADPH oxidase localization to the phagosome¹⁸⁷. Another CDC, like SLO, inhibits the respiratory burst in neutrophils, and reduction of reactive oxygen species also affects the elastase secretion, IL-8, and neutrophil extracellular trap formation¹⁸⁸.

2.13 CDCs mediated Adaptive immune responses

Although CDCs try to damage the macrophages, these cells and other APCs represent the CDCs to MHC molecule to generate the adaptive immune responses. Antibodies generated against the CDCs, including ALO, PFO, and SLY found to protect the mice from lethal infections^{189,190,191}. Anti-CDCs are found very antigenic for humans as Anti-SLO, and anti-PLY titers appeared in human serum. Interestingly, the hemolytic activity and anti- CDCs and B cell immune responses are independent of each other, indicating that using the non-toxic form of CDCs can be used for vaccine development¹⁹². Indeed, vaccine

¹⁸⁵Hancz, D., Westerlund, E., Valfridsson, C., Aemero, G.M., Bastiat-Sempe, B., Orning, P., Lien, E., Wessels, M.R. and Persson, J.J. Streptolysin O Induces the Ubiquitination and Degradation of Pro-IL-1 β . *Journal of Innate Immunology*. **11**, 457–468 (2019).

¹⁸⁶Littmann, M., Albiger, B., Frentzen, A., Normark, S., Henriques-Normark, B.; Plant, L. *Streptococcus pneumoniae* evades human dendritic cell surveillance by pneumolysin expression. *EMBO Molecular Medicine* **1**, 211–222 (2009).

¹⁸⁷ Lam, G.Y., Fattouh, R., Muise, A.M., Grinstein, S.; Higgins, D.E., Brumell, J.H. Listeriolysin O suppresses phospholipase C-mediated activation of the microbicidal NADPH oxidase to promote *Listeria monocytogenes* infection. *Cell Host Microbe*. **10**, 627–634 (2011).

¹⁸⁸Uchiyama, S., Döhrmann, S., Timmer, A.M., Dixit, N., Ghochani, M., Bhandari, T., Timmer, J.C., Sprague, K., Bubeck-Wardenburg, J., Simon, S.I. and Nizet, V. Streptolysin O rapidly impairs neutrophil oxidative burst and antibacterial responses to group A *Streptococcus*. *Frontiers in Immunology*. **6**, 581 (2016).

¹⁸⁹Nakouzi, A.; Rivera, J.; Rest, R.F.; Casadevall, A. Passive administration of monoclonal antibodies to anthraxolysin O prolong survival in mice lethally infected with *Bacillus anthracis*. *BMC Microbiology*. **8**, 159 (2008).

¹⁹⁰ Stevens, D.L.; Tweten, R.K.; Awad, M.M.; Rood, J.I.; Bryant, A.E. Clostridial gas gangrene: Evidence that α and θ toxins differentially modulate the immune response and induce acute tissue necrosis. *Journal of Infectious Diseases*. **176**, 189–195 (1997).

¹⁹¹ Jacobs, A.A.; Loefer, P.L.; van den Berg, A.J.; Storm, P.K. Identification, purification, and characterization of a thiol-activated hemolysin (sulfolysin) of *Streptococcus suis*. *Infection and Immunity*. **62**, 1742–1748 (1994).

¹⁹²Carrero, J.A.; Vivanco-Cid, H.; Unanue, E.R. Listeriolysin O is strongly immunogenic independently of its cytotoxic activity. *PLoS ONE*. **7**, e32310 (2012).

generated against PLY toxoid has been beneficial against *S. pneumonia* infections¹⁹³.

2.14 PFO mediated other cell responses in the host

As summarised in **figure 5**, PFO promotes the pathogenesis of *C. perfringens* by affecting different immune cells in different ways. PFO may also be involved in the toxic shock directly or indirectly after exerting their effect on myocardial and mononuclear cells (**Figure 6**). It plays a crucial role in the progression of gas gangrene caused by *C. perfringens* by interfering in leukocyte and other immune cell recruitment at the infection site. In a mouse myonecrosis model, PFO was found to affect the circulation of the leucocytes and other immune cells by aggregating leucocytes and platelets in microvasculature¹⁸⁴.

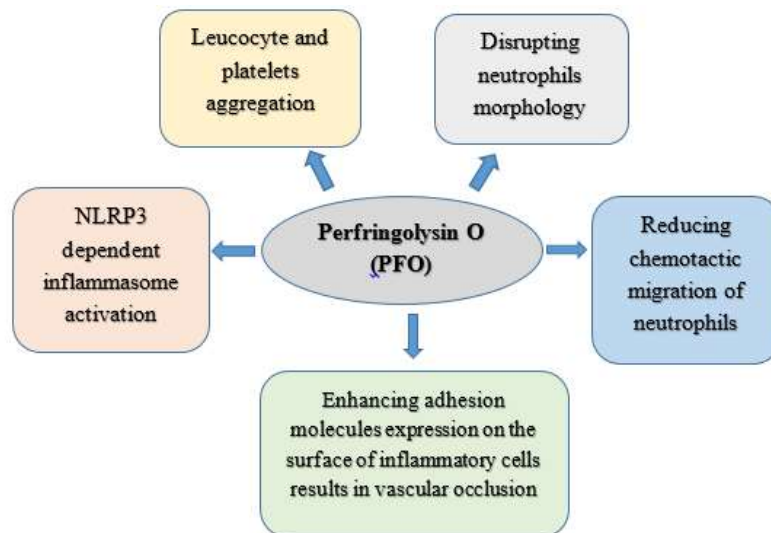


Figure 5. Different cellular responses and pathogenic outcomes occurred caused by PFO in *C. perfringens* infections.

Also, α -toxin and PFO synergistically increase the intravascular cell aggregation and vascular occlusion by enhancing the adhesion molecules on

¹⁹³Odutola, Aderonke, Martin OC Ota, Martin Antonio, Ezra O. Ogundare, YaubaSaidu, Patrick K. Owiafe, Archibald Worwui et al. "Immunogenicity of pneumococcal conjugate vaccine formulations containing pneumococcal proteins, and immunogenicity and reactogenicity of co-administered routine vaccines—A phase II, randomised, observer-blind study in Gambian infants. *Vaccine* **37** (19), 2586-2599 (2019).

the surface of inflammatory cells^{194,195}. Indeed, PFO was found to promoting neutrophil-dependent vascular occlusion and NLRP3 dependent inflammasome activation, which also promoted the leucocyte and platelets aggregation¹⁸⁰. Additionally, at sub lytic doses, PFO also affects the neutrophils' chemotactic migration and morphology by disrupting cytoskeleton polymerization and disassembly by upregulating adherence proteins. Thus PFO plays a significant role in the progress of gas gangrene and other pathogenic conditions caused by *C. perfringens*, which are described in the following sections¹⁹⁶.

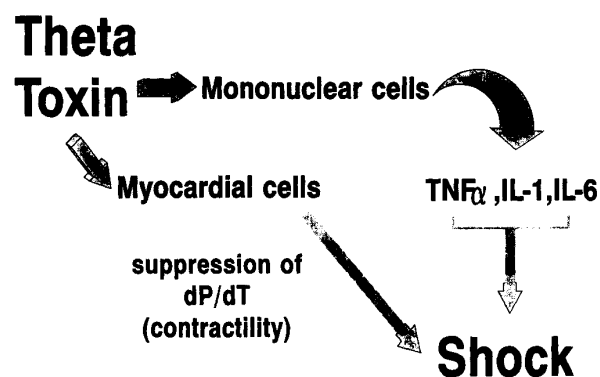


Figure 6. Mechanisms of PFO mediated toxic shock directly or indirectly during *Clostridium perfringens* infections. PFO can suppress myocardial contractility (dP/dT) directly resulted in declined cardiac output. Additionally, the cytokines, TNF α , IL-1, and IL-6 produced by mononuclear cells induced by PFO may also be involved indirectly in causing toxic shock. Reprinted with copyright permission from Oxford University Press Article Published in Infectious Diseases Society of America; Role of theta toxin, a sulfhydryl-activated cytolysin, in the pathogenesis of clostridial gas gangrene¹⁹⁷. (appendix no 2.2)

¹⁹⁴ Bryant, A.E., Bayer, C.R., Aldape, M.J., Wallace, R.J., Titball, R.W. and Stevens, D.L. *Clostridium perfringens* phospholipase C-induced platelet/leukocyte interactions impede neutrophil diapedesis. *J. Med. Microbiol.* **55**, 495–504 (2006).

¹⁹⁵ Bryant, A.E., Chen, R.Y., Nagata, Y.; Wang, Y., Lee, C.H., Finegold, S., Guth, P.H. and Stevens, D.L. Clostridial gas gangrene. I. Cellular and molecular mechanisms of microvascular dysfunction induced by exotoxins of *Clostridium perfringens*. *Journal of Infectious Diseases.* **182**, 799–807 (2000).

¹⁹⁶ Bryant, A.E., Bergstrom, R., Zimmerman, G.A., Salyer, J.L., Hill, H.R., Tweten, R.K., Sato, H. and Stevens, D.L. *Clostridium perfringens* invasiveness is enhanced by effects of theta toxin upon PMNL structure and function: The roles of leukocytotoxicity and expression of CD11/CD18 adherence glycoprotein. *FEMS Immunology and Medical Microbiology.* **7(4)**, 321–36 (1993).

¹⁹⁷ Stevens, D. L., and Bryant, A. E. Role of theta toxin, a sulfhydryl-activated cytolysin, in the pathogenesis of clostridial gas gangrene. *Clinical infectious diseases: an official publication of the Infectious Diseases Society of America*, **16 (4)**, S195–S199 (1993).

2.15 PFO Associated diseases

PFO was reported as one of the principal toxins secreted from *C. perfringens* isolates, type A after the α -toxin¹⁹⁸. Type A strains are one of the main causative agents of clostridial myonecrosis or gas gangrene in humans and several animals, including goats, horses, sheep, cats, dogs, and cattle¹⁹⁹. Although the α -toxin is widely accepted as the main toxin to cause clostridial myonecrosis, the involvement of PFO can also be considered in augmenting the pathological conditions in myonecrosis after determining its synergistic effect with α -toxin^{200,201}. Further, the synergistic action of PFO with α -toxin in causing myonecrosis was supported by determining the significantly decreased virulence effect of mutants lacking both genes in the mouse myonecrosis model.

PFO was also reported to assist the α -toxin in causing a type of enterotoxaemia in calves called necrohemorrhagic enteritis²⁰². Surprisingly, both α -toxin and PFO act in myonecrosis and necrohemorrhagic enteritis in different ways. Myonecrosis is characterized by thrombosis, tissue necrosis, and lack of leukocyte infiltration at the injection site, whereas necrohaemorrhagic enteritis is characterized by tissue congestion of the capillaries, hemorrhages, and inflammation. These different types of pathological conditions of the toxins in different organs indicate the toxins' organ-dependent effect.

¹⁹⁸Goossens, E., Verherstraeten, S., Valgaeren, B.R., Pardon, B., Timbermont, L., Schauvliege, S., Rodrigo-Mocholí, D., Haesebrouck, F., Ducatelle, R., Deprez, P.R. and Van Immerseel, F. Toxin-neutralizing antibodies protect against *Clostridium perfringens*-induced necrosis in an intestinal loop model for bovine necrohemorrhagic enteritis. *BMC veterinary research*. **12**, 1-8 (2016).

¹⁹⁹Beran, G.W. *Handbook of Zoonoses*, 2nd ed.; CRC Press: Boca Raton, FL, USA, x; 127–138 (1988).

²⁰⁰Awad, M.M., Ellemor, D.M., Boyd, R.L.; Emmins, J.J. and Rood, J.I. Synergistic effects of α -toxin and perfringolysin O in *Clostridium perfringens*-mediated gas gangrene. *Infect. Immun.*, **69**, 7904–7910 (2001).

²⁰¹Awad, M.M., Bryant, A.E., Stevens, D.L. and Rood, J.I. Virulence studies on chromosomal α -toxin and θ -toxin mutants constructed by allelic exchange provide genetic evidence for the essential role of α -toxin in *Clostridium perfringens*-mediated gas gangrene. *Molecular Microbiology*. **15**, 191–202 (1995).

²⁰²Verherstraeten, S., Goossens, E., Valgaeren, B., Pardon, B., Timbermont, L., Vermeulen, K., Schauvliege, S., Haesebrouck, F., Ducatelle, R., Deprez, P. and Van Immerseel, F. The synergistic necrohemorrhagic action of *Clostridium perfringens* perfringolysin and α -toxin in the bovine intestine and against bovine endothelial cells. *Veterinary Research*, **44**, 45 (2013).

2.15.1 Gas gangrene

Gas gangrene (myonecrosis) is a lethal pathogenic necrotic condition of the muscle tissue caused by an anaerobic bacterium, mainly *C. perfringens* isolates of type A. The introduction of bacteria to the host through open wounds results in traumatic injury. Deficiency of oxygen circulation in damaged tissue creates the anaerobic condition to facilitates the germination of spores and rapid growth of vegetative cells of *C. perfringens* that causes more necrosis, local edema, sepsis, fever, pain, and gas production that can lead to systemic toxemia, shock, and death, if not treated timely²⁰³. The soldiers have also been found dead in the wars due to this bacterium's infection after introducing the body's injured and open parts²⁰⁴. *Clostridial* myonecrosis is reported in animals (dogs, cats, horses, sheep, goats) and humans²⁰⁵. The two main toxins, alpha and PFO toxins secreted by *C. perfringens* type A, are responsible for necrosis and tissue damage in clostridial myonecrosis. Both toxins appeared to work synergistically in the progress of gas gangrene pathology as the lethal effect of both toxins was found to decline in the mutants lacking both genes in mouse myonecrosis model²⁰⁰. Clostridial infection stops the blood flow entirely at the infected site caused by trapping the blood vessel by aggregate formation mediated by alpha and PFO. Indeed, the two main characteristics of the gas gangrene pathogenesis, the vascular leukostasis and the paucity of leukocyte infiltration to the infection site, are caused by CPA and PFO^{46,206}. CPA and PFO both stimulate the ICAM-1 production and adherent glycoprotein CD11b/CD18 expression on the surface of endothelial cells that promote the

²⁰³ Bryant AE, Stevens DL. Clostridialmyonecrosis: new insights in pathogenesis and management. *Current Infectious Disease Report*. **12**, 383–391 (2010).

²⁰⁴ Alam, S. I., Dwivedi, P. Putative function of hypothetical proteins expressed by *Clostridium perfringens* type A strains and their protective efficacy in mouse model. *Infection Geneteics and Evolution*. **44**, 147–156 (2016).

²⁰⁵ Beran, G.W. *Handbook of Zoonoses*, 2nd ed.; CRC Press: Boca Raton, FL, USA. 127–138 (1994).

²⁰⁶ Ellemor, D.M.; Baird, R.N.; Awad, M.M.; Boyd, R.L.; Rood, J.I.; Emmins, J.J. Use of genetically manipulated strains of *Clostridium perfringens* reveals that both α -toxin and θ -toxin are required for vascular leukostasis to occur in experimental gas gangrene. *Infection and Immununity*. **67**, 4902–4907(1999).

leukostasis in vessels^{207,208}. Endothelial cells' integrity disruption promotes the local edema and, finally, systemic shock and multiorgan failure.

2.15.2 Treatment of gas gangrene

The rapid progressive nature of infection properly required early diagnosis and treatment to halt the infection, including surgical debridement of affected tissues or infected parts of the body, antibiotics, and hyperbaric oxygen therapy. Since the fast progressive nature of this disease's infection, only antibiotic therapy is not much effective. A combination of supportive therapies is required in a coordinated manner to halt the infection. Gas gangrene can be stopped early by adequate debridement of the wound and providing antibiotics and hyperbaric oxygen therapy simultaneously to halt the bacterium's growth and tissues' survival. There are many broad spectra of antibiotics recommended in necrosis conditions, including vancomycin and tazobactam or a carbapenem or ceftriaxone with metronidazole. However, penicillin plus clindamycin are strongly recommended if gas gangrene symptoms appeared, and clindamycin can inhibit the synthesis of exotoxins secreted by *Clostridium* bacterium. Penicillin and clindamycin can treat some other bacterial infections, such as group A streptococcal necrotizing fasciitis. Fasciotomy can also be advised to reduce compartment pressures to reduce ischemia and necrosis.

2.15.3 Enterotoxaemia

Enterotoxemia is a very lethal disease of veal calves and fast-growing suckler caused by *C. perfringens* isolates. Enterotoxemia characterized by sudden death without any pre-signatory symptoms within 24 h post-exposure to the bacterium. The mortality rate of veal calves in Belgium and thereby affecting

²⁰⁷Bryant, A.E. and Stevens, D.L. Phospholipase C and perfringolysin O from *Clostridium perfringens* upregulate endothelial cell-leukocyte adherence molecule 1 and intercellular leukocyte adherence molecule 1 expression and induce interleukin-8 synthesis in cultured human umbilical vein endothelial cells. *Infection and immunity*. **64(1)**, 358-362 (1996).

²⁰⁸Bryant, A.E., Bergstrom, R., Zimmerman, G.A., Salyer, J.L., Hill, H.R., Tweten, R.K., Sato, H. and Stevens, D.L. *Clostridium perfringens* invasiveness is enhanced by effects of theta toxin upon PMNL structure and function: the roles of leukocytotoxicity and expression of CD11/CD18 adherence glycoprotein. *FEMS Immunology & Medical Microbiology*. **7(4)**, 321-336 (1993).

the economic values²⁰⁹. The disease's significant symptoms are congestion of the capillaries, inflammation, hemorrhages, and necrosis of the small intestine and intestinal mucosa¹⁹⁸. Necrosis and hemorrhagic lesions in the small intestine of veal calves were identified by macro- post-mortem observation²¹⁰. It was suggested in a previous study that several toxins that could be present in all the isolates of *C. perfringens* could be responsible for the congestion of the capillaries within 30 min followed by starting intestinal necrosis and hemorrhages in 3-4h after the infection of the bacterium²¹¹. Subsequently, the synergistic alpha-toxin and PFO as the virulent toxins of *C. perfringens* were identified as causing bovine necrohemorrhagic enteritis, mainly in the veal calves²⁰²⁰². Additionally, PFO was also identified for the cytotoxicity on endothelial cells that line the small intestine wall in the development of necrohemorrhagic enteritis⁶¹.

CPA and PFO were also reported to enhance the lethal effect of the ETX toxin associated with type D enterotoxaemia on animals, including sheep and goats²⁹.

2.15.4 Treatment of enterotoxaemia

The rapid proliferation of bacterium in the gut's favorable condition leads to excess toxin production resulting in excessive intestinal necrosis, shock followed by death after the infection that makes less preventive measures. This condition could be controlled by inhibiting bacterial proliferation, preventing the absorption of toxins from the intestine, neutralizing already absorbed toxins (serotherapy), and additional treatment to counteract dehydration, acidosis, and shock, especially in pre-acute and acute cases. Bacterial proliferation can be inhibited by oral and parenteral antibiotic therapy.

²⁰⁹Pardon, B., De Bleecker, K., Hostens, M., Callens, J., Dewulf, J. and Deprez, P. Longitudinal study on morbidity and mortality in white veal calves in Belgium. *BMC Veterinary Research*, **8(1)**, 1-15 (2012).

²¹⁰Valgaeren BR, Pardon B, Verherstraeten S, Goossens E, TimbermontL, Haesebrouck F, Ducatelle R, Deprez PR, Van Immerseel F: Intestinal clostridial counts have no diagnostic value in the diagnosis of enterotoxaemia in veal calves. *Veterinary Record*. 172:237 (2013).

²¹¹Valgaeren B, Pardon B, Goossens E, Verherstraeten S, Schauvliege S, Timbermont L, Ducatelle R, Deprez P, Van Immerseel F: Lesion development in a new intestinal loop model indicates the involvement of a shared *Clostridium perfringens* virulence factor in haemorrhagic enteritis in calves. *Journal of Comparative Pathology*. **149**, 103–112 (2013)

Recently, extensive *in vitro* antibiotic sensitivity testing and *in vivo* antibiotic trials against *C. perfringens* in diarrhoeic sheep and goats revealed ciprofloxacin, penicillin, and ceftriaxone as the most effective antibiotics.

The involvement of PFO in causing other diseases from *C. perfringens* is remained to be explored. Moreover, it has also been reported to augment the virulence effect of ϵ toxin in causing type D enterotoxaemia in a mouse model²¹². Type D enterotoxaemia is one of the most dangerous clostridial diseases in animals that can lead to toxic shock and finally to death.

2.16 Vaccination

Vaccination is a type of approach to protecting humans and animals from infectious diseases. In this approach, vaccines are administrated in the body through different routes to develop the immune response, including adaptive and innate immune response against the outsider invaders²¹³. Vaccines could be live or killed microorganism or virus or proteins, or toxins from the pathogen²¹⁴. Moreover, emerging approaches enhance innate and adaptive immune responses by focussing on the immunological deconstruction of vaccines and mechanisms by which vaccines and adjuvant can sense the innate immune response. Vaccination is considered a more practical approach to eradicate infectious diseases. Indeed, vaccination has been very beneficial in eradicating smallpox worldwide and some very fatal diseases, including polio and tetanus^{215,216}. Moreover, WHO has also declared an estimation to save about 25 million lives from 2011 to 2020.

²¹²Fernandez-Miyakawa, M.E., Jost, B.H., Billington, S.J. and Uzal, F.A. Lethal effects of *Clostridium perfringens* epsilon toxin are potentiated by alpha and perfringolysin-O toxins in a mouse model. *Veterinary microbiology*. **127(3-4)**, 379-385 (2008).

²¹³Pulendran, B. and Ahmed, R. Immunological mechanisms of vaccination. *Nature immunology*. **12(6)**, 509 (2011).

²¹⁴Vetter, V., Denizer, G., Friedland, L.R., Krishnan, J. and Shapiro, M. Understanding modern-day vaccines: what you need to know. *Annals of medicine*. **50(2)**, 10-120 (2018).

²¹⁵Okwo-Bele, J.M. and Cherian, T. The expanded programme on immunization: a lasting legacy of smallpox eradication. *Vaccine*, **29**, D74-D79 (2011).

²¹⁶Aylward, B. and Tangermann, R. The global polio eradication initiative: lessons learned and prospects for success. *Vaccine*, **29**, D80-D85 (2011).

2.17 Vaccines

Vaccines are the biological preparation containing antigen and adjuvant to stimulate the generation of strong immune responses. Vaccines are broadly categorized into two groups, and the first group includes live attenuated vaccines (LAV) that could be bacteria or viruses that will have been rendered by reducing virulence property and believed not to be able to cause any disease²¹⁷. They can mimic the immune responses developed by the same pathogenic bacterium during infection²¹⁸. They can provide long-lasting immunity even in single immunization with developing strong cellular and antibody response⁷⁵. LAV has been recommended by WHO to use these vaccines against the pathogens causing infection, including smallpox, BCG, yellow fever, measles, mumps, rubella, and chickenpox^{219,220}. Although LAV is not considered a safe vaccine in immunocompromised individuals, it can revert into a virulent form²²¹.

Another class of vaccines is non-living, including subunit vaccines, toxoid vaccines, carbohydrate (vaccines against pneumococcus), and conjugate⁷⁵. As compared to live vaccines, they induce immune response for a shorter period, thereby requiring boosters to sustain the immune response for protection. Further, a part of the organism is made subunit vaccines to induce the immune response despite using the whole organism (live attenuated vaccines). Indeed, the surface protein and capsid are used against hepatitis B virus, human papillomavirus (HPV), respectively, and hemagglutinin and neuraminidase used against the influenza virus as the subunit vaccines^{222, 223}. Toxoid vaccines contain the inactivated toxins that are responsible for the pathogenesis of

²¹⁷Pulendran, B. and Ahmed, R., Immunological mechanisms of vaccination. *Nature immunology*, **12(6)**, 509 (2011).

²¹⁸Plotkin, S.A., Orenstein, W.A. and Offit, P.A. Vaccines 5th edn Saunders/Elsevier, Philadelphia, 2008.

²¹⁹Minor, P.D. Live attenuated vaccines: Historical successes and current challenges. *Virology*. **479**, 379-392 (2015).

²²⁰Benn, C.S., Fisker, A.B., Whittle, H.C. and Aaby, P. Revaccination with live attenuated vaccines confer additional beneficial nonspecific effects on overall survival: a review. *EBioMedicine*, **10**, .312-317 (2016).

²²¹Yang, H. and Ye, C. Reverse genetics approaches for live-attenuated vaccine development of infectious bursal disease virus. *Current Opinion in Virology*. **44**,139-144 (2020).

²²²Ho, J.K.T., Jeevan-Raj, B. and Netter, H.J. Hepatitis b virus (hbv) subviral particles as protective vaccines and vaccine platforms. *Viruses*. **12(2)**, 126 (2020).

microorganisms. These rendered harmless toxins are administered with aluminum or calcium-based adjuvants to elicit and increase the immune response. Tetanus and Diphtheria are an example of toxoid-based vaccines²²⁴. The conjugate vaccines are used to elicit the long-lasting protective immune response against weak immunogen, including bacterial outercoat polysaccharides, by linking with carrier proteins (diphtheria and tetanus toxoid). Example of conjugate vaccines includes *Haemophilus influenzae* type B vaccine and the meningococcal A vaccine introduced in Africa^{225,226}.

2.18 Adjuvants

An adjuvant is a substance that is essentially used in conjugated, inactivated, toxoid, and recombinant vaccines during vaccination and enhances the immune response for long-time protection by acting differently, as described in **Figure 7**. Mainly adjuvants are used with weak immunogen to improve the effectiveness of the vaccines. They also contribute to the better performance of vaccines. They help vaccine antigens to enhance an adaptive response by inducing innate responses like local inflammation. The meaning of an 'adjuvant' term is 'help' or 'aid' that comes from the Latin word adjuvant²²⁷. The adjuvant selection is a critical step in vaccination based on the balance between adjuvant properties and adverse effects.

Several adjuvant properties are listed below²²⁸:

- Biodegradable
- Stable
- Pure and defined composition

²²³Gupta, G., Glueck, R. and Patel, P.R. HPV vaccines: global perspectives. *Human vaccines & immunotherapeutics*. **13(6)**, 1421-1424 (2017).

²²⁴Havers, F.P., Moro, P.L., Hunter, P., Hariri, S. and Bernstein, H. Use of tetanus toxoid, reduced diphtheria toxoid, and acellular pertussis vaccines: updated recommendations of the Advisory Committee on Immunization Practices—United States, 2019. *Morbidity and Mortality Weekly Report*. **69(3)**, 77 (2020).

²²⁵Agrawal, A. and Murphy, T.F., 2011. *Haemophilus influenzae* infections in the H. influenzae type b conjugate vaccine era. *Journal of clinical microbiology*. **49(11)**, 3728-3732 (2011).

²²⁶Jódar, L., LaForce, F.M., Ceccarini, C., Aguado, T. and Granoff, D.M. Meningococcal conjugate vaccine for Africa: a model for development of new vaccines for the poorest countries. *The Lancet*. **361(9372)**, 1902-1904 (2003).

²²⁷Kool, M., Fierens, K. and Lambrecht, B.N., 2012. Alum adjuvant: some of the tricks of the oldest adjuvant. *Journal of medical microbiology*. **61(7)**, 927-934(2012).

²²⁸Aguilar, J.C. and Rodriguez, E.G. Vaccine adjuvants revisited. *Vaccine*. **25(19)**, 3752-3762 (2007)

- Immunopotenciating the vaccine antigen but not the host's tissue antigen

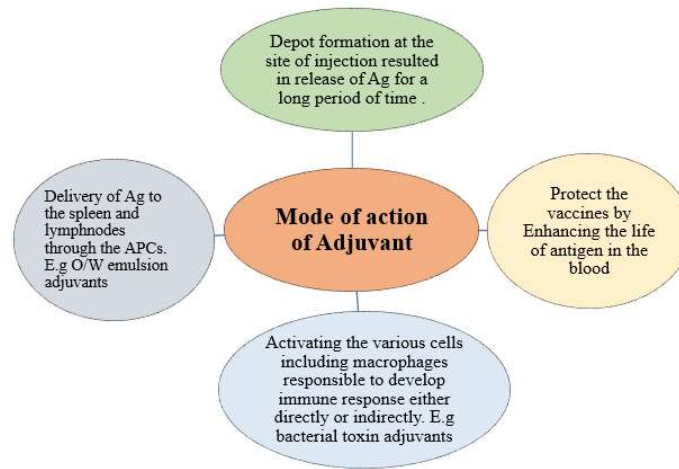


Figure 7. Action of Adjuvant in different way to enhance the immune responses generated by weak antigen²²⁹.

Different types of adjuvants are used with antigen in the vaccination with keeping things in mind the safety of the vaccine to enhance the immunogenic responses. However, the adjuvant classification is not very easy due to variability in adjuvant aspects of safety and other characteristics of the immunogenic vaccines. Nevertheless, the adjuvant can be classified as 1) antigen delivery system 2) immune potentiators (immunostimulatory) based on mechanism of action and mucosal adjuvants²³⁰.

The adjuvants that work as carriers of associated antigens to the target cells or antigen-presenting cells, including macrophages and dendritic cells, are considered antigen delivery systems, which are also known as particulate adjuvants. Additionally, these adjuvants can activate innate immunity. The mineral salts, including aluminum phosphate (AlPO_4), alum ($\text{Alk}(\text{SO}_4)_2 \cdot 12\text{H}_2\text{O}$), calcium phosphate (CaPO_4), and aluminum hydroxide

²²⁹Aguilar, J.C. and Rodriguez, E.G. Vaccine adjuvants revisited. *Vaccine*. **25(19)**, 3752-3762 (2007).

²³⁰Apostolico, J.D.S., Lunardelli, V.A.S., Coirada, F.C., Boscardin, S.B. and Rosa, D.S. Adjuvants: classification, modus operandi, and licensing. *Journal of immunology research*. **2016**, 1459394 (2016).

(Al(OH)₃), emulsion adjuvants, other lipid particles, and microparticles are used as the delivery system²²⁹. Alum is the most accepted adjuvant since it discovered in the 1920s as the safest adjuvant for the vaccination in human against many diseases, including hepatitis A (HAV), hepatitis B (HBV), diphtheria/ tetanus/pertussis (DTP), human papillomavirus (HPV), hepatitis B (HBV)²³¹. Although Alum was found to induce IgE antibody responses with some allergic reactions, it cannot induce the mucosal IgA antibody responses. Additionally, Alum is a weak adjuvant for antibody production by recombinant protein vaccines with inducing Th2 immune responses rather than Th1 responses²³². Thus, alum's use provides the limitation for those pathogens for that Th1 immune response is required that does not support using this alone.

Emulsion Adjuvants can be either water-in-oil or oil-in-water emulsion. Freund's adjuvant, a commonly used adjuvant in the mice experimental studies, is a type of water-in-oil emulsion. Further, this emulsion adjuvant consisting of an aqueous antigen in mineral oil was evolved during the study of tuberculosis, which was found to produce high antibody and delayed-type hypersensitivity in response to killed mycobacteria²³⁰. The mineral oil used in Freund's adjuvant was characterized by low specific gravity and low viscosity, including Drakeol 6VR (most commonly used in humans), branched-chain hydrocarbons, and aromatics and Article. Essentially, Freund's adjuvant is classified into two types, Complete Freund's adjuvant (CFA) and Incomplete Freund's adjuvant (IFA), based on the presence of heat-killed-mycobacteria. CFA, a water-in-oil emulsion containing heat-killed-mycobacteria, is generally used in experimental mice to evaluate vaccine potential and study autoimmune diseases. Indeed, the study on autoimmunity suggests that delayed-type hypersensitivity (DTH) is mediated by activation of Th1 immune responses through mycobacteria components. The major drawback of using CFA is to causing strong local inflammation formation of ulcer at the site of injection with severe pain, fever thereby CFA is allowed only for experimental animals

²³¹Lindblad E. B. Aluminium compounds for use in vaccines. *Immunology and Cell Biology*. **82(5)**, 497–505 (2004).

²³²Bajaj, A. K., Gupta, S. C., Pandey, R. K., Misra, K., Rastogi, S., and Chatterji, A. K. Aluminium contact sensitivity. *Contact Dermatitis*. **37(6)**, 307–308 (1997).

with numerous regulatory guidelines and not used for human or veterinary vaccines. Another Freund adjuvant IFA, a water-in-oil emulsion, is devoid of mycobacteria found to produce long-lived antibody titers against a human influenza vaccine²³³. It can induce first-line defense or local innate immunity characterized by phagocytosis, leukocyte infiltration, and cytokine production and enhance antigen lifetime due to the oily deposit antigen's continuous release²³⁴. However, the side effect of IFA included sterile abscesses reported by WHO, became the primary concern of the use²³⁵.

Another type of emulsion adjuvant, oil-in-water emulsion, including MF59 and AS03, highly participate adjuvants in developing potent immune responses against the flue. MF59 is licensed for use in routine flu vaccines and is considered a potent adjuvant as it can induce both cellular and humoral immune responses with a high titer of antibodies²³⁶. It was also approved for the H1N1 pandemic vaccine for pregnant women and young children licensed for pandemic and seasonal influenza vaccines in many countries. AS03 is squalene, α -tocopherol, and polysorbate containing oil-in-water adjuvant that was reported very effective adjuvant in developing robust and long-lasting immune responses using the influenza vaccine²³⁷.

Another type of delivery system adjuvant is the microparticles include *Virus-Like Particles (capsid, TLRs)*, virosomes, PML, PAML. Virus-like particles are very immunogenic due to their self-adjuvant characteristics and induce both cellular and humoral immune responses. Virosomes are non-virulent due to the absence of genetic material and works as a carrier of antigen through

²³³Salk J. E., and Laurent, A. M. The use of adjuvants in studies on influenza immunization. I. Measurements in monkeys of the dimensions of antigenicity of virus-mineral oil emulsions. *The Journal of Experimental Medicine*. **95(5)**, 429–447 (1952).

²³⁴Müssener, A., Klareskog, L., Lorentzen, J. C., and Kleinau, S. TNF- α dominates cytokine mRNA expression in lymphoid tissues of rats developing collagen- and oil-induced arthritis. *Scandinavian Journal of Immunology*. **42(1)**, 128–134 (1995).

²³⁵Miller, L. H., Saul, A., and Mahanty, S. Revisiting Freund's incomplete adjuvant for vaccines in the developing world. *Trends in Parasitology*. **121 (9)**, 412–414 (2005).

²³⁶Stephenson, I., Bugarini, R., Nicholson, K. G., Podda, A., Wood, J. M., Zambon, M. C., and Katz, J. M. Crossreactivity to highly pathogenic avian influenza H5N1 viruses after vaccination with nonadjuvanted and MF59-adjuvanted influenza A/Duck/Singapore/97 (H5N3) vaccine: a potential priming strategy. *Journal of Infectious Diseases*. **191(8)**, 1210–1215 (2005).

²³⁷Garçon, N., Vaughn, D. W., and Didierlaurent, A. M. Development and evaluation of AS03, an adjuvant system containing α -tocopherol and squalene in an oil-in-water emulsion. *Expert Review of Vaccines*. **11(3)**, 349–366 (2012).

reconstituted viral envelopes with membrane lipids and viral glycoproteins and induce strong and long-lasting immune responses. The most used virosomes platform is reported as influenza virosomes containing hemagglutinin (HA) and neuraminidase (NA) proteins within a membrane lipid²³⁸.

The second category of adjuvants is immunostimulators or immunopotentiators that help enhance the immune responses by inducing the APCs (dendritic cells, macrophages, natural killer cells, etc.) to release the pro-inflammatory cytokines. (IL-1, IL-2, IFN- γ , IL-12, and GM-CSF)²²⁹. Several immunostimulatory adjuvants, including Monophosphoryl lipid A (MPL), unmethylated CpG dinucleotides, and triterpenoid glycoside saponins, can induce the production of inflammatory cytokines including IL-1, IL-2, IFN- γ , IL-12, and GM-CSF.

The Third category of adjuvants described as mucosal adjuvants is used to potentiate the effect of mucosal vaccines. These adjuvants include the cholera toxin (CT) and heat-labile enterotoxin (LT) from *Vibrio cholerae* and *Escherichia coli*, respectively.

2.20 Vaccines against *C. perfringens*

C. perfringens associated diseases, including gas gangrene and enterotoxaemia, are fatal diseases due to the bacterium's fast-growing and heat-resistant spore formation nature. In gas gangrene, the bacterium or spores are responsible for causing tissue necrosis with reduced oxygen supply that antibiotics cannot adequately treat. The removal of infected tissues and other therapy, including administration of antibiotics and hyperbaric oxygen, has been only protective somehow. Therefore, using the vaccine to generate robust immune responses against *C. perfringens* infections could be considered an efficient and protective measure. Several approaches have been used to generate effective vaccine potential against *C. perfringens* in the past studies,

²³⁸Zurbriggen, R. Immunostimulating reconstituted influenza virosomes. *Vaccine*. **21(9-10)**, 921–924 (2003).

including denatured or formaldehyde inactivated toxoid and recombinant toxoid.

The use of denatured toxoids as the immunogens in animal models was protective against gas gangrene in the middle of the 20th century²³⁹. Also, a human experimental toxoid vaccine prepared by formalin-inactivated cultures was reported to be very effective in pigbel-related deaths in Papua New Guinea caused by *C. perfringens* type C¹¹⁵. However, this vaccine's production was not found to continue because the pigbel cases are still present in India's places, including Papua New Guinea²⁴⁰. Although the formaldehyde detoxified α -toxin was also used as experimental vaccines in humans, this toxoid's efficacy was reported quite variable. Therefore the formaldehyde inactivation approach of this toxin seemed not suitable to develop the vaccines^{241,242,243}.

Furthermore, the formaldehyde detoxified, and L-lysine protected formaldehyde inactivated α -toxin and PFO were reported to generate a high antibody titer after using it as the immunogen. However, the antisera were found to fail as a protective antibody and unable to be protective in the intestinal loop model¹⁹⁸. Nevertheless, formaldehyde inactivated toxins of *C. perfringens* other than α -toxin and θ -toxins, including NetB and epsilon toxoid, are reported to induce protective immunogenicity in cattle, sheep, goats, and piglets against types B, C, and D *C. perfringens* outbreaks^{244,245,246,247}. The

²³⁹ MacLennan, J.D. and MacFarlane. M.G. The treatment of gas gangrene. *British Medical Journal*. **683** (1944).

²⁴⁰ Duke, T., Poka, H., Myers, S., Radcliffe, J. and Pavlin, B.I. Pigbel in the 21st century: Still here, and still in need of an effective surveillance system. *Papua New Guinea Medical Journal*, **56**, 136–140 (2013).

²⁴¹ Kameyama, S., Sato, H. and Murata, R. The role of α -toxin of *Clostridium perfringens* in experimental gas gangrene in guinea pigs. *Japanese journal of medical science & biology*, **25**, 200 (1975).

²⁴² Boyd, N. A., Thomson, R. O. and Walker, P. D. The prevention of experimental *Clostridium novyi* and *C. perfringens* gas gangrene in high-velocity missile wounds by active immunisation. *Journal of Medical Microbiology*, **5**, 467–472 (1972).

²⁴³ Evans, D. G. The in-vitro production of alpha-toxin, theta-haemolysin and hyaluronidase by strains of *Cl. welchii* type A, and the relationship of in-vitro properties to virulence for guinea-pigs. *Journal of Pathology and Bacteriology*, **57**, 77–85 (1945).

²⁴⁴ Uzal, F.A. and Kelly, W.R. Protection of goats against experimental enterotoxaemia by vaccination with *Clostridium perfringens* type D epsilon toxoid. *Veterinary Record*, **142(26)**, 722–5 (1998).

²⁴⁵ Fernandes da Costa, S.P., Mot D, Bokori-Brown M., Savva CG, Basak AK, Van Immerseel F, Titball RW. Protection against avian necrotic enteritis after immunisation with NetB genetic or formaldehyde toxoids. *Vaccine*, **31(37)**, 4003–8 (2013).

toxoid-based veterinary vaccine against α -toxin is also commercially available and conditionally licensed by the FDA to protect the cattle by hemorrhagic bowel syndrome (HBS; or "bloody gut") and to control NE in chickens²⁴⁸. There are also some CPA, CPB, and ETX toxoid-based polyvalent veterinary vaccines that are commercially available. However, producing conventional toxoid-based clostridial vaccines has several weaknesses. It is dangerous for humans due to the pathogenic nature of bacteria, expensive, and inactivating toxin by formaldehyde, a very time-consuming process that can lose the toxoid's immunogenicity²⁴⁹. The lack of consistency in batch-to-batch fermentation affects the toxin production at a satisfactory level²⁵⁰.

These drawbacks of conventional vaccine production can be minimized by producing recombinant toxoid vaccines. These vaccines could be prepared using a non-pathogenic host, e.g., different *E. coli* strains for the expression of less toxic or non-toxic antigen in a large amount. Recombinant toxoid vaccines could be acceptable at the biosafety level and reduced time consumption for large-scale production. The antigen could be used as an immunologically active fragment, C-terminal or N-terminal domain of a toxin, and site-directed mutants of the toxins. These antigens could be safe and efficient for generating vaccine potential rather than using crude toxins, and formaldehyde inactivated toxins.

The formaldehyde-inactivated recombinant ETX (rETX) expressed in *E. coli* was reported for generating high antibody titer in rabbits compared to conventionally produced vaccines²⁵¹. Experimental recombinant vaccines as monovalent (single toxin) and polyvalent (two or more toxins) were generated

²⁴⁶ Kennedy, K.K. Norris, S.J.; Beckenhauer, W.H.; White, R.G. Vaccination of cattle and sheep with a combined *Clostridium perfringens* types C and D toxoid. *American Journal of Veterinary Research*. **38**, 1515–1517 (1977).

²⁴⁷ Schäfer, K., Wyder, M., Gobeli, S., Candi, A., Doherr, M.G., Zehnder, B., Zimmermann, W. Posthaus, H. Detection of *Clostridium perfringens* type C in pig herds following disease outbreak and subsequent vaccination. *Veterinary Record*. **171(20)**, 503 (2012).

²⁴⁸ Giri, B. and Kole, L. Combating the Perilous Consequence of Clostridial Gas Gangrene: An Overview. *Toxicology* (2014).

²⁴⁹ Titball, R.W. *Clostridium perfringens* vaccines. *Vaccine*. **27**, D44–D47 (2009).

²⁵⁰ Smith, L. Botulism and vaccines for its prevention. *Vaccine*. **27**, D33–9 (2009).

²⁵¹ Lobato, F.C.F., Lima, C.G.R.D., Assis, R.A., Pires, P.S., Silva, R.O.S., Salvarani, F.M., Carmo, A.O., Contigli, C. and Kalapothakis, E. Potency against enterotoxemia of a recombinant *Clostridium perfringens* type D epsilon toxoid in ruminants. *Vaccine*. **28**, 6125–6127 (2010).

against the toxins CPA, CPB, ETX, and NetBof *C. perfringens* have been studied extensively in previous studies. The C-terminal domain of CPA (CPA-C (247–370) identified as a robust immunogenic candidate as active immunization displayed protective responses in mice against experimental gas gangrene²⁵². The antibodies generated in calves against the C-terminal domain of CPA were found to have the neutralizing ability toward *C. perfringens*-induced endothelial cytotoxicity *in vitro*²⁵³. The antisera raised against the native toxin had a more robust neutralizing activity than those against the C-terminal fragment. However, antibodies against alpha-toxin alone were insufficient to completely neutralize the *C. perfringens*-induced necrosis in the intestinal loop model¹⁶⁷.

The multivalent vaccines or crude toxins were reported as more protective compared to monovalent that could be associated with the pathogenesis of *C. perfringens* mediated by secretion of a broad range of toxins. It is possible to design chimeras that consist of protective epitopes of different toxins and exclude the domains that do not confer immunity.

Together with perfringolysin O, the alpha-toxin has been identified as the principal toxin involved in the pathogenesis¹⁹⁸. The C-terminal alpha-toxin domain was identified as a robust immunogenic candidate generating immune responses in both mice and calves. The high antibody titer in sera obtained from immunized calves showed neutralizing antibodies against the toxins and the *C. perfringens*-induced endothelial cytotoxicity *in vitro*^{254, 255}. The antisera raised against the native toxin had a more robust neutralizing activity than

²⁵²Stevens, D.L., Titball, R.W., Jepson, M., Bayer, C.R., Hayes-Schroer, S.M. and Bryant, A.E. Immunization with the C-domain of α -toxin prevents lethal infection, localizes tissue injury, and promotes host response to challenge with *Clostridium perfringens*. *Journal of Infectious Diseases*. **190**(4), 767-773 (2004).

²⁵³Goossens, E., Verherstraeten, S., Valgaeren, B.R., Pardon, B., Timbermont, L., Schauvliege, S., Rodrigo-Mocholí, D., Haesebrouck, F., Ducatelle, R., Deprez, P.R. and Van Immerseel, F. The C-terminal domain of *Clostridium perfringens* alpha toxin as a vaccine candidate against bovine necrohemorrhagic enteritis. *Veterinary research*. **47**(1), 52 (2016).

²⁵⁴Jiang, Z., De, Y., Chang, J., Wang, F. and Yu, L. Induction of potential protective immunity against enterotoxemia in calves by single or multiple recombinant *Clostridium perfringens* toxoids. *Microbiology and immunology*. **58**(11), 621-627 (2014).

²⁵⁵Goossens, E., Verherstraeten, S., Valgaeren, B.R., Pardon, B., Timbermont, L., Schauvliege, S., Rodrigo-Mocholí, D., Haesebrouck, F., Ducatelle, R., Deprez, P.R. and Van Immerseel, F. The C-terminal domain of *Clostridium perfringens* alpha toxin as a vaccine candidate against bovine necrohemorrhagic enteritis. *Veterinary research*. **47**(1), 52 (2016).

those against the C-terminal fragment. However, antibodies against alpha-toxin alone were insufficient to completely neutralize the *C. perfringens*-induced necrosis in the intestinal loop model. The development of a multivalent vaccine combining the C-terminal fragment of alpha-toxin with other *C. perfringens* virulence factors might be necessary for complete protection against bovine necrohemorrhagic enteritis.

Thus, the above literature clearly reflects the important role of the PFO as a pore forming toxin in enhancing lethal effects of toxins, which it achieves by affecting macrophages and other immune cells during *C. perfringens* infections. Like other CDCs, PFO can generate the adaptive immune responses. Despite its effect in potentiating the effect of other *C. perfringens* toxins, and its antigenic characteristics, PFO has not yet been explored for its vaccine potential. The non-toxic variants could be used in multivalent vaccine generation to potentiate the effect of the vaccine against *C. perfringens* A. Its function with other toxins is also yet to be explored. In the present study, we have targeted the C-terminal domain of PFO and its non-toxic variants (V208C, A212C, and R467A) for their immunogenic potential in murine model. Antisera generated against these PFO variants is also assessed for their neutralizing potential. Results from the work are organized in the order of performance that includes expression and purification analysis, biological activity characterisation, evaluation of immune response, assessment of neutralization potential of immunization. The discussion chapter discusses these results in the same order.

Chapter 3

Materials and Methods

Bacterial strains and mammalian cell lines

Escherichia coli DH5 α and BL21(λ DE3)pLysS were obtained from GIBCO-BRL, USA and Novagen, USA respectively. The DH5 α and BL21(λ DE3)pLysS cells transformed with commercially procured gene constructs were used for the sequence analysis, and recombinant protein expression analysis, respectively.

THP-1 (human monocytic cell; phagocytic cells) used to determine the cytotoxicity of the WTrPFO and its mutants were procured from National Center for Cell Science (NCCS), Pune, India. The toxin is believed to be resistant to phagocytosis and cytotoxic to the phagocytic cells. THP-1 cells were maintained in complete RPMI-1640 containing 10 % FBS and (1% Penicillin-Streptomycin). The MDCK (Madin-Darby Canine Kidney; epithelial cells) cells were procured from NCCS, Pune and were maintained in complete DMEM medium (DMEM, 10%FBS, 1% Penicillin-Streptomycin).

Animals

Swiss albino female mice aged 4-6weeks old used in the study were bred and maintained at the Central Laboratory Animal Resources (CLAR), JNU. Each set/group of mice were housed there in separate cages as per the requirement in appropriate housing conditions (temperature 20-26°C, illumination 325-350 lux, humidity ~ 40-70%, room vent ~ 10-20 ACH). The animals were given drinking water (RO) and food *ad libitum*¹. Approval for the animal usage in the present study was granted by the Institutional Animal Ethics Committee of the University (Project code: IAEC # 03/2019).

Glassware, plasticware, and apparatus

Different wares and apparatuses used in the study are listed in Table 1.

¹Sharma, M., Dash, P., Sahoo, P.K. and Dixit, A. Th2-biased immune response and agglutinating antibodies generation by a chimeric protein comprising OmpC epitope (323–336) of *Aeromonas hydrophila* and LTB. *Immunologic Research*. **66(1)** 187-199 (2018).

Table 1. List of glassware, plastic ware, and apparatus

| Plastic Ware and glassware | Size | Source |
|--------------------------------------|---|---|
| Sterile conical bottom culture tubes | 15 ml and 50 ml | Falcon, USA, Nunc, USA |
| Disposable pipettes | 5ml, 10ml, 25ml, and 50ml | Greiner, Germany, Tarsons, India or Abdos, India. |
| Pipette tips | 10 μ l, 20 μ l, 200 μ l, and 1000 μ l | Greiner, Germany, Tarsons, India or Abdos, India. |
| Microcentrifuge tubes | 0.5ml, 1.5ml, and 2ml | Greiner, Germany, Tarsons, India or Abdos, India. |
| Petridish | | Greiner, Germany, Tarson, India or Abdos |
| ELISA plates | 96-well, flat bottom, high binding | Nunc, Corning |
| Glassbeakers and Flasks | 50 ml, 250 ml, 500ml, 1L, 2L, and 5L | Borosil, India |
| Filters | 0.22 micron, 0.45 micron | Advanced Microdevices Pvt. Ltd., India |
| Dialysis membrane | Cutoff 14 kDa, 3.5kDa | Sigma-Aldrich Chemical Co., USA |
| Centricons | Cut off 30 kDa | Millipore, Pall, USA |
| Mammalian cell culture plates | 6-, 12-, 24-, 96- well plates | Thermo Fisher Scientific. USA & Corning Incorporated, USA |
| Culture Flasks | 25 cm ² and 75 cm ² | Greiner, Falcon, Corning, USA |
| Syringes | 1 ml, 2 ml, 5 ml, 10 ml, and 50 ml | Dispovan, India |
| Whatman filters | 1 mm and, 3 mm | Advanced Microdevices Pvt. Ltd., India |
| Apparatuses | Agarose Gel electrophoresis, SDS-PAGE apparatus, Western blot | Biorad Laboratories, Inc., USA |

Chemicals, reagents, and kits

All the chemicals and reagents used in the study were of molecular biology grade. Different chemicals, reagents, and kits used in the study are listed in Table 2.

Table 2. List of chemicals, reagents, and kits with their sources

| Chemicals, reagents, and kits | Source |
|---|--|
| Roswell Park Memorial Institute medium (RPMI)- 1640, Dulbecco's modified eagle medium (DMEM), Foetal Bovine serum (FBS), Penicillin-streptomycin antibiotic solution, Trypan blue dye, XTT (2,3-Bis-(2-Methoxy-4-Nitro-5, Sulfophenyl)-2H-Tetrazolium-5-Carboxnilide) kit (cat. no. 20-300). | Biological industries, Israel |
| Propidium Iodide (PI), Dimethyl sulfoxide (DMSO), paraformaldehyde (PFA), Agarose (high melting and low melting), Ammonium persulphate, Bromophenol blue, 1,4-Dithiothreitol (DTT), Ethylene diamine tetraacetic acid (EDTA), Imidazole, Kanamycin monosulphate, Lysozyme, Methylene blue, RNaseA, Trizma base, Xylene cyanol, β -mercaptoethanol, Ficoll, Freund's complete adjuvant (FCA), Freund's incomplete adjuvant (IFA), Alkaline phosphatase-conjugated anti-Fc antibody, Alkaline phosphatase-conjugated anti-his antibody. | Sigma-Aldrich Chemical Co., USA |
| Potassium phosphate dibasic (K_2HPO_4), Monopotassium phosphate (KH_2PO_4), Sodium phosphate dibasic (Na_2HPO_4), Monosodium phosphate (NaH_2PO_4), Sodium chloride (NaCl), Ampicillin, p-Nitrophenyl Phosphate (PNPP), Bovine serum albumin (BSA), Glycerol, Hydrochloric acid (HCl). | Sisco Research Laboratories Pvt. Ltd., India |
| DNA molecular weight ladder (λ EcoRI/ HindIII) (Cat. No. SM0192), Prestained Protein molecular weight marker (Cat. No. 26620), Unstained protein molecular weight marker (Cat. No 26610). | Thermo Fisher scientific, USA |
| Ni^{2+} -NTAresin, Urea, Bicinchoninic acid assay (BCA) protein estimation kit (Cat. No. 786-570). | G-Biosciences, USA |
| LB (Luria Bertani)-agar, LB Broth, Bactotryptone, Bacto agar, Bactoyeast extract. | Hi-Media Laboratories, India |
| Tween-20, Triton-X-100, Methanol, Chloroform, Isoamylalcohol. | Merck, Germany |

Materials & Methods

| | |
|--|--------------------------|
| DNA molecular weight ladders. | New England Biolabs, USA |
| Acrylamide, Calcium chloride (CaCl ₂), Ethidium bromide (EtBr), Isopropyl thiogalactoside(IPTG), N-N'-N'-N'- tetramethylethylenediamine (TEMED), Western blue substrate, LDH assay kit (Cat. No C20300). | Promega, USA |
| Acetic acid, Formaldehyde, magnesium chloride (MgCl ₂), Potassium acetate (CH ₃ COOK), sodium acetate (CH ₃ COONa). | SD Fine chemicals, India |
| Horseshoe peroxidase (HRP)- conjugated anti-IgG1,anti-IgG2a, and anti-IgG2b antibodies | eBiosciences, USA |
| 3,3',5,5'-Tetramethylbenzidine (TMB) substrate reagent (Cat. No. 555214), Cytokine ELISA kit (Cat. No. 555138). | BD Biosciences, USA |

Gene constructs

For the construction of recombinant plasmids encoding various proteins, synthetic genes listed in Table.3 were obtained from GenScript, USA. The His-tagged gene constructs were designed by cloning synthetic genes encoding the wild type mature PFO (without the signal sequence), based on the sequence information available for *C. perfringens pfo* gene (GenBank Accession number: M36704), its mutant with single amino acid substitution (V208C, A212C and R467A), or deletion variant encoding only, the C-terminal domain comprising amino acid residues 390 to 499 (PFO_{C-ter}) in the expression vector pET22b(+) at the *Nde*I and *Xho*I restriction sites. The encoded recombinant proteins will have 9 additional residues (a methionine at the N-terminus and 8 additional amino acid residues (including 6 histidines at the C-terminus), contributed by the vector as a result of the cloning strategy.

Table3. Details of the plasmid constructs used in the study

| Name of the construct | GenScript Clone ID | Vector backbone | Recombinant Protein product | Recombinant protein length (including vector sequences) | Computed molecular weight (kDa) |
|------------------------------------|--------------------|-----------------|-----------------------------|---|---------------------------------|
| pET22. <i>PFO</i> _{wt} | K72803 | pET22b(+) | WTrPFO | 482 aa | 53922.24 |
| pET22. <i>PFO</i> _{C-ter} | K72110 | pET22b(+) | rPFO _{C-ter} | 119 aa | 13807.24 |
| pET22. <i>PFO</i> _{V208C} | C17576 | pET22b(+) | rPFO _{V208C} | 482 aa | 53926.25 |
| pET22. <i>PFO</i> _{A212C} | C17584 | pET22b(+) | rPFO _{A212C} | 482 aa | 53954.30 |
| pET22. <i>PFO</i> _{R467A} | C18249 | pET22b(+) | rPFO _{R467A} | 482 aa | 53837.13 |

3.2. Methodology

3.2.1. Bacterial cell cultures

Autoclaved LB-agar plates (1.5 % Bactoagar, 1 % NaCl, 1 % tryptone and 0.5% yeast extract, pH 7.4) and LB broth medium (1 % NaCl, 1 % tryptone and 0.5% yeast extract, pH 7.4) were used for culturing *E. coli* DH5 α and BL21(λ DE3) pLysS cells . Both *E. coli* strains, DH5 α and BL21(λ DE3) pLysS, were grown overnight using LB-agar medium in sterilized petri dish at 37°C and in LB broth medium in sterile culture tubes or culture flask at 37°C with continuous shaking at 200 rpm (Kuhner shaker LT-X, Switzerland). The overnight grown bacterial cells in agar or broth culture were kept in 4°C for short time storage. Sterile ampicillin (filtered using 0.45-micron filter) at the working concentration of 100 μ g/ml was added to LB-agar and LB broth for culturing the cells transformed with the recombinant plasmids.

3.2.3. Cryopreservation of the bacterial cells (Glycerol stock preparation)

Bacterial cells at their exponential phase were considered for cryopreservation. Bacterial cells were grown until the OD₆₀₀ reached 0.6-0.8 (exponential phase). Subsequently, 700µl of grown cells were mixed with 300µl of autoclaved glycerol (cryoprotectant) very gently with sterile pipette in a cryovial and stored at -80°C for long time storage and future use.

3.2.3. Medium preparation for animal cell culture

Dry 1-L RPMI-1640 or DMEM powder (very hygroscopic) was added in 900ml of autoclaved MilliQ water in a clean autoclaved transparent glass bottle and dissolved properly by continuous stirring. Subsequently, sodium bicarbonate was added in dissolved RPMI-1640 and DMEM medium (2g and 3.7g, respectively) The pH (pH 6.8-7.2) of the medium was adjusted with 1M HCl or 1N NaOH and the volume made up to 1 liter. The prepared 1×DMEM/RPMI-1640 medium was filter-sterilized using a 0.22-micron filter in biological safety cabinets and stored at 4°C. Complete medium was prepared by adding heat-inactivated fetal bovine serum (FBS) to a final concentration of 10 %. Penicillin-streptomycin antibiotic solution was added to the medium to a final concentration of 1× (penicillin, 100U/ml; streptomycin, 100µg/ml), just prior to use in cell culture.

3.2.4. Animal cell culture

The mammalian cells used in the study were cultured and maintained in the complete medium [1×medium (RPMI-1640 or DMEM) supplemented with 10% FBS, and Penicillin (100U/ml)-Streptomycin (100µg/ml)] at 37°C in 5% CO₂ atmosphere. To revive the frozen cells, the medium was warmed at 37°C and aliquoted about 30 ml in 50 ml falcon. A vial of the frozen cells (THP-1/MDCK cells in FBS and 10% DMSO) was defrosted at 37°C and quickly transferred to a culture tube (15 ml cell culture centrifuge tube) containing warm medium, followed by centrifugation at 1000rpm for 5min. The supernatant was discarded to remove the DMSO, and the cell pellet was resuspended with 5-8 ml medium in T25 flask at 37°C overnight in 5% CO₂ atmosphere. The next day, the medium was replaced with the fresh medium to remove the traces of DMSO. After that,

the cells were passaged upon attaining 80 %-90% confluency and monitored regularly. The MDCK cells are adherent in behavior. Therefore, after removing the medium, the cells were washed with 1×phosphate buffered saline (1× PBS, 137 mM NaCl, 2.7 mM KCl, 10 mM Na₂HPO₄, 1.8 mM KH₂PO₄, pH 7.4) to remove the debris. The cells were then resuspended in 1×Trypsin-EDTA solution (0.2% trypsin, 0.02%EDTA, 0.05% glucose in 1×PBS) for 5 min at 37°C to detach the cells from the surface. Freshly prepared complete medium was then added to reduce the trypsin activity. The cells were then centrifugated at 1000rpm (REMI R-4C centrifuge, R-41 rotor) for 5 min, the supernatant was removed and the cell pellet was resuspended in the complete medium and processed further i.e. counting, subculturing and preservation.

3.2.5. Cell counting

The counting of viable cells was performed using trypan blue exclusion assay using a hemocytometer². Trypan blue exclusion assay is based on the exclusion of trypan blue dye by the viable cells due to an intact cell membrane that appears bright under the illumination. On the other hand, the dead cells become blue due to the entry of the dye through the damaged or porous plasma membrane into the cytoplasm. The harvested cells were uniformly resuspended in the adequate medium. The cell culture suspension (10 µl) was aliquoted under sterile conditions and mixed with 10µl of trypan blue by gentle pipetting (1:1 dilution; dilution factor=2). Approximately, 10µl of the mixed cell suspension was put in both the chambers of a hemocytometer and covered with a glass coverslip. The cells were visualized and the viable cells (unstained) were counted in the 16 grids (4×4) in all the 4 squares of the hemocytometer under a bright-field microscope (Leica, USA) at 10 × magnification. All the viable cells counted in 4 squares were divided by 4 to determine the average number of cells per square. The viable cell density per ml was calculated using the following formula:

²Crowley, L.C., Marfell, B.J., Christensen, M.E. and Waterhouse, N.J. Measuring cell death by trypan blue uptake and light microscopy. *Cold Spring Harbor Protocols*, 7 (2016).

Total number of viable cells = Dilution factor × Average cell population of four square × 10⁴

3.2.6. Cryopreservation of the animal cells

After three passages at 80-90 % confluency, the cells were collected by centrifugation at 1000rpm for 5 min and resuspended in freezing medium (FBS and DMSO in 9:1 ratio), and transferred into labeled cryovials (the name of the cell line, passage no. and date). The cells were kept in a cryobox, and stored at -20°C for an hour, followed by transfer to -80°C for O/N and finally transferred into a liquid nitrogen tank for long time storage.

3.2.7. Plasmid isolation at mini scale (Miniprep)

Plasmid DNA for the screening of the transformed colonies was prepared at a mini scale by the method of Sambrook and Russel³. A single colony of *E. coli* cells harboring the plasmid was picked from the L-agar plate and inoculated into LB broth medium supplemented with ampicillin. The bacterial culture was allowed to grow at 37°C with shaking (200rpm). Overnight grown bacterial culture (1.5ml) was centrifuged at 6000rpm (Eppendorf centrifuge 5415R, UK) at RT for 10 min. The supernatant was discarded and the bacterial cell pellet was resuspended in 100µl of solution I (25 mM Tris-HCl-, 10 mM EDTA, pH 8.0, 50 mM glucose) containing lysozyme (freshly added at a final concentration of 4mg/ml), and incubated at RT for 5 min. Freshly prepared solution II (0.2% NaOH, 1% SDS, 200 µl) was then added to it and kept on ice for 5 min. The solution was mixed properly by gently inverting several times until the solution became clear. Subsequently, solution III (5M potassium acetate solution, pH 5.2, adjusted with glacial acetic acid; 3M with respect to potassium and 5M with respect to acetate) was added to the clear solution and incubated at 4°C for 15 min followed by centrifugation at 4°C (13000 rpm, Eppendorf centrifuge 5415R, UK) for 10 min. The supernatant layer was collected into a fresh Eppendorf tube

³Sambrook, J. and Russell, D.W. Preparation of plasmid DNA by alkaline lysis with SDS: mini preparation. *Cold Spring Harbor Protocols*. 1, 4084 (2006).

very carefully and extracted with Tris buffer (pH8.0)-saturated phenol: chloroform: isoamyl alcohol (PCI, 25:24:1) and chloroform: isoamyl alcohol solution (CI) to remove the proteins from the solution. The PCI extraction was carried out by adding an equal volume of the PCI solution to the supernatant, gently mixed by inverting about 10 times, followed by centrifugation (13000 rpm) at 4°C for 10 min. The aqueous layer obtained was collected in a fresh tube and further extracted by adding an equal volume of CI as for the PCI extraction. The aqueous layer thus obtained was transferred into a fresh tube and DNA was precipitated by adding two volumes of chilled 95% ethanol. The pelleted DNA was collected by centrifugation (12000×g, 4°C, 5 min). The pellet obtained was washed three times with 70% ethanol, dried under vacuum using Speed Vac (SAVANT ISS110 speed vac concentrator, Thermo scientific, USA), and resuspended in 20µl 1×TE (10mM Tris-HCl, -, 1mM EDTA, pH 8.0) containing RNase A (20µg/ml) and incubated at 37 °C for up to 2 h or overnight. DNA content was quantified by NanoDrop and the quality of the plasmid DNA was checked by Agarose gel (1%) electrophoresis. The DNA was stored at -20°C.

3.2.8. Plasmid isolation in large scale (Midiprep)

The alkaline lysis method was used for the isolation of DNA with some modifications⁴. A single colony of *E. coli* cells harboring plasmid construct was grown in 5ml LB broth medium supplemented with ampicillin(100µg/ml) overnight at 37 °C and 200 rpm (primary culture). A secondary culture (200 ml) was set by inoculating with 1% primary culture in LB medium containing ampicillin and grown overnight at the conditions mentioned earlier. The cells from the overnight grown culture were pelleted down by centrifugation at 6000rpm (Eppendorf centrifuge 5415R, UK) in Oakridge centrifuge tube at 4°C, for 10min. The pelleted cells were resuspended in 4ml solution I and incubated at RT for 10min. This was followed by the addition of 6ml of freshly prepared solution II, mixed very gentle mixing by inversion and incubation for 10 min at RT till the solution became clear. Subsequently, 5ml of solution III was added

⁴Sambrook J, Fritsch EF and Maniatis T) Molecular cloning: a laboratory manual, Cold Spring Harbor Laboratory Press, New York. (1989).

to this, mixed thoroughly and incubated at 4°C for 15 min, followed by centrifugation at 13000 rpm (Heraeus Stratos Biofuge, 3555 rotor) at 4°C for 30 min. The supernatant was collected in the round-bottom glass centrifuge tubes (Corex), and subjected to extraction with equal volume of PCI and CI as described before by mixing and centrifugation (6000 rpm, Heraeus Stratos Biofuge, 3555 rotor) at RT for 10 min. DNA present in the aqueous layer was precipitated by adding 0.7 volumes of isopropanol and incubation at RT for 15 min. This was followed by centrifugation forat 13000 rpm (4 °C, 30 min) to collect the precipitated DNA. The DNA was washed with 70% ethanol to remove excess salts. DNA thus obtained was dissolved in 1×TE containing 20µg/ml RNaseA and kept O/Nat37°C. Quantity and quality of the purified DNA were analyzed by agarose gel electrophoresis followed by visualization in a UV transilluminator (Bio-Rad Laboratories, USA).

3.2.9. Restriction enzyme Digestion analysis

The reaction mixtures consisting of the plasmid construct, restriction enzymes (*NdeI* and *XhoI*, 1U/µg of plasmid) and cutSmart Buffer (1×) was incubated at 37 °C for overnight. Subsequently the samples were analysed by agarose gel electrophoresis (1.2 %).

3.2.10. Agarose gel electrophoresis

This method was used for separating and analyzing the quality and quantity of the isolated DNA. The procedure was followed as per the lab manual with minor modifications⁴. For the agarose gel preparation, an appropriate amount of agarose to prepare 0.8% or 1.2% agarose gel (for resolving DNA fragment of 5-10kb and 0.2-1kb, respectively) was weighed and dissolved in 1×TAE buffer (40mMTris, 20mM acetic acid, and 1mM EDTA, pH 8.0) by boiling in the microwave with intermittent swirling till the solution became clear (minimum 45 sec). The boiled agarose was kept at RT to cool till the temperature reached approximately 40°C-45°C, followed by the addition of the intercalating dye, ethidium bromide (EtBr; 5µg/ml). The agarose solution was poured into the casting tray, and allowed to solidify after inserting an appropriate comb to create the sample slots in the gel. After solidification, the comb was removed

from the gel and the tray was placed into the electrophoresis tank. The tank was then filled with 1×TAE buffer, pH 8.3 to cover the gel. DNA samples were mixed with the 6× gel-loading dye to final concentration of 1× and loaded into the slots of gel. The gel was electrophoresed at constant voltage (5V/cm) until the loading dye reached the appropriate distance from the bottom (about 1cm). After electrophoresis, the gel was visualized using a UV transilluminator (Bio-Rad Laboratories, USA).

3.2.11. DNA quantification

The concentration of DNA was measured by spectrophotometric using NanoDrop⁵. Before starting the quantification of DNA, both lower and upper pedestals of the NanoDrop were cleaned with Milli-Q water and wiped using lint-free lab wipes. For the blank, 1× TE was used. DNA (2 µl) was used for quantification. Absorbance of the DNA was measured at 260-280 nm. The dsDNA absorbed the light at 260 nm and other contaminants such as protein absorb at 280 nm. The ratio of the absorbance at 260nm/280nm of 1.8 was considered good quality of DNA without protein and other contaminations. The optical density of DNA ~1 was correlated to DNA concentration of 50 ng/µl.

3.2.12. Competent cell preparation

Competent cells were prepared by CaCl₂ method as described earlier with minor modifications^{6,7}. *E. coli* cells (DH5α or BL21(λDE3)pLysS strains) from the glycerol stocks were streaked on sterilized LB agar plates and incubated (Kuhner incubator shaker LT-X, Switzerland) at 37°C overnight to generate the bacterial colonies. The next day, a single colony was inoculated in 10 ml LB broth medium and incubated at 37°C overnight with shaking at 200 rpm (primary culture). Next day 1 % of overnight grown culture was inoculated in 100ml LB

⁵Desjardins, P. and Conklin, D. Nano Drop micro volume quantitation of nucleic acids. *Journal of Visualized Experiments*. **45**, 2565 (2010).

⁶Mandel, M. and Higa, A., Calcium-dependent bacteriophage DNA infection. *Journal of molecular biology*. **53(1)**, 159-162 (1970).

⁷Tang, X., Nakata, Y., Li, H.O., Zhang, M., Gao, H., Fujita, A., Sakatsume, O., Ohta, T. and Yokoyama, K. The optimization of preparations of competent cells for transformation of *E. coli*. *Nucleic acids research*. **22(14)**, 2857 (1994).

broth medium (secondary culture) and incubated at 37°C with continuous shaking at 200rpm until the absorbance at 600 nm reached about 0.4-0.6. The bacterial culture then was chilled on ice by swirling gently for 30 min. The chilled culture was then centrifuged at 4°C for 10 min at 4000 rpm, the supernatant was discarded and the cells were re-suspended gently (gentle swirling) in chilled 100mM CaCl₂ (1/10th volume of bacterial culture) and incubated on ice for 30 min. Bacterial cells were then centrifuged at 4°C for 10 min at 4000 rpm. The supernatant was discarded and recovered bacterial cells were re-suspended in 100mM CaCl₂ and 20% glycerol (1/100th volume of bacterial culture) and incubated overnight at 4°C. The competent cells thus prepared were aliquoted in small aliquots of 100 µl and 200 µl in pre-chilled microcentrifuge tubes and stored at -80°C.

3.2.13. Transformation

Transformation of competent *E. coli* DH5α and *E. coli* BL21(λDE3)pLysS cells was carried out as per the protocol described by Sambrook *et al.* with some modifications⁴. The transformation of the competent cells was initiated by adding sufficient concentration (40-80 ng) of recombinant supercoiled plasmid DNA to 100µl aliquot of competent cells (thawed at 4°C) and mixing thoroughly but gently. The plasmid DNA-competent cells mixture was immediately kept on ice for 25 min. Subsequently, the cells were given a heat shock at 42°C for 90 sec. Heat shocked cells were immediately returned to ice for 2-10 min. Following this, 900µl LB broth medium was added to the cells, transferred into Oakridge tubes, and incubated at 37°C for 1h. To check the transformation, 100 µl -200µl cell suspension was plated onto the LB agar medium containing respective antibiotics and the plates were incubated overnight at 37°C. Other bacterial strains were also transformed using the same procedure.

3.2.14. Confirmation of sequence of synthesized gene constructs by gene sequencing

All the synthesized *pfo* gene constructs encoding WTrPFO, single site-directed mutants rPFO_{V208C}, rPFO_{A212C}, and rPFO_{R467A}, and N-terminal deletion variant containing only the C-terminals domain of PFO (rPFO_{C-ter}) were transformed in *E. coli* DH5 α cells. The transformed cells were spread onto LB agar plate containing ampicillin and incubated at 37°C overnight. A single colony from each of the transformed clones was subjected to automated gene sequencing at the DNA Sequencing Facility of the University of Delhi South Campus (UDSC), New Delhi, India, to confirm the insertion of mutation.

3.2.15. Expression analysis of WTrPFO and its mutants

Expression analysis of the WTrPFO, rPFO_{V208C}, rPFO_{A212C}, and rPFO_{R467A} and PFO_{C-ter} was performed by inoculating a single colony of *E. coli* BL21(λ DE3)pLysS cells harboring the respective gene construct. The inoculated culture was incubated at 37 °C overnight in a shaker incubator (200 rpm). The overnight grown cells were inoculated in a secondary culture at 1% inoculum and the secondary culture was allowed to grow till the OD₆₀₀ reached 0.6-0.8. The culture was then induced with 1mM IPTG for 6h. Uninduced culture (1ml) was collected in a separate microcentrifuge tube prior to induction and incubated along with the induced culture. Aliquots from both the uninduced and induced cultures were centrifuged at 6000 rpm (Eppendorf, centrifuge 5415R), 4°C for 5 min to harvest the cells. The cell pellet was lysed using lysis buffer (50 mM Tris-HCl, pH 6.8 and 2 % SDS) by vigorously vortexing, followed by boiling for 10 min and centrifugation at 13000rpm (Eppendorf centrifuge, 5415R.) at RT for 30 min. The supernatant fractions of both the uninduced and induced cell lysates were collected and analyzed by SDS-PAGE (12 %) to check the expression of the recombinant proteins.

3.2.16. Analysis of localization of expression of the recombinant protein

For the subcellular localization, the induced culture of the *E. coli* BL21(λ DE3)pLysS cells harboring different *pfo* gene construct were harvested as described earlier. The supernatant was collected as an extracellular fraction. The cell pellet was resuspended in sucrose buffer (50mM Tris pH

8.0, 10 mM EDTA and 20% sucrose) and incubated at 4° C for 15 min, followed by centrifugation at 5000 rpm (Eppendorf, centrifuge 5415R) for 10 min. The pellet was treated with autoclaved double distilled water (ddH₂O), incubated at 4° C for 15 min followed by centrifugation. The supernatant obtained from this centrifugation was taken as the periplasmic fraction. The pellet was resuspended in sonication buffer [50 mM, Tris-HCl, pH 8.0, 500 mM NaCl, 1 mM PMSF containing lysozyme (2 µg/ml)], and subjected to sonication (250W for 20 min) with 2s on and 4s off cycles. The sonicated solution was again centrifuged and the supernatant was taken as the cytoplasmic fraction. The pellet was treated with lysis buffer and incubated at RT for 15 min followed by centrifugation at 4° C for 10 min (5000 rpm) to get the membranous fraction. Finally, the residual pellet (inclusion body fraction) was treated with urea buffer (8 M urea, 10 mM Tris-HCl pH 8.0, 500 mM NaCl) to solubilize the proteins present in it. All the subcellular fractions were analyzed by 12% SDS-PAGE).

The temperature conditions for optimum recombinant protein expression by induction with 0.8 mM IPTG were optimized by incubation at 37 °C, 25 °C, 16 °C for 8 h with continuous shaking to acquire the protein in the soluble fraction, followed by harvesting the cells by centrifugation at 6000 rpm (Eppendorf, centrifuge 5415R), 4° C for 10 min. The harvested cells were lysed by sonication followed by centrifugation at 13000 rpm, 4° C for 30 min. Both the fraction soluble and pellet fractions were analyzed by 12% SDS-PAGE.

3.2.17. Optimization of expression of the recombinant protein

Inducer concentration and time of induction, were optimized to maximize the recombinant proteins' expression. For IPTG concentration optimization, secondary culture of the *E. coli* BL21(λDE3)pLysS cells harboring different gene constructs (pET22.*PFO*_{wt} and pET22.*PFO*_{C-ter}) were prepared as described before, and induced with different concentrations of IPTG (0.1 mM, 0.2 mM, 0.4 mM, 0.6 mM, 0.8 mM, 1.0 mM, and 2.0 mM) for 6 h at 37 °C with shaking at 200 rpm. For optimization of time of induction, the cells induced with 0.8 mM IPTG were grown in the conditions described earlier (37 °C, shaking at 200 rpm) for different periods i.e. 1 h, 2 h, 4 h, 6 h, 8 h, and overnight. For the temperature

optimization, the secondary culture of the *E. coli* BL21(λ DE3)pLysS cells harboring different gene constructs (pET22.*PFO*_{wt} and pET22.*PFO*_{C-ter}) were induced with 0.8 mM IPTG and cultured at different temperatures, 16 °C, 25 °C, and 37 °C for 8h. The cells from 1 ml of both the uninduced and induced cultures optimized at different IPTG conc., time intervals, and temperatures were harvested by centrifugation at 4 °C (6000 rpm, Eppendorf, centrifuge 5415R), followed by lysis and analysis by 12% SDS-PAGE.

3.2.18. Purification of the recombinant proteins (WTrPFO and rPFO_{C-ter}) from the soluble fraction

Analysis of localization of the WTrPFO and rPFO_{C-ter} showed that these proteins expressed as soluble proteins. Therefore, these were purified from the soluble fraction of the induced cell lysates. For large scale purification of WTrPFO and rPFO_{C-ter}, 1L LB broth was inoculated with 1% overnight grown primary culture and grown at 37°C with shaking 200 rpm till the OD₆₀₀ reached 0.6-0.8. The culture was then induced with 0.8mM IPTG, and incubated for 22 h at 16 °C to get the protein in the soluble fraction, as described in expression analysis. Induced cell culture was centrifuged at 6000rpm (Sorvall refrigerated centrifuge RC5B, rotor SS34),4°C for 10 min to harvest the cells. The harvested cells were re-suspended in ice-cold sonication buffer (20mM potassium phosphate buffer, pH 8.0, 500 mM NaCl, 1 mM PMSF and (2µg/ml lysozyme) and sonicated on ice as described before. The sonicated cell lysate was centrifuged at 13000 rpm (Heraeus Stratos Biofuge, 3555 rotor)) and 4 °C for 30 min. The supernatant (soluble fraction) was processed for purification of the histidine-tagged recombinant protein by Ni²⁺-NTA affinity chromatography as per the manufacturer's direction. The Ni²⁺-NTA agarose beads were washed with ddH₂O followed by equilibration with wash buffer (20 mM imidazole, 20 mM Tris-HCl, pH 8.0, 500 mM NaCl, 1 mM PMSF). The supernatant was then incubated with equilibrated Ni²⁺-NTA beads at 4 °C for 1 h with end-to-end rotation. The beads were packed in a syringe column followed by washing with wash buffer and elution of the recombinant protein in 5 ml aliquots using the elution buffer (20 mM Tris-HCl, pH 8.0, 500 mM NaCl, 1 mM PMSF),

containing different concentrations of imidazole (50 mM, 100 mM, 150 mM, 200 mM). Different eluted fractions with flow through were analyzed by SDS-PAGE (12% for WTrPFO and 14% for rPFO_{C-ter}).

3.2.19. Purification of recombinant proteins (rPFO_{V208C}, rPFO_{A212C}, and rPFO_{R467A}) from inclusion bodies

Inclusion bodies from the induced culture of *E. coli* BL21 (λ DE3)pLysS strain harboring the PFO mutant plasmids (pET22.PFO_{V208C}, pET22.PFO_{A212C}, and pET22.PFO_{R467A}) were prepared as described earlier by Yadav *et al*⁸. *E. coli* cells transformed with the above constructs were harvested from the induced secondary culture (1 L) 8 h post-induction, by centrifugation at 8000 rpm for 10 min at 4°C. The cells were resuspended in 40 ml of lysis buffer (50 mM Tris-HCl, pH 8.0, 10 mM EDTA, 10 mg/ml lysozyme) followed by sonication (250W, 2s on and 4s off cycles) till the lysate became clear. The sonicated solution was centrifuged at 13,000 rpm (Heraeus Stratos Biofuge, 3555 rotor) for 20 min at 4°C and the supernatant was discarded. The pellet was washed with PENGU buffer (0.2 M sodium phosphate buffer pH 7.3, 1 mM EDTA, 50 mM NaCl, 5 % glycerol and 1 M urea) three times, followed by 3 washes with homogenization buffer (50 mM Tris-HCl, pH 8.0, 100 mM NaCl, 0.5 % Triton-X-100, 0.1 % sodium-Azide). After a final wash with 50 mM Tris-HCl, pH 8.0, 100 mM NaCl, the pellet was solubilized in urea buffer (8 M urea, 10 mM Tris-HCl pH 8.0, 500 mM NaCl) at RT for 1 h and centrifuged at 13,000 rpm for 20 min at 4°C. The supernatant thus obtained contained the solubilized inclusion bodies fraction, which was used for purification of the recombinant mutant proteins. The solubilized inclusion bodies were allowed to bind to Ni⁺²-NTA resins pre-equilibrated with urea buffer for 1 h at RT. The non-specific proteins were removed by washing with 10 column volumes (CV) of wash buffer-I (8 M urea, 20 mM Tris-HCl, pH 8.0, 500 mM NaCl, 20 mM imidazole). The bound proteins were eluted with elution buffer (8 M urea, 20 mM Tris-HCl, pH 8.0, 500

⁸Yadav, S.K., Sahoo, P.K. and Dixit, A. Characterization of immune response elicited by the recombinant outer membrane protein OmpF of *Aeromonas hydrophila*, a potential vaccine candidate in murine model. *Molecular biology reports*. **41(3)**, 1837-1848 (2014)

mM NaCl) containing 50mM, 100 mM and, 150mM and, 200mM imidazole. Eluted fractions (5 ml each) were collected and analyzed by SDS-PAGE (12%). The fractions containing the desired proteins were pooled and dialyzed using the urea gradient dialysis method. Finally, the purified proteins were dialyzed against 1×PBS using a 14 kDa (WTrPFO, and its substitution mutants, ~54kDa) and 3.5 kDa (rPFO_{C-ter}, ~14kDa) cut-off dialysis membranes, respectively. The protein concentration was estimated using a bicinchoninic acid (BCA) protein assay⁹. The proteins were stored in small aliquots (100µl) at -80°C for further use.

3.2.20. Protein concentration estimation

Protein was quantified by bicinchoninic acid (BCA) protein assay using a BCA kit procured from G Biosciences, USA as described by Smith *et al*⁹. An appropriate amount of cell lysates/purified protein (2µl) was diluted in Milli-Q water to make a final volume of 25µl (dilution factor=12.5) in duplicate in a 96-well plate. Standard BSA solution (2mg/ml) was serially diluted from 2000µg/ml to 15.625 µg/ml in Milli-Q water to generate the standard curve in the same plate. The BCA solution and the copper solution were mixed in the ratio of 50:1, and 200 µl of the mixed solution was added to each well. The plate was incubated at 37°C for 30 min, followed by measurement of the absorbance at 562nm in an ELISA plate reader (Tecan, USA). The protein concentration was calculated using slope values obtained by a straight-line fit curve of the standard.

3.2.21. Sodium dodecyl sulfate-polyacrylamide gel electrophoresis (SDS-PAGE)

SDS-PAGE was performed as described by Laemmli¹⁰. Firstly, all the gel casting plates (one thin and the thick or spacer plate) were cleaned very carefully by 70% ethanol. Plates were tightly adjusted in the casting frame to form the

⁹Smith, P.K., Krohn, R.I., Hermanson, G.T., Mallia, A.K., Gartner, F.H., Provenzano, M.D., Fujimoto, E.K., Goeke, N.M., Olson, B.J. and Klenk, D.C. BCA protein assay. *Anal Biochem.* **150**, 76-85 (1985).

¹⁰Laemmli, U.K. Cleavage of structural proteins during the assembly of the head of bacteriophage T4. *Nature.* **227**, 680-685 (1970).

casting chamber (space between the plates) by closing the green gates of the frame. The casting frame along with the plates was clamped in the casting stand. Before starting the gel polymerization process, leakage through the chamber was checked by filling ddH₂O. After confirming of no leakage, H₂O was removed with a filter paper. Resolving gel (12%) and stacking gel solutions (5%) were prepared as per the composition given in Table 4. TEMED was mixed in the gel solution just before adding in the casting chamber to avoid polymerization. Resolving gel solution was added up to the marked point of the plate (about 0.7 cm from the top). Isopropanol or ddH₂O was then poured above the gel and the gel solution was allowed to polymerize at RT. After polymerization of the gel, isopropanol was removed carefully using filter paper, washed with ddH₂O and allowed to dry. Stacking gel solution was poured immediately on top of the resolving gel, after addition of TEMED. A suitable comb was placed very carefully in the stacking carefully,

Table 4. Composition of resolving and stacking gel

| Components | 12% Resolving (10ml) | 14% Resolving (10ml) | 5% Stacking (5ml) |
|-----------------------|-------------------------|----------------------------|----------------------|
| H ₂ O | 3.4 ml | 2.63 | 3.4 ml |
| Acrylamide (30%) | 4.0 ml | 4.66 | 0.85 ml |
| 1.5M Tris-HCl, pH 8.8 | 2.5 ml | 2.50 | ----- |
| 1M Tris-HCl, pH 6.8 | ----- | ----- | 0.625 ml |
| SDS(10%) | 100 µl | 100µl | 50 µl |
| APS(10%) | 100 µl | 100µl | 50 µl |
| TEMED | 5 µl | 4µl | 2 µl |

avoiding formation of any bubble and the gel was allowed to polymerize. The comb was removed very carefully. For the loading samples preparation, 30µg of the purified proteins or or 50 µg of the cell lysate were mixed with an appropriate

volume of 5× loading dye (0.01% bromophenol, 62.5 mM Tris-Cl, pH 6.8, 2% SDS, 5% β-mercaptoethanol and 10% Glycerol) to a final concentration of 1×. The sample was boiled for 10 and 15 min, respectively and loaded into the wells. The samples were electrophoresed at constant current 30mA in 1× SDS-running buffer (192mM glycine, 25mM Tris-HCl, pH 8.3 and 0.1% SDS). Electrophoresed protein bands were visualized by staining the gel with Coomassie Brilliant blue staining solution (0.25 % Coomassie Brilliant Blue R-250 in 50 % ddH₂O, 40 % methanol and 10 % glacial acetic acid) for 1 h, followed by destaining (50 % ddH₂O, 40 % methanol and 10 % glacial acetic acid) for 2 h to 3h.

3.2.22. Western blotting /Immunoblotting analysis

Western blot analysis was carried out as described earlier with minor modifications¹¹. Purified protein samples or the cell lysates prepared from the uninduced and induced cell cultures were resolved by SDS-PAGE (12%) together with pre-stained marker. Electrophoresed proteins were transferred onto nitrocellulose membrane (0.45µm) at constant voltage (50V) for 2h at 4°C using 1×transfer buffer [25 mM Tris-HCl, pH 8.3, 192 mM glycine and 20 % (v/v) methanol]. After the transfer, the membrane was incubated in blocking buffer [2%BSA in 1× PBST solution (137 mM NaCl, 2.7 mM KCl, 10 mM Na₂HPO₄, 1.8 mM KH₂PO₄, pH 7.4, and 0.05 % Tween 20)] with shaking at RT for 1h or at 4°C overnight without shaking. Next morning, the blot was washed three times (10 min each) using 1× PBST with continuous shaking. The membrane was then incubated with primary antibody (anti-his antibody or antisera generated against the recombinant protein in mice at 1:10,000 dilution, for 1h at RT with continuous shaking. Further, the membrane was washed three times with 1× PBST (each wash 10 min) to remove the unbound antibodies, followed by incubation with secondary antibody [alkaline phosphatase(AP)-conjugated goat anti-mouse/ rabbit antibody; 1:10000] at RT for 1h. The membrane was again washed three times to remove unbound antibodies,

¹¹Fido, R.J., Tatham, A.S. and Shewry, P.R. Western blotting analysis. *Plant Gene Transfer and Expression Protocols*. 423-437 (1995).

followed by the addition of with the enzyme substrate BCIP/NBT [5-Bromo-4-chloro-3-indolyl phosphate (BCIP)/nitro blue tetrazolium (NBT)] to develop the color. The image was captured using a Gel-doc (Bio-Rad Laboratories, USA).

3.2.23. Oligomerization behavior of WTrPFO and its mutants

Oligomerisation behavior analysis of the recombinant proteins was carried out as described earlier with minor modifications¹². MDCK cells were seeded at a density of $4-5 \times 10^5$ cells/ml/well in a 6-well tissue culture plate and allowed to adhere for minimum 12h or overnight. The cells were treated with recombinant WTrPFO or its mutants (10 μ g in 1 ml DMEM medium with 10% FBS) for 1h at 37°C. After this, the medium was removed and the adhered cells were washed thrice with 1 \times PBS. The cells were then lysed with 1 \times RIPA buffer (20 mM Tris-HCl, pH 7.5, 150 mM NaCl, 1 mM EDTA, , 1% NP-40, 1% sodium deoxycholate, 2.5 mM sodium pyrophosphate 1mM β -glycerophosphate, 1 mM Na₃PO₄, 1 μ g/ml leupeptin).The crude cell lysates were mixed with denaturing loading dye containing SDS and heated at 95°C for 10 min. The samples were then electrophoresed on 12% SDS-PAGE, followed by Western blotting using monoclonal anti-polyhistidine antibodies and developed with BCIP/NBT substrate. The image was acquired using a Gel-documentation system (Bio-Rad Laboratories, USA).

3.2.24. Hemolytic assay

Erythrocytes were separated from the mice blood as described by Hanson *et al.*, with minor modifications¹³. For hemolytic activity assay, 1 ml blood was collected from mice through retro-orbital route with a glass capillary, in a tube containing EDTA (1.5mg/ml) to prevent coagulation. The blood was centrifuged at 500 \times g at 4°C for 5 min. The supernatant (plasma fraction) was discarded and

¹²Wu, Y., Li, Q. and Chen, X.Z. Detecting protein–protein interactions by far western blotting. *Nature protocols*. **2**(12), 3278. (2007).

¹³Hanson MS, Stephenson AH, Bowles EA et al. Phosphodiesterase 3 is present in rabbit and human erythrocytes and its inhibition potentiates iloprost-induced increases in cAMP. *Am.J.Physiol Heart Circ.Physiol*. **295**, H786-H793 (2008).

the pellet was washed three times with 1× PBS at 4°C. The washed pellet was resuspended in 1× PBS to a final volume that was 10 times to blood pellet volume. The RBC suspension (2.5×10⁶ in 50 µl) was treated with different concentrations (0.4 µg/ml to 2.0 µg/ml) of the test proteins in a final volume of 150 µl, and incubated at 37 °C for 1 h. The cells treated with 1% SDS were included as a positive control. The treated samples were then centrifuged at 1000 rpm (Eppendorf centrifuge 5415R, UK) at 4 °C for 5 min to remove the cell debris. The released hemoglobin in the supernatant was measured by measuring the absorbance at 540 nm. One hemolytic unit (HU) activity was defined as the difference in the absorbance at 550 nm between the sample and blank per microgram of protein present in each sample¹⁴. The percentage of hemolysis in each assay reaction was calculated by using the following formula.

$$\% \text{ Hemolysis} = \frac{A_{540}(\text{Sample}) - A_{540}(\text{Blank})}{A_{540}(\text{Control}) - A_{540}(\text{Blank})} \times 100$$

3.2.25. Cytotoxicity activity assay

Cytotoxicity of the recombinant WTrPFO and its mutants rPFO_{A208C}, rPFO_{V212C}, and rPFO_{R467A} were determined towards phagocytic monocytes THP1 cells and macrophages isolated from the mice peritoneal cavity as described earlier using LDH cytotoxicity assay (Pierce, USA)¹⁴. Mice macrophages were isolated from peritoneal cavity as per described protocol by Ray and Dittel¹⁵. Macrophages (5×10³ cells/100µl/well, in triplicates) in a 96-well plate were treated with different concentrations of the WTrPFO (10µg/ml - 100µg/ml) and incubated at 37°C for 24h in a 5% CO₂ atmosphere. Post-treatment, the cells were subjected to LDH assay as per the manufacturer's protocol, in which the released lactate dehydrogenase was measured using coupled assay followed by measuring the absorbance at 570nm. The absorbance

¹⁴O'Brien, D.K. and Melville, S.B., Effects of *Clostridium perfringens* alpha-toxin (PLC) and perfringolysin O (PFO) on cytotoxicity to macrophages, on escape from the phagosomes of macrophages, and on persistence of *C. perfringens* in host tissues. *Infection and immunity*. **72**, 5204-5215 (2004).

¹⁵Ray, A. and Dittel, B.N., Isolation of mouse peritoneal cavity cells. *Journal of Visualized Experiments*. **35**, 1488 (2010).

was considered directly proportional to the cytotoxicity of the WTrPFO. The cytotoxicity of all the recombinant mutant proteins was determined at 100 µg/ml (highest used concentration of the WTrPFO).

3.2.26. Pore formation analysis

Pore formation ability of the recombinant proteins was analyzed using Propidium Iodide (PI) dye¹⁶. The MDCK cells were seeded on a coverslip in a 6-well plate at a density of $4-5 \times 10^5$ cells/ml/well and incubated for 12 h or overnight at 37°C in 5%CO₂ atmosphere. Next morning, the medium was removed and the cells were washed with 1×PBS very gently 2-3 times. Different dilutions of the WTrPFO (10µg/ml) prepared in DMEM containing 10% FBS were added to the cells and incubated at 37°C for 1h in a 5% CO₂ incubator. The control cells were treated with medium only. Following this, the cells were washed with 1×PBS 2-3 times. Finally, the cells were treated with a solution of 1×PBS and paraformaldehyde in a ratio of 1:1 to fix the cells onto the coverslips, and kept at RT in dark for 10-15 min. The solution was aspirated very carefully and the cells on the coverslip were again washed very gently with 1× PBS 2-3 times. A membrane-impermeable DNA intercalating dye propidium iodide (PI) diluted in the medium (5µg/ml) was added to the cells and allowed to internalize and intercalate to DNA for 15 min. Fluorescence of the entered and intercalated PI inside the cells was observed through Nikon fluorescence microscopy using a green filter (510nm to560nm).

3.2.27. Mice immunization

Female Swiss albino mice (a group of 5-6 mice for each protein, 4-6 weeks old) were housed in the animal house of the University under observation for immunizing. The approval for animal usage for this study has been granted by the Institutional Animal Ethics Committee of the University (Project code IAEC# 03/2019). All the experimental procedures such as bleeding and

¹⁶Skalman, L.N., Holst, M.R., Larsson, E. and Lundmark, R. Plasma membrane damage caused by listeriolysin O is not repaired with through endocytosis of the membrane pore. *Biology open*. **7**(10), (2018).

sacrificing were performed as per the guidelines laid down by the committee. The mice were immunized with the recombinant proteins through the intraperitoneal route (i.p.) in the form of an emulsion (30µg/100µl/mice). The emulsion was prepared by continuous mixing of protein (30µg/mice) and Complete Freund's adjuvant(CFA) in a 1:1 ratio and thoroughly vortexing it for ~2 h-3h. The Freund's Complete (CFA) and Freund's Incomplete Adjuvant (IFA) were used for the emulsion preparations for primary immunization on day 0, and for giving boosters on 14th, 28th, and 42nd day of primary immunization, respectively. Mice immunized with 1× PBS (50 µl/mice) emulsified in CFA (for primary immunization) and IFA (for boosters) were included as controls. The mice were bled through retro-orbital plexus before immunization (day 0), and 1 week after each booster i.e. on day 21 after first booster, day 35 after second booster and day 49 after the third booster. The blood was allowed to clot at 25°C in a stagnant position for 1 h, followed by centrifugation at 5000rpm, 4°C for 10 min¹⁷. The supernatant (serum) was stored at -20°C in small aliquots for subsequent analysis.

3.2.28. Enzyme-linked immunosorbent assay(ELISA)

Indirect ELISA was performed for quantifying antibody titer in the antisera generated against the recombinant protein(s) as per the method described by Sharma and Dixit¹⁸. The purified recombinant protein (500 ng/100µl in each well) in coating buffer (carbonate-bicarbonate buffer; 100mM NaHCO₃, 3.3 mM Na₂CO₃, pH 9.8) was coated in a flat bottom high binding 96-well ELISA plate and left at 4 °C overnight. Next morning, the wells were washed three times with (200-300µl/well) to remove the unbound proteins, followed by blocking with 2 % BSA prepared in 1 × PBST (200µl/well) for 2h at 37°C. The plates were again washed with 1× PBST as mentioned for the previous step. One hundred microliter of different dilutions of primary antibodies (1:20,000 to 1: 160,000 in

¹⁷Harlow, E. D., and David Lane. "A laboratory manual." *New York: Cold Spring Harbor Laboratory*. 579 (1988).

¹⁸Sharma, M. and Dixit, A., . Identification and immunogenic potential of B cell epitopes of outer membrane protein OmpF of *Aeromonas hydrophila* in translational fusion with a carrier protein. *Applied microbiology and biotechnology*. 99(15),6277-6291 (2015).

1×PBS) collected on different days post-immunization was added to the protein-coated wells (in triplicates) and incubated at 37 °C for 1h to allow the complex formation. The plates were again washed three times with 1× PBST to remove excess or unbound antibodies. AP-conjugated anti-mouse antibody (secondary antibody; 100 µl/well; 1:10,000 dilution in 1×PBS) was then added and incubated at 37 °C for 1h, after covering the plate with adhesive plastic. After washing with 1× PBST, the PNPP substrate (1 mg/ml) in substrate buffer (50mM Na₂CO₃ and 1mM MgCl₂, pH 9.8) was added (50µl/well) and incubated at 37 °C for 15 min. The reaction was stopped with 3.0 M NaOH (100µl/well). The absorbance of the yellow color reaction product was measured at 450 nm.

3.2.29. Antibody Isotyping

Levels of different isotypes of the IgG (IgG1, IgG2a, IgG2b) present in the antisera were determined for evaluating the type of immune responses (Th1 and Th2 type immune response related to the generation of IgG2a and IgG1, respectively) by indirect ELISA using isotype-specific horseradish peroxidase (HRP)-conjugated secondary antibodies. Recombinant protein in the coating buffer was aliquoted in a 96-well plate (500 ng/100µl/well, in triplicates) and incubated at 4 °C overnight, followed by washing with 1 × PBST as described for ELISA. The washed protein-coated wells were blocked with 2 % BSA prepared in 1 × PBST (200µl/well) and incubated at 37°C for 2 h, followed by washing with 1× PBST. Antisera generated against different proteins (primary antibody; 1:5000 in 1×PBS) was added to the protein-coated wells, and allowed to incubate at 37 °C for 1 h for the antigen-antibody complex formation. Residual primary antibodies were removed by washing with 1× PBST three times. Each isotype (anti-IgG1, anti-Ig2a, and anti-IgG2b)-specific horseradish peroxidase (HRP)-conjugated secondary antibodies (1:5000 in 1×PBS) was added to the wells (100µl/well in triplicates) followed by three 1× PBST washes. The TMB substrate solution (prepared by mixing both TMB solutions A and B in a 1:1 ratio, just prior to use) was then added (100µl/well) to the wells in dark, followed by incubation at 37°C to develop the color. The absorbance was measured at 450 nm.

3.2.30. Lymphocyte proliferation assay

After one week of the second booster, a set of the immunized mice was sacrificed as per the guidelines of the IAEC. The spleen was surgically removed under aseptic conditions and splenocytes were isolated by chopping the spleen with a surgical blade and crushing the chopped spleen between the rough edges of sterile autoclaved glass slides. The crushed spleen was resuspended in RPMI medium under aseptic conditions¹⁸. The medium was removed by centrifugation at 1000rpm for 5min and the recovered splenocytes were treated with 0.9% NH₄Cl (1ml) to remove the RBCs by lysis, followed by washing with 1×PBS to remove the traces of NH₄Cl. The splenocytes were suspended uniformly in a suitable amount of RPMI supplemented with 10% FBS, 100U/ml penicillin and 2mM glutamine) and subjected to cell counting using trypan blue dye exclusion assay in a hemocytometer. The splenocytes from the recombinant protein-immunized mice and PBS-immunized mice (control) were seeded (1×10^5 cells/100 μ l/well, in triplicates) in 2 sets of 96-well plates in parallel. The splenocytes were then stimulated with the respective proteins (20 μ g/100 μ l/well) or with 1×PBS in both the sets and cultured at 37°C for different time durations i.e. 24h, 48h and 72h, under 5% CO₂ humidified conditions (Hera Cell 150, Heraeus, USA). The supernatant (culture medium) was aspirated from a set of cells cultured for different time durations and stored at -80 °C for the cytokine ELISA. Another set of cultured plate was subjected to cell proliferation analysis by XTT assay as per the manufacturer's instructions. The absorbance was recorded at 450nm with reference at 630 nm in an ELISA plate reader. Proliferation was expressed as the stimulation index (S.I.) i.e. the ratio of the absorbance at 450 nm for the protein-stimulated splenocytes from the protein-immunized mice and the protein-stimulated splenocytes from the PBS-immunized mice.

3.2.31. Cytokine ELISA

Immune response (CD4⁺T-helper cell proliferation) generated by the splenocytes from the recombinant protein- and PBS-immunized mice after stimulation with either the protein or PBS *in vitro* was evaluated by estimating the IL-4 & IFN- γ levels employing an Indirect sandwich ELISA using BD cytokine ELISA kit as per the protocol described by the manufacture. Briefly, Both IL-4 and IFN- γ capture antibody (1:250) in freshly prepared 0.1M Sodium carbonate buffer (pH 9.5) was coated in 96-well high binding ELISA plates (100 μ l/well), and incubated overnight at 4°C. Residual capture antibodies were aspirated and the plate was washed with 1 \times PBST three times. The plate was inverted onto a blotting paper after the last wash to drain out the residual amount of washing buffer from the wells. The coated wells were blocked with Assay Diluent (PBS with 10% FBS pH 7; 200 μ l/well) at RT for 1h, followed by washings as described in the last step. The standard solutions of both IL-4 and IFN- γ (IL-4, 500pg/ml to 7.8pg/ml; IFN- γ , 2000pg/ml to 31.3 pg/ml) prepared in Assay Diluent were added to the wells (in triplicates). The supernatants from the cultured splenocytes proliferation assay collected post-stimulation (stored at -80 °C and thawed at 4°C) were added to different wells and the plate was incubated at RT for 2h, followed by 5 washes as described for the previous step. The working detector for IL-4(1;500) and IFN- γ (1:500) were added (100 μ l/well) to the wells, and incubated at RT for 1h, followed by 10 washes. Finally, the TMB substrate solution was added to each well (100 μ l/well) and the plate was incubated at RT for 30 min in dark to develop the color. The stop solution (1M orthophosphoric acid) was added to stop the reaction and the absorbance was measured at 450nm (with reference at 570nm).

3.2.32. *In vitro* inhibition of the hemolytic activity of WTrPFO by the antisera

Antisera were collected from each set of mice immunized with WTrPFO and its mutants on day 42 post-immunization. The pooled antisera from all the mice of each set (5 mice) were analyzed for their ability to inhibit the hemolytic activity of the WTrPFO. A range of dilutions (50% - 5%) of the control antiserum (raised

against PBS) and the anti-recombinant protein antisera were prepared in 1×PBS. An equal volume of the diluted antisera (50µl) was mixed with the WTrPFO (50 µl of a stock of 0.2mg/ml that caused 80% hemolysis) and incubated for 30 min at 37°C for 1h¹⁹. The mixture was then added to the RBC suspension (2.5×10⁶ in 50µl PBS, in duplicate) to make the final volume 150 µl for each reaction and incubated at 37 °C for 1 h. This was followed by centrifugation (1000 rpm, 5 min) and measurement of the absorbance of the supernatant at 540nm. A decrease in the absorbance in comparison to control cells treated with the protein alone indicated inhibition of hemolysis.

3.2.33. *In vitro* neutralization capacity of the antisera towards cytotoxicity of the WTrPFO in phagocytic cells

The antisera against the WTrPFO and rPFO_{C-ter} collected on day 35 post-immunization were evaluated for their neutralization capacity against the WTrPFO toxicity in mice peritoneal macrophages. The WTrPFO (100µg/ml, 25 µl) was pre-incubated with equal volume (25 µl) of different dilutions of the antisera (1:10-1:10, 000) for 37°C for 30 min. Mice peritoneal macrophages were isolated by the method described by Ray and Dittel¹⁴. Macrophages, seeded in a 96 well plate (5×10⁴/100µl/well, in triplicates) were treated with WTrPFO pre-incubated with different dilutions of antiserum in a final volume of 150µl and incubated for 24h at 37°C and 5% CO₂ atmosphere.

The cells treated with WTrPFO incubated the neat pre-immune serum were included as negative control. Percentage neutralization of cytotoxicity in the samples pre-incubated with different antisera was calculated with respect to cells treated only with the WTrPFO (100% cytotoxicity).

¹⁹Verherstraeten, S., Goossens, E., Valgaeren, B., Pardon, B., Timbermont, L., Haesebrouck, F., Ducatelle, R., Deprez, P. and Van Immerseel, F. Non-toxic perfringolysin O and α -toxin derivatives as potential vaccine candidates against bovine necrohaemorrhagic enteritis. *The Veterinary Journal*. **217**, 89-94 (2016).

Statistical analysis.

The data represent mean and standard deviation (SD) of the individual experiments performed in triplicates. Statistical significance was calculated using One-way ANOVA (Prism 8.0 software, Graphpad, CA, USA) and a p value of ≤ 0.05 (*) was considered significant. Other p values are indicated with different symbols in the figures and $p \leq 0.01$ (**) and $p \leq 0.001$ or 0.0001 (***) were considered very significant and extremely significant respectively.

Chapter 4

Results

4.1 Sequence confirmation of the synthetic gene constructs (*pET22.PFO_{wt}*, and its mutants)

4.1.1 Restriction digestion analysis of synthetic gene constructs *pET22.PFO_{wt}* and its mutants *pET22.PFO_{C-ter}*, *pET22.PFO_{V208C}*, *pET22.PFO_{A212C}* and *pET22.PFO_{R467A}*

Plasmid DNA isolated from the cells transformed with different PFO constructs was subjected to restriction enzyme digestion for confirmation of the presence of the synthetic gene insert. Release of the expected inserts size (~ 1.4 kb) of the plasmids *pET22.PFO_{wt}*, and its mutants *pET22.PFO_{V208C}*, *pET22.PFO_{A212C}*, and *pET22.PFO_{R467A}* upon digestion with *NdeI* and *XhoI* restriction enzyme (**Figure 1a, lanes 2, 4, 6 and 8**, respectively). Absence of any such bands in the respective undigested plasmids (lanes 1, 3, 5 and 7, respectively) confirmed the correctness of the digestion. Likewise, the expected size of the insert (~ 340 bp) was released upon restriction digestion of the gene construct *pET22.PFO_{C-ter}*, with *NdeI* and *XhoI* (**Figure 1b, lane 2**), whereas undigested DNA did not show any such band.

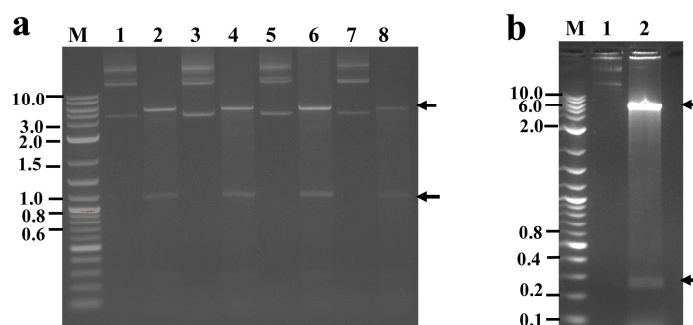


Figure 1. Restriction enzyme digestion analysis of PFO gene constructs in *pET22+vector*. (a) Lanes 2, 4, 6, and 8 represent *NdeI* and *XhoI* digested *pET22.PFO_{wt}*, *pET22.PFO_{V208C}*, *pET22.PFO_{A212C}*, and *pET22.PFO_{R467A}* respectively. Lanes 1, 3, 5, and 7 depict the respective undigested gene constructs. (b) Lane 1 represents the undigested plasmid *pET22.PFO_{C-ter}* whereas lane 2 represents the *pET22.PFO_{C-ter}* plasmid DNA digested with *NdeI* and *XhoI* restriction enzymes. M in both the panels depicts the DNA molecular size markers (2-Log DNA Ladder; 0.1-10.0 kb). Arrow points to the released inserts of ~1.4 kb (expected size 1431 bp) and ~ 350 bp (expected size 342bp) in panels “a” and “b”, respectively

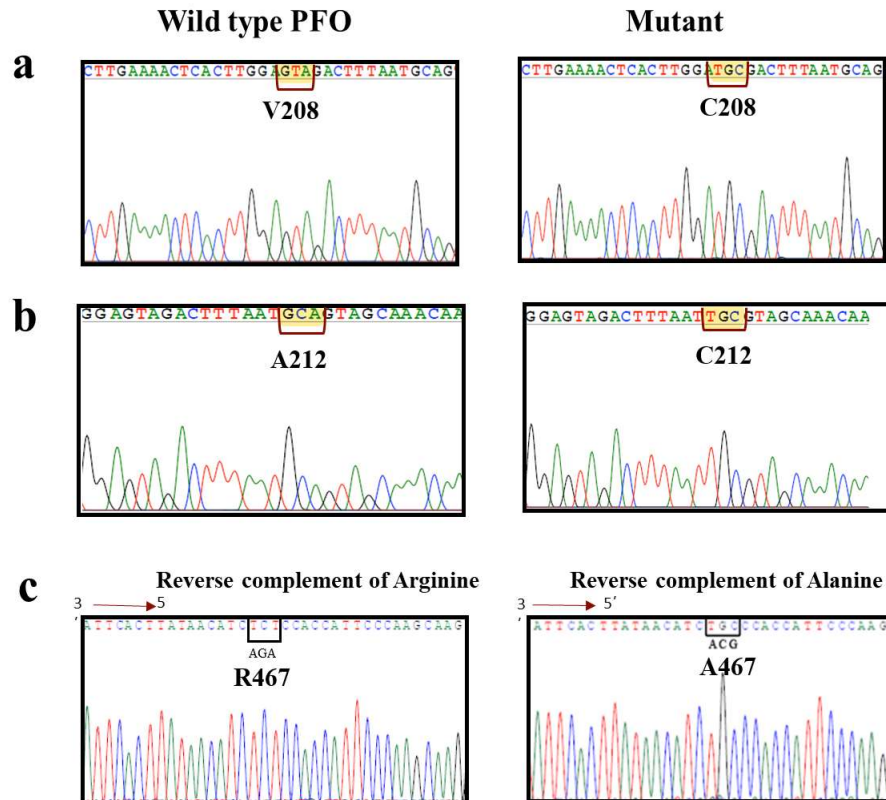


Figure 2. Electropherogram of the wild type PFO (Panel a) and mutant PFO (Panel b) sequences encompassing the residue position 208, 212 and 467. The codon sequences of Valine (panel a, V208, GTA) and alanine (panel b, A212, GCA) in the wild type *pfo* gene are shown in the left panel (highlighted bases) The mutated *pfo* codon at the respective positions (V208C, TGC and A212C, TGC) are shown on the right sides of panels a and b, respectively. Panel c shows the reverse complement sequence of the *pfo* gene showing the codon sequence of Arginine (TCT; R467 in the wild type, left panel-), mutated to Alanine (TGC; A467) in the right panel.

4.1.2 Confirmation of mutations by gene sequencing of the gene constructs *pET22.PFO_{wt}* and its mutants

The constructs were subjected to automated DNA sequencing for confirmation of the induced mutations. The codon sequence encoding V208 and A212 (GTA and GCA, respectively) are displayed as highlighted in wild type *pfo* gene sequence (left) panel (Wild type, **Figure 2a and 2b**, respectively). Substitution of codon sequence of V208 (GTA) and A212 (GCA) resulted in C208 (TCG) and C212(TCG) as shown in the mutated *pfo* gene sequence (right panel labelled ‘Mutant’, **Figure 2a and**

2b, respectively). The codon sequence of R467 and mutation at the same position resulted in A467 of the wild type *pfo* gene sequence (TCT) and mutated gene sequence respectively (TGC) as evident from their reverse complement sequences shown in **Figure 2c** (left and right panels, respectively).

4.2 Recombinant expression analysis and purification of WTrPFO and its mutants

4.2.1 Expression analysis of WTrPFO and its N-terminal deletion variant (rPFO_{C-ter})

The expression of WTrPFO and rPFO_{C-ter} were achieved in the induced cell lysates of *E. coli* BL21(λDE3) pLysS harboring the pET22.PFO_{wt} and pET22.PFO_{C-ter}, respectively upon induction with 1mM IPTG (**Figure 3a**). A strong band of ~ 14 kDa and ~54 kDa was exclusively observed in the induced cell lysates (**lane I**) of *E. coli* BL21(λDE3)pLysS cells expressing rPFO_{C-ter} and WTrPFO, respectively. No bands were detected in the uninduced cell lysates (**lane UI**) of both the cells harboring pET22.PFO_{C-ter} and pET22.PFO_{wt}. Western blot analysis using the monoclonal anti-histidine tag antibody confirmed the authenticity of the expressed proteins as a distinct band at the expected position of WTrPFO (~ 54 kDa) and rPFO_{C-ter} (~14kDa) were observed in the respective induced cell lysates only (**Figure 3b**, lane I).

4.2.2 Expression analysis of rPFO substitution mutants (rPFO_{V208C}, rPFO_{A212C} and rPFO_{R467A})

Induction of the *E. coli* BL21(λDE3)pLysS cells harboring pET22.PFO_{V208C}, pET22.PFO_{A212C}, and pET22.PFO_{R467A} with 1 mM IPTG for 8 h resulted in expression of the respective proteins (**Figure 4a**, lanes I of the respective proteins labelled as V208C for rPFO_{V208C}, A212C for

rPFO_{A212C}, and R467A for rPFO_{R467A}). Detection of an intense band at the expected position of ~ 54 kDa only in the induced cell lysates of the cells harbouring the respective gene constructs confirms tight regulation of expression.

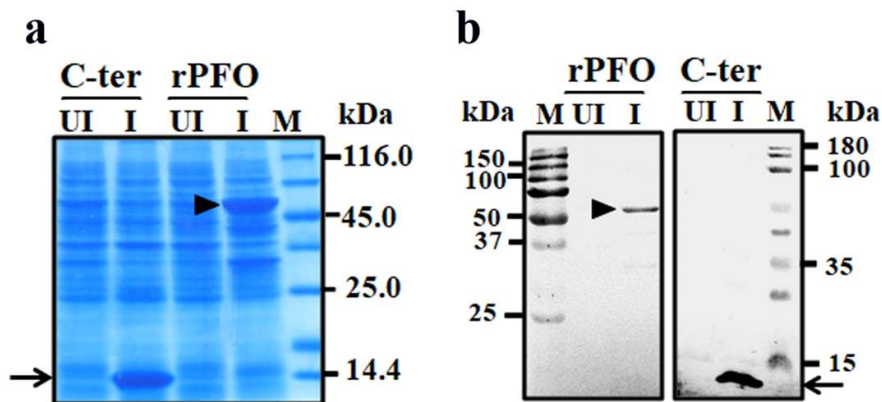


Figure 3. Expression analysis of WTrPFO and rPFO_{C-ter}. **a.** Uninduced and induced cell lysates (~30 µg each) of both *E. coli* BL21(λDE3)pLysS cells harboring pET22.*PFO*_{wt} and pET22.*PFO*_{C-ter} were analyzed by SDS-PAGE (12%). An intense band of the WTrPFO (~54 kDa, rPFO) and rPFO_{C-ter} (~ 14 kDa, C-ter), respectively is present only in the induced cell lysates of the respective constructs. **b.** Western blot analysis of the induced and uninduced cell lysates of *E. coli* BL21(λDE3)pLysS cells expressing WTrPFO and rPFO_{C-ter} using anti-His monoclonal antibody. Lanes ‘UI’ and ‘I’ represent uninduced and induced cell lysates of *E. coli* BL21(λDE3)pLysS cells harboring pET22.*PFO*_{wt} (rPFO) and pET22.*PFO*_{C-ter} (C-ter) in both the panels. Lane M denotes the protein molecular weight marker (kDa). Arrowhead and arrow in both the panels point to the WTrPFO at ~54 kDa and rPFO_{C-ter} at ~14 kDa respectively.

Western blot analysis using anti-histidine monoclonal antibodies confirmed the authenticity of the expressed proteins to be recombinant histidine tagged mutants as a single and intense band at the position of recombinant mutant proteins (rPFO_{A212C}, rPFO_{V208C}, and rPFO_{R467A}). was detected only in the respective induced cell lysates (**Figure 4b, lanes I**) respectively). No such band was present in the uninduced cell lysates (**Figure 4b, lanes UI**).

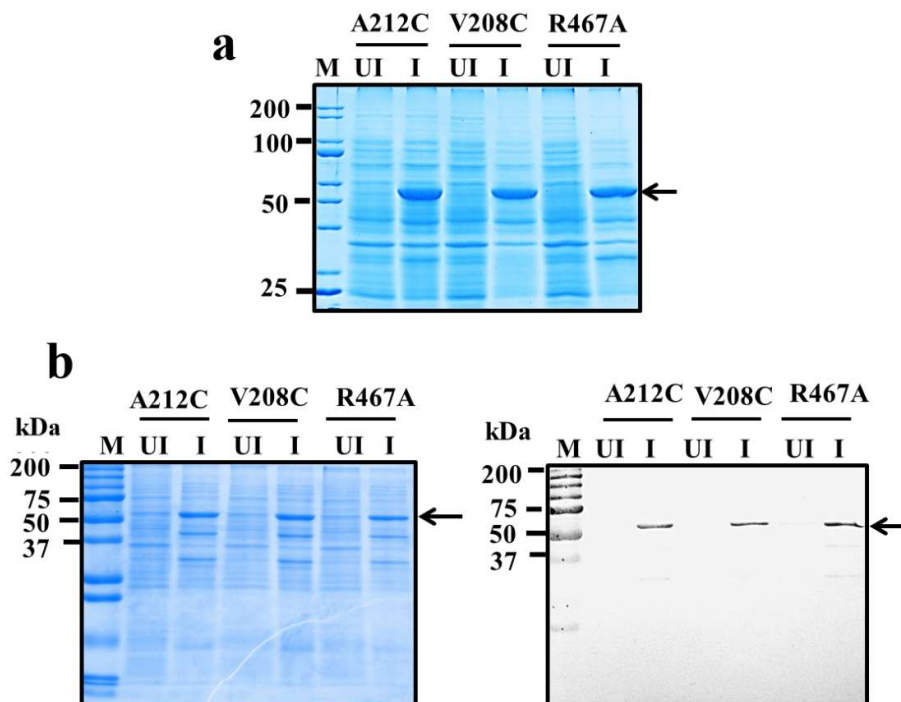


Figure 4. Expression analysis of rPFO substitution mutants (rPFO_{V208C}, rPFO_{A212C}, and rPFO_{R467A}). The uninduced (UI) and induced (I) cell lysates (~30 μ g each) of each *E. coli* BL21(λ DE3)pLysS cells harboring pET22.PFO_{V208C} (V208C), pET22.PFO_{A212C} (A212C) and pET22.PFO_{R467A} (R467A) were analyzed by SDS-PAGE (12 %). The arrow points to the three recombinant mutant PFOs at ~54 kDa observed only in the induced cell lysates. **(b)** Western blot analysis of the uninduced (U) and induced (I) cell lysates of *E. coli* BL21(λ DE3)pLysS cells expressing three PFO mutants shown in panel a, using an anti-His monoclonal antibody to confirm the expression of the mutants (right panel). The left panel shows parallelly run SDS-PAGE of the same stained with Coomassie Brilliant blue stain. Lane M denotes the protein molecular weight marker (kDa). Arrow points to the detected mutant recombinant PFO in the induced cell lysates for all the three mutants.

4.2.3 Optimization of inducer concentration and duration (h) for recombinant WTrPFO and rPFO_{C-ter} expression.

Inducer concentration optimization showed the expression of WTrPFO and rPFO_{C-ter} to occur at a concentration as low as 0.1 mM. (**Figure 5a and 5b** respectively). The expression of WTrPFO increased slightly with increase in IPTG concentration with maximum expression at 0.8mM. Unlike the WTrPFO, rPFO_{C-ter} expression did not significantly increase with increasing inducer concentration.

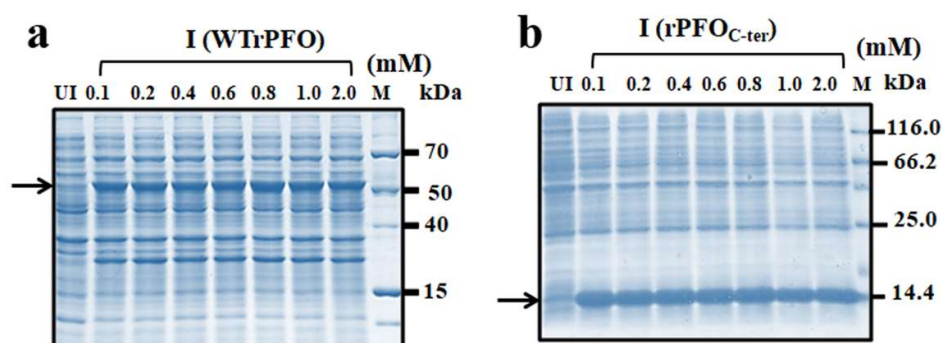


Figure 5. Optimization of inducer concentration for WTrPFO and rPFO_{C-ter} expression. Expression of WTrPFO (**panel a**) and rPFO_{C-ter} (**panel b**) at different concentrations of IPTG (0.1 mM – 2.0 mM) for 8 h. Lane UI represents the uninduced cell lysates and lanes under “I” represent the culture induced with the indicated concentrations of IPTG. M indicates protein molecular weight markers (kDa). Arrow in both the panels points to the respective recombinant protein.

Time kinetics of protein WTrPFO expression showed an increase in expression with induction time till 8 h, beyond which no further increase in expression with increase in induction time (**Figure 6a**) The rPFO_{C-ter} expression was found to increase with induction time with maximum expression observed in overnight induced culture (**Figure 6b**).

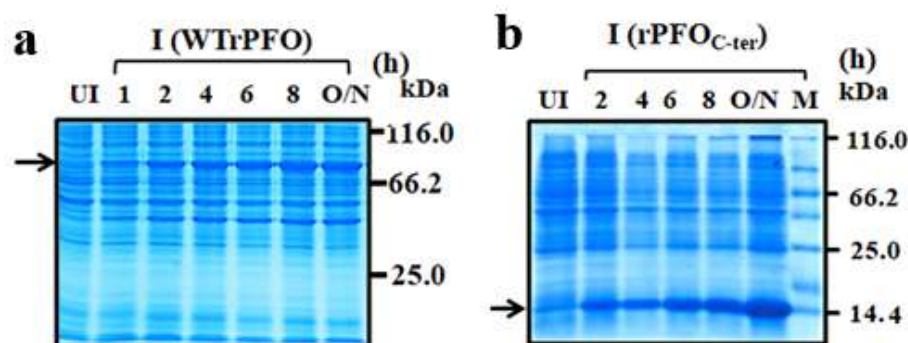


Figure 6. Time optimization for WTrPFO and rPFO_{C-ter} expression at constant IPTG concentrations for different durations (1h to overnight). Lane UI denotes the uninduced cell lysate of *E. coli* BL21(λDE3)pLysS cells expressing WTrPFO and rPFO_{C-ter} in **panel a** and **panel b**, respectively. Lanes under “I” represent the WTrPFO and rPFO_{C-ter} expression, respectively the cell lysates of the cells induced for 1h, 2h, 4h, 6h, 8h and overnight (O/N). Arrow in both the panels point to the respective recombinant protein. “M” denotes the protein molecular weight marker (kDa).

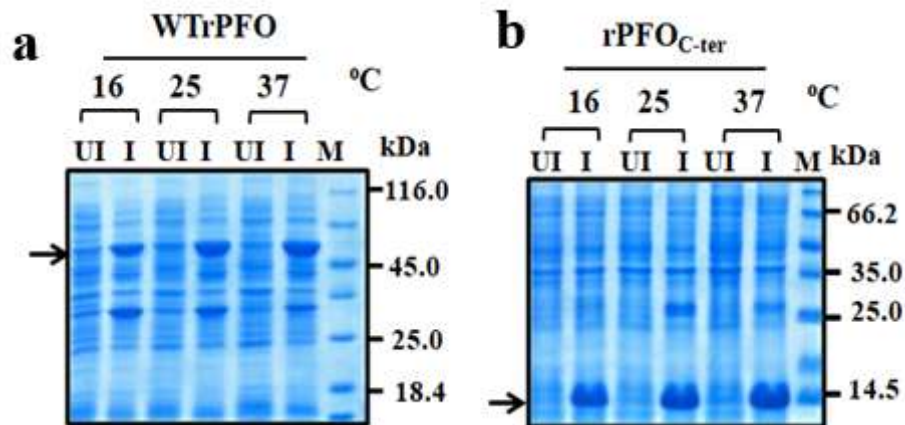


Figure 7. Optimization of temperature for WTrPFO and rPFO_{C-ter} expression. The *E. coli* BL21(λ DE3)pLysS cells harboring pET22.*PFO*_{wt} (panel a) and pET22.*PFO*_{C-ter} (panel b) were induced with 1 mM IPTG for 8 h at different temperatures. The cell lysates were analyzed by 12 % SDS-PAGE. Lanes UI and I depict the uninduced and induced cell lysates of the respective cells. “M” indicates the protein molecular weight marker (kDa). Arrow in panel a and panel b points to the WTrPFO (~54 kDa) and rPFO_{C-ter} (~14 kDa), respectively.

The expression analysis of both the proteins, WTrPFO and rPFO_{C-ter} at different temperatures i.e. 16 °C, 25 °C, and 37 °C, for 8 h showed the presence of a dominant band at the respective positions of the two proteins (Figure 7a and 7b, respectively), with maximum expression taking place at 37 °C for both the proteins. At 16 °C, expression of both the proteins was slightly lower, therefore, for further analysis, the induction at 16 °C was performed for 22 h (overnight) to obtain higher amounts of the protein

4.2.4 Localization of expression analysis

Analysis of the different fractions extracellular (EC), periplasm (P), membranous (M), soluble (S), and pellet or insoluble fraction (I) prepared from the induced cell lysates of *E. coli* BL21(λ DE3)pLysS cells harboring pET22.*PFO*_{wt} (37 °C, 1mM IPTG) showed the presence of the recombinant protein WTrPFO in periplasm (P), membranous (M), and insoluble (I) fractions (Figure 8). However, no protein was detected in the soluble (S) fraction.

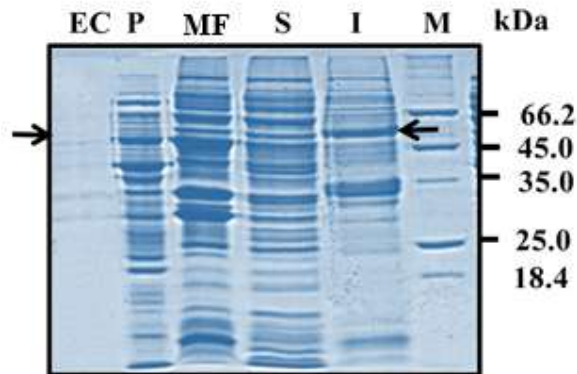


Figure 8. Localization of expression WTrPFO. Subcellular localization of WTrPFO expression was analyzed by preparing different fractions of the induced cell lysates of *E. coli* BL21(λ DE3)pLysS cells harboring pET22.*PFO*_{wt}. EC (extracellular fraction), P (periplasmic fraction), MF (membranous fraction), S (soluble fraction), and I (inclusion bodies). “M” indicates protein molecular weight marker (kDa). Arrow points to the recombinant WTrPFO

In order to direct the expression of the recombinant proteins to soluble fractions, the cultures were induced at different temperatures and the soluble (lane S) and insoluble (lane I) fractions of the induced cell lysates were analyzed. Analysis of the soluble (lane S) and insoluble (lane P) fractions of the induced cell lysates cultured at 25 °C and 37 °C for 8 h showed WTrPFO (**Figure 9a**) and rPFO_{C-ter} (**Figure 9b**) to be exclusively present in the insoluble fraction (lane P). However, when the expression of the WTrPFO and rPFO_{C-ter} was induced at 16°C for 8 h, the recombinant proteins were predominantly present in the soluble fractions (lane S in both the panels). Since expression of both the proteins was slightly lower, at in the cultures induced at 16 °C, for 8 h, therefore, for large scale purification of the WTrPFO and rPFO_{C-ter}, the cultures were induced at 16 °C for 22 h.

Temperature optimization to direct the expression of PFO mutants (**rPFOA_{212C}**, **rPFOV_{208C}**, and **rPFOR_{467A}**) to soluble fractions did not direct the expression of the recombinant proteins to soluble fractions at any temperature (data not shown). Since maximum expression of these

proteins occurred at 37 °C, soluble (lanes S) and insoluble (lanes P) fractions prepared from the induced cell lysates of the

E. coli BL21(λDE3)pLysS cells harboring pET22.*PFO*_{V208C} (V208C), pET22.*PFO*_{A212C} (A212C) and pET22.*PFO*_{R467A} (R467A), cultured at 37 °C are shown in **Figure 9c**.

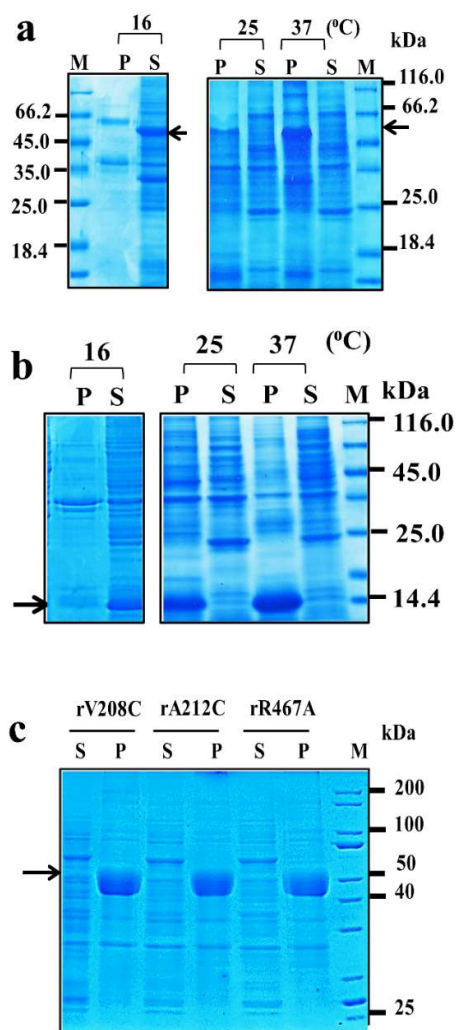


Figure 9. a and b. Subcellular localization of recombinant WTrPFO and rPFO_{C-ter} (panel b) induced at different temperatures. Soluble (S) and insoluble (P) fractions of the *E. coli* BL21(λDE3)pLysS cells harboring pET22.*PFO*_{wt} (**panel a**) and pET22.*PFO*_{C-ter} (**panel b**) induced at different temperatures (16 °C, 25 °C, and 37 °C) were analyzed by SDS-PAGE (12 %). **c. Soluble (S) and insoluble (P) fractions** (30 μg each) of the *E. coli* BL21(λDE3)pLysS cells harboring pET22.*PFO*_{V208C} (V208C), pET22.*PFO*_{A212C} (A212C), and pET22.*PFO*_{R467A} (R467A), induced at 37 °C were analyzed by SDS-PAGE (12 %). Lane M in all the panels denotes the protein molecular weight marker (kDa). The arrows in all the panels denote the respective recombinant protein.

4.2.5 Purification of WTrPFO & its mutants (rPFO_{C-ter}, rPFOA_{212C}, rPFO_{V208C}, and rPFOR_{467A})

Purification of the proteins **WTrPFO** and **rPFO_{C-ter}** from the soluble fraction of the induced cell lysates using Ni²⁺-NTA agarose chromatography showed that both the proteins started to elute with 100 mM imidazole. However, initial fractions eluted with 100 mM imidazole showed the presence of some high molecular weight contaminants (**Figure 10a, lanes 5-6 and Figure 10b, lanes 3-4**). However, subsequent fractions eluted with 100 mM imidazole were free from any contaminant.

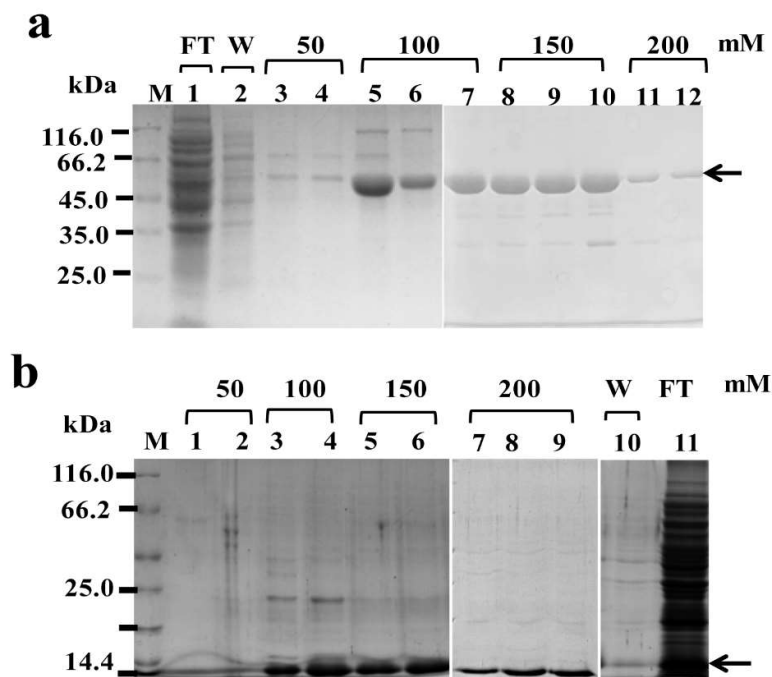


Figure 10. Purification of recombinant proteins WTrPFO and rPFO_{C-ter}.

The soluble fractions of the cell lysates of *E. coli* BL21(λDE3)pLysS cells harboring pET22.*PFO_{wt}* (**panel a**) and pET22.*PFO_{C-ter}* (**panel b**) induced with 1 mM IPTG at 16 °C for 22 h were subjected to Ni²⁺-NTA chromatography and analyzed by SDS-PAGE (12 %). Lanes 1 and 11 in **panel a** and **panel b** represent the flowthrough (FT) and lanes 2 and 10 represent the wash (W) fractions in panel a and panel b, respectively. The other lanes show fractions eluted with buffer containing 50 mM, 100 mM, 150 mM, and 200 mM imidazole, respectively. “M” in both the panels denotes the protein molecular weight markers (kDa) and the arrow points to the respective recombinant protein.

In order to get high yield of purified proteins, the fractions showing the presence of purified proteins were pooled, dialyzed and re-subjected to affinity chromatography, which resulted in the purified proteins to near homogeneity (>99 %), as evident from a single band of the purified WTrPFO (**Figure 11a, lane P**) and rPFO_{C-ter} (**Figure 11b, lane P**) at their expected positions (~54 kDa and ~14kDa, respectively) were detected on SDS-PAGE. The yield of the purified WTrPFO and rPFO_{C-ter} were determined to be 70 mg and 75 mg respectively from 1L culture at shake flask level.

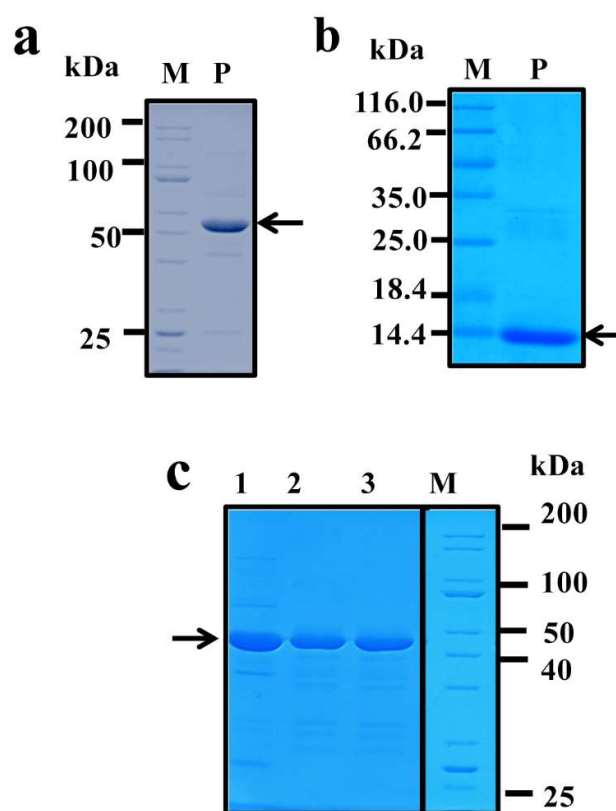


Figure 11. SDS-PAGE analysis of the purified WTrPFO, rPFO_{C-ter} and its mutants. Lane P in **panel a** and **panel b** depicts the purified WTrPFO and rPFO_{C-ter}, respectively obtained after re-purification of the pooled fractions showing the presence of recombinant protein using Ni²⁺-NTA chromatography and eluted with 100 mM imidazole (obtained from figure 10). **c.** The figure shows the SDS-PAGE (12 %) analysis recombinant mutant PFOs purified from solubilized inclusion bodies using Ni²⁺-NTA chromatography and eluted with 150 mM imidazole. Lanes 1, 2, and 3 represent purified rPFO_{A212C}, rPFO_{V208C}, and rPFO_{R467A}, respectively. “M” in all the panels depicts the protein molecular weight marker (kDa). The arrow indicates the purified recombinants proteins.

The rPFO_{V208C}, rPFO_{A212C}, and rPFO_{R467A} were purified from solubilized inclusion bodies using Ni²⁺-NTA agarose chromatography (**Figure 11c**). The proteins eluted with 150 mM imidazole. As shown in the figure, the three mutants were purified and a single band at the expected size of ~ 54 kDa was seen for rPFO_{V208C}, rPFO_{A212C}, and rPFO_{R467A} (lanes 1, 2 and 3, respectively). The three mutants were purified to > 99 % homogeneity as no other band was detected in SDS-PAGE analysis. The yields of the purified recombinant proteins from 1 L culture at shake flask level are shown in **Table 4.1**.

4.3 Biological activity of the WTrPFO toxin and its mutants

4.3.1 Haemolytic activity of the WTrPFO and its mutants.

In order to see if the histidine-tagged WTrPFO retained its biological activity, it was evaluated for its hemolytic and cytotoxic activities using mice RBCs and mice peritoneal macrophages, respectively. As shown in **Figure 12a**, hemolysis (~ 20 %) could be seen at a concentration of 0.8 µg/ml of WTrPFO with respect to 1 % SDS (included as a positive control and considered to cause 100 % lysis). A dose dependent increase in the hemolysis was observed and at the 2 µg/ml of WTrPFO, ~80 % lysis was observed. Hemolytic activity of purified WTrPFO from the soluble fraction was determined as 10⁵HU/mg.

Unlike the WTrPFO, treatment of RBCs with the PFO mutants (rPFO_{V208C}, rPFO_{A212C}, and rPFO_{R467A}) did not show any hemolysis. The percentage of haemolysis by various mutants was determined with respect to the haemolysis by WTrPFO (2 µg/ml), taken as 100 %. Even at the highest

concentration of 2 $\mu\text{g/ml}$ of the mutants, more than 90% of RBCs remained viable (**Figure 12b**).

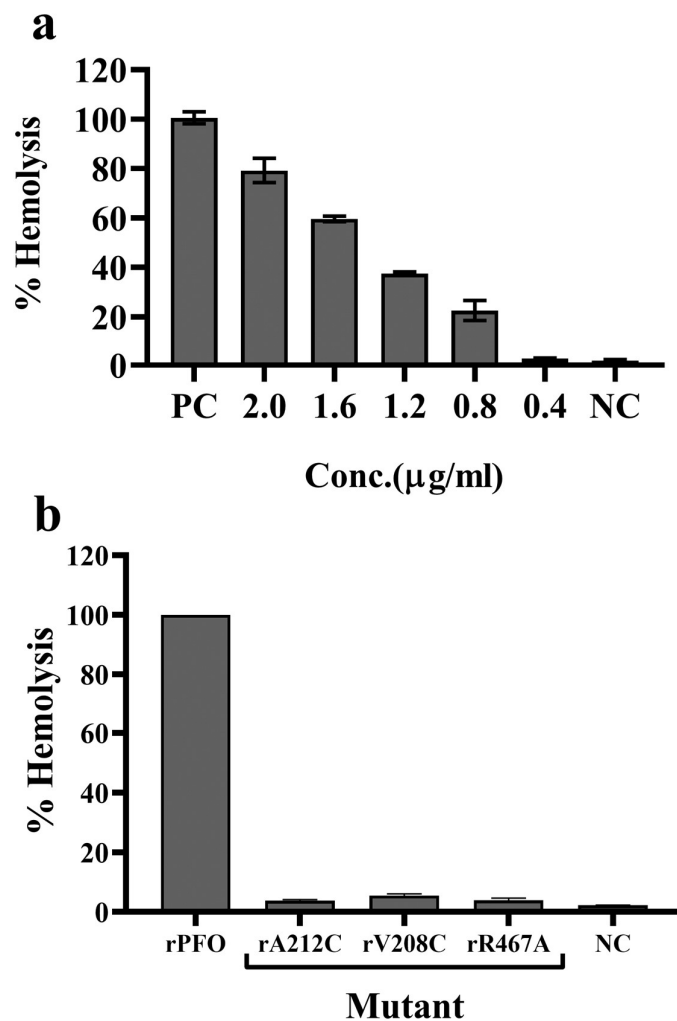


Figure 12. Hemolytic activity analysis of **WTrPFO** and **its mutants**. **(a)** Hemolytic activity analysis of WTrPFO. Mice RBCs (2.5×10^6 in $50 \mu\text{l}$) were treated with different concentrations of WTrPFO ($0.4 \mu\text{g/ml}$ - $2.0 \mu\text{g/ml}$). Percentage hemolysis was determined with respect to 1 % SDS, included as a positive control (PC), and considered as 100% hemolysis. **(b)** Hemolytic activity analysis of PFO mutants. Mice RBCs (2.5×10^6 in $50 \mu\text{l}$) were treated with the PFO mutants (rPFO_{A212C}, rPFO_{V208C}, and rPFO_{R467A}) at conc. $2 \mu\text{g/ml}$ and the % hemolytic activity was determined with respect to WTrPFO-treated RBCs. All the mutants are showing negligible haemolysis as compared to WTrPFO. The RBCs treated with $1 \times \text{PBS}$ were included as negative control (NC) represents the negative control.

4.3.2 Cytotoxicity of the WTrPFO and its mutants towards phagocytic cells/Macrophages and monocytes (THP1)

The purified WTrPFO was biologically active as evident from its cytotoxicity towards mice peritoneal macrophages evaluated by LDH release assay (**Figure 13a**). Like the hemolytic activity, an increase in percentage cytotoxicity was observed with an increase in WTrPFO concentration and ~ 84 % cytotoxicity was observed at 100 µg/ml concentration with respect to 10× lysis buffer, included as positive control and considered to cause 100 % cell death.

Whether or not substitution mutation has resulted in affecting the cytotoxicity of the PFO, cytotoxicity of the three PFO mutants (rPFO_{V208C}, rPFO_{A212C}, and rPFO_{R467A}) was evaluated both in mice peritoneal cells and THP1 (human monocytes). Significantly reduced cell death was observed when the mice peritoneal macrophages (**Figure 13b**) and THP-1 cells (**Figure 13c**) were treated with the mutant proteins at 100 µg/ml, compared to the cytotoxicity observed with the same concentration of WTrPFO. The three mutants were found to be less than 30 % toxic with respect to WTrPFO. The rPFO_{V208C} and rPFO_{R467A} were more toxic (27.54±6.3 % and 28.88±2.4 %, respectively in mice peritoneal macrophages; 14.32±1.4 % and 14.32±9.4 %, respectively in THP-1 cells) in comparison to rPFO_{A212C} (18.88±4.3 % and 8.86±4.81 % in mice peritoneal macrophages and THP-1 cells, respectively). Comparative analysis of the two cell lines showed that they were less cytotoxic to THP-1 cells when compared to mice peritoneal macrophages.

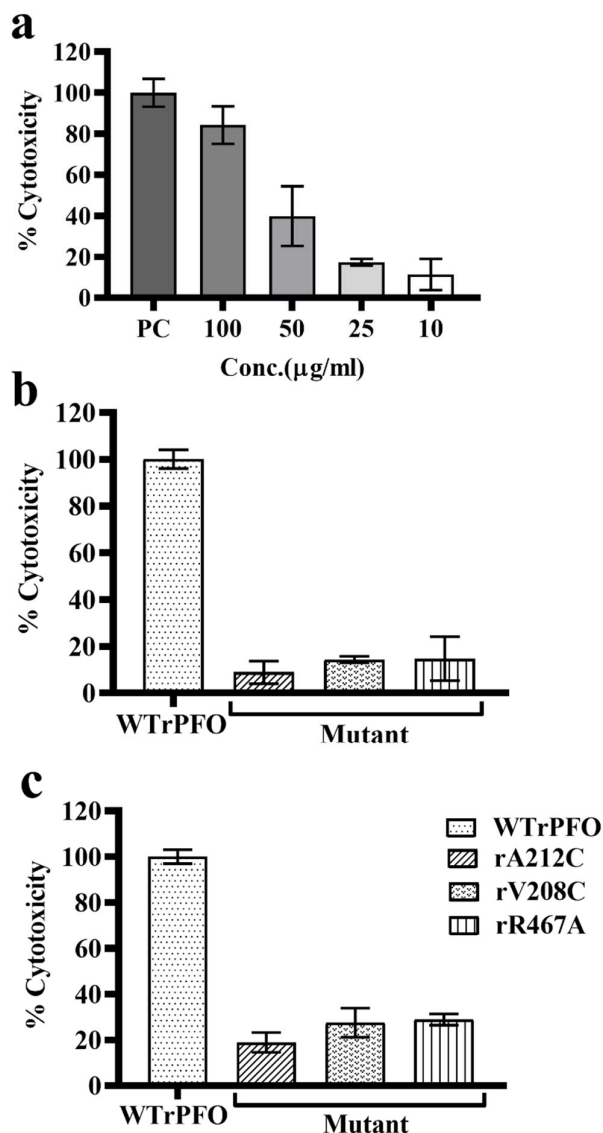


Figure 13. Cytotoxic activity of WTrPFO and its mutants (a) Cytotoxic activity of WTrPFO. Mice peritoneal macrophages ($5 \times 10^4/100 \mu\text{l/well}$) were treated with different concentrations (10 $\mu\text{g/ml}$ -100 $\mu\text{g/ml}$) of WTrPFO (in triplicates) at 37 °C for 24 h in 5 % CO_2 humidified atmosphere. LDH release was taken as a measure of cytotoxicity and the absorbance at 490 nm was considered as an indicator of lysis. Percentage cytotoxicity was calculated with respect to lysis caused by lysis buffer included as a positive control (PC) and considered to cause 100 % lysis. Data represent mean \pm SD of three independent experiments performed in triplicates. **(b and c)** Cytotoxic activity of the PFO mutants (**rPFO_{V208C}**, **rPFO_{A212C}**, and **rPFO_{R467A}**) towards the mice peritoneal macrophages (**panel b**) and THP1 cells (**panel c**). Mice peritoneal macrophages or THP1 cells ($5 \times 10^3/100 \mu\text{l/well}$) were treated with different mutants at 100 $\mu\text{g/ml}$ for 24 h at 37 °C in 5 % CO_2 humidified atmosphere and the cytotoxicity was measured using LDH release assay. Percentage cytotoxicity of the three mutants was calculated with respect to lysis caused by WTrPFO included as a positive control (PC) and considered to cause 100 % lysis. Data represent the mean \pm S.D. of the assays performed in triplicates.

4.3.3 Complex formation behaviour analysis

The binding and oligomer/complex formation ability of the WTrPFO with the eukaryotic cells was analyzed *in vitro* using MDCK cells. To determine if the reduced toxicity of the mutants is due to the loss of binding and oligomerization ability of the mutants, the mutants were also analyzed for their binding ability to MDCK cells. Western blot analysis of the electrophoresed cell lysates of the MDCK cells pre-treated with different proteins (WTrPFO and its mutants; 10 µg/ml) was carried out to detect oligomer formation, if any. As evident from **Figure 14 (lane 1)**, incubation of MDCK cells with WTrPFO resulted in appearance of two bands at ~54 kDa and ~110 kDa positions, corresponding to monomeric and dimeric forms of the protein. An intense band at ~54 kDa indicates effective binding of the WTrPFO to the plasma membrane in the monomeric state. Unlike the cell lysates of the MDCK cells incubated with WTrPFO, the cell lysates of the MDCK cells incubated with the three PFO substitution mutants (rPFO_{V208C}, and rPFO_{A212C}) showed a very faint band at the position of monomeric and oligomeric positions of the proteins, indicating reduction in binding of the mutant proteins (**Figure 14, lanes 2 and 3**). No band at the same position (~54 kDa) was detected in the cell lysates incubated with the rPFO_{R467A} suggesting complete loss of binding with the membrane (**Figure 14, lane 4**). Surprisingly, the cell lysates of the MDCK cells incubated with the rPFO_{V208C}, rPFO_{A212C} showed a band at slightly lower position (~100 kDa) in comparison to the oligomer observed with the WTrPFO, suggesting that the proteins did not properly oligomerize on the plasma membrane and possibly aggregated. Likewise, a negligible intense band was noted in the cell lysates of the MDCK cells incubated with rPFO_{R467A}. The intensity of the band at the ~100 kDa position was in the order of rPFO_{A212C} > rPFO_{V208C} > rPFO_{R467A}. No band was detected at either monomeric or dimeric position in the cells incubated with PBS, indicating the specificity of detection.

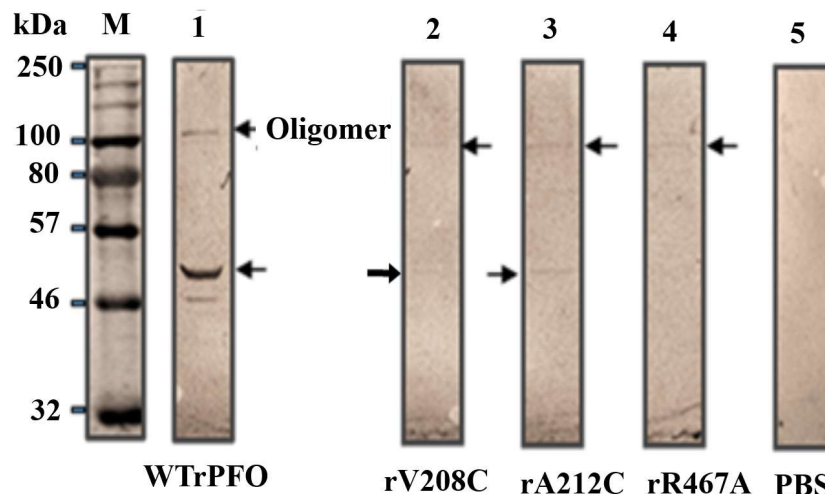


Figure 14. Determination of binding to MDCK cells and oligomerization ability of the WTrPFO and its mutants with the plasma membrane of MDCK cells by western blot analysis. Western blot analysis of the cell lysates of MDCK cells (5×10^5 /ml) were incubated with $10 \mu\text{g/ml}$ of WTrPFO, rPFO_{V208C}, rPFO_{A212C}, rPFO_{R467A}, and vehicle ($1 \times \text{PBS}$) (lanes 1-5, respectively) for 1 h at 37°C in 5 % CO_2 humidified atmosphere using anti-histidine monoclonal antibodies. Lane M shows the migration of protein molecular weight markers (kDa). Arrows point to the monomeric and oligomeric forms of the proteins in different lanes.

4.3.4 Pore formation analysis

To assess that the WTrPFO was able to make functional pores on the plasma membrane, propidium iodide influx assay was performed. Fluorescence microscopy of the MDCK cells incubated with the WTrPFO ($10 \mu\text{g/ml}$) and stained with PI showed red fluorescent cell population (**Figure 15b**), whereas no fluorescence was noted in the control cells treated with corresponding volume of PBS (**Figure 15a**). Increased fluorescent cell population indicated that WTrPFO could form pores on the MDCK cells.

Unlike WTrPFO, the MDCK cells pre-treated with the mutants rPFO_{V208C} (**Figure 15c**), rPFO_{A212C} (**Figure 15d**), and rPFO_{R467A} (**Figure 15e**) at the same concentration used for WTrPFO showed negligible fluorescent cell population in fluorescence microscopy. These data confirm that the substitution mutations have resulted in the loss of toxicity due to failure of

oligomerization and complex formation on thplasma membrane, as observed in the last figure (Figure 14).

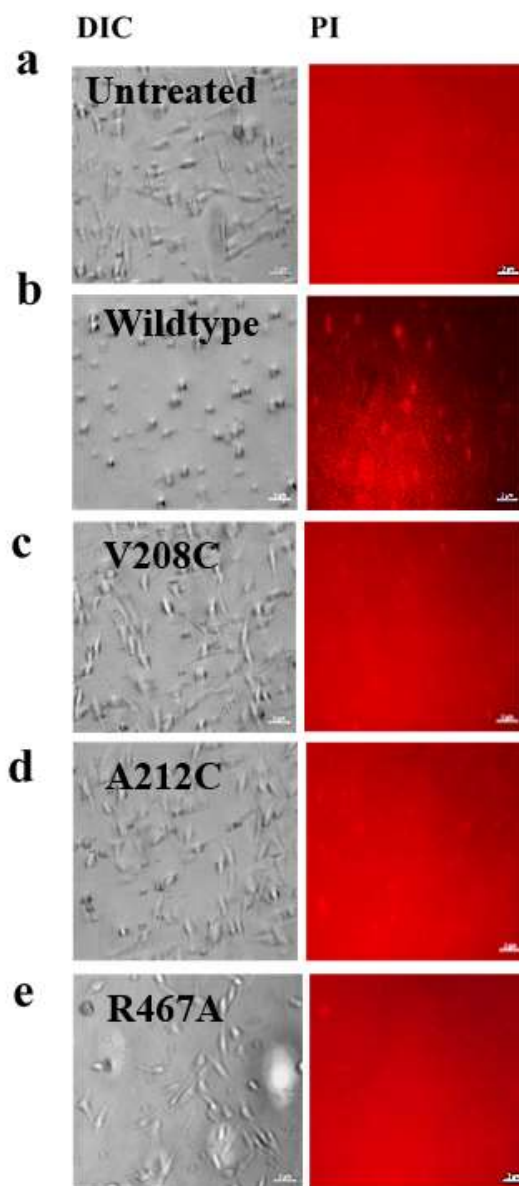


Figure 15. Analysis of pore formation ability of the WTrPFO and its mutants on MDCK cells using propidium iodide influx assay through fluorescence microscopy. The MDCK cells (5×10^5 cells/ml) were treated with the WTrPFO, rPFO_{V208C} (rV208C), rPFO_{A212C} (rA212C), rPFO_{R467A} (rR467A), (10 μ g/ml) in a 6-well plate (panels b-e) respectively). The cells treated with 1 \times PBS were included as negative controls (panel a). The cells were then stained with propidium iodide (PI, 5 μ g/ml) for 15 min. Internalization of PI was visualized by fluorescence microscopy. The left and right panels show the DIC (Differential Interference Contrast) images and the fluorescence microscopy images of the treated cells, respectively.

4.4 Evaluation of immune response generated against recombinant PFO and its mutants.

Since the study was targeted to carry out comparative analysis of the immunogenic and neutralizing potential of the WTrPFO and its mutants, immunization studies with the recombinant proteins were performed.

The Immunoglobulin (IgG) levels in antisera of both WTrPFO (**Figure 16a**) and rPFO_{C-ter} (**Figure 16b**) immunized mice were found to be higher on day 14 after immunization and increased further on day 21, day 35, and day 49 after the administration of the boosters. Although the IgG level against the rPFO_{C-ter} was lower than that observed with the WTrPFO (indicated by relatively lower absorbance), the IgG levels still remained significantly higher than that of pre-immune serum. The endpoint titers of the anti-WTrPFO antisera were determined to be much greater than 1:80,000 drawn on day 21 and day 35, and much greater than 1:160,000 drawn on day 49 post-immunization as the absorbance remained significantly higher ($p \leq 0.001$) than that obtained with pre-immune serum. On the other hand, the endpoint titers for anti-rPFO_{C-ter} were determined to be >1: 20,000, >1: 80,000, & >1: 160,000 on day 21, day 35, and day 49 post-immunization, respectively.

Antibody titers of the antisera generated against the three mutants i.e. anti-rPFO_{V208C}, anti-rPFO_{A212C}, and anti-rPFO_{R467A} antisera, collected on day 21, day 35, and day 49 post-immunization were determined using different dilutions (1: 20,000 to 1: 160,000) of the respective antisera. As shown in the **Figure 17a-c**, all the three antisera showed significantly higher absorbance ($p \leq 0.001$) of all mutants antisera in comparison to that obtained with PI. Even at 1:160,000 dilution, the absorbance obtained with the antisera generated against the three mutants collected on day 21, day 35 and day 49 post-immunization was found to be significantly ($p \leq 0.001$) higher than that obtained with PI, with the exception of anti-rPFO_{V208C} antiserum collected on day 21 post-immunization (**Figure**

17a). Thus, the antibody titers of the antisera generated against the three mutants were determined to be $>1:160,000$, except for the day 21 -anti-rPFO_{V208C} antiserum, for which the titer was found to be $>1:80,000$. As evident from the figure, booster administration resulted in an increase in absorbance with successive boosters, indicating stimulation of immune response.

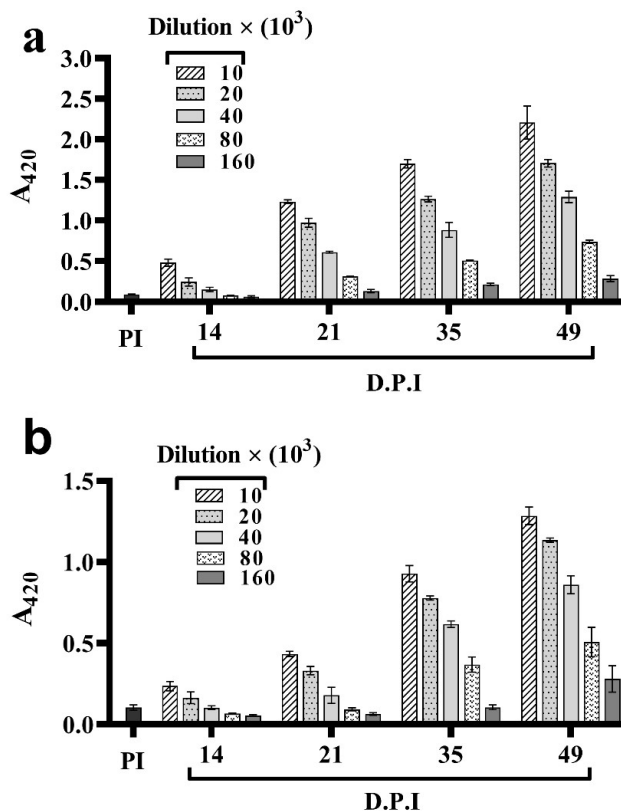


Figure 16. Antibody titers of the anti-WTrPFO and anti-rPFO_{C-ter} antisera. Different dilutions of the antisera drawn on different days post-immunization (D.P.I.) from mice immunized with WTrPFO (**panel a**) and rPFO_{C-ter} (**panel b**) were subjected to ELISA for determination of antigen-specific antibody titers. Anti-mouse Fc-specific alkaline phosphatase-conjugated antibody was used as a secondary antibody. End point titers of the anti-WTrPFO antisera (**a**) were determined to be $\geq 1:20,000$ on day 14, $\geq 1:80,000$ on day 21 and 35, and $\geq 1:160,000$ on day 49 post-immunization. End point titers for anti-rPFO_{C-ter} antisera were determined to be $>1:10,000$, $>1:20,000$, $>1:80,000$, & $>1:160,000$ on day 14, day 21, day 35, and day 49 post-immunization, respectively. Absorbance at 420 nm (A_{420}) depicts mean \pm S. D. of pooled antisera samples ($n=5$ mice per group) analyzed in triplicates. One-way ANOVA was used to determine the significant difference between PI and different antisera dilutions.

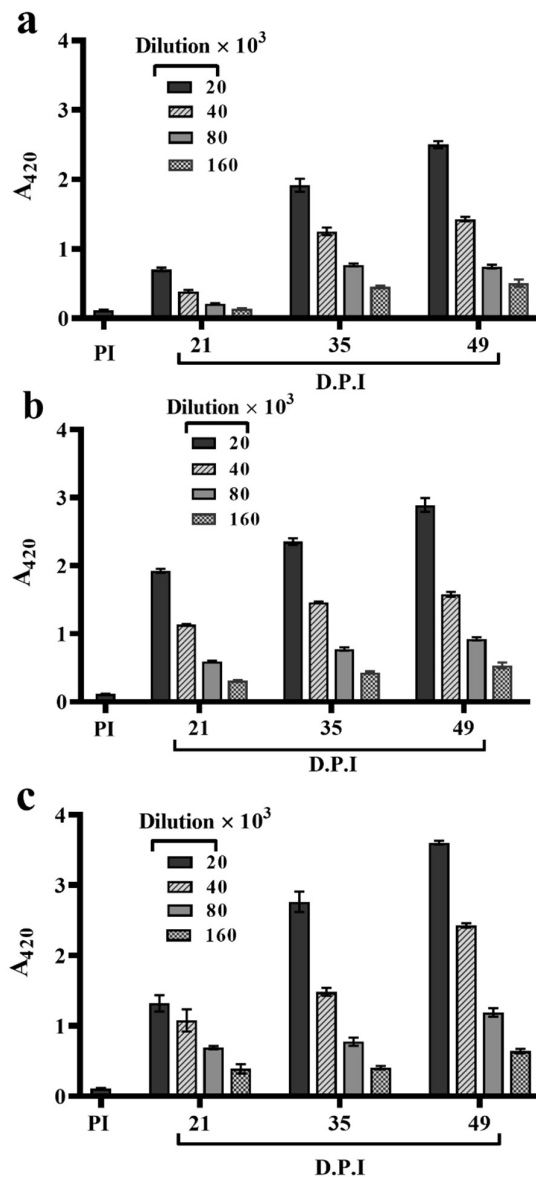


Figure 17. Antibody titers of the PFO mutant antisera. Different dilutions of the antisera drawn on different days' post-immunization (D.P.I.) from mice immunized with **rPFO_{V208C}** (panel a), **rPFO_{A212C}** (panel b) and **rPFO_{R467A}** (panel c) were subjected to ELISA for determination of antigen-specific antibody titers using anti-mouse Fc-specific alkaline phosphatase-conjugated secondary antibody. Endpoint titers of the antisera generated against the three mutants on day 21, day 35, and day 49 post-immunization were determined to be >1: 160,000, except for anti-rPFO_{V208C} antiserum on day 21, for which the titer was found to be > 1: 80,000. Absorbance at 420 nm (A₄₂₀) depicts mean \pm S.D. of pooled antisera samples (n=5 mice per group) analyzed in triplicates. One-way ANOVA was used to determine the significant difference between PI and antisera dilutions.

4.4.2 Specificity determination of anti-WTrPFO and anti-PFO mutant's antisera

The antisera from the mice immunized with the WTrPFO, PFO_{C-ter}, rPFO_{V208C}, rPFO_{A212C}, and rPFO_{R467A} collected on day 35 after immunization were used as the primary antibodies in immunoblotting analysis of the respective proteins for determination of the antigen-specificity of the antisera. Immunoblotting of uninduced (UI) and induced cell lysates (I) of the bacterial cells expressing WTrPFO or its mutants with the respective antisera resulted in detection of a band at the expected position of the recombinant proteins only in the induced cell lysates (**Figure 18a-e, respectively**). However, no such band was detected in the uninduced cell lysates of the *E. coli* BL21(λDE3)pLysS cells harboring the respective constructs indicating the generation of highly specific antibodies by the WTrPFO and all its mutants generated in the present study.

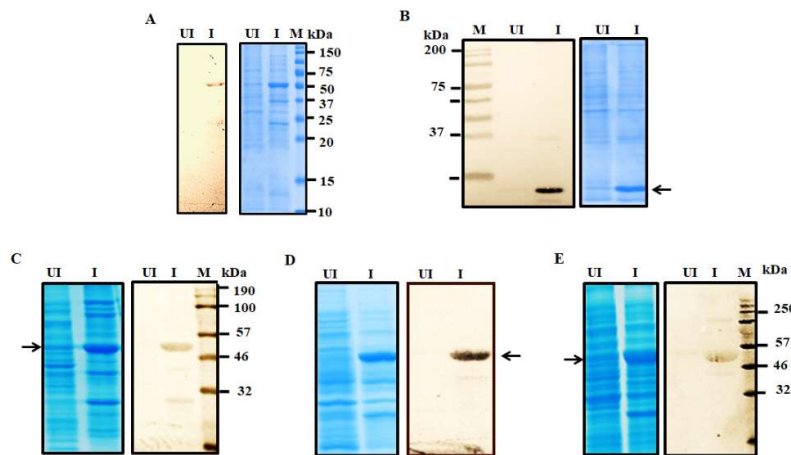


Figure 18. Specificity determination of antisera generated against the WTrPFO, rPFO_{C-ter}, rPFO_{V208C}, rPFO_{A212C} and rPFO_{R467A}. The uninduced (UI) and induced (I) cell lysates (10 g each) of *E. coli* BL21(λDE3) pLysS cells expressing WTrPFO, rPFO_{C-ter}, rPFO_{V208C}, rPFO_{A212C} and rPFO_{R467A} (panels a-e, respectively) were electrophoresed and immunoblotted with the respective antiserum (1:10, 000). Alkaline phosphatase (AP)-conjugated goat anti-mouse/rabbit antibody (1:10,000) dilution was used as the secondary antibody. The left panels show the parallelly run SDS-PAGE stained with Coomassie blue stain and the right panels show the Western blot images of the same lysates. The arrow in all the panels points to the position of the recombinant proteins (WTrPFO and its mutants at ~54 kDa; rPFO_{C-ter} at ~14 kDa) only in the induced cell lysates. All antisera (anti-WTrPFO, and antisera of the mutants) are used in 1:10, 000 dilutions for immunoblot analysis. “M” denotes protein molecular weight markers (kDa) in all the panels.

4.4.3 Cross-reactivity analysis

Immunoblot analysis of the induced cell lysates of the *E. coli* BL21(λ DE3) pLysS cells harboring pET22.*PFO*_{wt} and pET22.*PFO*_{C-ter} showed that the anti-WTrPFO antiserum collected on day 35 (a week after the second booster) was able to detect a single band corresponding to the recombinant protein in the induced cell lysates (**Figure 19a, lane I, rPFO**).

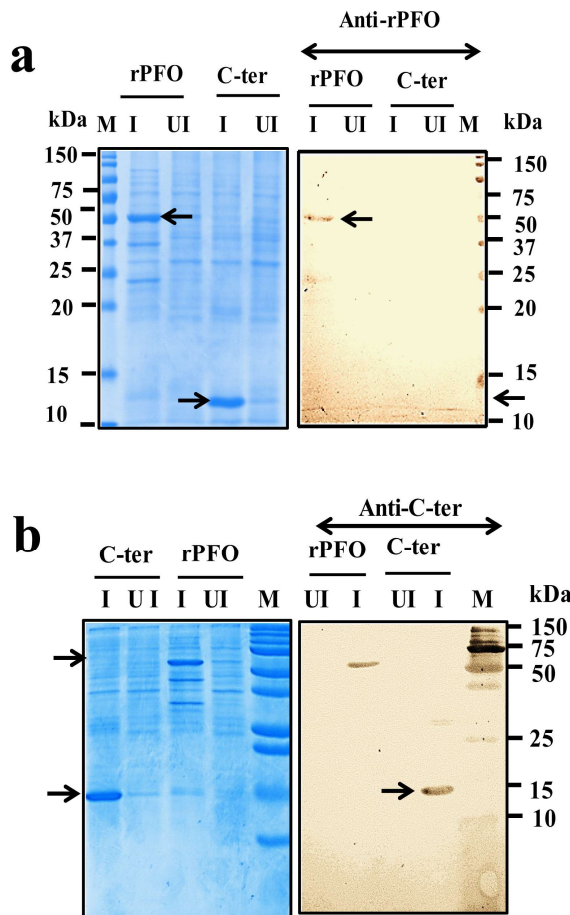


Figure 19. Cross-reactivity Analysis of anti-WTrPFO and rPFO_{C-ter} antisera. Antigen specificity of the (a) anti-WTrPFO and (b) anti-rPFO_{C-ter} antisera was determined by immunoblot analysis. Ten micrograms of the uninduced (UI) and induced (I) cell lysates of the *E. coli* BL21(λ DE3) pLysS cells expressing WTrPFO (rPFO) or rPFO_{C-ter} (C-ter) were resolved on SDS-PAGE and immunoblotted either with anti-WTrPFO antiserum (anti-rPFO, panel a) or anti-rPFO_{C-ter} antiserum (anti-C-ter, panel b) at 1:10,000 dilution. Alkaline phosphatase (AP)-conjugated goat anti-mouse/rabbit antibody (1:10,000) dilution was used as secondary antibody. In both the panels, the image on the left shows the parallelly run SDS-PAGE of the same lysates stained with Coomassie blue stain. Lane M denotes the pre-stained protein molecular weight (kDa) marker.

Absence of the band in the uninduced cell lysate indicates the specificity of the anti-WTrPFO antibodies (**Figure 19a, lane UI, rPFO**). Surprisingly, the anti-WTrPFO antiserum could not detect the rPFO_{C-ter} protein (**Figure 19a, lane I, C-ter**) in the cell lysates of *E. coli* BL21(λ DE3)plysS expressing rPFO_{C-ter}.

Likewise, the antigen-specificity and the cross-reactivity analysis of anti-rPFO_{C-ter} antiserum was analyzed by immunoblotting the induced cell lysates of the *E. coli* BL21(λ DE3) plysS expressing WTrPFO. Detection of a single band at ~54 kDa position clearly revealed that the anti-rPFO_{C-ter} antiserum (raised against only the C-terminal of the PFO) could specifically cross-react with the full length protein (**Figure. 19b, lane I, rPFO**). Detection of a band at ~14 kDa position in the cells expressing the rPFO_{C-ter} revealed the antigen-specificity of the anti-rPFO_{C-ter} antiserum (**Figure 19b, lane I, C-ter**).

Likewise, the cross-reactivity of the antisera raised against the WTrPFO and its substitution mutants against each other was analyzed by resolving all the four proteins on SDS-PAGE and immunoblotting with each antiserum separately on different blots. As shown in the **Figure 20 a-d**), all the four antisera were able to cross-react with each of the four proteins and a band at the expected ~54 kDa position was detected in each of the four lanes corresponding to WTrPFO (**lane 1**), rPFO_{A212C} (**lane 2**), rPFO_{V208C} (**lane 3**) and rPFO_{R467A} (**lane 4**) in the four blots developed using anti-WTrPFO, anti-rPFO_{A212C}, anti-rPFO_{V208C} and anti-rPFO_{R467A} antisera (**Figure 20 a-d**, respectively). Effective cross-reactivity of each antiserum with WTrPFO and other mutants revealed the structural similarity of the antigen binding region (Fab fragment) of the antibodies present in the antisera.

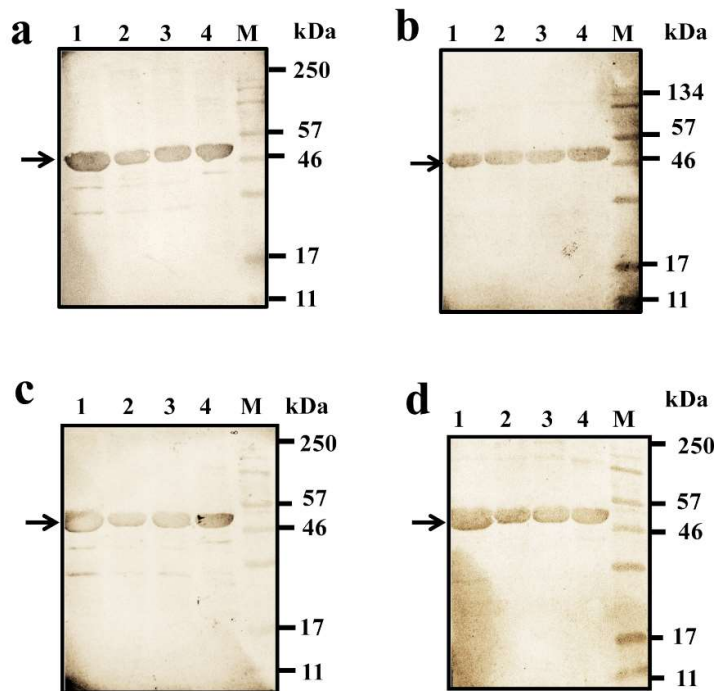


Figure 20. Cross-reactivity Analysis of antisera generated against the WTrPFO and its substitution mutants. Thirty micrograms of the purified proteins (lanes 1-4, WTrPFO, rPFO_{V208C}, rPFO_{A212C}, and rPFO_{R467A}, respectively) were resolved on SDS-PAGE and immunoblotted with the anti-WTrPFO (**panel a**), anti-rPFO_{V208C} (**panel b**), anti-rPFO_{A212C} (**panel c**), and anti-rPFO_{R467A} (**panel d**) antisera (each at 1:10,000 dilution). Alkaline phosphatase (AP)-conjugated goat anti-mouse/ rabbit antibody (1:10,000) dilution was used as the secondary antibody. Lane M in all the panels denotes the color-coded pre-stained protein molecular weight marker and the arrow points to the detected recombinant protein band.

4.4.4 Analysis of the type of immune response by antibody Isotyping

Different IgG isotypes namely IgG1, IgG2a, and IgG2b in the anti-WTrPFO, anti-rPFO_{C-ter} antisera (**Figure 21a and b, respectively**) and the antisera generated against other mutants (**Figure 22a-c**) collected on day 21, day 35, and day 49 post-immunization were assayed to determine the type of immune response generated against the test proteins. Significantly elevated levels of all the three isotypes in the anti-WTrPFO (**Figure 21a**) and anti-rPFO_{C-ter} (**Figure 21b**) antisera collected on day 21, 35, and 49 when compared to the respective pre-immune sera. The ratios of IgG1/IgG2a and IgG1/IgG2b in the anti-WTrPFO collected on day 21, day 35, and day 49 were found to be >1 that reflects the Th2- biased

immune response (Figure 21a). The ratio of IgG1/IgG2a in the anti-rPFO_{C-ter} antisera was determined to be much >1 on all study intervals (8.67, 7.89 and 8.64 on day 21, day 35, and day 49, respectively), whereas the ratio of and IgG1/IgG2b was determined to be slightly <1 (0.962, 0.867 and 0.925 on day 21, day 35, and day 49, respectively), suggesting predominantly Th2-biased mixed immune response (Figure 21b).

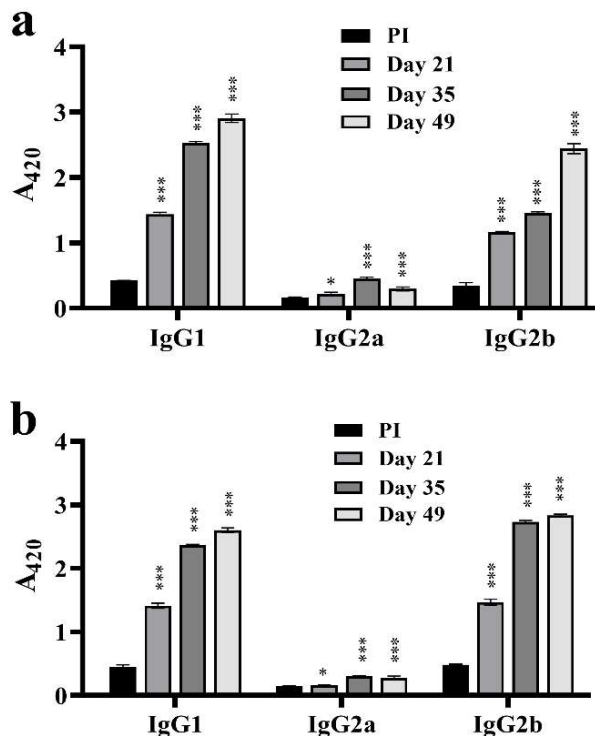


Figure 21. Determination of different isotypes of IgG present in the antisera of WTrPFO and rPFO_{C-ter}. The anti-WTrPFO (panel a) and anti-rPFO_{C-ter} (panel b) antisera, collected on day 21, 35, and 49 post-immunization were analyzed for different IgG isotypes' levels by ELISA using respective HRP-conjugated isotype-specific secondary antibodies. Pre-immune (PI) was included as a control. Data represent mean \pm S.D. of absorbance (A_{420}), of analyses performed in triplicates. Significance of difference in the different isotypes in the antisera collected on different days with respect to PI was determined using a one-way ANOVA and is denoted as $p \leq 0.05$ (*), $p \leq 0.01$ (**), and $p \leq 0.001$ (***)

The IgG1 and IgG2b levels were also found to be significant increase in the antisera generated against the mutants rPFO_{V208C}, rPFO_{A212C}, and rPFO_{R467A} (Figure 22). On day 21, significance of change for IgG1 for all

the three antisera was determined to be $p \leq 0.01$ whereas the IgG1 levels increased further on subsequent intervals post-boosters and attained more significant change ($p \leq 0.001$) when compared to pre-immune sera. The IgG2b levels were found to be significantly higher at $p \leq 0.001$ in all the three antisera (anti-rPFO_{V208C}, rPFO_{A212C} and rPFO_{R467A}), at all the time intervals, except on day 21 for rPFO_{R467A}, when it was slightly lower at $p \leq 0.05$.

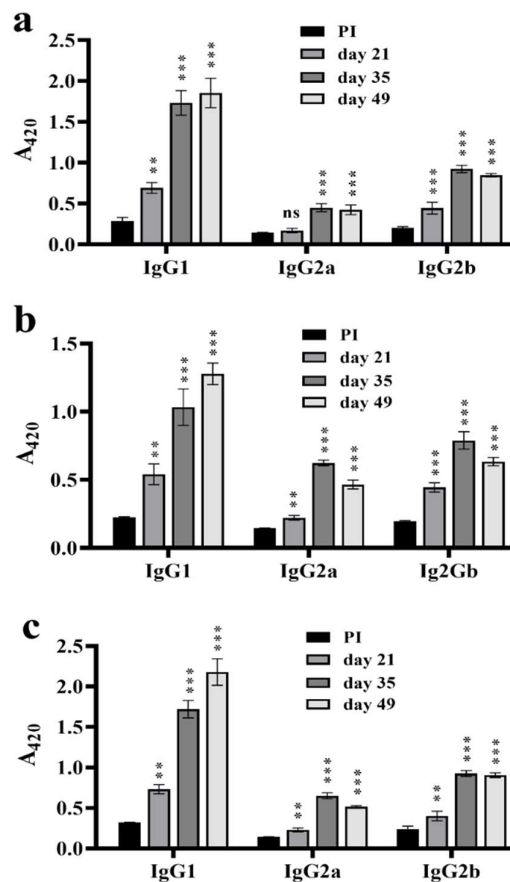


Figure 22. Antibody isotyping of the anti-rPFO substitution mutant antisera. The anti-rPFO_{V208C} (panel a), anti-rPFO_{A212C} (panel b), and anti-rPFO_{R467A} (panel c) antisera, collected on day 21, 35, and 49 post-immunization were analyzed for different IgG isotypes' levels by ELISA using respective HRP-conjugated isotype-specific secondary antibodies. Pre-immune (PI) was included as a control. Data represent mean \pm S.D. of absorbance (A_{420}), of analyses performed in triplicates. Significance of difference in the different isotypes in the antisera collected on different days with respect

to PI was determined using a one-way ANOVA and is denoted as $p \leq 0.05$ (*), $p \leq 0.01$ (**), and $p \leq 0.001$ (***)).

However, No significant increase was found in IgG2a levels in the antisera against the rPFO_{V208C} on day 21, whereas it was significantly increased in the anti-rPFO_{A212C} and anti-rPFO_{R467A} antisera ($p \leq 0.01$) on day 21. The antisera drawn on day 35 and 49 after booster administration also showed significantly higher levels of IgG2a for all the three mutants ($p \leq 0.001$) in all the three mutants was observed significant increased (**Figure 22a-c**). Thus, antibody isotyping of the antisera generated against the rPFO_{V208C}, rPFO_{A212C}, and rPFO_{R467A} on all the study intervals indicated a Th2-biased immune response as the ratio of IgG1 to IgG2a and IgG1:IgG2b absorbance were determined to be > 1 .

4.4.5 Generation of T-cell memory and analysis of immune response by WTrPFO and its mutants

In vitro proliferation of the splenocytes isolated from the mice immunized with the WTrPFO and rPFO_{C-ter} and stimulated with the respective proteins resulted in significantly higher proliferation, in comparison to that stimulated with PBS at all study intervals (**Figure 23**). No increase in the proliferation was noted when the splenocytes isolated from the PBS immunized mice were stimulated with the test proteins. The significance level for the splenocytes isolated from the WTrPFO-immunized mice, stimulated with the same protein were found to be at $p \leq 0.01$, $p \leq 0.001$ and $p \leq 0.05$ at 24 h, 48 h and 72 h post-stimulation, respectively (**Figure 23a**). The significance levels of change with rPFO_{C-ter} were found to be $p \leq 0.01$ at all the three intervals post-stimulation (**Figure 23b**). The stimulation index of the WTrPFO- and rPFO_{C-ter}-stimulated splenocytes was determined to be 1.4 and 2.08, respectively, which was noticeably higher than that of the control splenocytes (~1.12 and ~1.15) indicating significant T cell activation and proliferation in response to antigens.

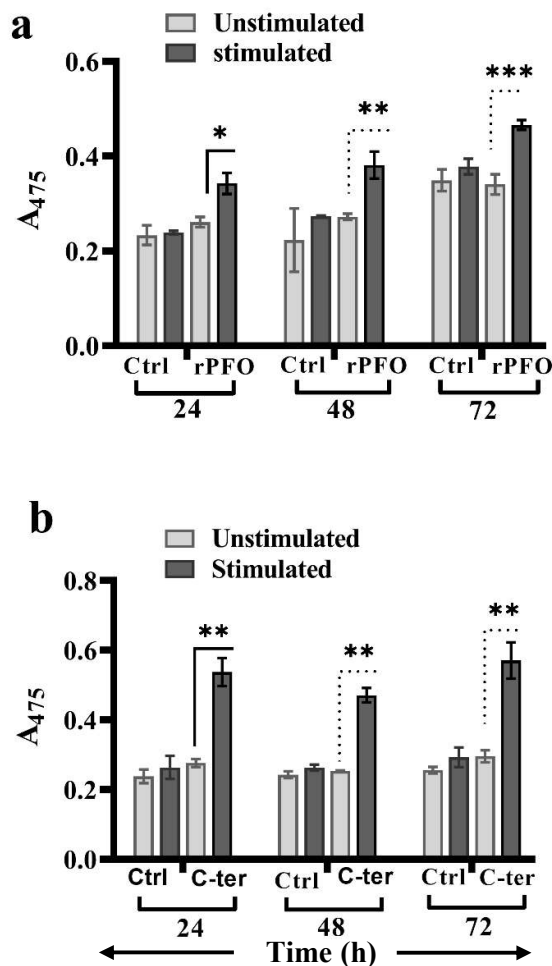


Figure 23. Assessment of *in vitro* T cell proliferation response generated against the WTrPFO and rPFO_{C-ter}. Splenocytes (1×10^5 cell /well in 100 μ l) isolated from mice immunized with WTrPFO (**panel a**) and rPFO_{C-ter} (**panel b**) (i.p; 30 μ g/mice) were stimulated with the respective protein (20 μ g/ml, stimulated) and vehicle (1 \times PBS, unstimulated). ‘Ctrl’ in both the panels indicates splenocytes isolated from mice immunized with 1 \times PBS (control) and stimulated with either WTrPFO (panel a) or rPFO_{C-ter} (panel b) or PBS (unstimulated). Splenocyte proliferation was measured by XTT assay at different time intervals post-stimulation. Data represent the mean \pm S.D. of 3 independent experiments performed in triplicates. Statistical significance (p value) was calculated with respect to PBS-stimulated splenocytes of the same group using Student’s two-tailed t -test. $p \leq 0.05$ (*), $p \leq 0.01$ (**), and $p \leq 0.001$ (***)

No significant change in proliferation in the splenocytes isolated from the rPFO_{V208C}- immunized mice and stimulated with the same protein was observed at 24 h post-immunization. However, at 48 h and 72 h post-stimulation, a significant increase ($p < 0.01$) in proliferation as evidenced by increased absorbance was noted (**Figure 24a**).

When the splenocytes isolated from the rPFO_{A212C} and rPFO_{R467A} immunized mice were stimulated with the respective proteins, significantly increased proliferation at all the three time intervals was noted (rPFO_{A212C}, $p < 0.01$ at all the three intervals; rPFO_{R467A}, $p < 0.05$ at 24 h and $p < 0.01$ at 48 h and 72h) (**Figures 24 b and c**, respectively).

For calculation of the stimulation index in different sets of splenocyte, both experimental and control mice were considered for stimulation with the respective experimental proteins (antigen) as shown in Table 4.2. Stimulation indices (S.I.) of the protein-stimulated splenocytes from the rPFO_{V208C}-, rPFO_{A212C}-, and rPFO_{R467A}-immunized mice at 72 h were determined to be ~1.94, ~1.55 and ~ 2.40, respectively, which were significantly higher than that of the respective splenocytes stimulated with the PBS stimulated splenocytes (~1.0505, ~1.02, and ~1.05, respectively). These data highlighted the T cell activation by antigenic stimulation and generation of T cell memory.

| | 24 | | 48 | | 72 | |
|-------------------|------|----------------|------|----------------|------|----------------|
| Proteins | SI | <i>p</i> value | SI | <i>p</i> value | SI | <i>p</i> value |
| WTrPFO | 1.12 | 0.0018 | 1.4 | 0.009 | 1.23 | 0.0052 |
| rA212C | 1.13 | 0.0101 | 1.48 | 0.0061 | 1.55 | 0.0061 |
| rV208C | 1.13 | 0.1221 | 1.93 | 0.0011 | 1.94 | 0.0011 |
| rR467A | 1.27 | 0.0301 | 2.15 | 0.0026 | 2.4 | 0.0026 |
| C-terminal domain | 2.08 | 0.0313 | 1.86 | 0.0083 | 1.75 | 0.0022 |

Table.4.2. T cell stimulation indices (S.I.) of stimulated splenocytes isolated from immunized mice with different recombinants proteins at different time post-stimulation. Significance (*p* value) is calculated with respect to the control cells at respective time durations.

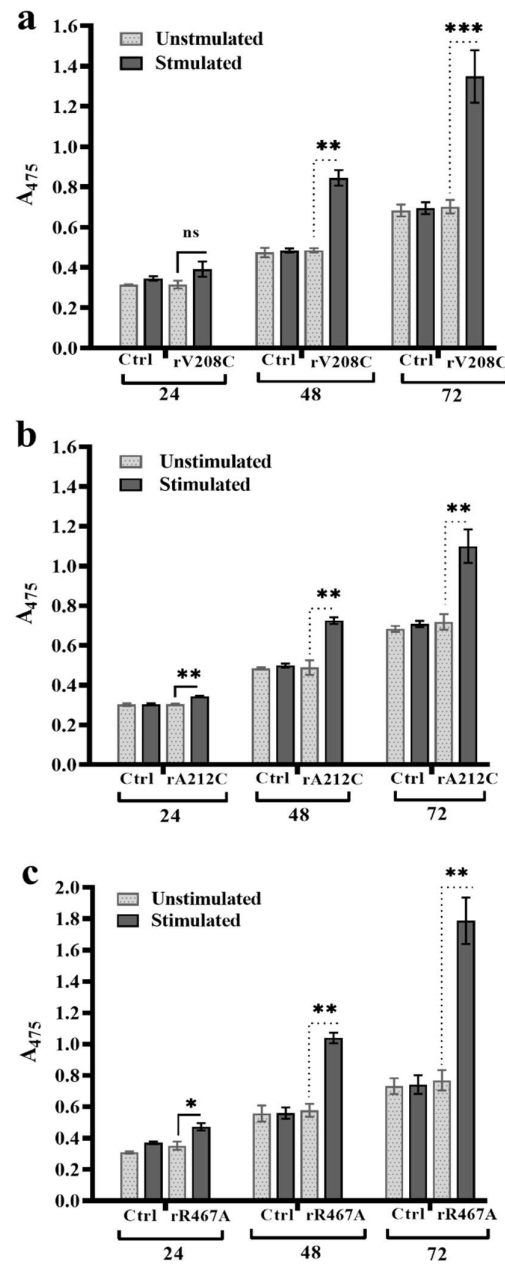


Figure 24. Assessment of T cell proliferation response *in vitro* generated against the recombinant PFO mutants (rPFO_{V208C}, rPFO_{A212C}, and rPFO_{R467A}). Splenocytes (1×10^5 cell/well in 100 μ l) isolated from the mice immunized with rPFO_{V208C} (**panel a**), (**panel b**) and rPFO_{R467A} (**panel c**) (i.p.; 30 μ g/mice) were stimulated with the respective proteins (20 μ g/ml, stimulated) and vehicle (1 \times PBS, unstimulated). ‘Ctrl’ in all the panels indicates splenocytes isolated from mice immunized with 1 \times PBS (control) and stimulated with either proteins or PBS (unstimulated). Splenocyte proliferation was measured by XTT assay at different time intervals post-stimulation. Data represent the mean \pm S.D. of 3 independent experiments performed in triplicates. Statistical significance (p value) was calculated with respect to PBS-stimulated splenocytes of the same group using Student’s two-tailed t -test and is denoted as $p \leq 0.05$ (*), $p \leq 0.01$ (**), and $p \leq 0.001$ (***)

4.4.6. Immune response analysis by cytokine profiling of the culture supernatants of splenocytes

The type of T cell immune response (evaluated by antibody isotype analysis) generated by the WTrPFO, rPFO_{C-ter} and its mutants (rPFO_{A212C}, rPFO_{V208C} and rPFO_{R467A}) on day 7 after second booster (on day 35 post immunization) was further confirmed by assessing the levels of IFN- γ (Th1 marker) and IL-4 (Th2 marker) in the splenocyte culture supernatants post-stimulation of splenocytes isolated from mice immunized with the respective proteins.

A significant increase ($p \leq 0.05-0.01$) in both IL-4 and IFN- γ levels in splenocytes isolated from WTrPFO (**Figure 25a and 25c**) and rPFO_{C-ter} (**Figure 25b and 25d**) immunized mice stimulated with the respective proteins demonstrated that both proteins are able to generate mixed T cell immune response at all the time points. IFN- γ level increased significantly ($p < 0.05-0.01$) in the culture supernatant of splenocytes of WTrPFO-immunized mice after stimulation with the WTrPFO, (~ 4.98 fold and 4.51 folds at 48 h and 72 h post-stimulation) as compared to that of the splenocytes from PBS-immunized mice stimulated with the protein. The IFN- γ levels remained higher than the control splenocytes from 48h to 72h (~573.12 pg/ml at 48 h, and 965 pg/ml at 72 h post-stimulation). The splenocytes isolated from rPFO_{C-ter} immunized mice upon stimulation with the same protein showed 4.45 and 3.04-fold increase in IFN- γ levels at 48 h and 72 h, respectively ($p < 0.05$), in comparison to the control splenocytes isolated from the PBS-immunized mice post-stimulation with the same protein. The IFN- γ levels were determined to be 473.75pg/ml at 48 h and 666.87pg/ml at 72 h. It was noted that at 48 h, the increase in IL-4 levels was more prominent indicative of Th2 immune response), in the WTrPFO-stimulated splenocytes isolated from the immunized mice. At 72 h, there was a shift to Th1 response as IFN- γ levels increased further with a concomitant decrease in IL-4 levels in the splenocytes isolated from both the WTrPFO (**Figure 25a and 25c**) and rPFO_{C-ter} (**Figure 25b and 25d**)

immunized mice, suggesting a shift to Th1-biased mixed immune response at later intervals.

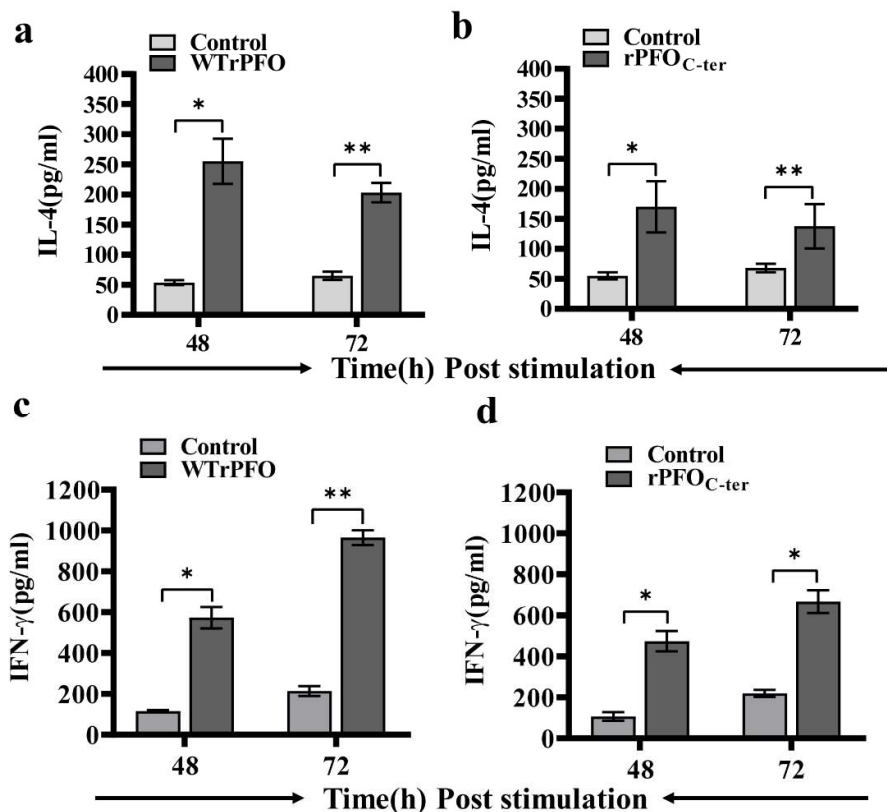


Figure 25. Analysis of T cell immune response (Th1 and Th2 type) against WTrPFO and rPFO_{C-ter} by cytokine ELISA. **(a and b)** IL-4 levels (pg/ml) in the culture supernatants (harvested at different time points) of splenocytes isolated from the WTrPFO and rPFO_{C-ter} immunized mice and stimulated with the respective proteins, respectively. **(c and d)** IFN-γ levels in the culture supernatants (harvested at different time points) of splenocytes isolated from the WTrPFO and rPFO_{C-ter} immunized mice and stimulated with the respective proteins. Control in each panel represents the cytokine produced by splenocytes of PBS-immunized mice, stimulated with respective proteins. Data represent the mean± SD of three experiments, performed in triplicates. The Statistical significance (*p* value) levels are as follows: $p \leq 0.05$ (*), $p \leq 0.01$ (**), $p \leq 0.001$ (***)

The supernatant of splenocytes isolated from the mutants rPFO_{V208C}, and rPFO_{A212C}, rPFO_{R467A}-immunized mice and stimulated with the same proteins also showed significantly increased levels of IL-4 at 48 h and 72 h ($p \leq 0.01$) post-stimulation. Increase in the IL-4 level was found to be increased by approximately, 4.6, 4.3 and 4.5 folds at 48 h in the supernatant of the splenocytes isolated from mice immunized with, the

rPFO_{V208C}, rPFO_{A212C} and rPFO_{R467A}, respectively upon stimulation with the respective proteins (**Figure 26a-c**). Further culturing of the splenocytes till 72 h post-stimulation showed a significant increase ($p \leq 0.01$) in the IL-4 levels and the fold increase was determined to be to be 4.09, 4.20, and 4.45 folds, respectively, with respect to control splenocytes (isolated from the PBS-immunized mice stimulated with the respective proteins). Greater release of the IL-4 by splenocytes isolated from the mice immunized with the PFO mutants (rPFO_{A212C}, rPFO_{V208C} and rPFO_{R467A}) in comparison to that of WTrPFO and PFO_{C-ter}-immunized mice suggest greater humoral immune response generated by the mutants and is also in agreement with the antibody isotyping data.

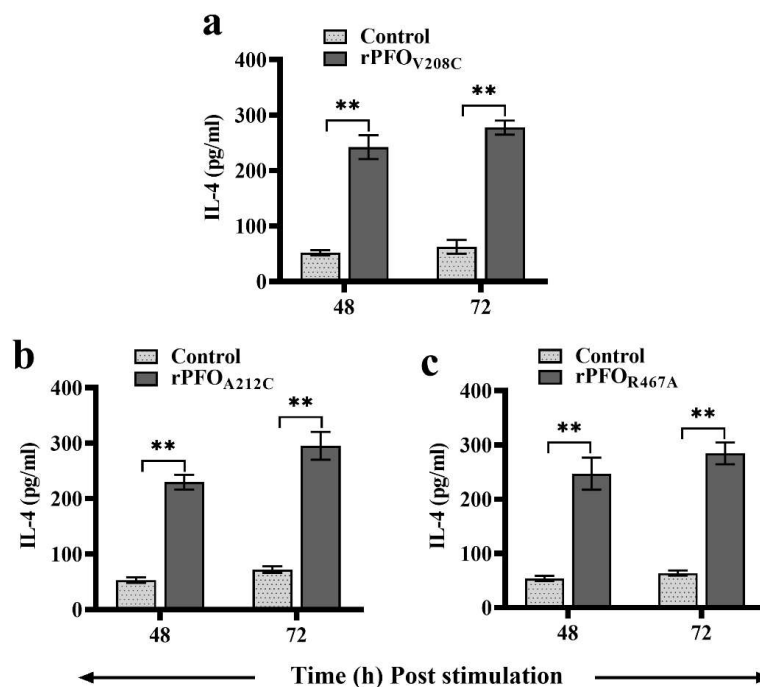


Figure 26. Analysis of Th2-type T cell immune response against the recombinant PFO substitution mutants by cytokine (IL-4) ELISA. (**a-c**) IL-4 levels (pg/ml) in the culture supernatants (harvested at different time points) of splenocytes isolated from the rPFO_{V208C} (panel a), rPFO_{A212C} (panel b) and rPFO_{R467A} (panel c)- immunized mice on day 35 post-immunization, and stimulated with the respective proteins, respectively. Control in each panel represents the cytokine produced by splenocytes of PBS-immunized mice, stimulated with respective proteins. Data represent the mean \pm SD of three experiments, performed in triplicates. The Statistical significance (p value) levels are as follows: $p \leq 0.05$ (*), $p \leq 0.01$ (**), $p \leq 0.001$ (***)

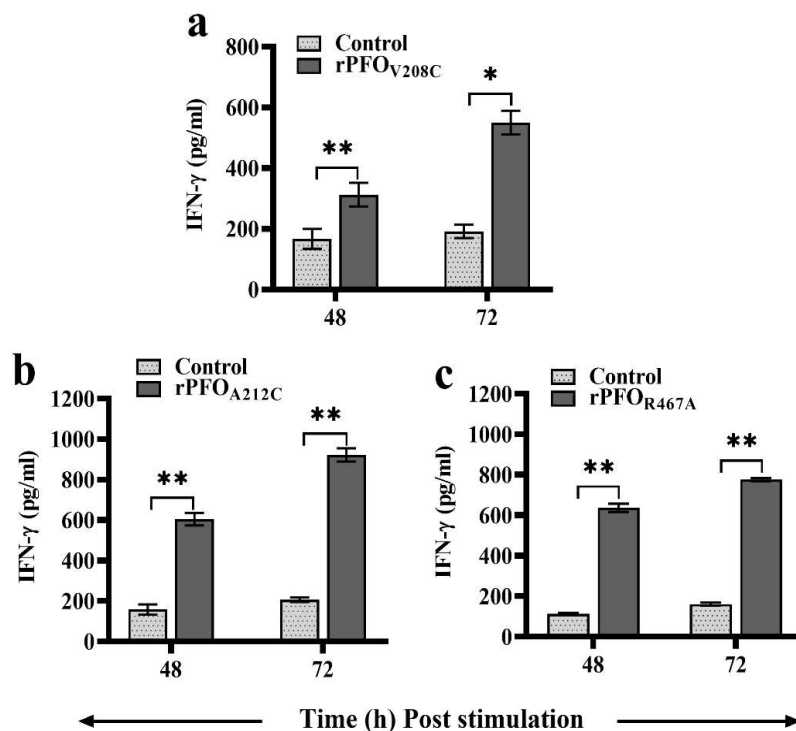


Figure 27. Analysis of Th1-type T cell immune response against the recombinant PFO substitution mutants by cytokine (IFN- γ) ELISA. **(a-c)** IFN- γ levels (pg/ml) in the culture supernatants (harvested at different time points) of splenocytes isolated from the rPFO_{V208C} (panel a), rPFO_{A212C} (panel b) and rPFO_{R467A} (panel c)- immunized mice on day 35 post-immunization, and stimulated with the respective proteins ((20 μ g/ml), respectively. Control in each panel represents the cytokine produced by splenocytes of PBS-immunized mice, stimulated with respective proteins. Data represent the mean \pm SD of three experiments, performed in triplicates. The Statistical significance (p value) levels are as follows: $p \leq 0.05$ (*), $p \leq 0.01$ (**), $p \leq 0.001$ (***)).

The IFN- γ levels were also found to be increased significantly ($p < 0.05$ -0.01) in the supernatant of the splenocytes from rPFO_{V208C}, rPFO_{A212C}-, and rPFO_{R467A}-immunized mice (stimulated with the respective proteins (1.87, 3.82, and 5.59.7 folds, respectively at 48 h, and, 2.86, 4.45, and 5.01 folds, respectively at 72 h post-stimulation) (**Figure 27 a-c**). IFN- γ levels in the culture supernatants of the splenocytes isolated from the rPFO_{V208C}-, rPFO_{A212C}- and rPFO_{R467A}-immunized mice were determined to be

~604.37 pg/ml, ~312.50 pg/ml, and ~636.87.3 pg/ml at 48 h and ~921.87 pg/ml, ~550 pg/ml, ~776.87 pg/ml at 72 h post-stimulation with the respective proteins. These levels were comparatively less than that released by the splenocytes isolated from the WTrPFO- and rPFO_{C-ter} immunized mice, stimulated with the respective proteins, suggesting a relatively reduced cell mediated immune response by the mutants. Significant increase in both the IL-4 and IFN- γ levels by the splenocytes from the mice immunized with WTrPFO, rPFO_{C-ter} and, the three mutants and stimulated with the respective proteins, in comparison to that released by control splenocytes suggested a Th1 and Th2 bipolar response.

Analysis of cytokines secreted from the splenocytes isolated from the mice immunized with the WTrPFO, rPFO_{C-ter}, rPFO_{V208C}, rPFO_{A212C}, and rPFO_{R467A} after 32 weeks of primary immunization and stimulation with the respective protein resulted in significant increase in IFN- γ levels ($p \leq 0.05-0.01$) at different time post-stimulation. The IFN- γ levels increased significantly from 395.5pg/ml at 24 h to 651.1pg/ml at 48 h and 1688.9 pg/ml at 72 h in the splenocytes from WTrPFO-immunized mice upon stimulation with the same (**Figure 28a**). IFN- γ levels also increased in the supernatants of spleen cells isolated from rPFO_{C-ter}, and rPFO_{A212C}-immunized mice incubated for different time points with the respective proteins with increase in incubation time ($p \leq 0.05$ to 0.01) (**Figure 28b and d**). Stimulation of spleen cells of the rPFO_{V208C} and rPFO_{R467A}-immunized mice with respective proteins didn't show any increment in IFN- γ at 24h; however IFN- γ levels significantly increased at 48 h and 72h post-stimulation ($p \leq 0.05-0.01$). (**Figure 28c and 28e**). On the other hand, the IL-4 levels sharply declined in spleen cells from mice immunized with the WTrPFO and its all mutants (rPFO_{A212C}, rPFO_{V208C}, rPFO_{R467A} and rPFO_{C-ter}) upon stimulation with the respective proteins at any time interval (Data not shown). These data suggest that prolonged

immune response switched to only Th1 type immune upon administration with boosters.

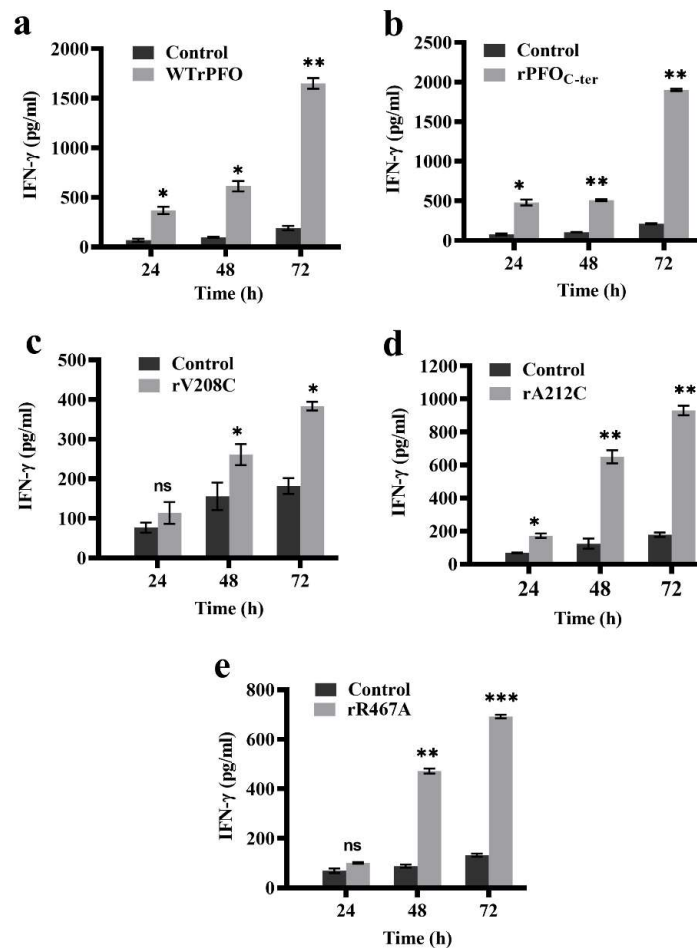


Figure 28. *In vitro* analysis of long term (32 weeks post-immunization) T cellular immune (Th1 type, IFN- γ) by cytokine ELISA. The IFN- γ (pg/ml) levels in the culture supernatants of splenocytes (1×10^5 cell /well in 100 μ l) isolated from the WTrPFO (panel a), rPFO_{C-ter} (panel b), rPFO_{V208C} (panel c), rPFO_{A212C} (panel d) and rPFO_{R467A} (panel e) immunized mice on 32 weeks post-immunization and stimulated with the respective proteins (20 μ g/ml) was analysed. Control in each panel represents the cytokine produced by splenocytes of PBS-immunized mice, stimulated with the respective proteins. Data represent the mean \pm SD of three experiments, performed in triplicates. The statistical significance (p value) calculated with respect to control is denoted as $p \leq 0.05$ (*), $p \leq 0.01$ (**), $p \leq 0.001$ (***). “ns” indicates not significant.

4.5 Assessment of neutralization potential of immunization with the WTrPFO and its mutant against the wild type rPFO toxicity

4.5.1 Neutralization of hemolytic activity of the WTrPFO by the anti-WTrPFO and anti-mutant PFO antisera

Treatment of RBCs with the WTrPFO (2 µg/ml) caused ~ 80 % lysis when compared to the cells treated with PBS. Pre-incubation of WTrPFO at 2 µg/ml (that caused 80 % hemolysis) with different dilutions (50 % - 5 %) of both the anti-WTrPFO and anti-rPFO_{C-ter} antisera prior to addition to mice RBCs (2.5×10^6 , 50 µl) resulted in inhibition of hemolytic activity to a great extent, indicating the excellent inhibitory capacity of both antisera (**Figure 29**). Inhibition of hemolytic activity of the WTrPFO was maximum (more than 90 %) at the dilution of 25 % of both the antisera. Incubation of the toxin (WTrPFO) with other dilutions of the antisera (50 %, 10 %, and 5%) also resulted in more than 80 % inhibition of hemolytic activity. No significant inhibition (~4.56 %) was observed when the WTrPFO was pre-incubated with neat pre-immune serum.

Likewise, significant inhibition of hemolytic activity was observed when the WTrPFO was incubated with different dilutions of the antisera generated against the three substitution mutants (Figure 29). Although neat antisera of all the mutants showed relatively lower inhibition of hemolysis as compared to the diluted antisera, the number of viable cells was still

significantly higher than the RBCs treated with the WTrPFO alone.

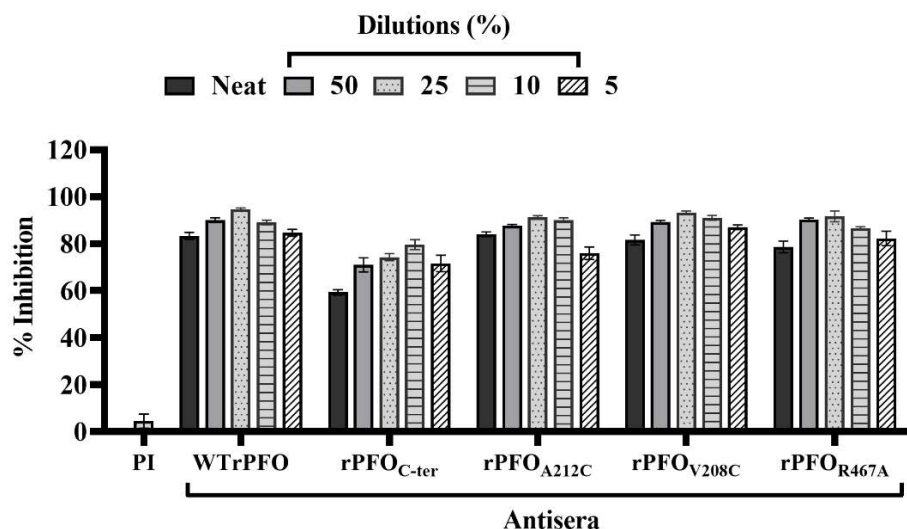


Figure 29. Neutralization of hemolytic activity of WTrPFO by different antisera (antisera generated against WTrPFO, its substitution mutants and rPFO_{C-ter}). The WTrPFO (2.0 µg/ml) was incubated with different dilutions of the antisera (neat and 50 % - 5 %) in a total volume of 150 µl for 1 h at 37 °C before addition to the mice RBCs (2.5×10⁶ cells in 50 µl). After incubation at 37 °C for 60 min, the absorbance of the supernatant was measured at 540 nm for released haemoglobin. WTrPFO (20 µg/ml) pre-incubated with vehicle (1×PBS) was included as positive control and considered to cause 100 % hemolysis. WTrPFO pre-incubated with PI (neat) was included as negative control. Percentage inhibition of hemolysis was calculated with respect to the absorbance obtained with WTrPFO incubated with 1×PBS

4.5.2 *In vitro* neutralization of WTrPFO cytotoxicity by the anti-WTrPFO and anti-PFO mutant antisera

Treatment of the mice peritoneal macrophages with the WTrPFO at 100 µg/ml showed 80 % cytotoxicity. Neutralization capacity of different antisera was determined as the percentage of reduced cytotoxicity of the purified WTrPFO pre-incubated with different dilutions (1:10-1:10,000) of each antiserum, with respect to the cells incubated with the WTrPFO alone (considered as 100 %). Pre-incubation of the WTrPFO with the antisera generated against the WTrPFO, rPFO_{C-ter} and other mutants at all the dilutions (1:10-1: 10,000) was able to neutralize the cytotoxicity of the purified WTrPFO (100 µg/ml) significantly towards the mice peritoneal macrophages.

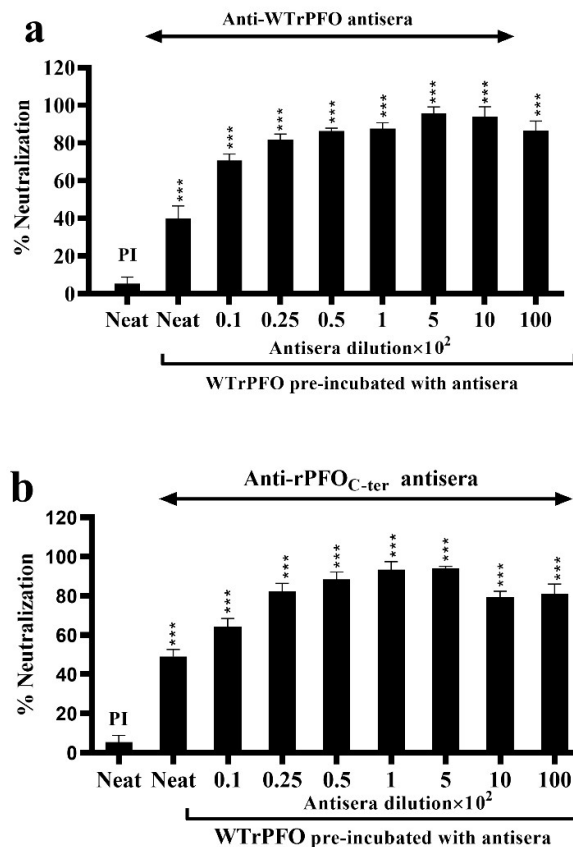


Figure 30. Neutralization of cytotoxic activity of WTrPFO in mice peritoneal macrophages by anti-WTrPFO and anti-rPFO_{C-ter} antisera. Mice peritoneal macrophages (5×10^4 macrophages/100 μ l) were treated with WTrPFO (100 μ g/ml) pre-incubated with different dilutions (1:10, 1:25, 1:50, 1:100, 1:500, 1:1000, and 1:10,000) of the anti-WTrPFO (**panel a**) and anti-rPFO_{C-ter} (**panel b**) for 1 h at 37 °C. The cells were then incubated at 37 °C for 24 h in 5 % CO₂ atmosphere, followed by LDH release. WTrPFO pre-incubated with PI (neat) was considered as negative control. Percentage neutralization was calculated with respect to LDH released by the cells treated with WTrPFO incubated with 1×PBS, taken as 100 % cytotoxicity. Data represent mean \pm SD of neutralization percentage of experiments performed in triplicates. Ordinary one-way ANOVA was used to determine the significance of neutralization ability of the antiserum with respect to control cells treated with WTrPFO incubated with PI. $p \leq 0.05$ (*), $p \leq 0.001$ (**), $p \leq 0.001$ (***)).

The cytotoxicity neutralization of toxin by the anti- WTrPFO and anti-PFO_{C-ter} antisera was between 70 % -96 % and 64 %- 94%, respectively, at 1:10 and 1:100 dilutions. However, at 1: 10,000 of the anti-WTrPFO and anti-rPFO_{C-ter} antisera, percentage neutralization was determined to be 87 % and 81 %, respectively (**Figure 30a and 30b**).

Neutralization of the WTrPFO toxicity upon pre-incubation with the antisera against rPFO_{V208C} and rPFO_{A212C} ranged between 50%-93% and 50-82%, respectively, with increase in dilution from 1:10 to 1:1000. **(Figure 31 a and 31b)**. Pre-incubation of the WTrPFO with the anti-rPFO_{R467A} antiserum was also able to reduce the WTrPFO cytotoxicity and percentage neutralization ranged from 60 % to 86 % with increasing dilutions of 1:10-1:500. At 1:10,000 dilution of the anti-rPFO_{R467A} antiserum, 76 % neutralization of the WTrPFO's toxicity was observed **(Figure 31c)**. Maximum neutralization of the toxin was noted at 1:1000 dilution of the antisera against WTrPFO, rPFO_{A212C}, and rPFO_{V208C} (~96%, ~93 % and ~83 %, respectively). Pre-incubation of the WTrPFO at 1:500 dilution of the antisera against the rPFO_{C-ter} and rPFO_{R467A} showed significant neutralization (94 % and 86 %, respectively) of the WTrPFO toxicity **(Figure 30b and 31c)**. The neat antisera of rPFO_{V208C} ($p \leq 0.01$), rPFO_{A212C} ($p \leq 0.05$) and rPFO_{R467A} ($p \leq 0.05$) could also neutralize the cytotoxicity of the toxin. Interestingly, the neat fraction of all the antisera showed least neutralization as observed in the *in vitro* inhibition of the WTrPFO's haemolytic activity. After reaching the equivalence zone, increase in the antibodies concentration by reducing the dilution, did not result in an increase in percentage neutralization. Thus, the targeted mutations resulted in rendering the rPFO mutants non-toxic. Further, the antisera generated against the WTrPFO, its N-terminal deletion variant rPFO_{C-ter} and substitution mutants (rPFO_{V208C}, rPFO_{A212C} and rPFO_{R467A}) neutralized the haemolytic activity in RBCs as well as the cytotoxic effect in mice peritoneal macrophages.

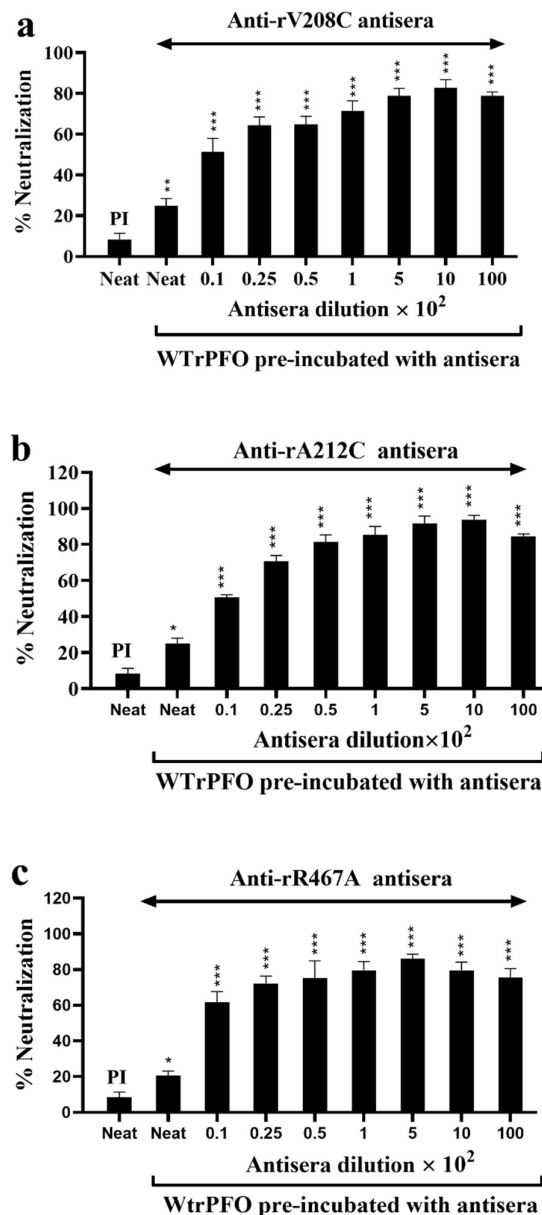


Figure 31. Neutralization of cytotoxic activity of WTrPFO in mice peritoneal macrophages by anti-rPFO_{V208C}, anti-rPFO_{A212C}, and anti-rPFO_{R467A} antisera. Mice peritoneal macrophages (5×10^4 macrophages/100 μ l) were treated with WTrPFO (100 μ g/ml) pre-incubated with different dilutions (1:10, 1:25, 1:50, 1:100, 1:500, 1:1000, and 1:10,000) of the anti-rPFO_{V208C} (**panel a**), anti-rPFO_{A212C} (**panel b**), and anti-rPFO_{R467A} (**panel c**) for 1 h at 37 °C. The cells were then incubated at 37 °C for 24 h in 5 % CO₂ atmosphere, followed by LDH release. WTrPFO pre-incubated with PI (neat) was considered as negative control. Percentage neutralization was calculated with respect to LDH released by the cells treated with WTrPFO incubated with 1×PBS, taken as 100 % cytotoxicity. Data represent mean \pm SD of neutralization percentage of experiments performed in triplicates. Ordinary one-way ANOVA was used to determine the significance of neutralization ability of the antiserum with respect to control cells treated with WTrPFO incubated with PI. $p \leq 0.05$ (*), $p \leq 0.01$ (**), $p \leq 0.001$ (***)

Chapter 5

Discussion

Different types of *C. perfringens* strains cause a variety of diseases both in humans and animals, which are attributed to a single or multiple toxin(s) secreted by different strains. The bacterium is ubiquitously present in the environment, highly pathogenic and causes a high proliferation rate, and results in death of animals either within hours of appearance of symptoms or without any clinical symptoms. Though, it is susceptible to several antibiotics including penicillin, clindamycin, its rapid proliferation rate results in death without a premonitory sign making antibiotics ineffective¹. This endorses the development of vaccines against the toxins involved in the pathogenesis of *C. perfringens* to counteract the infection. Though attempts have been made to develop vaccines against different toxins secreted by a specific type, these can be used against a specific type of *C. perfringens*. Therefore, a toxin which is secreted by all types is likely to assist in protecting the animals from all types of *C. perfringens*. PFO is one of the toxins of *C. perfringens* that contributes to the pathogenesis of *C. perfringens* and believed to be encoded by all the isolates². Although PFO is not the main disease-causing toxin, it acts synergistically with α -toxins in causing myonecrosis and necrohemorrhagic enteritis in calves^{3,4}. PFO has also been reported to augment the toxicity of ϵ -toxin in a mouse model for enterotoxaemia caused by *C. perfringens* type D, a disease of goat and sheep⁵. These data highlight the importance of PFO in supporting the outbreak of different *C. perfringens* associated diseases and make it an attractive vaccine candidate that could be used in combination with the existing vaccine

¹Muylaert, A., Lebrun, M., Duprez, J.N., Labruzzo, S., Theys, H., Taminiau, B. and Mainil, J. Enterotoxaemia-like syndrome and *Clostridium perfringens* in veal calves. *Veterinary Record*. **167**, 64–65 (2010).

²Kiu, R. and Hall, L.J. An update on the human and animal enteric pathogen *Clostridium perfringens*. *Emerging microbes & infections*. **7(1)**, 1-15 (2018).

³Awad, M.M., Ellemor, D.M., Boyd, R.L., Emmins, J.J. and Rood, J.I. Synergistic effects of alpha-toxin and perfringolysin O in *Clostridium perfringens*-mediated gas gangrene. *Infection and Immunity*. **69(12)**, 7904-7910 (2001)

⁴Verherstraeten, S., Goossens, E., Valgaeren, B., Pardon, B., Timbermont, L., Vermeulen, K., Schauvliege, S., Haesebrouck, F., Ducatelle, R., Deprez, P. and Van Immerseel, F. The synergistic necrohemorrhagic action of *Clostridium perfringens* perfringolysin and alpha toxin in the bovine intestine and against bovine endothelial cells. *Veterinary research*. **44(1)**, 1-8 (2013)

⁵Fernandez-Miyakawa, M.E., Jost, B.H., Billington, S.J. and Uzal, F.A. Lethal effects of *Clostridium perfringens* epsilon toxin are potentiated by alpha and perfringolysin-O toxins in a mouse model. *Veterinary Microbiology*. **127**, 379-385 (2008).

preparation against the toxin secreted by a specific type. Earlier reports by Goossen and his associates demonstrated the α -toxin and PFO to be the most immunogenic proteins in vaccine preparations, and immunization with the native toxin(s) or toxoids conferred protection against the toxin-induced necrotic lesions in the intestinal loop model⁶. *In vitro* neutralizing capacity of a PFO derivative with a single amino acid substitute (PFO^{L491D}) against the hemolytic activity and cytotoxic effect of PFO in horse red blood cells and bovine endothelial cells has been reported⁷. However, detailed *in vivo* immune response analysis against these proteins has not been carried out. As the type of immune response generated against an antigen is critical in inducing a long-lasting protective immune response, we carried out the present study to assess the vaccine potential of soluble recombinant PFO (WTrPFO). Since the native toxins are generally not considered safe for the vaccine development, as these can cause local tissue damage at the site of administration and the vaccination dose need to be closely monitored so as to not cause adverse effects in the organism, other approaches including genetically modified toxins by site-directed mutagenesis or by using a non-toxic immunogenic fragment of the toxin could be used to generate an effective and protective immune response as has

⁶Goossens, E., Verherstraeten, S., Valgaeren, B.R., Pardon, B., Timbermont, L., Schauvliege, S., Rodrigo-Mocholí, D., Haesebrouck, F., Ducatelle, R., Deprez, P.R. and Van Immerseel, F. Toxin-neutralizing antibodies protect against *Clostridium perfringens*-induced necrosis in an intestinal loop model for bovine necrohemorrhagic enteritis. *BMC veterinary research*. **12**, 1-8 (2016).

⁷Verherstraeten, S., Goossens, E., Valgaeren, B., Pardon, B., Timbermont, L., Haesebrouck, F., Ducatelle, R., Deprez, P. and Van Immerseel, F. Non-toxic perfringolysin O and α -toxin derivatives as potential vaccine candidates against bovine necrohaemorrhagic enteritis. *The Veterinary Journal*. **217**, 89-94 (2016).

been reported with the C-terminal domain of α -toxin^{8,9,10,11}. In the present study, we targeted the receptor binding C-terminal domain of the PFO that is crucial for the initiation of oligomer formation in the membrane by recognition and binding of the toxin to the host cell membrane¹². Also, earlier investigations have established that PFO variants including the C-terminal domain, V209C, A213C, and R468A to be non-toxic variants of PFO. These variants showed reduced pore formation ability, hemolytic activity, and destabilization of the structure^{13,14,15}. The single site-directed mutants of PFO V208C, A212C, and R467A are therefore also included in the present study. The numbering of these positions vary by one amino acid residue as compared to the position of the same amino acid residue found in the literature as V209C, A213C, and R468A^{14,15} due to variation in the considered nucleotide sequence of PFO available in Gen Bank accession no. M36704. The amino acid derivative V208 and A212 located in the domain 3(D3) are involved in the insertion of the molecule in pore formation, and the residue R467 is present in the most conserved region undecapeptide (457-ECTGLAWEWWR-467) in the D4 domain which is

⁸Goossens, E., Verherstraeten, S., Valgaeren, B.R., Pardon, B., Timbermont, L., Schauvliege, S., Rodrigo-Mocholi, D., Haesebrouck, F., Ducatelle, R., Deprez, P.R. and Van Immerseel, F. The C-terminal domain of *Clostridium perfringens* alpha toxin as a vaccine candidate against bovine necrohemorrhagic enteritis. *Veterinary Research*. **47**, 1-9 (2016).

⁹Williamson, E.D. and Titball, R.W. A genetically engineered vaccine against the alpha-toxin of *Clostridium perfringens* protects mice against experimental gas gangrene. *Vaccine*. **11**, 1253–1258 (1993).

¹⁰Stevens, D.L., Titball, R.W., Jepson, M., Bayer, C.R., Hayes-Schroer, S.M. and Bryant, A.E. Immunization with the C-domain of α -toxin prevents lethal infection, localizes tissue injury, and promotes host response to challenge with *Clostridium perfringens*. *Journal of Infectious Diseases*. **190**, 767–773 (2004).

¹¹Jiang, Z., De, Y., Chang, J., Wang, F. and Yu, L. Induction of potential protective immunity against enterotoxemia in calves by single or multiple recombinant *Clostridium perfringens* toxoids. *Microbiology and Immunology*. **58**, 621–627(2014).

¹²Dunstone, M.A., and Tweten, R.K., Packing a punch: the mechanism of pore formation by cholesterol dependent cytolysins and membrane attack complex/perforin-like proteins. *Current Opinion in Structural Biology*. **22**,342–349 (2012).

¹³Shimada, Y., Maruya, M., Iwashita, S. and Ohno-Iwashita, Y. The C-terminal domain of perfringolysin O is an essential cholesterol-binding unit targeting to cholesterol-rich microdomains. *European journal of biochemistry*. **269**, 6195-6203 (2002).

¹⁴Shepard, Laura A., Alejandro P. Heuck, Brian D. Hamman, Jamie Rossjohn, Michael W. Parker, Kathleen R. Ryan, Arthur E. Johnson, and Rodney K. Tweten. Identification of a membrane-spanning domain of the thiol-activated pore-forming toxin *Clostridium perfringens* perfringolysin O: an α -helical to β -sheet transition identified by fluorescence spectroscopy. *Biochemistry*. **37**, 14563-14574(1998).

¹⁵Kulma, M., Kacprzyk-Stokowiec, A., Kwiatkowska, K., Traczyk, G., Sobota, A. and Dadlez, M. R468A mutation in perfringolysin O destabilizes toxin structure and induces membrane fusion. *Biochimica et Biophysica Acta (BBA)-Biomembranes*. **1859**, 1075-1088 (2017).

responsible for allosteric coupling and insertion of β -barrel in the membrane¹⁴.¹⁵. These proteins were produced through recombinant routes and comparative analysis of the immune response generated against these proteins (WTrPFO and its mutants) were carried out. We expressed the WTrPFO, rPFO_{C-ter}, and single substitution mutants of PFO (rPFO_{V208C}, rPFO_{A212C}, and rPFO_{R467A}) using heterologous host *E. coli* for analyzing their immunogenic and neutralizing potential. A tight and intense band of the proteins WTrPFO (~ 54 kDa), rPFO_{C-ter} (~14kDa), and its site-directed mutants (~ 54 kDa) in the induced cell lysate at the expected positions established tight regulation of the T7 expression system. Initial attempts to express the proteins WTrPFO and rPFO_{C-ter} at 25 °C and 37 °C resulted in the expression of the two proteins as insoluble proteins. Likewise, site-directed mutants expressed at these temperatures also expressed as insoluble proteins. This is expected as higher expression of recombinant protein(s) without the signal sequence results in misfolding of the protein in the cytoplasm and leads to aggregation to form inclusion bodies. Other recombinant cytolysin such as the C-terminal domain of streptolysin O has also been reported to express as inclusion bodies¹⁶. For biologically active protein, the protein must express as soluble protein (native form). Therefore, initially optimization of expression conditions was carried out to direct the expression of WTrPFO and rPFO_{C-ter} in soluble fraction. Induction of expression at lower temperature for a prolonged period led to the expression of the two proteins predominantly in the soluble fraction. Significantly higher yields of the purified recombinant proteins (70 mg/l and 75 mg/l for WTrPFO and rPFO_{C-ter}, respectively) were obtained than that reported by Tweten (1988, 15 mg/l) who purified the protein from a clone identified from a *C. perfringens* genome library in bacteriophage λ ¹⁷. Tweten (1988)'s PFO clone from the genomic library contained the signal sequence and directed the expression of rPFO in the periplasm, resulting in

¹⁶Weis, S. and Palmer, M. Streptolysin O: the C-terminal, tryptophan-rich domain carries functional sites for both membrane binding and self-interaction but not for stable oligomerization. *Biochimica et Biophysica Acta (BBA)-Biomembranes*. **1510(1-2)**, .292-299 (2001).

¹⁷Tweten, R.K. Cloning and expression in *Escherichia coli* of the perfringolysin O (theta-toxin) gene from *Clostridium perfringens* and characterization of the gene product. *Infection and Immunity*. **56**, 3228–3234 (1988).

significantly lower yield. In the present study, the proteins were expressed without the signal sequence and with a histidine tag which facilitated a single-step purification, thus improving the yield. This is of importance as higher production of the protein is desirable for assessment of its biological activity as well as vaccine potential. Unlike the WTrPFO and rPFO_{C-ter}, the mutants rPFO_{A212C}, rPFO_{V208C}, and rPFO_{R467A} expressed as insoluble proteins even at lower temperature. Since the expression of these mutants was higher at 37 °C in comparison to the other two temperatures, these proteins (rPFO_{A212C}, rPFO_{V208C}, and rPFO_{R467A}) were purified by solubilising the inclusion bodies using urea buffer (denaturant) and removing contaminants by using mild detergents followed by purification via Ni²⁺-NTA affinity chromatography. To achieve the proteins in biologically active form, the removal of denaturants from the proteins is very necessary to start refolding of proteins. Dialysis is used to remove the denaturants from the proteins. The proper folding of protein undergoes both aggregation and correct refolding process continuously in the cellular environment¹⁸. One-step dialysis was not found convenient for getting biologically active proteins as more misfolding and aggregation occurred along with refolding. Therefore, using gradient dialysis or step-wise dialysis method has been very helpful for proper folding of proteins by maintaining equilibrium between denatured proteins and the denaturant concentration thus ensuring gradual removal of the denaturant and proper refolding of proteins¹⁹. The purification of the mutants rPFO_{A212C}, rPFO_{V208C}, and rPFO_{R467A} on a large scale was acquired by inclusion bodies followed by refolding by gradient urea dialysis method for developing the immune responses in mice. Significant high yields (50 mg/L, 75 mg/L, and 90 mg/L for mutants rPFO_{A212C}, rPFO_{V208C}, and rPFO_{R467A} respectively) of the recombinants proteins were obtained from the inclusion bodies.

¹⁸Baneyx, F. and Mujacic, M. Recombinant protein folding and misfolding in *Escherichia coli*. *Nature Biotechnology*. **22**, 1399-1408 (2004).

¹⁹Yamaguchi, H. and Miyazaki, M. Refolding techniques for recovering biologically active recombinant proteins from inclusion bodies. *Biomolecules*. **4**(1), 235-251 (2014).

The mature WTrPFO purified from the soluble fraction was biologically active and its hemolytic activity (10^5 HU/mg) was comparable with that reported by Tweten (1988)¹⁶. Sufficient cytotoxicity (close to SDS, included as positive control) observed with WTrPFO in mice peritoneal macrophages and human macrophage further confirmed that the presence of histidine tag did not affect its biological activity and the structural conformation of the soluble WTrPFO was similar to that of native PFO. On the other hand, as expected the mutants of PFO, and PFO substitution mutants (rPFO_{A212C}, rPFO_{V208C}, and rPFO_{R467A}) caused negligible hemolysis of the mice RBCs and also showed reduced cytotoxicity towards mice peritoneal macrophages (~10%) and human macrophage THP1 cells (~20-30%), thus conforming them to be non-toxic nature. Earlier reports have shown that the R468A (R467A of the present study) had reduced PFO activity at lower protein concentrations (0.01-0.1 μ M). However at higher concentrations (4 μ M), this mutant PFO_{R468A} exhibited lytic activity that was determined by release of carboxyfluorescein from liposome composed of cholesterol: DOPC (1,2-di-(9Z-octadecenoyl)-sn-glycero-3-phosphocholine (1:1)¹⁵. In the present study, the WTrPFO was found to be toxic to RBCs and macrophages at much lower concentrations. This difference in the cytotoxic dose of the protein in the present study and earlier reports could be due to the differential susceptibility of the cells used for carrying out the analysis. The hemolytic activity of the rPFO_{A212C} and rPFO_{V208C} in the present study was found to be negligible when compared to the equivalent mutants (PFO_{A213C} and PFO_{V209C}) reported earlier¹⁴. This is of significance as the idea of the present study was to produce non-toxic variants of PFO. The relatively reduced hemolytic activity of the recombinant mutants could possibly be due to purification of the mutants from misfolded inclusion bodies. Membrane binding, homo-oligomer formation and pore formation ability of WTrPFO in MDCK cell lines also confirmed that the recombinant protein has attained its native structural conformation as the pore-forming toxins damage the epithelial cells during bacterial infections²⁰. The membrane binding ability of the mutants

²⁰Los, F.C., Randis, T.M., Aroian, R.V. and Ratner, A.J. Role of pore-forming toxins in bacterial infectious diseases. *Microbiology and Molecular Biology Reviews*. **77**(2), 173-207 (2013).

rPFO_{A212C} and rPFO_{V208C} in MDCK cells indicated that these mutations did not affect the cholesterol binding ability of the proteins. However, homooligomerization in the membrane and pore formation ability was declined. These further confirmed the non-toxic nature of the variants. The declination of cholesterol/membrane binding ability of the rPFO_{R467A} in the present study is in agreement with the earlier reports where in loss of cholesterol binding ability of rPFO_{R468A} has been established¹⁵.

Surprisingly, the cell lysates of the MDCK cells incubated with the rPFO_{V208C}, rPFO_{A212C} showed a band at slightly lower position (~100 kDa) in comparison to the oligomer observed with the WTrPFO, suggesting, that the proteins did not properly oligomerized on the plasma membrane and possibly aggregated. Likewise, a negligible intensity band was noted in the cell lysates of the MDCK cells incubated with rPFO_{R467A}. The intensity of the band at the ~100 kDa position was in the order of rPFO_{A212C} > rPFO_{V208C} > rPFO_{R467A}. These data suggest that the refolding of the protein using gradient dialysis method though directed them to come in soluble form, the mutation resulted in affecting the native conformation and thereby affecting their oligomerization in the membrane.

Immunization of mice with the WTrPFO, non-toxic rPFO_{C-ter}, and the mutants rPFO_{A212C}, rPFO_{V208C}, and rPFO_{R467A} emulsified with Freund adjuvant resulted in robust immune response as evidenced with very high antigen-specific antibody titers in the antisera generated against the all respective proteins. Although the end-point titers of the rPFO_{C-ter} antiserum appeared to be slightly lower than the full-length WTrPFO, the antigen-specific immune response (determined by immunoblotting) of the anti-rPFO_{C-ter} was found to be as strong as the anti-WTrPFO.

The end-point titers of antisera raised against the mutants rPFO_{A212C}, rPFO_{V208C}, and rPFO_{R467A} were found more than WTrPFO. These strong immune responses including high antibody titer and antigen-specificity of generated antibodies revealed the efficient humoral immune responses generated against the toxin and its mutants that protect the body from the different type of pathogens including bacteria, viruses, and fungi. The effective and specific cross-reactivity of

antiserum raised against the non-toxic rPFO_{C-ter} and the mutants rPFO_{A212C}, rPFO_{V208C}, and rPFO_{R467A} with the WTrPFO toxin suggested that the antibodies present in the antisera of the respective proteins could possibly neutralize WTrPFO toxicity and thus can serve as the non-toxic vaccine candidates.

Further, for a vaccine candidate to act effectively, generation of immune memory is desirable criterion so that the immune cells can get activated upon exposure to the respective pathogen. The stimulation of lymphocytes isolated from WTrPFO, rPFO_{C-ter}, rPFO_{A212C}, rPFO_{V208C}, and rPFO_{R467A} immunized mice with the respective proteins resulted in enhanced proliferation of splenocytes indicating that the WTrPFO and non-toxic mutants were able to generate the T-cell memory in the mice after immunization. An increase in the IgG1, IgG2a, and IgG2b with a ratio of IgG1/IgG2a and IgG1/IgG2b rPFO_{C-ter} more than 1 in WTrPFO and all the mutants and IgG1/IgG2b almost close to 1 in the rPFO_{C-ter} antisera had indicated a Th2-biased immune response. The cytokine ELISA of the culture supernatants of the splenocytes isolated from the WTrPFO, rPFO_{C-ter}, rPFO_{A212C}, rPFO_{V208C}, and rPFO_{R467A}-immunized mice stimulated with the respective protein also confirmed the Th2-biased mixed immune response as a significant increase in both IFN- γ (a marker of Th1 type immune response) and IL-4 (a marker of Th2 type immune response) was noted. A vaccine that generates a mixed immune response considered a better candidate than that which either stimulates Th1 or Th2 type response^{21,22}. Thus, the WTrPFO and its non-toxic mutants, which generated mixed immune response are likely to prove promising vaccine candidates against the PFO toxicity of all types of *C. perfringens* strains.

The above mentioned all IgG subclasses have been also found produced in animals challenged with different types of antigens including DNA vaccines, recombinant *Ascarissuum* antigens, recombinant *Plasmodium* antigens, and

²¹Cheers, C., Janas, M., Ramsay, A. and Ramshaw. Use of recombinant viruses to deliver cytokines influencing the course of experimental bacterial infection. *Immunology and Cell Biology*. **77**, 324–330(1999).

²²Yadav, S.K., Sahoo, P.K. and Dixit, A. Characterization of immune response elicited by the recombinant outer membrane protein OmpF of *Aeromonashydrophila*, a potential vaccine candidate in murine model. *Molecular Biology Reports*. **41**, 1837–1848 (2014).

bacterial adhesins and after infections with bacteria and viruses²³. The IgG1 subclass can neutralize toxins and viruses and also plays a very important role in controlling auto antibody-induced inflammation in mice and humans by blocking the complement activation²⁴. The IgG2a has been linked to strengthen the antigen clearance by FcγR-mediated activity and thereby clearing the viruses through antibody-dependent cellular cytotoxicity mechanism^{25,26,27}. Further, effective cross-reactivity of each antiserum (anti-WTrPFO, anti-PFO_{C-ter}, anti-rPFO_{V208C}, anti-rPFO_{A212C}, and anti-rPFO_{R467A}) with the WTrPFO and other mutants revealed the structural similarity of the antigen-binding region (Fab fragment) of the antibodies present in the antisera.

For efficient immune responses, both humoral and T cell-mediated immune responses must be developed significantly. The significant increase of all antigen-specific lymphocyte proliferation as compared to unstimulated control after exposure with respective proteins WTrPFO, rPFO_{C-ter}, rPFO_{A212C}, rPFO_{V208C}, and rPFO_{R467A} *in vivo* indicates the capacity of all the proteins to generate T-cell memory in the mice. The more stimulation indices of the rPFO_{C-ter}, rPFO_{A212C}, rPFO_{V208C}, and rPFO_{R467A} (1.75, 1.55, 1.94, and 2.4) compared to WTrPFO reflect greater antigenicity and robust immune response development by the non-toxic variants of the PFO.

PFO is known to cause hemolysis and is also responsible for *C. perfringens* dependent macrophages cytotoxicity by resisting the *C. perfringens* to be killed by phagocytosis of macrophages²⁸. Therefore, these two assays were used for

²³Collins, A.M. IgG subclass co-expression brings harmony to the quartet model of murine IgG function. *Immunology and cell biology*. **94**(10),949-954 (2016).

²⁴Lilienthal, G.M., Rahmöller, J., Petry, J., Bartsch, Y.C., Leliavski, A. and Ehlers, M. Potential of murine IgG1 and human IgG4 to inhibit the classical complement and Fcγ receptor activation pathways. *Frontiers in immunology*. **9**, 958 (2018).

²⁵Nimmerjahn, F. and Ravetch, J.V. Divergent immunoglobulin g subclass activity through selective Fc receptor binding. *Science*. **310**, 1510–1512 (2005)

²⁶Fang, Y., Banner, D., Kelvin, A.A., Huang, S.S., Paige, C.J and Corfe, S.A. Seasonal H1N1 influenza virus infection induces cross-protective pandemic H1N1 virus immunity through a CD8-independent, B cell-dependent mechanism. *Journal of virology*. **86**, 2229–2238 (2012).

²⁷Collins, A.M., Wang, Y., Roskin, K.M., Marquis, C.P. and Jackson KJ. The mouse antibody heavy chain repertoire is germline-focused and highly variable between inbred strains. *Philosophical transactions of the Royal Society of London. Series B, Biological sciences*. **370**, 1676 (2015).

²⁸O'Brien, D.K. and Melville, S.B. Effects of *Clostridium perfringens* alpha-toxin (PLC) and perfringolysin O (PFO) on cytotoxicity to macrophages, on escape from the phagosomes of

assessing the toxin neutralization ability of the antisera. The ability of the anti-WTrPFO, anti-rPFO_{C-ter}, anti-rPFO_{A212C}, anti-rPFO_{V208C}, and anti-rPFO_{R467A} antisera to neutralize the hemolytic activity in mice RBCs and cytotoxicity of WTrPFO towards mice peritoneal macrophages confirmed that the antibodies present in these antisera are neutralizing type. Surprisingly the hemolytic inhibition by neat and antisera diluted two folds (50%) appeared less than the 4 folds diluted antiserum (25%), despite the presence of higher concentrations of antibodies in these in comparison to 25% diluted antisera dilutions. Similarly, the neutralization capacity of neat anti-WTrPFO, anti-PFO_{C-ter}, anti-rPFO_{C-ter}, anti-rPFO_{V208C}, anti-rPFO_{A212C}, and anti-rPFO_{R467A} antisera against the cytotoxic effect of WTrPFO was found to be lower (~40%, ~49%, ~24, ~25, ~20 respectively), when compared to other dilutions of the antisera (1:10-1: 10,000; 50-80 %) keeping the amount of the WTrPFO constant (100 µg/ml). The neutralization percentage of anti-WTrPFO was $\geq 80\%$ at the dilutions of 1:250-1:10,000 and attained maximum neutralization (99%) at the dilution fraction 1:500 that indicated the equivalence zone of antigen-antibody interaction. The higher neutralizing capacity of the diluted antiserum in comparison to neat antiserum could be attributed to the Lattice theory that explained the precipitation reactions in fluid media in which antigen-binding sites in concentrated polyclonal antibodies became saturated, thereby reducing their antigen-binding ability²⁹.

Comparable neutralization (~90 %) of the WTrPFO cytotoxicity by the anti-WTrPFO and antisera generated against its mutants rPFO_{C-ter}, rPFO_{V208C}, and rPFO_{A212C} in mice peritoneal macrophages demonstrate the effectiveness of non-toxic rPFO_{C-ter} and substitution non-toxic mutants in negating the PFO toxicity. The same can be employed as a promising alternative to native PFO toxin in combination with the non-toxic C-terminal domain of alpha-toxin or with another non-toxic alternative of main virulent disease-causing toxins of different

macrophages, and on persistence of *C. perfringens* in host tissues. *Infection and Immunity*. **72**,5204–5215 (2004).

²⁹VIRELLA, G. and TSOKOS, G.C. Pathogenic role of antigen-antibody complexes. *Medical Immunology*. **321** (2019).

types of *C. perfringens* to generate a protective immune response against the bacterium.

Thus, the present study reports recombinant expression and purification of the full-length PFO of *C. perfringens* and its C-terminal receptor-binding domain as soluble proteins and the variants of PFO V208C, A212C, and R467A as insoluble proteins followed by solubilizing in denaturing buffer (8M urea). Comparative analysis of the immunogenicity and antigenicity of the WTrPFO, its deletion variant (i.e. C-terminal receptor-binding domain, rPFO_{C-ter}) and single substitution variants (rPFO_{V208C}, anti-rPFO_{A212C}, and anti-rPFO_{R467A}) showed that all the non-toxic variants were capable of generating a robust immune response, though the IgG levels in the antiserum generated against the C-terminal domain were relatively lesser than full-length PFO. Despite relatively lower IgG levels in the anti-rPFO_{C-ter} antiserum, it could specifically recognize the full-length PFO and also neutralized the hemolytic and cytotoxic activity of the PFO *in vitro*. All the proteins generated T cell memory and mixed immune response, which is a characteristic of a good vaccine candidate as both the arms of immune response play an important role in conferring protection against the pathogen/toxin. The anti-WTrPFO and the antiserum generated against the C-terminal domain and rPFO_{V208C}, anti-rPFO_{A212C}, and anti-rPFO_{R467A} could specifically recognize the full-length PFO, and also neutralized the hemolytic and cytotoxic activity of the PFO *in vitro*. Specific and robust cross-reactivity of the antiserum against the non-toxic variants (rPFO_{C-ter}, rPFO_{V208C}, and rPFO_{A212C}, rPFO_{R467A}) with the full-length PFO and their ability to neutralize its toxicity clearly demonstrate that these variants of PFO could be the potential non-toxic vaccine candidates against the PFO that is secreted by all *Clostridial* toxinotypes. Both WTrPFO and its non-toxic variants could also be used as an adjuvant vaccine together with other *Clostridial* toxins as PFO has been reported to aid in the action of other *clostridial* toxins. Also, since the structure of PFO secreted by *C. perfringens* strains shares similarities with other cholesterol-dependent cytolysins of other genera such as *Streptococcus*,

*Bacillus, Listeria etc*³⁰, the non-toxic variants of PFO reported in the present study could be assessed as a candidate for potentiating the protective immune responses against other bacterial infections as well.

³⁰ Petit, L., Gibert, M. and Popoff, M.R. *Clostridium perfringens*: toxinotype and genotype. *Trends in Microbiology*. **7**, 104–110 (1999).

Summary

- Different variants of the PFO namely V208C, A212C, R467A (according to accession no. M36704), and the C-terminal domain of PFO were identified as non-toxic variants from the literature, and, therefore considered for the comparative evaluation of their immunogenic potential with wild type PFO.
- The gene constructs harboring the mature full-length *pfo* of *C. perfringens* (without the signal sequence), its deletion variant harboring only the C-terminal domain comprising 390 to 499 (PFO_{C-ter}) residues and a single amino acid substitution mutation in the mature *pfo* (V208C, A212C, R467A) were designed on the basis of sequence information available for *C. perfringens pfo* gene (GenBank Accession number: M36704).
- The synthetic gene constructs cloned into expression vector pET22b (+) at the *Nde*I and *Xho*I restriction sites (procured from GenScript, USA) were designated as pET22.PFO_{wt} and pET22.PFO_{C-ter}, pET22.PFO_{V208C}, pET22.PFO_{A212C} and pET22.PFO_{R467A}.
- Synthesized gene constructs were confirmed by restriction enzyme digestion analysis using *Nde*I and *Xho*I restriction enzymes and by gene sequencing.
- The synthetic constructs transformed in *E. coli* BL21 (λDE3) pLysS cells were used for recombinant protein production.
- Recombinant proteins WTrPFO and rPFO_{C-ter} were expressed at different temperatures (16 °C, 25 °C, and 37 °C), different inducer concentration (IPTG, 0.1 mM to 2mM) and for different time intervals (1 h –O/N) post-induction to optimize the protein expression and to obtain the recombinant protein as a soluble protein. The expression at 25 °C and 37 °C resulted in the expression of the two proteins as insoluble fraction. Induction of expression at lower temperature (16 °C) for prolonged period (overnight, 22 h) led to the expression of the WTrPFO and rPFO_{C-ter} in soluble fractions as the expression was relatively slower, and did not allow the proteins to aggregate.

- Recombinant proteins were purified from the soluble fraction (WTrPFO, and rPFO_{C-ter}) or inclusion bodies (rPFO_{V208C}, rPFO_{A212C}, and rPFO_{R467A}) using Ni²⁺-NTA affinity chromatography. The proteins purified from the solubilized inclusion bodies were refolded using urea-gradient dialysis method.
- The WTrPFO was Biologically active and exhibited hemolytic activity of 10⁵ HU/mg against mice RBCs. The WTrPFO showed 84 % cell death at 100µg/ml in mice peritoneal macrophages. The WTrPFO was capable of forming homooligomer and pores in MDCK cell membranes.
- The deletion variants and substitution variants of the PFO were found to be non-toxic and did not show any haemolytic activity towards mice RBCs and cytotoxic activity in mice peritoneal macrophages and human macrophages (THP1 cells) *in vitro*. The mutants also exhibited failure of proper oligomerization and failed to form pores in MDCK cell lines. The WTrPFO, its deletion and substitution variants generated robust humoral immune response, as evident from very high end-point titers (>1:160, 000) of the antisera generated against these proteins. Although the end-point titers of the rPFO_{C-ter} antiserum appeared to be slightly lower than the WTrPFO, the antigen-specific immune response (determined by immunoblotting) of the anti-rPFO_{C-ter} was found to be as strong as the anti-WTrPFO antisera. The antisera generated against the mutants also exhibited high antigen specificity.
- Immunoblotting analysis showed effective cross-reactivity of the antisera raised against the WTrPFO and its substitution mutants against each other suggesting the structural similarity of antigen-binding region (Fab fragment) of the antibodies present in the antisera.
- Immunization with all the five recombinant proteins (WTrPFO and its mutants rPFO_{C-ter}, rPFO_{V208C}, rPFO_{A212C}, and rPFO_{R467A}) generated Th2 biased mixed immune response, established by increased levels of all the three types of key anti-isotypes (IgG1, IgG2a, and IgG2b).

- The WTrPFO and its mutants were capable of generating T cell memory, evidenced by enhanced proliferation of splenocytes isolated from the immunized proteins post-stimulation with the respective proteins.
- Increased levels of both IL-4 (a Th2 response indicator) and IFN- γ (a Th1 response indicated) in the culture supernatant of the splenocytes isolated from the immunized mice upon stimulation with respective proteins further confirmed the mixed T cell-mediated immune response.
- The WTrPFO and its mutants generated long lasting immune response. However, a response switch towards Th1 was noted as the splenocytes isolated 32 weeks post-immunization upon stimulation with the respective protein showed significantly increased IFN- γ levels ($p \leq 0.05-0.001$) with negligible IL-4 levels.
- The antibodies present in the anti-WTrPFO, anti-rPFO_{V208C}, anti-rPFO_{A212C} and anti-rPFO_{R467A} and anti-rPFO_{C-ter} antisera were of neutralizing type and completely negated the hemolytic activity of WTrPFO in mice RBCs. Similarly, the antisera generated against all the five recombinant proteins were capable of neutralizing the cytotoxic effect of WTrPFO towards mice peritoneal macrophages.

Publications and conference presentation

Published Manuscript

- Sunita Kumari Yadav, Deepak Panwar, Ankita Singh, Meenakshi B Tellis, Rakesh Shamsunder Joshi & Aparna Dixit (2021): Molecular phylogeny, structure modeling and *in silico* screening of putative inhibitors of aerolysin of *Aeromonas hydrophila* EUS112, Journal of Biomolecular Structure and Dynamics, DOI: 10.1080/07391102.2021.1918254

Poster presented

- Presented on “Effect of Severe and Mild Galactosemia Mutations on Structural and Functional Characteristics of *E. Coli* Galactose-1-phosphate uridylyltransferase (GALT) in the Annual Symposium of the INDIAN BIOPHYSICAL SOCIETY (IBS 2017) held at IISER Mohali, India during March 23-25, 2017.
- Presented on “Expression, purification and immunogenic potential of recombinant perfringolysin O, PFO and C-terminal receptor-binding domain in murine model” in Biospectrum 2020 International Conference on Biotechnology & Biological Sciences held from 19th to 21st November 2020.






Molecular phylogeny, structure modeling and *in silico* screening of putative inhibitors of aerolysin of *Aeromonas hydrophila* EUS112

Sunita Kumari Yadav, Deepak Panwar, Ankita Singh, Meenakshi B Tellis, Rakesh Shamsunder Joshi & Aparna Dixit



To cite this article: Sunita Kumari Yadav, Deepak Panwar, Ankita Singh, Meenakshi B Tellis, Rakesh Shamsunder Joshi & Aparna Dixit (2021): Molecular phylogeny, structure modeling and *in silico* screening of putative inhibitors of aerolysin of *Aeromonas hydrophila* EUS112, Journal of Biomolecular Structure and Dynamics, DOI: [10.1080/07391102.2021.1918254](https://doi.org/10.1080/07391102.2021.1918254)

To link to this article: <https://doi.org/10.1080/07391102.2021.1918254>

 View supplementary material 

 Published online: 30 Apr 2021.

 Submit your article to this journal 

 View related articles 

 View Crossmark data 



Molecular phylogeny, structure modeling and *in silico* screening of putative inhibitors of aerolysin of *Aeromonas hydrophila* EUS112

Sunita Kumari Yadav^{a†}, Deepak Panwar^{b†}, Ankita Singh^c, Meenakshi B Tellis^{d,e}, Rakesh Shamsunder Joshi^d and Aparna Dixit^c

^aDepartment of Zoology, Daulat Ram College, University of Delhi, Delhi, India; ^bGene Regulation Laboratory, National Institute of Immunology, New Delhi, India; ^cGene Regulation Laboratory, School of Biotechnology, Jawaharlal Nehru University, New Delhi, India; ^dBiochemical Sciences Division, CSIR – National Chemical Laboratory, Dr. Homi Bhabha Road Pune, India; ^eDepartment of Botany, Savitribai Phule Pune University, Ganeshkhind Rd, Ganeshkhind, Pune, India

Communicated by Ramaswamy H. Sarma

ABSTRACT

Aeromonas hydrophila, a Gram-negative bacterium, causes diseases in fish, resulting in excessive loss to the aquaculture industry. *Aeromonas* is a highly heterogeneous group of bacteria, and the heterogeneity of the genus is attributed to variation and diversity in the virulence factors and toxins among various *Aeromonas* strains. One of the major toxins aerolysin, secreted by the bacterium, causes hemorrhagic-septicemia and diarrhea and can serve as a drug target. Here, we describe characterization, molecular phylogeny, and homology modeling of the aerolysin of *A. hydrophila* strain EUS112 (*Ah*_{EUS112}) cloned in our lab. The encoded aerolysin is 485 amino acids long with an N-terminal signal sequence of 23 amino acids. Phylogenetic analysis of the aerolysin of *Ah*_{EUS112} revealed that it belongs to a diverse group of toxins, showing maximum similarity with aerolysins of other *Aeromonas* strains followed by *Vibrio* toxin. The homology model of the mature aerolysin of *Ah*_{EUS112} was generated using the crystal structure of a mutant aerolysin (PDB#3g4n) as the template, which showed that the encoded aerolysin exists as a channel protein. Validation of the generated model using bioinformatics tool confirmed it to be a good quality model that can be used for drug design. Molecular dock analysis revealed that drugs, aralia-saponin I, cyclamin, ardisiacrispin B, and aralia-saponin II bind to aerolysin with a higher affinity as compared to other drugs and at functionally important amino acids of aerolysin. Hence, these molecules can act as an effective therapeutics for inhibiting the aerolysin pore formation and curtail the severity of *Aeromonas* infection.

ARTICLE HISTORY

Received 18 November 2020
Accepted 11 April 2021

KEYWORDS


Aerolysin; homology modeling; molecular docking; molecular dynamic simulation; phylogenetic tree

1. Introduction

A. hydrophila is a motile, Gram-negative rod-shaped enterobacterium established as one of the major pathogens that affect fish. It is a ubiquitously present bacterium, accountable for causing necrosis in fish tissues besides ulcers, hemorrhagic septicemia, and many other diseases, resulting in high fish mortality and substantial economic losses to the aquaculture industry (Rasmussen-Ivey et al., 2016). It is an opportunistic pathogen and occasionally causes diseases in amphibians, reptiles, and mammals, including humans. In humans, it is a causative agent of diarrhea and septicemia. The pathogenicity of *Aeromonas* is attributed to its intricate network of virulence factors such as a surface layer, adhesins (porins help in attachment), various secretion systems (releases enzymes and toxins), and biofilm formation (Rasmussen-Ivey et al., 2016). Among various extracellular toxins secreted by *Aeromonas*, aerolysin and hemolysin are the best characterized that are involved in the development of hemorrhagic septicemia and contribute significantly to its

pathogenicity in fish and other animals. Though *Aeromonas* are ubiquitously present in the aquatic environment, a significant heterogeneity has been noted in this genus among various species and subspecies with respect to its distribution, host range, and growth parameters (Gauthier et al., 2017; Janda & Abbott, 2010). The heterogeneity in various parameters and virulence among various *Aeromonads* has been attributed to genomic heterogeneity and due to variations in the structure of toxins owing to amino acid difference. Cytotoxic and hemolytic activities reported for many *Aeromonas* species have been attributed to both hemolysin and aerolysins (Cumberbatch et al., 1993; Ferguson et al., 1995; Gosling, 1996). Aerolysin is a heat-labile type of β -hemolysin displaying phospholipase A and C activity. It can form a channel by inserting itself into the cell membrane's bilayer, initiating leakage of essential cytoplasmic contents resulting in cell lysis (Abrami et al., 2003). The toxin is secreted as an inactive precursor (proaerolysin) and traverses the membrane with the help of its N-terminus sequence. The toxin is then secreted into the periplasm, where it attains a

CONTACT Aparna Dixit  adixit7@gmail.com, adix2100@mail.jnu.ac.in  School of Biotechnology, Jawaharlal Nehru University, New Delhi-110067, India
†Equal contribution.

 Supplemental data for this article can be accessed online at <https://doi.org/10.1080/07391102.2021.1918254>.

© 2021 Informa UK Limited, trading as Taylor & Francis Group

dimeric form before being released outside the cell. Removal of 45 amino acids from C-terminus converts proaerolysin to aerolysin, diffuses its target cell to bind to the specific surface receptors having the common property of being glycosylphosphatidylinositol (GPI) anchored. Proaerolysin may be cleaved by trypsin or chymotrypsin prior to receptor binding (Zhu et al., 2007). Once processed, the toxin oligomerizes into a ring-like heptameric structure that inserts into the membrane and forms a channel. Finally, channel formation leads to permeabilization of the plasma membrane to small ions, activation of G-proteins, and apoptosis in specific cell types resulting in osmotic swelling and lysis of RBCs (Abrami et al., 2003).

Significant genotypic diversity has been reported in these genes in clinical isolates of several *Aeromonas* sp. (Wang et al., 2003 and references therein). Due to this heterogeneity, it is crucial to characterize the toxin from different strains and isolates due to environmental heterogeneity for drug targeting; even though it has been characterized in few *Aeromonas* species (Singh et al., 2010; Zhu et al., 2007). In the present study, we have carried out the characterization of the aerolysin gene of an Indian strain EUS112 of *Aeromonas hydrophila*, isolated from a diseased Puntius fish in Mangalore. Further, molecular phylogeny and homology modeling (using a known aerolysin structure) of the deduced amino acid sequence of aerolysin of *A. hydrophila* EUS112 was carried out.

The biological nanopore produced by aerolysin of *Aeromonas* sp. have been used to study the protein dynamics (conformation and length), enzyme kinetics, and mass of PEGs (Cao et al., 2018). A biological pore has also been employed for biotechnological applications (Schneider & Dekker, 2012; Stefureac et al., 2006). Understanding the structure may also give insight by which the aerolysin gene can be engineered for heterologous expression in expression host *Escherichia coli* for specific size nanopore formation, which can then be applied for enhancing recombinant protein production.

The generated model was further screened for potential inhibitors/ligands by molecular docking, a highly useful and competent tool to search for a suitable ligand that can fit in protein's binding site efficiently based on energy and geometry. It plays a vital role in rational drug designing via *in silico* screening of drugs. Among several docking software types, protein-ligand docking is most popular (if the protein structure is known) to search for accurate ligand conformations that would effectively fit into the pocket of protein of interest. Regarding aerolysin, there are only a few molecules that have been reported to bind to it. DockThor docking program has been used in the current study to reveal the interaction between aerolysin and the molecules that have been reported to inhibit oligomerization and biofilm formation of aerolysin (Dong et al., 2018; 2020; Singh & Somvanshi, 2009).

2. Materials and methods

2.1. Cloning of aerolysin gene of *A. hydrophila* in cloning vector

The *aerolysin* gene was amplified using the genomic DNA of *A. hydrophila* EUS 112 (isolated from a diseased Puntius fish

in Mangalore) as template and *aerolysin* gene-specific primers (designed on the basis of sequence information available for *A. hydrophila* ATCC7966, Sigma Aldrich, USA), *Taq* DNA polymerase with PCR reaction at the following conditions: initial denaturation at 94 °C for 5 min, followed by 30 cycles of thermal denaturation at 94 °C for 45 sec; annealing at 50 °C for 1 min; and extension at 72 °C for 2 min. Final extension was performed for 10 min at 72 °C. The purified amplicon of ~1.5 kb was cloned into pGEM-T vector and subjected to sequence analysis at the DNA sequencing facility, University of Delhi, South Campus, New Delhi. The cloned aerolysin gene sequence has been submitted to Genbank (MT491733).

The amino acid sequence of *A. hydrophila* (EUS112) aerolysin was deduced using the ExPasy translate tool (<http://www.expasy.org>).

2.2. Physical and chemical properties of aerolysin

Physical and chemical analyses of the encoded aerolysin of *A. hydrophila* EUS112 were carried out using PROSCAN (Bairoch et al., 1997) and PredictProtein (Rost et al., 2004; URL: PredictProtein.org) bioinformatics tools.

2.3. Multiple sequence alignment and molecular phylogeny analysis of *A. hydrophila* (EUS112) aerolysin

Aerolysin amino acid sequences of 35 bacterial species (*Aeromonas* and other bacteria) were retrieved from the GenBank and subjected to multiple sequence alignment with the *Ah*_{EUS112} aerolysin amino acid sequence. MEGAX tool was used for constructing neighbor-joining (NJ) tree and evolutionary analysis (Kumar et al., 2018; Saitou & Nei, 1987). The numbers next to the branches show the percentage of replicate trees in which the associated taxa clustered together in the bootstrap test (500 replicates) (Felsenstein, 1985). The branch length of the phylogenetic tree is equivalent to the evolutionary distances and is drawn to scale. P-distance method (Nei & Kumar, 2000) was used to compute evolutionary distances directly correlated with the number of amino acid differences per site. The final data set used for analysis consisted of 523 positions after removing all ambiguous positions for each sequence pair (pairwise deletion option).

2.4. Structural analysis of aerolysin

To search for the best suitable template for homology modeling, BLAST-P analysis of the amino acid sequence of the *Ah*_{EUS112} aerolysin (Accession no. MT491733) was performed. The available crystal structures of the best-aligned aerolysins reported in the protein data bank (PDB) were then searched for similarity, and the structure of a mutant aerolysin (PDB # 3g4n, Resolution = 2.10 Å, R-value = 0.216, Rfree value = 0.261) was used as the template for modeling using Swiss-Model homology modeling program. The generated 3D structure was visualized by Swiss-PDB viewer software (<http://www.expasy.org/spdbv>) without any filters and

subjected to various validation analyses using structure verification servers such as WHAT_CHECK (<http://swift.cmbi.ru.nl/gv/whatcheck>), Verify3D (Eisenberg et al., 1997) and QMEANDisCo (Studer et al., 2020). Ramachandran plot (Ramachandran & Sasisekharan, 1968) clarifying various aspects of the model was produced using PROCHECK (Laskowski et al., 1993). The energy of the generated model was calculated using PROSA (Sippl, 1993).

2.5. Ligand screening and molecular docking for identification of suitable inhibitor

Based on a literature survey, 11 potent saponin variants reported to inhibit aerolysin oligomerization were chosen to study their interaction with aerolysin and identify the critical residues involved in binding. Also, we have screened two more therapeutically important molecules, namely morin, a flavonoid present in green tea, vegetables, and red wine, and thymol, a major constituent of essential oils of thyme (*Thymus vulgaris* L., *Lamiaceae*), which have also been reported to inhibit the hemolytic activity and biofilm formation (Dong et al., 2018; 2020). The 2D structure of each drug was downloaded from the PubChem database in the structure-data file (SDF) format (<https://pubchem.ncbi.nlm.nih.gov/>), and Online SMILES Translator (<https://cactus.nci.nih.gov/translate/>) was used to convert SDF to PDB format.

To simulate binding affinity between aerolysin protein and ligands, *in silico* docking analysis was performed using the DockThor server (<https://dockthor.incc.br/v2/>). The DockThor program is a flexible-ligand and rigid-receptor grid-based method that employs a multiple solution genetic algorithm and MMFF94S molecular force field scoring function. The search parameters blind docking by programming 25 runs and 10^6 evaluations for each ligand (Santos et al., 2020). DockThor simulation was carried out to confirm binding of aerolysin with the test molecules, saponin, colhiside 6 (saponin 4), aralia-saponin I, aralia-saponin II, aralia-saponin III, aralia-saponin IV, kalopanax (saponin C), gypsogenin, cyclamin, berneuxia (saponin A), ardisiacrispin B, thymol, and morin. Interacting residues of aerolysin involved in the molecular interaction with these molecules were assessed by Protein-Ligand Interaction Profiler (PLIP) (<https://projects.biotec.tu-dresden.de/plip-web/plip/index>) (Salentin et al., 2015). To validate the docking scores of the molecules obtained from DockThor, we also used Python Prescription Virtual Screening Tool (PyRx) version 0.8 (<https://pyrx.sourceforge.io/>). Following this, structure-based virtual screening applying docking simulations was performed using the AutoDockVina tool compiled in PyRx (Dallakyan & Olson, 2015; Trott & Olson, 2010). The molecules were imported into Open Babel within the PyRx and subjected to energy minimization. The energy minimization was performed with the Universal Force Field (UFF) using the conjugate gradient algorithm. The total number of steps was set to 200 and number of steps for update set to 1. In addition, the minimization was set to stop at an energy difference of less than 0.1 kcal/mol. Docked complexes and 2D protein-ligand interactions were

visualized in PyMol (Delano & Palo Alto, 2002) and Discovery studio visualizer (<http://accelrys.com>).

2.6. Molecular dynamic simulation (MDS)

The best ranked docked complex was used for molecular dynamics (MD) simulation. All the MD simulations were performed using Charmm36feb2021 force field using GROMACS 5.1.4 package (Abraham et al., 2015; GROMACS User Manual version 5.1.4). Topologies for both ligand and protein were prepared by the CGenFF server (<https://cgenff.umaryland.edu/>). During the MD simulations, all the protein atoms were surrounded by a dodecahedron water box (14^*14^*10 cubic units) of TIP3P water molecules. The systems were neutralized with two Na^+ counter ions replacing the water molecules, and energy minimization was performed using the steepest descent algorithm. NVT and NPT equilibrations were done for 100 ps each using PME electrostatics and Parrinello-Rahman pressure coupling. Production MD simulations of 100 ns with a time step of 2 fs was performed. RMSD calculations were done for the backbone of protein over the complete simulation.

3. Results and discussion

3.1. In silico physicochemical characterization of the Ah_{EUS112} aerolysin

The gene Ah_{EUS112} aerolysin encodes for a protein product of 485 amino acid residues, of which 23 amino acids at the N-terminus constituted the signal sequence (Figure 1). Theoretical PI and molecular weight of the protein was determined to be 7.6 and ~ 53 kDa, respectively.

ProScan analysis showed that the aerolysin contains 48 negatively charged residues (acidic) and 49 positively charged residues (basic). The glycine content was highest at 9.3%, followed by serine, leucine, and alanine (8–9%). The presence of five cysteine residues suggests a strong possibility of disulfide bond formation while attaining secondary or tertiary structure. The instability index was estimated to be 26.8 that revealed the stable nature of the protein. The aliphatic index (relative volume of a protein occupied by its aliphatic side chains) of Ah_{EUS112} aerolysin was calculated to be 75.01, indicating high thermal stability owing to high hydrophobic amino acids. Being a membrane toxin, the high number of hydrophobic amino acids is expected to be present for the trans-membrane toxic structure-activity of the aerolysin. The GRAVY index (hydropathicity) was found to be -0.460 . The structure revealed 6.6% helix, 45.8% β -strands, and 47.6% loop. A significant percentage of β -strands is known to be involved in activating and oligomerization of aerolysin to prepre state constituted by two β barrels held together by hydrophobic interactions. The loops and the β barrels extend toward the membrane to create a trans-membrane β barrel, eventually resulting in a pore (Cirauqui et al., 2017).

PredictProtein analysis showed presence of 8 motifs for enzyme recognition in the Ah_{EUS112} aerolysin that are: Casein kinase II phosphorylation sites ([ST].[2]{DE}) at four positions

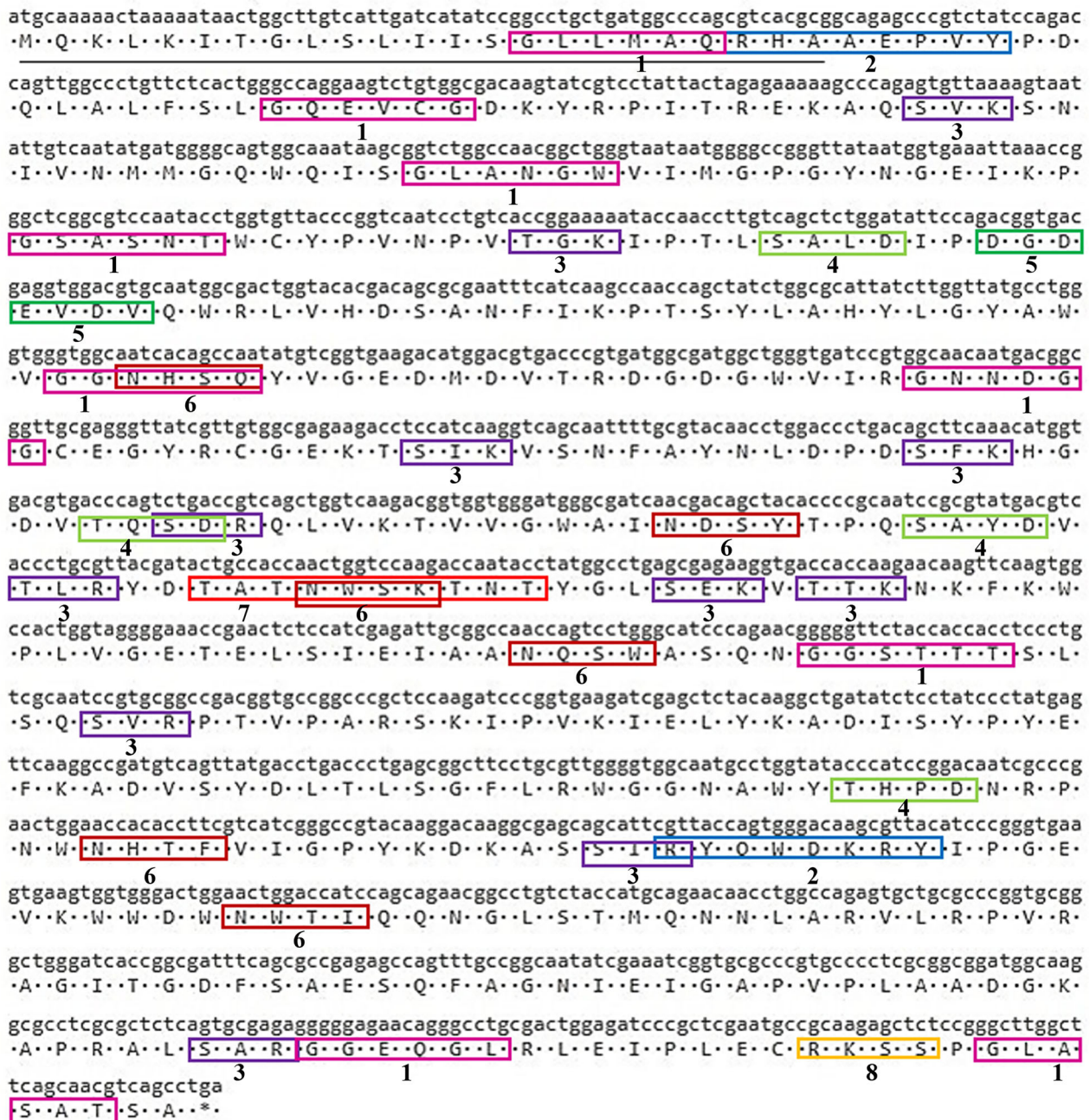


Figure 1. Nucleotide and deduced amino acid sequence of aerolysin of *Ah_{EUS112}*. The open reading frame encodes for a protein of 485 amino acids. Underlined nucleotide sequence shows the region encoding the signal peptide (amino acid residues 1–23). The stop codon is marked with an asterisk (*). The 8 motifs for enzyme recognition in aerolysin sequence are indicated as boxed sequences: (1) N-myristoylation site, G^{[^]E}DRKH^{[^]P}FWY.₂[STAGCN]^{[^]P}; (2) Tyrosine kinase phosphorylation site, 2 ([RK].₃)[DE].₂Y; (3) Protein kinase C phosphorylation site, [ST].[RK]; (4) Casein kinase II phosphorylation sites, [ST].₂[DE]; (5) Inorganic pyrophosphatase signature site, D[SGDN]D[PE][LIVMF]D[LIVMGAC]; (6) N-glycosylation site, N^{[^]P}[ST]^{[^]P}; (7) Aerolysin type toxins signature, TATNWSKTNT; and (8) cAMP- and cGMP dependent protein kinase phosphorylation site, [RK]₂.^{[^]P}[ST].

(112–115, 213–216, 236–239 and 354–357), N-glycosylation sites (N^{[^]P}[ST]^{[^]P}) at six locations (154–157, 229–232, 249–252, 285–288, 363–66 and 397–400), protein kinase C phosphorylation sites ([ST].[RK]) at eleven positions (56–58, 105–107, 192–194, 206–208, 215–217, 241–243, 259–261, 263–265, 303–305, 377–379 and 456–458), N-myristoylation sites (G^{[^]E}DRKH^{[^]P}FWY)₂[STAGCN]^{[^]P} at nine locations, (15–20, 38–43, 72–77, 91–96, 152–157, 176–181, 293–298, 459–464 and 478–483), cAMP- and cGMP-dependent protein kinase phosphorylation sites ([RK]₂.^{[^]P}[ST]) spanning positions 473–476, aerolysin type toxins signature (TATNWSKTNT)

spanning positions 246–255 amino acid residues, inorganic pyrophosphatase signature (D[SGDN]D[PE][LIVMF]D[LIVMGAC]) at 118–124 position (DGDEVDV), and tyrosine kinase phosphorylation sites ([RK].₃)[DE].₂Y at two positions, (21–28 and 379–386) (Figure 1).

3.2. Phylogenetic analysis of the aerolysin of *Ah_{EUS112}*

Multiple sequence alignment of the *Ah_{EUS112}* aerolysin with other bacterial aerolysin showed ~90–96% identities with the

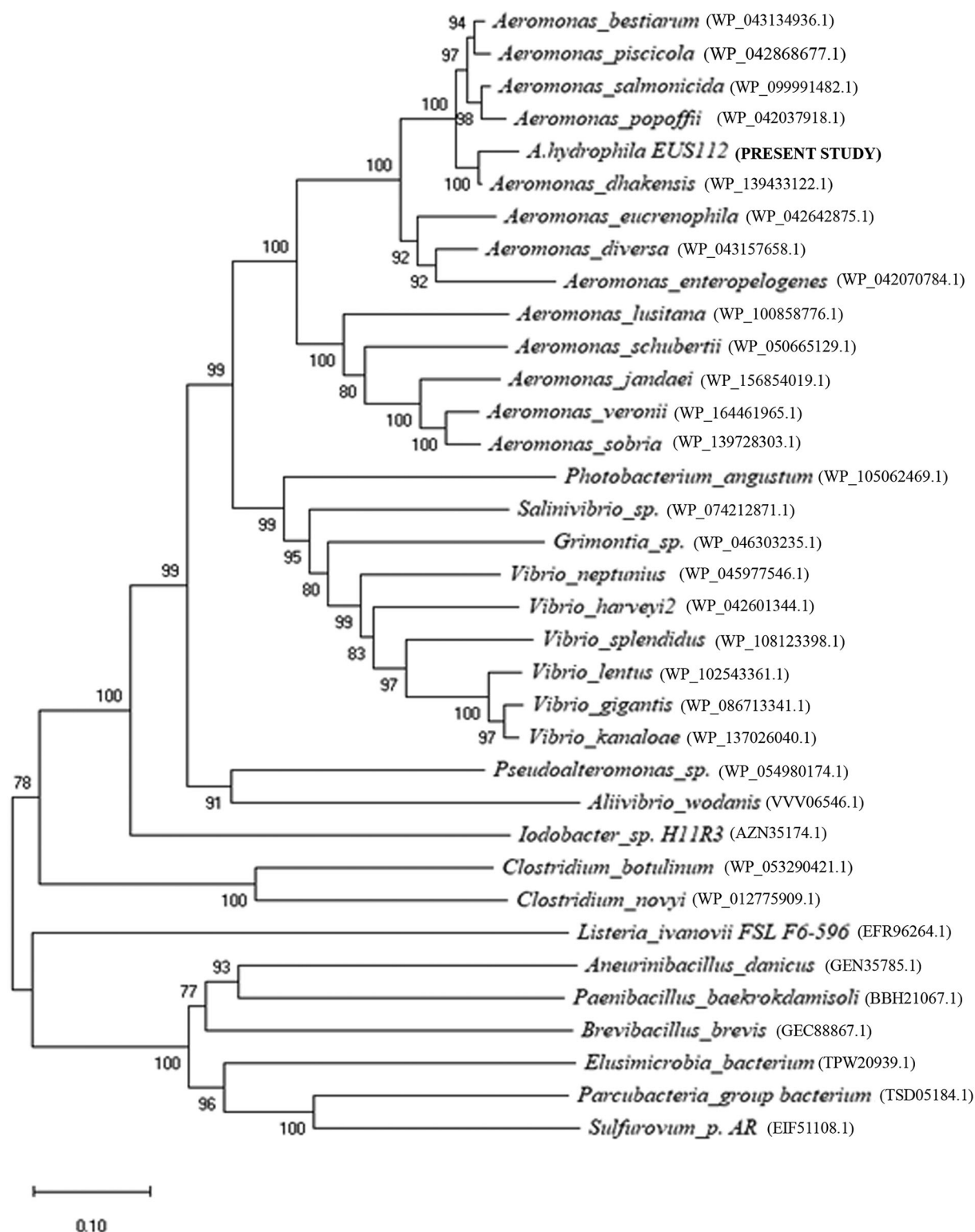


Figure 2. Rooted phylogenetic tree of the deduced amino acid sequence of aerolysin of *Ah_{EUS112}*. Amino acid sequences of aerolysin of 35 bacterial species were retrieved from the NCBI database. Multiple sequence alignment was performed using MEGAX. Sequence divergence is represented by the distances from the nodes i.e. the branch length (denoted by numbers).

aerolysins of other *Aeromonas* species. The evolutionary history of aerolysin of *A. hydrophila* analysis using the neighbor-joining method (Saitou & Nei, 1987) resulted in an optimal tree with the sum of branch length = 6.42708017. The phylogenetic tree generated from the multiple sequence alignment of the *Ah_{EUS112}* aerolysin with 35 bacterial

aerolysin showed the presence of multiple branches indicating the diverse architectural structure of a protein (Figure 2). In the *Aeromonas* species itself, at least three clusters could be distinctly seen, with *Ah_{EUS112}* aerolysin to be closest to that of *A. dhakensis* (98% similarity). In contrast, the similarity with other *Aeromonas* sp. varied from 60% to 96%,

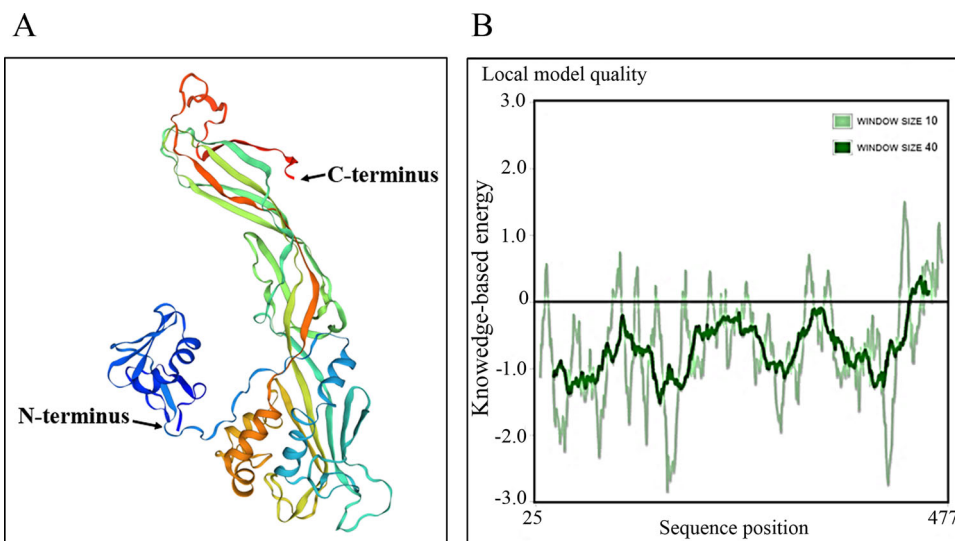


Figure 3. A. Homology model of the aerolysin of *AhEUS112*. Homology model of the *AhEUS112* aerolysin generated using PDB#3g4n as a template. The structure was visualized by Swiss-PDB Viewer and represented in the form of ribbons. B. Comparison of energy plot of the modeled *AhEUS112* aerolysin with the template to verify the reliability of the generated model using PROSA energy plot.

confirming this genus' heterogeneity. The *AhEUS112* aerolysin exhibited ~50% identity with the aerolysin of *Vibrio* (second highest after *Aeromonas* aerolysins). Another pathogenic bacterium, *Clostridium botulinum*, displayed ~17% identity with *A. hydrophila* aerolysin, indicating a highly diverse structure of aerolysin attained by different bacteria. The least similarity of only 1% was found to be with the aerolysin of *Parcubacteria*.

3.3. Structural model and overall architecture

The amino acid sequence of the aerolysin of *A. hydrophila* (PDB entry# 3g4n) showed 93.39% similarity with that of *AhEUS112*; therefore, this structure was used as a template for the generation of the Swiss-PDB most acceptable model of the aerolysin of *AhEUS112* (Figure 3(a)). The quality of the model was assessed using PROCHECK. The Ramachandran plot thus generated showed 90.3% residues in the most favorable regions, 9.4% residues in the allowed regions, while 0.3% residues in the disallowed regions (Supplementary material, Figure 1).

The G-factor score for the model revealed by the Ramachandran plot was: -0.29 for dihedral bonds, 0.03 for covalent bonds, and overall was -0.15. The G-score greater than -0.50 confirms that these are within limits, and hence the G-factor score of the model is satisfactory and acceptable. The structure was also verified using verify3D, WHAT_CHECK, QMEANDisCo and PROSA. Verify3D has shown that 96.03% of the residues have averaged 3D-1D score ≥ 0.2 , which is acceptable and approved by the program. Quality of homology modeling was also checked using QMEANDisCo. As the reliability of the prediction heavily depends on model size, the provided error estimate is calculated based on models of similar size to the input verification tool, and the global score was found to be 0.88 ± 0.05 , which is in acceptable range as structure less than 0.6 range is expected to be of low quality. The energy of the *AhEUS112*

aerolysin model (Z scores) calculated by PROSA with mutant aerolysin was determined to be -8.58 (Figure 3(b)). The Z score of a similar model is found to be -6.57. Therefore, our model is within the range of PROSA energy and can be accepted for further analysis.

3.4. Docking interaction analysis

In the present study, the primary purpose of *in silico* docking analysis is to determine the favorable binding conformations between aerolysin and drugs that would inhibit its pore forming ability. Molecular docking was carried out to interpret the ligands' best binding pose and search the drugs that can bind strongly with the active site residues of aerolysin. Multiple poses were generated and evaluated based on binding conformations and common interacting residues at the binding pocket. On the basis of binding energies and interacting residues, the best-docked complexes obtained with aerolysin were aralia-saponin I (-8.969 kcal/mol), cyclamin (-8.449 kcal/mol), ardisiacrispin B (-8.166 kcal/mol) and aralia-saponin II (-8.097 kcal/mol) (Table 1). These drugs exhibited better binding affinity than other drugs and bound to the functionally important domain of aerolysin. The binding poses in 3D and 2D interaction of drugs with aerolysin are shown in Figures 4 and 5. Further, the ligands poses are stabilized by a combination of hydrophobic and van der Waals interactions with active site residues. Analysis of results revealed that all the test molecules mostly shared common interacting residues in aerolysin (Table 1). DockThor analysis results were also validated employing AutoDockVina tool compiled in PyRx software. Analysis of binding energy and binding pose of each molecule using PyRx confirmed the results obtained from DockThor server (Supplementary material, Table S1). The best ranked poses obtained from PyRx interacting with the aerolysin were aralia-saponin I (-12.1 kcal/mol), followed by cyclamin (-12.0 kcal/mol), ardisiacrispin B (-11.4 kcal/mol) and aralia-saponin II (-11.1 kcal/

Table 1. Molecular docking results and interaction analysis of most effective putative inhibitors of *Aeromoans hydrophila* (EUS112) aerolysin.

| S.No. | PubChem CID | Drug Name | Binding Affinity (kcal/mol) | ΔE_{total} (kcal/mol) | ΔE_{vdw} (kcal/mol) | ΔE_{ele} (kcal/mol) | Interacting residues |
|-------|-------------|-----------------------|-----------------------------|--------------------------------------|------------------------------------|------------------------------------|---|
| 1. | 101028180 | Aralia-saponin_I | -8.969 | 237.978 | -49.905 | -21.118 | Pro180, Asp181, Lys241, Lys245 and Tyr347 |
| 2. | 441916 | Cyclamin | -8.449 | 349.623 | -15.387 | -14.389 | Asp181, Lys245 and Leu248 |
| 3. | 10441164 | Ardisiacrispin B | -8.166 | 317.339 | -14.631 | -17.018 | Met40, Asn177, Asp179, Asp181, Lys243 and Asp310 |
| 4. | 101028181 | Aralia-saponin_II | -8.097 | 239.050 | -13.099 | -34.017 | Asp179, Asp181, Lys245, Asp310, Tyr347 and Pro394 |
| 5. | 195332 | Kalopanax (Saponin C) | -7.934 | 419.841 | -12.071 | -34.867 | Asp179, Asp181 and Lys245 |
| 6. | 85229914 | Aralia-saponin_III | -7.86 | 325.225 | -12.074 | -20.24 | Met40, Asp181, Lys245 and Leu248 |
| 7. | 198016 | Saponin | -7.506 | 349.905 | -10.431 | -21.603 | Asn177, Asp179, Lys241, Asp310 |
| 8. | 73109902 | Aralia-saponin_IV | -7.499 | 364.172 | -5.553 | -27.393 | Asn39, Asp181 and Lys245 |
| 9. | 92825 | Gypsogenin | -7.218 | 145.345 | -6.325 | -19.929 | Asp179, Gly347, Tyr347, Pro394 and Arg396 |
| 10. | 102438569 | Berneuxia | -7.126 | 334.671 | -0.528 | -31.057 | Asn61, Asp179 and Asp181 |
| 11. | 482163 | Colhiside (Saponin 4) | -7.002 | 232.133 | -2.136 | -32.539 | Asp181, Lys245, Glu253 and Ser255 |
| 12. | 5281670 | Morin | -6.929 | 24.719 | -1.729 | -30.199 | Asp181, Lys245, Pro247 and Leu248 |
| 13. | 6989 | Thymol | -6.34 | 12.471 | -1.89 | -14.793 | Asn39, Asp181 and Pro394 |

ΔE_{total} , ΔE_{vdw} and ΔE_{ele} denote total energy, van der Waals energy and electrostatic energy, respectively.

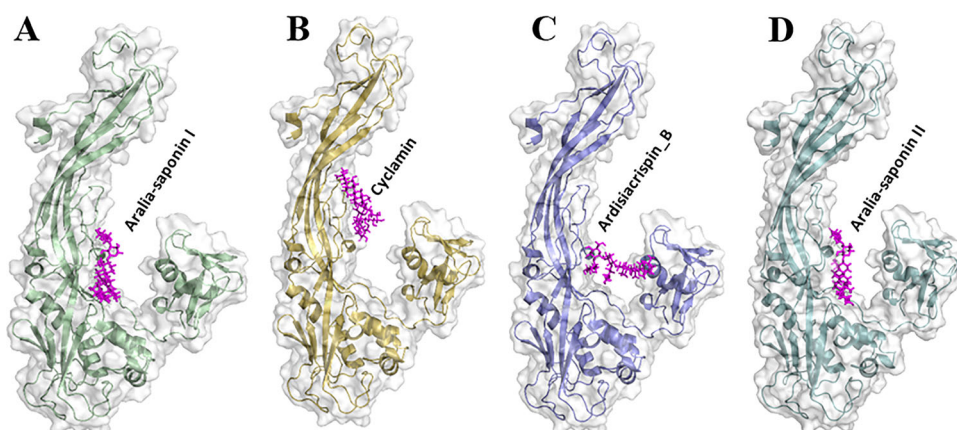


Figure 4. Visualization of docked complexes. 3-D models of the four best docked complexes of the modeled aerolysin structures and aralia-Saponin I (A), cyclamin (B), ardisiacrispin B (C) and aralia-Saponin II (D) visualized in PyMol.

mol). The best molecules in terms of binding energy were further taken for interacting interface analysis using DockThor server. The Asp179, Asp181, Lys241, Lys245, Pro247, and Leu248 were the central amino acid residues of aerolysin involved in hydrogen bonding with the test drugs. These residues have shown lowest docking energy that is proportional to highest binding affinity (more potent compound) with aerolysin. It is also seen that aralia-saponin I could more strongly bind to and interact with the binding site of the aerolysin when compared to other drugs. Detailed analysis showed that the residues Asp181 and Lys245 are the most common amino acids of aerolysin that interact with all the drugs forming strong van der Waals and hydrophobic interactions. Docking results also revealed that all binding residues across all the drugs reside in the pore forming domain of aerolysin. Pore-forming domain helps aerolysin in binding to the glycan core of glycosylphosphatidyl inositol

(GPI)-anchored proteins and subsequently forms a pore in the plasma membrane (Abrami et al., 2003). Thus, binding of these test drugs to the critical amino acids present in the pore forming domain would prevent pore formation, possibly by inhibiting oligomerization. Earlier *in silico* studies by Singh and Somvanshi (2009) demonstrated that aralia, gypsogenin, saponin and TS-saponin are highly effective in inhibiting oligomerization of aerolysin monomer of *A. hydrophila* Ah 14 through robust binding affinity between aerolysin and drugs. Another study by Abrami and Goot (1999) had reported the role of saponin in inhibiting the oligomerization of aerolysin by preventing its clustering on plasma membrane that reduces the probability of encounter of toxin monomers and thereby the efficiency of oligomerization. Hence, molecular docking explained the interactions between aerolysin and drugs, which provided useful information on identification of key interacting residues, which in turn could help develop

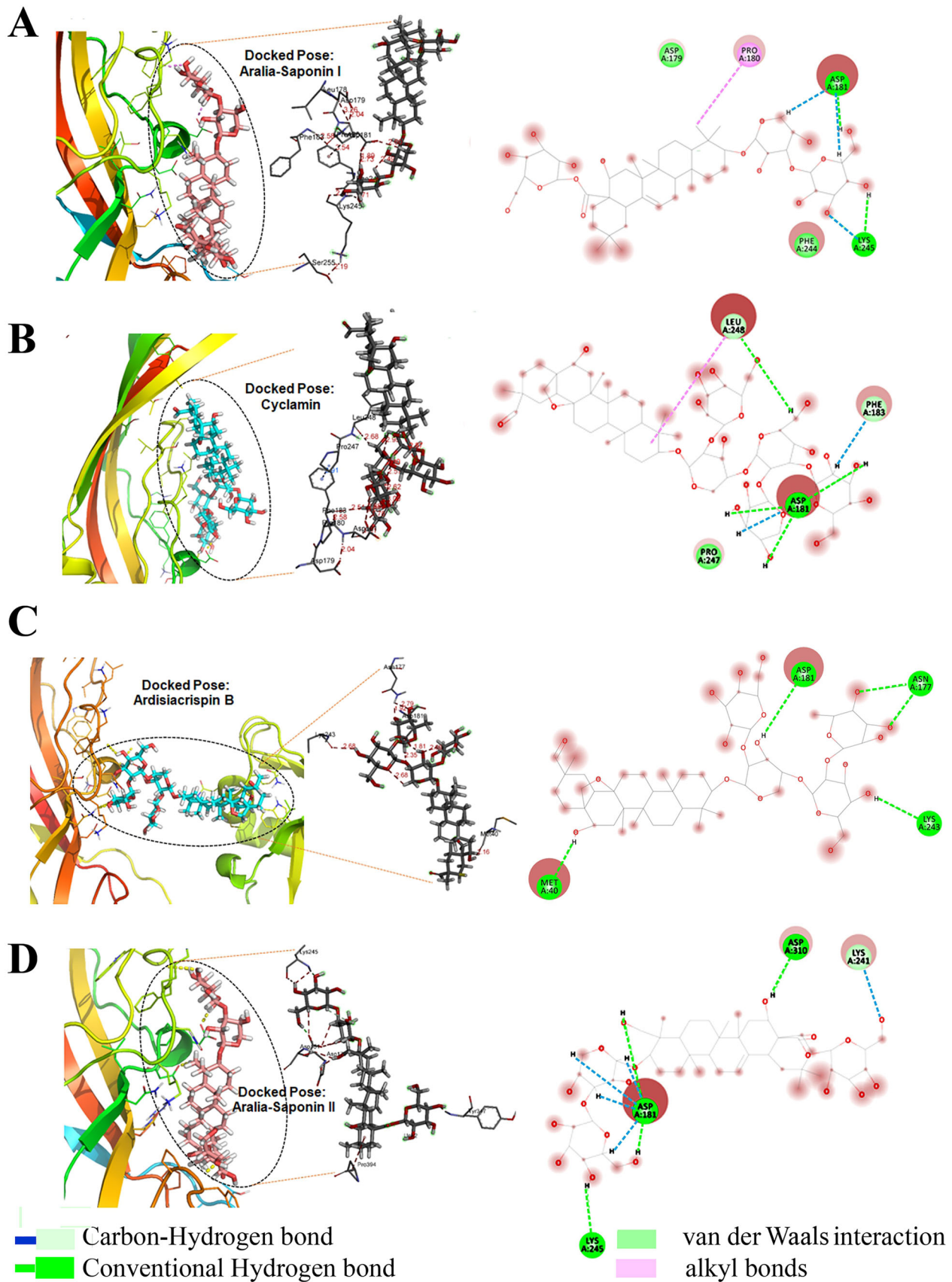


Figure 5. Docked poses of the modeled aerolysin with different drugs. 2D view of the interaction of drugs [aralia-saponin I (A), cyclamin (B), ardisiacrispin (C) and aralia-Saponin II (D)] with surrounding amino acids of aerolysin. Docked poses are enlarged. Figures were constructed using PyMol and Discovery Studio Visualizer.

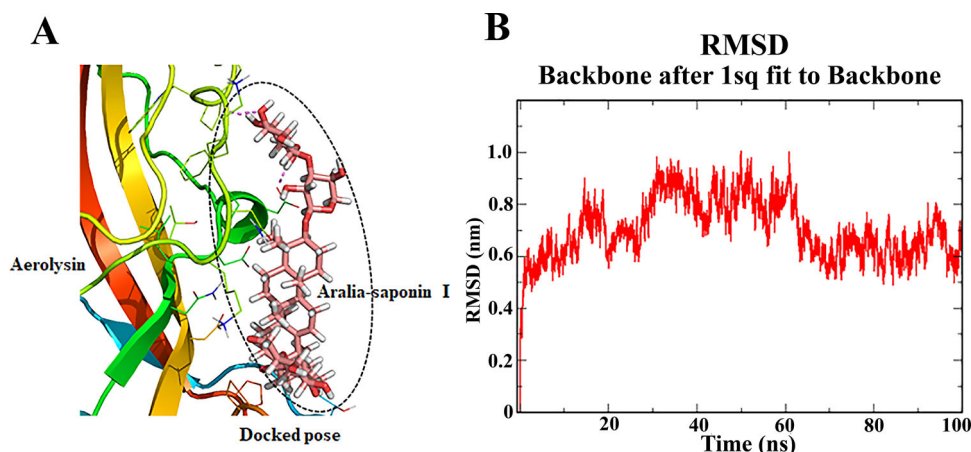


Figure 6. Molecular dynamics simulation (A) Best ranked docked complex of aerolysin with aralia-saponin I (B) RMSD of backbone over the simulation of 100 ns.

novel molecules against aerolysin to inhibit its binding to GPI anchored proteins. Molecular dynamic simulation offers a deeper insight into the proper binding of the ligand candidates with the protein under analysis. A workflow combined with molecular docking, molecular dynamic, and free energy calculation has been engaged in understanding the properties of individual natural products in solvation state. In the present study, a 100 ns MDS was performed to calculate the binding affinity and conformational stability of best docked molecule araliasaponin I to the aerolysin. The MD simulation yielded total energy of -2.2036 kJ/mol and potential energy of -2.712 kJ/mol for the aerolysin-araliasaponin I complex. The RMSD calculation of backbone atoms over the whole simulation ranged from 0.05 nm to a maximum of 0.75 nm. Initially, the RMSD increased slightly, fluctuated in the period of 20 ns to 40 ns and then stabilized to a reasonable extent. It rose again and became stable from around 27 ns to 62 ns, and again reduced and remained stable until 100 ns. Majorly it remained within 0.5 to 0.7 nm (Figure 6). Thus, MD simulation analysis clearly demonstrated that the araliasaponin I forms a stable complex with aerolysin. Collectively, it is reasonable to infer that aralia-saponin I followed by cyclamin, ardisiacrispin and aralia-saponin II possibly have the potential to inhibit aerolysin heptamer formation, thus blocking the binding on membrane. Further *in vitro* studies are required to be carried out to confirm the mechanism of aerolysin inhibition by the drugs used in current study.

4. Conclusion

The sequence analysis of gene encoding aerolysin of *A. hydrophila* has revealed that it possesses the characteristics of a cytological toxin. Multiple sequence alignment and the phylogenetic tree revealed significant heterogeneity with similarity varying between 60% – 96% in the aerolysin sequence of different *Aeromonas* species. The *Ah*_{EUS112} aerolysin showed considerable similarity with *Vibrio* toxin and thus justified the earlier placement of *A. hydrophila* in the *Vibrionacea* family. Since the sequence homology of aerolysin amongst *Aeromonas* strains has revealed the presence of conserved residues, it can be tested as a broad spectrum drug target for different *Aeromonas* isolates/strains. Based on

molecular docking analysis, we also propose that aralia-saponin I, cyclamin, ardisiacrispin B, and aralia-saponin II may be a more potent effective drug for inhibiting the pore formation in aerolysin infection. Further, the study of proposed inhibitors needs to be carried out to explore their binding and inhibitory potential *in vivo*. In the absence of a high-resolution crystal structure of aerolysin available, the cloned *AhaerA*_{EUS112} of *A. hydrophila* can be expressed and purified to validate the *in silico* results reported in the present study, and investigate the effect of the identified drugs on its activity *in vitro* using cell based assays.

Acknowledgements

AD acknowledges the Jawaharlal Nehru University, New Delhi for intramural funding.

Disclosure statement

No potential conflict of interest was reported by the authors.

References

- Abraham M. J., Murtola T., Schulz R., Páll S., Smith J. C., Hess B., & Erik L. (2015). GROMACS: High performance molecular simulations through multi-level parallelism from laptops to supercomputers. *SoftwareX*, 1/2, 19–25. <https://doi.org/10.1016/j.softx.2015.06.001>
- Abrami, L., & van der Goot, F. G. (1999). Plasma membrane microdomains act as concentration platforms to facilitate intoxication by aerolysin. *The Journal of Cell Biology*, 147(1), 175–184. <https://doi.org/10.1083/jcb.147.1.175>
- Abrami, L., Fivaz, M., Glauser, P. E., Sugimoto, N., Zurzolo, C., & van der Goot, F. G. (2003). Sensitivity of polarized epithelial cells to the pore-forming toxin aerolysin. *Infection and Immunity*, 71(2), 739–746. <https://doi.org/10.1128/iai.71.2.739-746.2003>
- Bairoch, A., Bucher, P., & Hofmann, K. (1997). The PROSITE database, its status in 1997. *Nucleic Acids Research*, 25(1), 217–221. <https://doi.org/10.1093/nar/25.1.217>
- Bendtsen, J. D., Nielsen, H., von Heijne, G., & Brunak, S. (2004). Improved prediction of signal peptides: SignalP 3.0. *Journal of Molecular Biology*, 340(4), 783–795. <https://doi.org/10.1016/j.jmb.2004.05.028>
- Cao, C., Li, M. Y., Cirauqui, N., Wang, Y. Q., Dal Peraro, M., Tian, H., & Long, Y. T. (2018). Mapping the sensing spots of aerolysin for single oligonucleotides analysis. *Nature Communications*, 9(1), 2823. <https://doi.org/10.1038/s41467-018-05108-5>

- Cao, C., Liao, D. F., Yu, J., Tian, H., & Long, Y. T. (2017). Construction of an aerolysin nanopore in a lipid bilayer for single-oligonucleotide analysis. *Nature Protocols*, 12(9), 1901–1911. <https://doi.org/10.1038/nprot.2017.077>
- Cirauqui, N., Abriata, L. A., van der Goot, F. G., & Dal Peraro, M. (2017). Structural, physicochemical and dynamic features conserved within the aerolysin pore-forming toxin family. *Scientific Reports*, 7(1), 13932. <https://doi.org/10.1038/s41598-017-13714-4>
- Cumberbatch, N., Gurwith, M. J., Langston, C., Sack, R. B., & Brunton, J. L. (1993). Cytotoxic enterotoxin produced by *Aeromonas hydrophila*: Relationship of toxigenic isolates to diarrheal disease. *Infection and Immunity*, 23(3), 267–277. <https://doi.org/10.1128/IAI.23.3.829-837.1979>
- Dallakyan, S., & Olson, A. J. (2015). Small-molecule library screening by docking with PyRx. In J. E. Hempel, C. H. Williams, & C. C. Hong (Eds.), *Chemical biology: Methods and protocols, methods in molecular biology* (pp. 243–250). Springer.
- Delano, W. L., & Palo Alto, C. A. (2002). The PYMOL molecular graphics system.
- Discovery Studio Visualizer Software, Version 4.0. (2012). <http://www.accelrys.com>
- Dong, J., Liu, Y., Xu, N., Yang, Q. & Ai, X. (2018). Morin protects channel catfish from *Aeromonas hydrophila* infection by blocking aerolysin activity. *Frontiers in Microbiology*, 9, 2828. <https://doi.org/10.3389/fmicb.2018.02828>
- Dong, J., Zhang, L., Liu, Y., Xu, N., Zhou, S., Yang, Q., Yang, Y., & Ai, X. (2020). Thymol protects channel catfish from *Aeromonas hydrophila* infection by inhibiting aerolysin expression and biofilm formation. *Microorganisms*, 8(5), 636. <https://doi.org/10.3390/microorganisms8050636>
- Eisenberg, D., Lüthy, R., & Bowie, J. U. (1997). VERIFY3D: Assessment of protein models with three-dimensional profiles. *Methods in Enzymology*, 277, 396–404. [https://doi.org/10.1016/s0076-6879\(97\)77022-8](https://doi.org/10.1016/s0076-6879(97)77022-8)
- Felsenstein, J. (1985). Confidence limits on phylogenies: An approach using the bootstrap. *Evolution International Journal of Organic Evolution*, 39(4):783–791. <https://doi.org/10.1111/j.1558-5646.1985.tb00420.x>
- Ferguson, M. R., Xu, X. J., Houston, C. W., Peterson, J. W., & Chopra, A. K. (1995). Amino-acid residues involved in biological functions of the cytolytic enterotoxin from *Aeromonas hydrophila*. *Gene*, 156(1), 79–83. [https://doi.org/10.1016/0378-1119\(95\)00043-6](https://doi.org/10.1016/0378-1119(95)00043-6) [https://doi.org/10.1016/0378-1119\(95\)00043-6](https://doi.org/10.1016/0378-1119(95)00043-6)
- Gauthier, J., Vincent, A. T., Charette, S. J., & Derome, N. (2017). Strong genomic and phenotypic heterogeneity in the *Aeromonas sobria* species complex. *Frontiers in Microbiology*, 8, 2434. <https://doi.org/10.3389/fmicb.2017.02434>
- Gosling, P. J. (1996). Pathogenic mechanisms. In B. Austin, M. Altwegg, P. J. Gosling, & S. W. Joseph (Eds.), *The genus Aeromonas* (pp. 245–265). John Wiley & Sons Ltd..
- Janda, J. M., & Abbott, S. L. (2010). The genus *Aeromonas*: Taxonomy, pathogenicity, and infection. *Clinical Microbiology Reviews*, 23(1), 35–73. <https://doi.org/10.1128/CMR.00039-09>
- Kumar, S., Stecher, G., Li, M., Nknyaz, C., & Tamura, K. (2018). MEGA X: Molecular evolutionary genetics analysis across computing platforms. *Molecular Biology and Evolution*, 35(6), 1547–1549. <https://doi.org/10.1093/molbev/msy096>
- Laskowski, R. A., MacArthur, M. W., Moss, D. S., & Thornton, J. M. (1993). PROCHECK: A program to check the stereo chemical quality of protein structures. *Journal of Applied Crystallography*, 26(2), 283–291. <https://doi.org/10.1107/S0021889892009944>
- Nei, M., & Kumar, S. (2000). *Molecular evolution and phylogenetics*. Oxford University Press.
- Ramachandran, G. N., & Sasisekharan, V. (1968). Conformation of polypeptides and proteins. *Advances in Protein Chemistry*, 23, 283–438. [https://doi.org/10.1016/s0065-3233\(08\)60402-7](https://doi.org/10.1016/s0065-3233(08)60402-7)
- Rasmussen-Ivey, C. R., Figueras, M. J., McGarey, D., & Liles, M. R. (2016). Virulence factors of *Aeromonas hydrophila*: In the wake of reclassification. *Frontiers in Microbiology*, 7, 1337. <https://doi.org/10.3389/fmicb.2016.01337>
- Rost, B., Yachdav, G., & Liu, J. (2004). The PredictProtein server. *Nucleic Acids Research*, 32 (Web Server issue), W321–W326. <https://doi.org/10.1093/nar/gkh377>
- Saitou, N., & Nei, M. (1987). The neighbor-joining method: A new method for reconstructing phylogenetic trees. *Molecular Biology and Evolution*, 4(4), 406–425. <https://doi.org/10.1093/oxfordjournals.molbev.a040454>
- Salentin, S., Schreiber, S., Haupt, V. J., Adasme, M. F., & Schroeder, M. (2015). PLIP: Fully automated protein-ligand interaction profiler. *Nucleic Acids Research*, 43(W1), W443–W447. <https://doi.org/10.1093/nar/gkv315>
- Santos, K. B., Guedes, I. A., Karl, A., & Dardenne, L. E. (2020). Highly flexible ligand docking: benchmarking of the DockThor Program on the LEADS-PEP protein-peptide data set. *Journal of Chemical Information and Modeling*, 60(2), 667–683. <https://doi.org/10.1021/acs.jcim.9b00905>
- Schneider, G. F., & Dekker, C. (2012). DNA sequencing with nanopores. *Nature Biotechnology*, 30(4), 326–328. <https://doi.org/10.1038/nbt.2181>
- Singh, V., & Somvanshi, P. (2009). Inhibition of oligomerization of aerolysin from *Aeromonas hydrophila*: Homology modeling and docking approach for exploration of hemorrhagic septicemia. *Letters in Drug Design & Discovery*, 6(3), 215, 223. <https://doi.org/10.2174/157018009787847864>
- Singh, V., Somvanshi, P., Rathore, G., Kapoor, D., & Mishra, B. N. (2010). Gene cloning, expression, and characterization of recombinant aerolysin from *Aeromonas hydrophila*. *Applied Biochemistry and Biotechnology*, 160(7), 1985–1991. <https://doi.org/10.1007/s12010-009-8752-3>
- Sippl, M. J. (1993). Recognition of errors in three-dimensional structures of proteins. *Proteins*, 17(4), 355–362. <https://doi.org/10.1002/prot.340170404>
- Stefureac, R., Long, Y. T., Kraatz, H. B., Howard, P., & Lee, J. S. (2006). Transport of alpha-helical peptides through alpha-hemolysin and aerolysin pores. *Biochemistry*, 45(30), 9172–9179. <https://doi.org/10.1021/bi0604835>
- Studer, G., Rempfer, C., Waterhouse, A. M., Gumienny, R., Haas, J., & Schwede, T. (2020). QMEANDisCo-distance constraints applied on model quality estimation. *Bioinformatics (Oxford, England)*, 36(6), 1765–1771. <https://doi.org/10.1093/bioinformatics/btz828>
- Trott, O., & Olson, A. J. (2010). AutoDock Vina: improving the speed and accuracy of docking with a new scoring function, efficient optimization, and multithreading. *Journal of Computational Chemistry*, 31(2), 455–461. <https://doi.org/10.1002/jcc.21334>
- Véron M. (1965). La position taxonomique des *Vibrio* et de certaines bactéries comparables [The taxonomic position of *Vibrio* and certain comparable bacteria]. *Comptes Rendus Hebdomadaires Des Seances de L'Academie Des Sciences. Serie D: Sciences Naturelles*, 261(23), 5243–5246.
- Wang, G., Clark, C. G., Liu, C., Pucknell, C., Munro, C. K., Kruk, T. M., Caldeira, R., Woodward, D. L., & Rodgers, F. G. (2003). Detection and characterization of the hemolysin genes in *Aeromonas hydrophila* and *Aeromonas sobria* by multiplex PCR. *Journal of Clinical Microbiology*, 41(3), 1048–1054. <https://doi.org/10.1128/JCM.41.3.1048-1054.2003>
- Wang, Y. Q., Cao, C., Ying, Y. L., Li, S., Wang, M. B., Huang, J., & Long, Y. T. (2018). Rationally designed sensing selectivity and sensitivity of an aerolysin nanopore via site-directed mutagenesis. *ACS Sensors*, 3(4), 779–783. <https://doi.org/10.1021/acssensors.8b00021>
- Zhu, D., Li, A., Wang, J., Li, M., & Cai, T. (2007). Cloning, expression and characterization of aerolysin from *Aeromonas hydrophila* in *Escherichia coli*. *Indian Journal of Biochemistry & Biophysics*, 44(4), 204–208. PMID: 17970277

Appendices

MDPI Open Access Information and Policy

All articles published by MDPI are made immediately available worldwide under an open access license. This means:

- everyone has free and unlimited access to the full-text of *all* articles published in MDPI journals;
- everyone is free to re-use the published material if proper accreditation/citation of the original publication is given;
- open access publication is supported by the authors' institutes or research funding agencies by payment of a comparatively low **Article Processing Charge (APC)** ([/about/apc](#)) for accepted articles.

Permissions

No special permission is required to reuse all or part of article published by MDPI, including figures and tables. For articles published under an open access Creative Common CC BY license, any part of the article may be reused without permission provided that the original article is clearly cited. Reuse of an article does not imply endorsement by the authors or MDPI.

External Open Access Resources

MDPI is a RoMEO **green publisher** (<http://www.sherpa.ac.uk/romeo/search.php?type=publisher&search=mdpi>) — RoMEO is a database of Publishers' copyright and self-archiving policies hosted by the **University of Nottingham** (<http://www.nottingham.ac.uk/>)

Those who are new to the concept of open access might find the following websites or 'Open Access 101' video informative:

Wikipedia article on 'Open Access' ([https://en.wikipedia.org/wiki/Open_access_\(publishing\)](https://en.wikipedia.org/wiki/Open_access_(publishing)))
Peter Suber's 'Open Access Overview' (<http://www.earlham.edu/~peters/fos/overview.html>)
Information Platform Open Access [in **English** (<https://open-access.net/en/information-on-open-access>)] , in **German** (<https://open-access.net/informationen-zu-open-access>)]
SHERPA's 'Authors and Open Access' (<http://www.sherpa.ac.uk/guidance/authors.html>)

Meaning of Open Access

In accordance with major definitions of open access in scientific literature (namely the Budapest, Berlin, and Bethesda declarations), MDPI defines *open access* by the following conditions:

- peer-reviewed literature is freely available without subscription or price barriers,

Open Access Explained!

Back to Top

4/7/2021

RightsLink Printable License

OXFORD UNIVERSITY PRESS LICENSE TERMS AND CONDITIONS

Apr 07, 2021

This Agreement between Ms. Ankita Singh ("You") and Oxford University Press ("Oxford University Press") consists of your license details and the terms and conditions provided by Oxford University Press and Copyright Clearance Center.

| | |
|------------------------------|---|
| License Number | 5043590790023 |
| License date | Apr 07, 2021 |
| Licensed content publisher | Oxford University Press |
| Licensed content publication | Clinical Infectious Diseases |
| Licensed content title | Role of θ Toxin, a Sulfhydryl-Activated Cytolysin, in the Pathogenesis of Clostridial Gas Gangrene |
| Licensed content author | Stevens, Dennis L.; Bryant, Amy E. |
| Licensed content date | Jun 1, 1993 |
| Type of Use | Thesis/Dissertation |
| Institution name | |
| Title of your work | Vaccine potential of PerfringolysinO (PFO) of Clostridium perfringens and its mutants |
| Publisher of your work | Jawaharlal Nehru University |
| Expected publication date | Jan 2023 |

4/7/2021

RightsLink Printable License

OXFORD UNIVERSITY PRESS LICENSE
TERMS AND CONDITIONS

Apr 07, 2021

This Agreement between Ms. Ankita Singh ("You") and Oxford University Press ("Oxford University Press") consists of your license details and the terms and conditions provided by Oxford University Press and Copyright Clearance Center.

| | |
|------------------------------|---|
| License Number | 5043590790023 |
| License date | Apr 07, 2021 |
| Licensed content publisher | Oxford University Press |
| Licensed content publication | Clinical Infectious Diseases |
| Licensed content title | Role of θ Toxin, a Sulfhydryl-Activated Cytolysin, in the Pathogenesis of Clostridial Gas Gangrene |
| Licensed content author | Stevens, Dennis L.; Bryant, Amy E. |
| Licensed content date | Jun 1, 1993 |
| Type of Use | Thesis/Dissertation |
| Institution name | |
| Title of your work | Vaccine potential of PerfringolysinO (PFO) of Clostridium perfringens and its mutants |
| Publisher of your work | Jawaharlal Nehru University |
| Expected publication date | Jan 2023 |